Anticancer Activity of *Ceratotheca triloba*

Submitted in complete fulfilment for the Degree of Doctorate of Philosophy in Biotechnology in the Department of Biotechnology and Food Technology, Durban University of Technology, Durban, South Africa

Leeann Naicker

SUPERVISOR: **Professor B. Odhav**

CO-SUPERVISORS: **Dr M.G Matsabisa**

Dr V. Mohanlall

REFERENCE DECLARATION

I, **Miss Leeann Naicker - (Student number: 20509633)** and **Prof Bharti Odhav** (full name of supervisor) do hereby declare that in respect of the following dissertation:

Title: **Anticancer activity of *Ceratotheca triloba***

1. As far as we ascertain:

(a) no other similar dissertation exists:

2. All references as detailed in the dissertation are complete in terms of all personal communications engaged in and published works consulted.

_____ _____

Signature of student **Date**

_____ _____

Signature of supervisor **Date**

_____ _____

Signature of co-supervisor **Date**

_____ _____

Signature of co-supervisor **Date**

AUTHORS DECLARATION

This study presents original work by the author. It has not been submitted in any form to another academic institution. Where use was made of the work of others, it has been duly acknowledged in the text. The research described in this dissertation was carried out in the Department of Biotechnology and Food Technology, Faculty of Applied Sciences, Durban University of Technology, South Africa, under the supervision of Prof Bharti Odhav, Dr Viresh Mohanlall and Dr M.G. Matsabisa.

_____

Students signature

TABLE OF CONTENTS

ACKNOWLEDGEMENTS

I would like to extend my sincere thanks and gratitude to:

- My God, the Lord almighty, my protector and defender, my saviour and redeemer for teaching me that I can do all things through him who strengthens me. Jeremiah 29:11- For I know the plans I have for you," declares the LORD, "plans to prosper you and not to harm you, plans to give you hope and a future.

- My supervisors, Dr M.G. Matsabisa, Prof. B. Odhav and Dr. V. Mohanlall for their patience, guidance, constructive criticism and words of encouragement throughout the course of this project;

- Prof. H. Baijnath (Durban University of Technology) for collection of plant material;

- Mr J. Nyelimane (Indigenous Knowledge Systems, Medical Research Council) for technical assistance;

- Miss J. Petersen (Indigenous Knowledge Systems, Medical Research Council) for administrative assistance;

- Dr C. Kaschula (ICGEB, University of Cape Town) for technical assistance and provision of cell lines;

- Miss N. Kolesnikova (Council for Scientific and Industrial Research, Biosciences) for provision of cell lines;

- Prof. P. Steenkamp, (Council for Scientific and Industrial Research, Biosciences) for his technical assistance;

- Dr. S. Kumar, (Durban University of Technology) for their technical assistant during the course of the project;

- National Research Foundation (NRF) for funding this project.

LIST OF ABBREVIATIONS

%GI	Percentage of growth inhibition
7-AAD	7-Aminoactinomycin D
AIF	Apoptosis inducing factor
APAF1	Apoptotic protease-activating factor 1
CAD	Caspase-activated deoxyribonuclease
CARD	Caspase activation and recruitment domain
CCM	Complete culture medium
CLL	Chronic lymphocytic leukemia
CSIR	Council of Scientific and Industrial Research
DCM	Dichloromethane
DD	Death domain
DED	Death effector domain
DISC	Death inducing signalling complex
DMEM	Dulbecco‘s Modified Eagle Medium
DMSO	Dimethyl sulphoxide
EI-LC-MS	Electron Ionization- Liquid Chromatography-Mass Spectroscopy
FADD	Fas associated death domain
FDA	Food and Drug Administration
FITC	Fluorescein isothiocyanate
IAC’s	Independently active compounds
IAPs	Inhibitor of apoptosis proteins
IARC	International Agency for Research on Cancer
ICAD	Inhibitor caspase-activated deoxyribonuclease

JC-1	5,5’,6,6’-tetrachloro-1,1’,3,3’-tetraethylbenzimidazolcarbocyanine iodide
MCL1	Myeloid cell leukemia 1
MDR	Multi-drug resistance
MTT	3-(4,5-dimethylthiazol-2-yl)-2,5-diphenyltetrazolium bromide
NCI	National Cancer Institute
PARP	Poly-(ADP-ribose) polymerase
PBS	Phosphate saline buffer
PE	Phycoerythrin
PHPLC	Preparative High Performance Liquid Chromatography
PI	Propidium iodide
PI3K	Phosphatidylinositol 3-kinase
PS	Phospholipid phosphatidylserine
PTLC	Preparative Thin Layer Chromatography
R*f*	Resolution factor
Rt	Retention time
SDS	Sodium dodecyl sulphate
SEM	Standard mean of error
TGI	Total growth inhibition
TLC	Thin layer chromatography
UKZN	University of Kwa-Zulu Natal
WHO	World Health Organization

SUBMITTED AND ACCEPTED PUBLICATIONS

Naicker, L., Kaschula, C., Steenkamp, P., Matsabisa, M. G., Mohanlall, V. & Odhav, B. 2016. Anticancer compounds from *Ceratotheca triloba*. *International Journal of Pharmacognosy and Phytochemical Research.* Manuscript number: 04122016PPRN.

Naicker, L., Mohanlall, V., & Odhav, B. 2016. Genetic transformation of *Ceratotheca triloba* for the production of anthraquinones from hairy root cultures. *Afr J Tradit Complement Altern Med*, 13, 85-94.

CONFERENCE PRESENTATIONS/WORKSHOPS

Screening of *Ceratotheca triloba* plant extracts for antibacterial and anticancer activity. South African Society of Microbiology (SASM), Limpopo (2013).

NRF and DST Research Conference, Centre for Rural Development, Walter Sisulu University, East London (2012).

International Workshop on Good Laboratory Practice (GLP), World Health Organization, University of Free State, Bloemfontein (2011).

Stakeholder consultation workshop on the amendment of the Bioprospecting, Access and Benefit Sharing Regulations, Medical Research Council, Cape Town (2012).

LIST OF FIGURES

LIST OF TABLES

ABSTRACT

Plants have provided a source of medicine from the beginning of human history and are the core of modern medicine. Moreover, plant based drug discovery has led to the development of various anticancer drugs (such as vincristine, vinblastine, etoposide, paclitaxel, camptothecin, topotecan and irinotecan). The use of botanical, phytochemical, biological and molecular techniques have facilitated the discovery of anthraquinones from *Ceratotheca triloba* that can inhibit the human topoisomerase II enzyme (target for anticancer drugs) and kill cancer cells. However, the *C. triloba* plant has not been extensively studied for its anticancer activity. Therefore, the aim of this study was to further investigate the anticancer activity of *C. triloba* and determine the classes of compounds that contributed towards its activity.

In this study the leaf and root extracts were prepared by using hexane, DCM, hexane: DCM (1:1), methanol and/or water. These extracts were examined for their growth inhibitory potential on three cancer cell lines (A375 [melanoma], MDA-MB-231[breast] and WHCO1 [esophageal]) by using the MTT assay. Then, different mobile phases were prepared for optimizing the separation of the compounds of the active extract by TLC. Column chromatography was performed with the active extract by using five mobile phases (hexane : DCM [60 : 40, 40 : 60], DCM, DCM : ethyl acetate [90 : 10, 70 : 30, 60 : 40, 50 : 50, 50 : 60, 30: 60, 20 : 80], ethyl acetate and ethyl acetate: methanol [80 : 20, 70 : 30, 50 : 50]). The fractions collected from the column were examined for their growth inhibitory potential on two melanoma cell lines (A375 and UACC-62). The IC_{50} and TGI (total growth inhibition) values of the active fractions were determined. Also, the apoptosis inducing effects of the active fractions and standards (camptothecin and doxorubicin) were determined by using flow cytometer based assays (FITC annexin assay, PE active caspase 3 assay and BD MitoScreen assay). Subsequently, the chemical structures of the compounds that contributed towards the activity of these fractions were obtained by EI-LC-MS analysis.

The results demonstrated that the hexane root extract exhibited the best percentage of growth inhibition (%GI) on all three cancer cell lines. The separation of the compounds of the hexane root extract was optimized on TLC plates by using different ratios of hexane and DCM. Column

chromatography allowed for fractionation of this extract. Purified compounds were not obtained due to co-elution. Further research would have to be conducted to obtain purified compounds. This may involve the use of mini-column chromatography and PTLC. Overall a total of ten combined fractions were collected from the column. Four of these fractions (F2, F4, F5 and F8) displayed a high %GI on the A375 and UACC-62 cell lines. Moreover, fraction F4 was the most active fraction as it had the lowest IC_{50} (0.70 $\mu g.ml^{-1}$ [A375] and 0.39 $\mu g.ml^{-1}$ [UACC-62]) and TGI (12.50 $\mu g.ml^{-1}$[A375] and 25 $\mu g.ml^{-1}$ [UACC-62]) values in comparison to the other fractions.

All four fractions induced depolarization of the mitochondria membrane potential ($\Delta\Psi$), caspase 3 activation, early apoptosis (phospholipid phosphatidylserine exposure) and/or late apoptosis in the melanoma cells. The results also revealed that fraction F4 (25 $\mu g.ml^{-1}$) induced depolarization of the $\Delta\Psi$ in a higher percentage of A375 (78.11%) and UACC-62 (87.4%) cells than the other fractions and standards. This fraction also induced caspase 3 activation in a high percentage of A375 (90.56%) and UACC-62 (96.78%) cells. Therefore fraction F4 was also the most active fraction in terms of apoptosis activity. Based on our results and literature findings we can deduce that the active fractions induced the intrinsic or extrinsic (type II) apoptosis pathway in the melanoma cells.

Six classes of compounds were identified from the four active fractions. These were: benzothiophenones, benzopyranones, naphthoquinones, anthraquinones, androstanes and quinazolines.

In conclusion, this is the first study that evaluated the growth inhibition potential of the leaf and root extracts of *C. triloba* on a panel of cancer cells. This research indicated that the hexane root extract displayed the best levels of cell growth inhibition. The active constituents of this extract were isolated into four fractions which elicited apoptosis inducing effects that promoted the extrinsic (type II) or intrinsic apoptosis pathway in the melanoma cells. Furthermore, fraction F4 contained the most active compounds from *C. triloba* as it had the lowest IC_{50} and TGI values (in comparison to the other fractions) and induced depolarization of the $\Delta\Psi$ in the highest percentage of melanoma cells. It was confirmed that six classes of compounds were accountable

for the anticancer activity of these fractions. Thus, the *C. triloba* plant is a rich source of anticancer compounds.

Key words: *Ceratotheca triloba*, cancer, growth inhibition potential, hexane root extract, column chromatography, flow cytometry, apoptosis, anticancer activity.

1. INTRODUCTION AND LITERATURE REVIEW

1.1 Introduction

"Cancer is the name given to a collection of related diseases. In all types of cancer, some of the body's cells begin to divide without stopping and spread into surrounding tissues" (National Cancer Institute, 2015a). Also, cancer cells can be transferred to other parts of the body through the blood and lymph systems. The majority of cancers are named after the organ or type of cells from which they originated. Over 100 types of different cancers can occur (National Cancer Institute, 2015a). Moreover, cancers are grouped into five main categories: i) Carcinoma - cancer that starts in the skin or in the tissue that surrounds internal organs. ii) Sarcoma - cancer that starts in bone, cartilage, fat, muscle, blood vessels or other connective or supportive tissue. iii) Leukemia - a type of cancer that is initiated in blood-forming tissue such as bone marrow. This leads to the formation of abnormal blood cells that get transported into the blood. iv) Lymphoma and myeloma - cancer that starts in the immune system. v) Central nervous system cancers - cancers that starts in the tissues of the brain or spinal cord (Cancer Research UK, 2014a).

The International Agency for Research on Cancer (IARC) and World Health Organization (WHO) highlighted the prevalence of cancer by estimation of the following statistics. "Cancer is a leading cause of disease worldwide" as in 2012 an estimated 14.1 million new cases were documented (Cancer Research UK, 2014b, International Agency for Research on Cancer, 2015). Globally, lung, breast, colon, and stomach cancers were accountable for over 40% of all diagnosed cases. Lung cancer was more prevalent in males (16.7% of cancer cases) while breast cancer was more prevalent in females (25.2% of cancer cases) (Cancer Research UK, 2014b). Moreover, Central and Eastern Europe had the most cancer deaths worldwide (123 cancer deaths per 100 000 deaths) while Southern Africa had the fourth most cancer deaths (113 cancer deaths per 100 000 deaths). The most prevalent cancer deaths in Southern Africa was due to cancer of the lung (13%), cervix (9%), breast (8%) and oesophagus (8%) (Cancer Research UK, 2014c). These statistics have shown that cancer has affected people worldwide as well as locally. This is an indication that new medicines need to be developed for the treatment of cancer to overcome the death rate due to this disease.

1.2 Mechanism of cancer formation

The formation of cancer involves three stages: initiation, promotion and progression. During the initiator stage a carcinogen (ultraviolet radiation, oxidative stress, and genotoxic chemicals) induces a mutation in the DNA of a cell (Kang et al., 2005, Rastogi et al., 2009). The cell then reacts by activating tumour suppressor proteins such as p53. This protein detects the DNA mutation, blocks genes that are responsible for regulation of cell growth and activates the cell's repair mechanism. However, if the DNA is severely damaged, the cell will commit suicide through a cell death process referred to as apoptosis (refer to section 1.3). On the other hand, if one of these two processes does not occur the mutated cell will survive and replicate. Hence the resulting daughter cells (initiator cells) will contain the same damaged DNA (John, 2001).

The promotion stage can occur next. During this stage the initiator cells can accumulate and form a benign, localized mass of cells. These cells can also be eliminated by apoptosis. If the initiator cells are not eliminated, they can undergo selective clonal expansions due to their ability to escape apoptosis and growth inhibitory signals (DiGiovanni, 1992). Also, clonal expansion of the initiator cells increases the possibility of other genetic mutations (Xi, 2003).

The last stage involves progression of the mutated cells into a malignant or cancerous tumour with amplified metastatic and invasive potential (Kang et al., 2005, Lee and Surh, 2005). This phase occurs because of the ability of the cells to adapt to the harsh micro-environmental conditions such as acidosis and hypoxia (Gatenby and Gillies, 2004). Hence, cancer cells can be characterized by having dysfunctional and uncontrolled proliferation through resistance of apoptosis and growth inhibitory signals which in turn causes metastasis and invasiveness to transpire (Jorgen et al., 2011).

1.3 An overview of apoptosis

Apoptosis can be defined as programmed or suicidal cell death whereby activated enzymes are responsible for degradation of the cell's nuclear DNA and cytoplasmic proteins (Bahr and Groner, 2004, Elmore, 2007). As described earlier, apoptosis plays a critical role in eliminating cells with altered genetic integrity in order to prevent the development of cancer. Therefore, the following sections focuses on the morphological characteristics of apoptosis (as well as necrosis), key molecules involved in apoptosis and three extensively studied apoptosis pathways.

1.4 Morphological characteristics of apoptotic and necrotic cells

1.4.1 Apoptotic cells

Cells undergoing apoptosis show distinct morphological changes in their cytoplasm, plasma membrane and nucleus. The onset of apoptosis involves the rounding up and condensing of cells that loose contact with neighbouring cells. This is followed by loss of microvilli and dilation of the endoplasmic reticulum and outer nuclear envelope in the cytoplasm. Vacuoles and vesicles are then formed as a result of swelling of the reticulum cisternae. The vacuoles and vesicles fuse with the plasma membrane giving the cells a sponge appearance. Thereafter, the cytoplasm loses water and becomes shrinked. This subsequently leads to membrane budding or blebbing and the formation of membrane bound spears known as apoptotic bodies. In the nucleus, condensation and margination of the chromatin occurs. This leads to the budding off of many DNA fragments as well as the formation of apoptotic bodies. These are rapidly phagocytosed by neighbouring cells and macrophages. Therefore an inflammatory response of the tissue is inhibited (Figure 1 and 2) (Apraiz et al., 2011, Bowen et al., 1998).

1.4.2 Necrotic cells

Necrosis is another type of cell death that is more passive than apoptosis and occurs as a result of lethal trauma or pathology. During necrosis, cells swell and loose calcium and sodium due to damage of the plasma membrane. This leads to loss of water balance, acidosis and shock. The decrease in pH causes chromatin precipitation and the formation of a pyknotic nucleus. Inside

the mitochondria, distension of both the inner and outer compartments occurs and dense deposits of lipoprotein can be observed. This is followed by swelling and bursting of the endoplasmic reticulum and lysosomes. These organelles contain digestive enzymes that are responsible for further disintegration of the cell. This results in the release of cellular debris which elicits an inflammatory response (Figure 1) (Bowen et al., 1998).

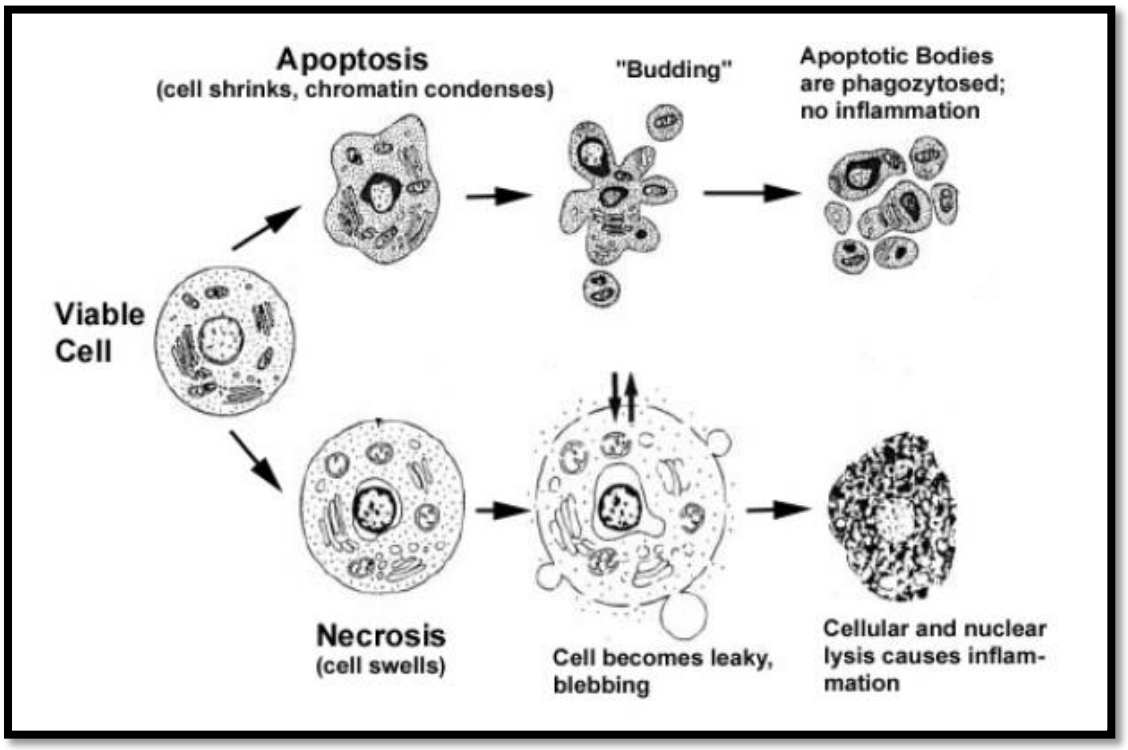

Figure 1: Morphological changes of a cell undergoing apoptosis or necrosis (Van Cruchten and Van Den Broeck, 2002).

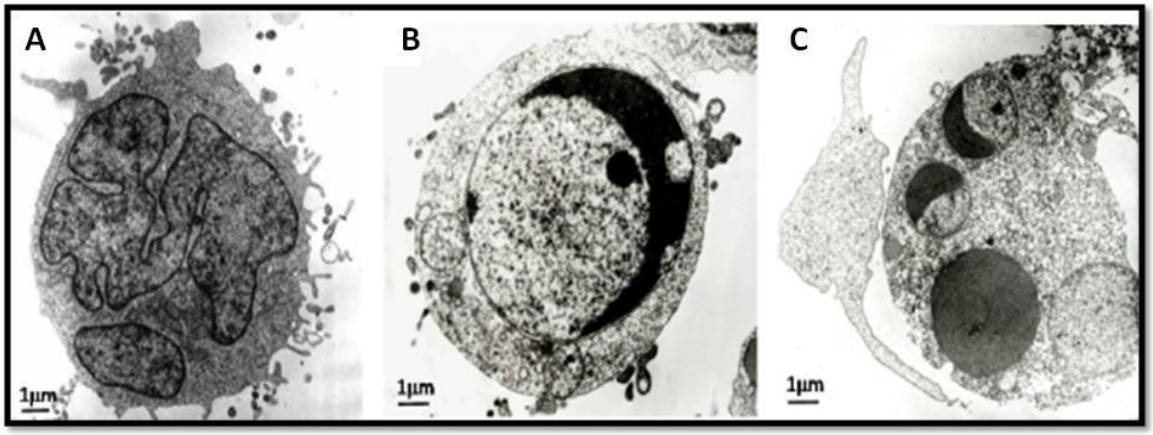

Figure 2: Electron micrographs of human T-cell acute lymphoblastic leukemia (CCRF-CEM) cells (5000x). Untreated cells had large nuclei and lacked visible vacuoles (A). Drug treated cells underwent apoptosis and had visible vacuoles, condensed chromatin (B) and micronuclei (C) (Apraiz et al., 2011).

1.5 Key molecules involved in apoptosis signalling pathways

The initiation, mediation, execution and regulation of the apoptosis signalling pathways are orchestrated by molecular machinery that determines the fate of a cell. Therefore this section provides an overview of the key molecules that are involved in these processes.

1.5.1 Caspases

Caspases are involved in apoptosis. These enzymes are a family of proteases which derives its name from the fact that they are cysteine-dependent aspartate-specific proteases. Their catalytic activity is dependent on a cysteine residue that is highly conserved within an active pentapeptide site (QACRG) (Denault and Salvesen, 2002). The caspases are synthesized as inactive zymogens known as procaspases which consist of an N- terminal domain (a signal peptide with a cleavage site for activation of procaspases), a p20 large subunit and a p10 small subunit (Li and Yuan, 2008, Molloy and Thomas, 2002) (Figure 3 and 4). The procaspases are processed by autoproteolysis (rupturing of a peptide bond in a protein due to an intra-molecular reaction) of the prodomains and small and large subunits. These reactions lead to the linking of two large subunits with two small subunits (from two procaspase molecules) and the subsequent formation of an active tetrameric caspase enzyme (Figure 3) (Blair and Semler, 1991, Boatright and

Salvesen, 2003, Nicholson, 1999, Paulus, 2000, Perler et al., 1997, Rastogi et al., 2009, Yan and Shi, 2005).

There are 14 mammalian caspases (caspase 1 to 14) that have been identified. These enzymes have been categorized into three functional groups. The first group consists of the initiator caspases. They contain domains known as death domains (DD's) which exists as the caspase activation and recruitment domain (CARD) (present in caspases 1, 2, 4, 5, 9, 11 and 12) or the death effector domain (DED) (present in caspases 8 and 10) (Figure 4). These death domains direct the activation of procaspases when they interact with other molecules. The second group consists of the effector caspases (includes caspase 3, 6 and 7) (Figure 4). These caspases are activated by initiator caspases and they carry out the downstream execution steps of apoptosis by cleaving multiple cellular substrates. The third group consists of the inflammatory caspases (includes caspase 1, 4, 5, 11, 12 and 13; some of the initiator caspases also function as inflammatory caspases). They are involved in cytokine activation (Cohen, 1997, Elmore, 2007, Li and Yuan, 2008, Martinon and Tschopp, 2007, Pop and Salvesen, 2009, Rai et al., 2005). In addition, caspase 14 is a unique member of the caspase family as it is involved in the formation of the skin barrier (Denecker et al., 2008).

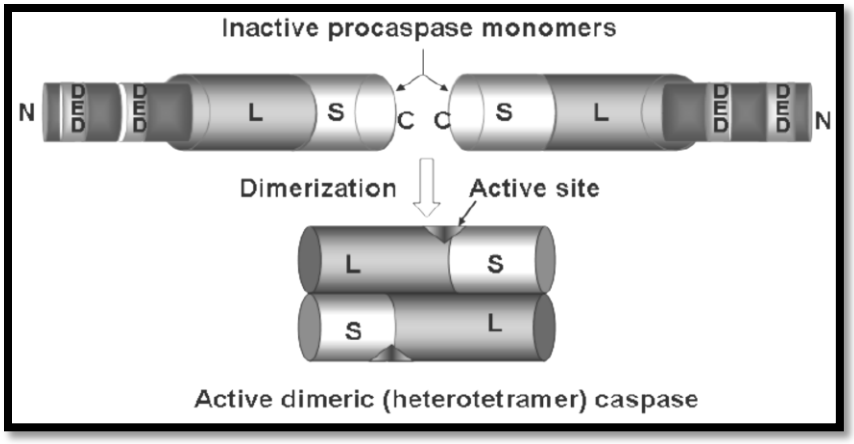

Figure 3: A diagrammatic representation of the activation of procaspase 8 molecules which exists as inactive zymogen monomers. These are processed by autoproteolysis of the prodomain and small and large subunits. These reactions lead to the linking of two large subunits with two small subunits (from two procaspase molecules) and the subsequent formation of a tetrameric caspase enzyme with two active sites. L refers to large subunit and S refers to small subunit (Rastogi et al., 2009).

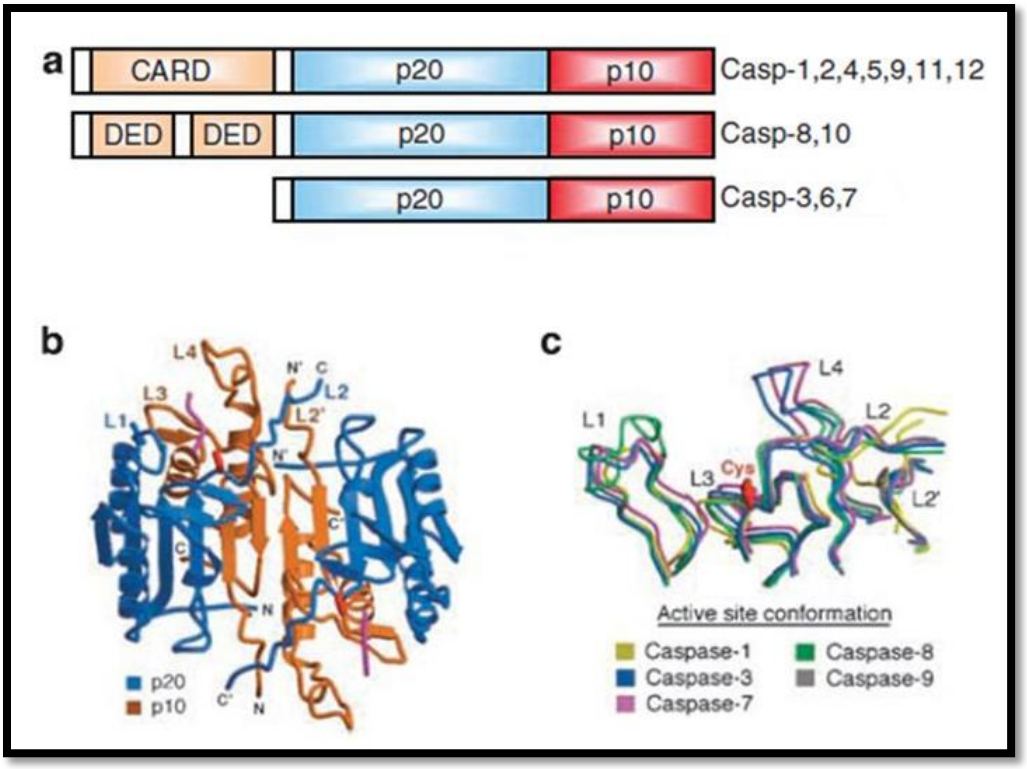

Figure 4: The structural and prodomain organization of caspases. The caspases consist of a p20 large subunit and a p10 small subunit. The initiator caspases contain prodomains which exist as the CARD (present in caspases 1, 2, 4, 5, 9, 11 and 12) or DED (present in caspases 8 and 10). The effector caspases (includes caspase 3, 6 and 7) do not have prodomains (a). A ribbon representation of caspase 3 (b). The active site (Cys) conformation of caspases 1, 3, 7, 8 and 9 (c) (Li and Yuan, 2008, Shi, 2002).

1.5.2 B Cell Lymphoma-2 (Bcl-2) family of proteins

Amongst the molecules that are involved in apoptosis are the Bcl-2 family of proteins. The Bcl-2 protein was the first protein to be identified in this family. It derives its name from the fact that it was the second member of a group of proteins to be discovered in human B-cell lymphomas with the t (14; 18) chromosomal translocation (Gross et al., 1999, Tsujimoto et al., 1984). The Blc-2 family of proteins is divided into two groups (Figure 5). The first group consists of the anti-apoptotic proteins which contain all four Bcl-2 Homology (BH) domains (BH1, BH2, BH3 and BH4). They protect the cell from apoptotic stimuli. The second group consists of the pro-apoptotic proteins which contain multi-domains or the BH3 domain only. They initiate apoptosis

when cellular stresses such as DNA damage, growth factor deprivation and endoplasmic reticulum stress occurs (Dewson and Kluc, 2010, Kuwana and Newmeyer, 2003, Yip and Reed, 2008).

A disruption in the balance of anti-apoptotic and pro-apoptotic proteins of the Bcl-2 family can cause dysregulation of apoptosis in affected cells. This can occur as a result of overexpression of an anti-apoptotic protein or impaired expression of a pro-apoptotic protein or a combination of both (Wong, 2011). For instance, the overexpression of Bcl-2 prevented prostate cancer, neuroblastoma, glioblastoma and breast cancer cells from undergoing apoptosis (Fulda et al., 2000, Raffo et al., 1995). On the other hand, the impaired expression of Bax (mutated) resulted in the resistance of colorectal cancer cells to anticancer drugs (Miquel et al., 2005). In chronic lymphocytic leukemia (CLL) cells, Bcl-2 was expressed at high levels while Bax was expressed at low levels (Goolsby et al., 2005). This condition reduced the chances of apoptosis from occurring.

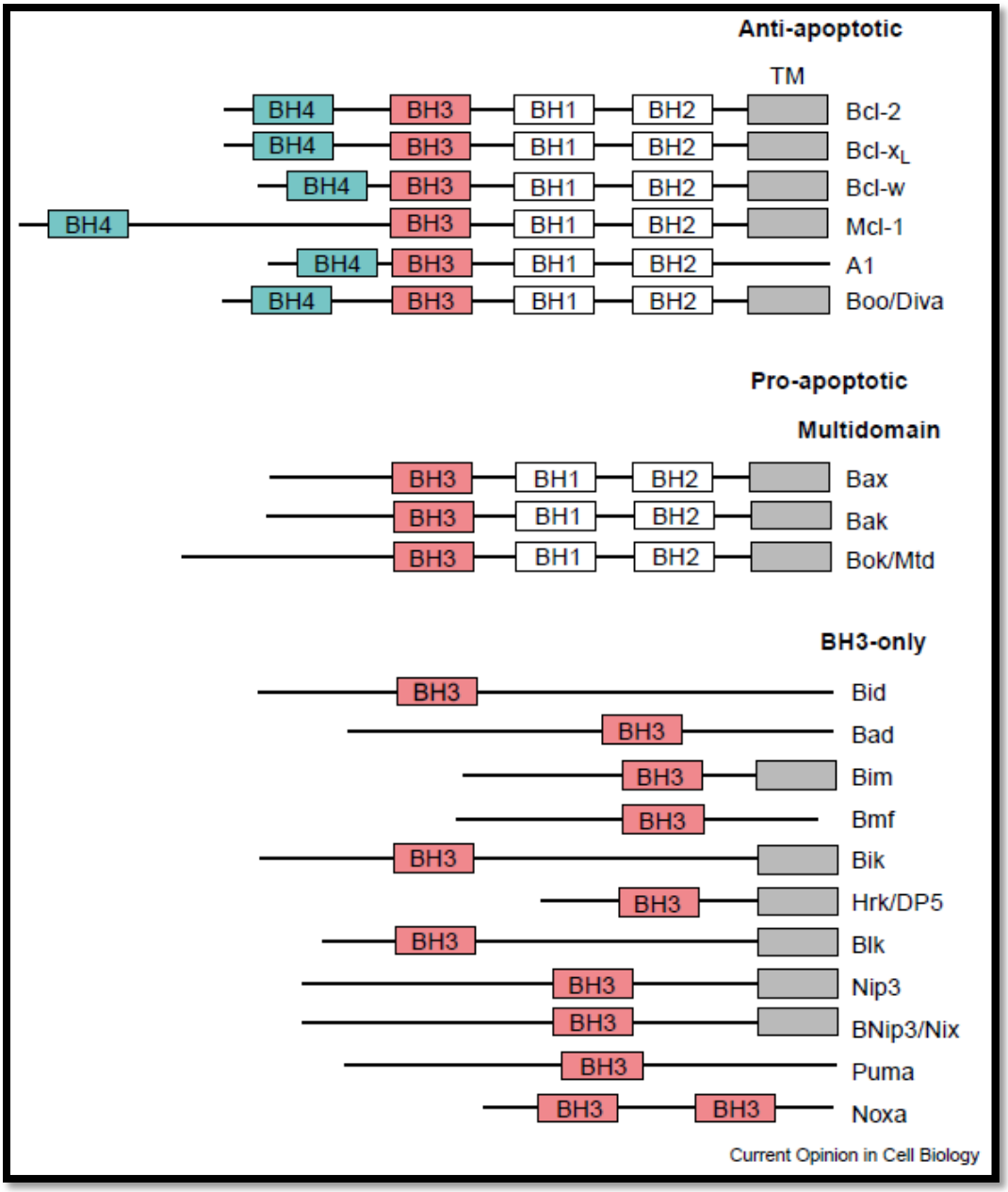

Figure 5: The Blc-2 family of proteins is divided into two groups. The first group consists of the anti-apoptotic proteins which contain all four BH domains (BH1, BH2, BH3 and BH4). The second group consists of the pro-apoptotic proteins which contain multi-domains or the BH3 domain only. TM refers to the transmembrane domain which is responsible for anchoring the protein onto the mitochondrial membrane (Kuwana and Newmeyer, 2003).

1.5.3 Inhibitor of apoptosis proteins (IAPs)

The IAPs are important regulators of apoptosis pathways. So far eight IAPs have been identified, these are: NAIP (BIRC1), c-IAP1(BIRC2), c-IAP2 (BIRC3), X-linked IAP (XIAP, BIRC4), Survivin (BIRC5), Apollon (BRUCE, BIRC6), Livin/MLIAP (BIRC7) and IAP-like protein 2 (BIRC8) (Vucic and Fairbrother, 2007). IAPs can inhibit apoptosis by: binding onto the active sites of caspases, promoting the degradation of activated caspases or blocking caspases from their substrates (Wei et al., 2008). The effect of IAPs on cancers has been studied. The expression of cIAP-2 caused pancreatic cancer cells to become resistant to chemotherapy (Lopes et al., 2007). Also, the up-regulation of Apollon caused gliomas to become resistant to cisplatin and camptothecin (Chen et al., 1999).

1.6 The most extensively studied apoptosis pathways

This section focuses on the various apoptosis pathways which are facilitated by a series of signal molecules (receptors, enzymes and gene regulating proteins) that act together to passively destroy a cell. The three most extensively studied apoptosis pathways are the intrinsic and extrinsic pathways (type I and II). A detailed account of these pathways is presented below.

1.6.1 The intrinsic apoptosis pathway

The intrinsic apoptosis pathway occurs through the mitochondria and therefore it is also known as the mitochondrial apoptosis pathway (Figure 6) (Igney and Krammer, 2002). It is triggered as a result of DNA damage (caused by factors such as carcinogenic chemicals or irradiation) which activates the synthesis of p53. This protein induces the production of pro-apoptotic proteins: Bad Bid, Bim and Bax (Igney and Krammer, 2002, Voet and Voet, 1995). Bad migrates to the mitochondria and inhibits the anti-apoptotic proteins Bcl-2 and Bcl- X_L (Letai, 2011). Bid and Bim induces permeabilization of the outer mitochondrial membrane. Then, Bax inserts itself into the outer mitochondrial membrane and stimulates the release of cytochrome c and SMAC/Diablo (second mitochondria-derived activator of caspase/direct IAP binding protein with low pI) into the cytosol (Crow et al., 2004, Kim et al., 2006). Thereafter apoptotic protease-activating factor 1 (APAF1) molecules link up to cytochrome c (in a dATP dependant manner) and procaspase 9

molecules (through their CARD). This results in the formation of an apoptosome (a wheel like structure that has a seven fold symmetry) (Figure 7). Then, procaspase 9 is activated to caspase 9 (by autoproteolysis) which in turn activates executioner procaspases 3, 6 and 7 to caspases 3, 6 and 9 (Acehan et al., 2002, Igney and Krammer, 2002, Slee et al., 1999). Subsequently, these caspases cleave specific death substrates. Caspase 9 mediates the cleavage of nuclear poly-(ADP-ribose) polymerase (PARP) which is an enzyme that aids in the repair of DNA breaks. Caspases 3, 6 and 7 attacks nuclear ribonucleoproteins. Caspase 3 cleaves DNA dependent protein kinase (repairs double-stranded DNA). It also cleaves fodrin (a membrane-associated cytoskeletal protein that maintains normal membrane structure and supports the function of cell surface proteins) which results in blebbing of the cell. Caspase 6 cleaves nuclear lamins and permits the packaging of condensed chromatin into apoptotic bodies (Bennett and Gilligan, 1993, Bowen et al., 1998, Weterings et al., 2003). These actions result in the impairment of the cell's DNA system and consequential cell death.

Anti-apoptotic proteins can inhibit the intrinsic apoptosis pathway. For example, growth factors and cytokines activate phosphatidylinositol 3-kinase (PI3K) which stimulates AKT (Protein Kinase B) to phosphorylate and inactivate the pro-apoptotic protein BAD (Figure 6). On the other hand, pro-apoptotic proteins allow for the survival and regulation of the apoptotic signal. For example pro-apoptotic protein, SMAC/DIABLO interacts with anti-apoptotic proteins such as Bcl-2, Bcl- X_L and IAPs to prevent them from attenuating apoptosis (Figure 6) (Igney and Krammer, 2002).

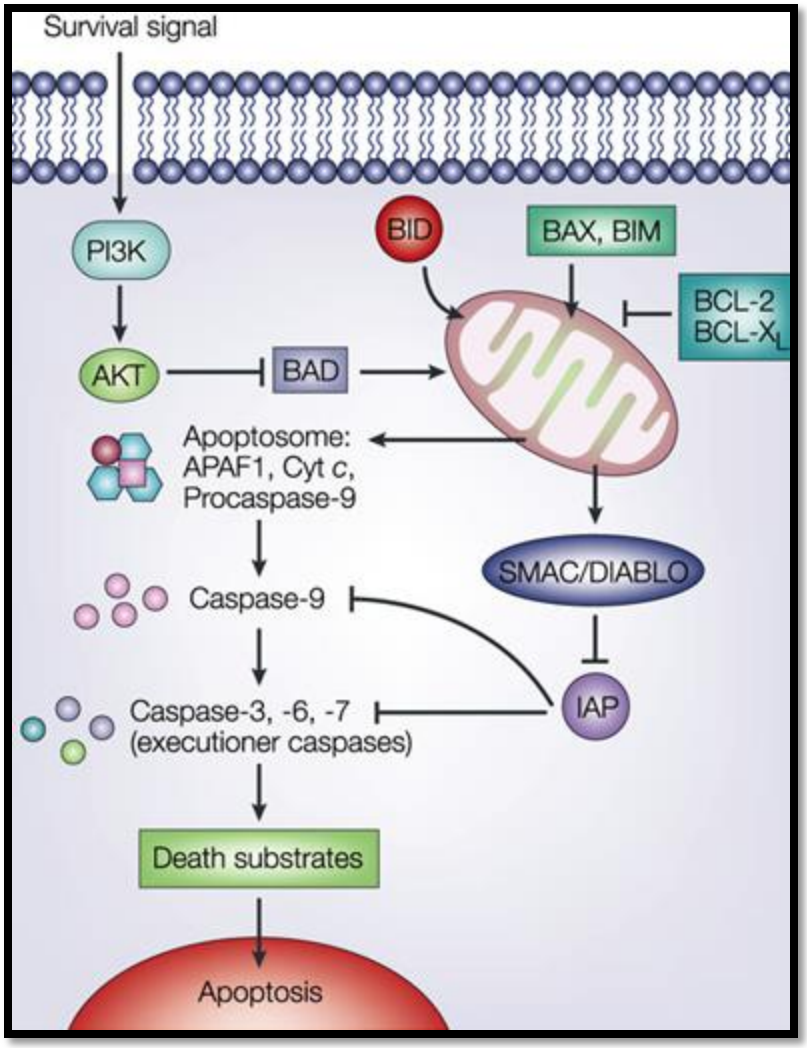

Figure 6: The intrinsic apoptosis pathway (Igney and Krammer, 2002).

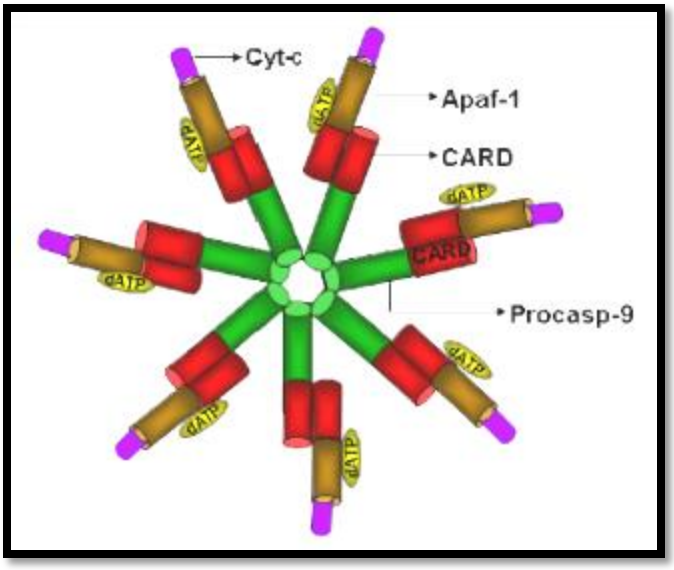

Figure 7: A diagrammatic representation of an apoptosome. This is a wheel-like structure that forms when APAF1 molecules link up to cytochrome c (in a dATP dependant manner) and procaspase 9 molecules (through their CARD). Cyt-c refers to cytochrome c and Procasp-9 refers to procaspase 9 (Rastogi et al., 2009).

1.6.2 The extrinsic apoptosis pathway - type I

The extrinsic apoptosis pathway can occur via the type I or type II pathway. The type I pathway is also known as the death-receptor-mediated apoptosis pathway as it involves the activation of the death receptors (Figure 8) (Igney and Krammer, 2002). These are cell surface receptors that belong to the tumor necrosis factor receptor (TNFR) family. Members of this family contain cysteine-rich extra-cellular sub-domains (death domains) which allow them to bind to their ligands for transmission of apoptotic signals (Fulda and Debatin, 2006). For example, in the type I pathway the death receptor C95 is activated when it binds to its ligand, C95L. This leads to the death domain (DD) of C95 to bind to the DD of the cytosolic adaptor molecule, Fas associated death domain (FADD) protein. These interactions result in the formation of the death inducing signalling complex (DISC). Thereafter, the death effector domain (DED) of FADD binds to the DED of procaspase 8 and 10 which are activated to caspase 8 and 10 by autoproteolysis. They are released from the DISC into the cytoplasm to activate the effector procaspases 3, 6 and 7 to caspases 3, 6 and 7 (Bodmer et al., 2000, Igney and Krammer, 2002). These caspases cleave

specific death substrates (as mentioned for the intrinsic apoptosis pathway) (Bowen et al., 1998). Consequently, the cell becomes impaired and dies through apoptosis.

The extrinsic apoptosis pathway – type I can be inhibited by several anti-apoptotic proteins. Soluble decoy receptors such as soluble C95 (sCD95) can prevent the ligand CD95L from binding to its receptor CD95. FLICE (FADD-like interleukin-1 beta-converting enzyme) inhibitory proteins (FLIPs) can inhibit the activation of procaspase 8 and 10 by binding to the DISC. Also, IAPs can inhibit caspases by binding to them (Figure 8) (Igney and Krammer, 2002).

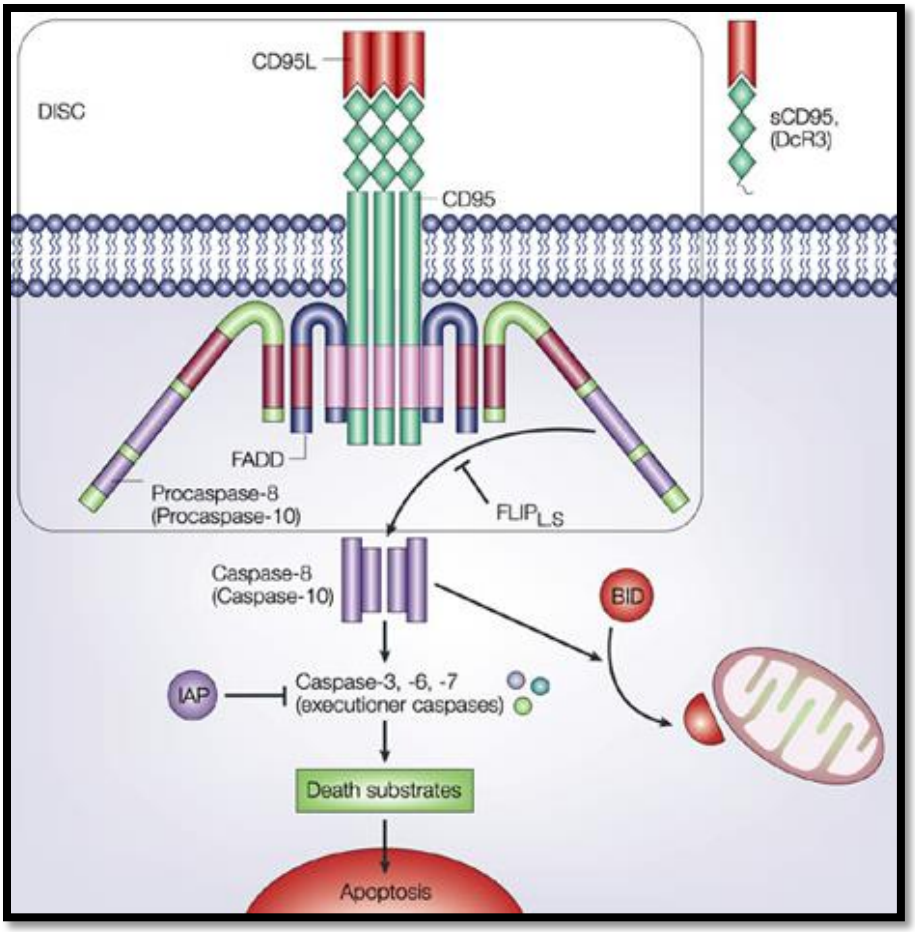

Figure 8: The extrinsic apoptosis pathway – type I. $FLIP_{LS}$ refers to long and short forms of the FLICE (FADD-like interleukin-1 beta-converting enzyme) inhibitory protein, respectively (Igney and Krammer, 2002).

1.6.3 The extrinsic apoptosis pathway - type II

The extrinsic apoptosis pathway - type II is also known as the mitochondrial-dependent caspase activation pathway because it involves the linking of a weak caspase signal to the mitochondria signal molecules (Kuo et al., 2009, Pope, 2002) (Figure 9). This pathway is initiated by the formation of the DISC which in turn releases active caspase 8. Subsequently, this enzyme cleaves BID to form truncated BID (tBID) which translocates to the mitochondria and activates Bak and Bax (Luo et al., 1998, Pope, 2002). Inside the mitochondria, Ca^{2+} is produced and it reaches a critical threshold. Then, a permeable transition pore is formed across the inner membrane. Bak and Bax regulates the opening of this pore to facilitate the release of cytochrome

c, apoptosis inducing factor (AIF) and SMAC/Diablo into the cytosol (Belizario et al., 2007, Bonora and Pinton, 2014, Brenner et al., 2000, Du et al., 2000, Jeong and Seol, 2008, Liu et al., 1996b, Narita et al., 1998, Susin et al., 1999). APAF1 molecules then link up to cytochrome c (in a dATP dependant manner) and procaspase 9 molecules (through their CARD). As a result an apoptosome is formed. Thereafter, procaspase 9 is activated to caspase 9 by autoproteolysis. This enzyme in turn activates procaspase 3 to caspase 3 (Acehan et al., 2002, Slee et al., 1999). Then, caspase 3 cleaves inhibitor caspase-activated deoxyribonuclease (ICAD) to form caspase-activated deoxyribonuclease (CAD) which fragments DNA into approximately 200 base pair fragments. Hence, the cell's DNA repair mechanism becomes impaired and cell death occurs (Sakahira et al., 1998, Zhao et al., 2001).

The extrinsic apoptosis pathway – type II can be inhibited by several anti-apoptotic proteins. Bcl-2 and Bcl-X_L can block the action of Bak and Bax on the mitochondria by sequestering the BH3-only proteins (Cheng et al., 2001). Also, MCL1 (Myeloid cell leukemia 1) can bind to Bak and neutralize it (Figure 9) (Zhai et al., 2008).

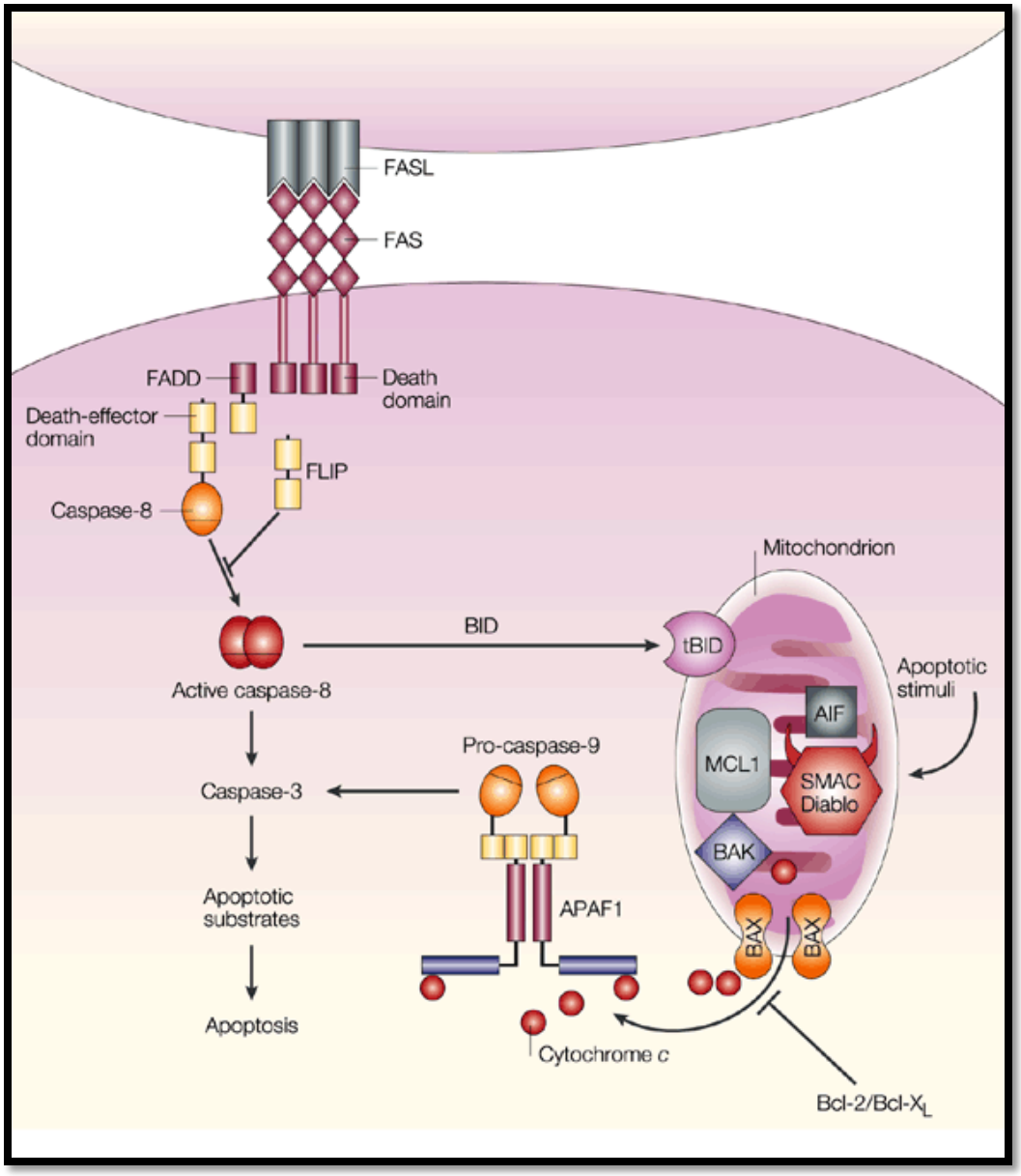

Figure 9: The extrinsic apoptosis pathway – type II (Pope, 2002).

1.7 How do anticancer drugs induce apoptosis?

Anticancer drugs are classified according to their mechanism of action. There are four main classes of anticancer drugs: antimetabolites, genotoxic agents, anti-mitotic agents and targeted therapies (Druker and David, 2003, Gascoigne and Taylor, 2009, Kaye, 1998, Smith et al., 1997, Swift and Golsteyn, 2014) (Table 1). Through their mechanism of action, anticancer drugs can initiate apoptosis by switching on the expression of signal molecules such as Fas and FasL (for initiation of the extrinsic pathway type I and II) or p53 (for initiation of the intrinsic pathway) (Igney and Krammer, 2002, Micheau et al., 1999, Pope, 2002, Wang and Sun, 2010). For instance, emodin induces topoisomerase II inhibition which causes DNA damage that activates the expression of FasL for initiation of the extrinsic pathway type I (Li et al., 2010, Mo and Beck, 1999, Yaoxian et al., 2013). On the other hand, 6-Mercaptopurine incorporates itself into DNA and subsequently activates the expression of p53 for initiation of the intrinsic pathway (Kanemitsu et al., 2009, Payne and Miles, 2008). Thus, anticancer drugs work in a very intricate manner to facilitate the death of cancer cells.

Table 1: Classes and mechanisms of anticancer drugs.

Class	Mechanism of action	Example of a drug	Reference
Antimetabolites	Interferes with the function of metabolites that are involved in normal metabolism.	*Gemcitabine*- Pancreatic cancer *Methotrexate*- Acute lymphoblastic leukemia *6-Mercaptopurine*- Acute lymphoblastic leukaemia	(Adam de Beaumais et al., 2011, Kaye, 1998, Kotopoulis et al., 2013, Mantadakis et al., 2005, Smith et al., 1997)
Genotoxic agents	Causes DNA damage by reacting with DNA or by targeting enzymes that are essential for DNA replication (for example, topoisomerases).	*Cisplatin*- Sarcomas *Epirubicin*- Breast and ovarian cancer *Doxorubicin*-Breast cancer	(Champoux, 2001,Coukell and Faulds, 1997, Florea and Büsselberg, 2011, Smith et al., 2006,Swift and Golsteyn, 2014, Vermorken et al., 1999)
Anti-mitotic agents	Disturbs the mitotic progression of cells by interfering with their microtubules (organelles that are responsible for controlling cell division by mitosis).	*Paclitaxel*- Ovarian, breast, lung and other cancers	(Gascoigne and Taylor, 2009, Kintzios and Barberaki, 2004, Milross et al., 1996)
Targeted therapies	Inhibits biochemical pathways and mutant proteins that are essential for tumor growth and survival.	*Imatinib*- Chronic myeloid leukemia and certain acute lymphoblastic leukemias *Gefitinib*- Non-small cell lung cancer *Bortezomib*- Multiple myeloma and mantle cell non-Hodgkin's lymphoma	(Cross and Lyseng-Williamson, 2007, Druker and David, 2003, Giaccone, 2004, Piperdi et al., 2011, Smith, 2011)

1.8 Treatment of cancer

The treatment of cancer can involve surgical intervention, radiation, chemotherapy, targeted therapy and/or other therapies (National Cancer Institute, 2015b). The objective of any cancer treatment is to remove all cancerous tissue without harming normal tissues. Severe cases of cancer are treated by surgery which allows for the removal of cancerous tissue with less damage to healthy tissues but surgery can also have certain risks (such as bleeding, drug reactions and damage to nearby tissues or organs) and side effects (such as pain and infection) (American Cancer Association, 2014, Erhabor and Adias, 2011). In less severe cases of cancer, radiation or chemotherapy can be used to remove the cancerous tissue but these treatments are limited due to the toxicity imposed on healthy tissues (Brannon-Peppas and Blanchette, 2004, Phillips and Fu, 1976). The side effects of radiation therapy depend on the part of the body that is exposed to the treatment. The following side effects may be experienced: diarrhea, hair loss, fatigue, mouth and throat changes, nausea, vomiting, sexual changes, fertility changes, skin changes and urinary changes (National Cancer Institute, 2014a). The side effects of chemotherapeutic drugs may include: anemia, appetite changes, bleeding problems, constipation, diarrhea, fatigue, hair loss, infection, memory changes, mouth changes, throat changes, nausea, vomiting, nerve changes, pain, sexual changes, fertility changes, skin changes, nail changes, swelling and urination changes (National Cancer Institute, 2014b). In addition, a major complication that can occur while chemotherapy is administered is multi-drug resistance (MDR). This occurs as a result of: i) the up-regulation of membrane proteins which pump the drugs out of the cell to decrease the intracellular drug concentration, ii) the interruption of the balance between bioactivation and detoxification pathways, iii) alterations in DNA repair response and iv) alterations in apoptosis response. Thus, MDR can hinder the success of treating cancers by chemotherapy (Kumar and Clark, 1990, Riddick et al., 2005).

On the other hand, some cancers are treated with targeted therapy. This involves the use monoclonal antibody drugs which target and disrupt molecular pathways that are responsible for promoting tumorigenesis (Majidi et al., 2009). However, some of these drugs are associated with serious side effects. For example, trastuzumab causes cardio-toxicity in women with metastatic breast cancer (Force et al., 2007, Guglin et al., 2008). Cetuximab and panitumumab are used for the treatment of refractory metastatic colorectal cancer but these drugs cause skin rash on the

face and upper torso (Jean and Shah, 2008, Perez-Soler and Saltz, 2005). Rituximab is used to treat non-Hodgkin's lymphoma but it is associated with serious infections such as the John Cunningham virus which infects the central nervous system (Aksoy et al., 2007, Carson et al., 2009, Hansel et al., 2010, Major, 2010). Hence due to the side effects caused by the current cancer treatments, there is a need to discover and develop new drugs to effectively and safely treat cancer.

1.9 Plant as a source of medicine

Thousands of years ago, ancient civilizations in many countries such as China, India and Thailand used plants for medicinal purposes (Chang and But, 1986, Kapoor, 1990, Subchareon, 1998). The traditional use of plants has continued into modern times as the World Health Organization (WHO) estimated that 80% of people living in developing countries depend on traditional medicine (mostly herbal medicines) to fulfil their primary health care needs (Chaudhary et al., 2010). Moreover, herbal medicines are highly valuable in the international market place. In Western Europe, herbal medicine revenue amounted to US$ 5 billion in 2003-2004. In China, sales of herbal medicine products reached US$ 14 billion in 2005. In Brazil, herbal medicine revenue reached US$ 160 million in 2007 (Chaudhary et al., 2010). Locally, over 70 plant species are used in Africa to treat both veterinary and human patients (Stark et al., 2013). In addition South Africa has a long history of using plants in traditional healing as it hosts a variety of around 30,000 flowering species (Louw et al., 2002). This accounts for almost 10 % of the world's higher plant species (Van wyk and Gericke, 2000b). Thus, plants have been an integral component of the health care system both locally and internationally.

1.10 Why plants are used in the treatment of cancer?

There are several advantages of using plants to treat cancer. The complex synergistic interaction of various compounds in plants allows for the designing of herbal formulations that attack cancerous cells without harming normal cells of the body. This is possible as some plants can protect the body against cancer by enhancement of its detoxification functions. Certain plants contain biological response modifiers that can prevent the growth of cancer by modulating the activity of specific hormones and enzymes. Some plants have good immunomodulatory and

antioxidant properties which can promote anticancer activity (Larkin, 1983, Saxe, 1987). Moreover, a survey documented that over 60% of cancer patients depend on the use of vitamins or herbs as therapy (Madhuri and Pandey, 2008, Sivalokanathan et al., 2005). Therefore medicinal plants play an important role in the treatment of cancer.

1.11 Discovery of anticancer compounds from plants

Although traditional practices involve the use of complex plant extracts, scientists have focused on purifying and identifying independently active compounds (IACs) from plant extracts. The advantage is that once the structures of the IACs are determined they can be chemically or semi-chemically synthesized. The disadvantage is that some compounds found in plants act in a synergistic manner with other compounds to bring about biological activity.

Plants produce two distinct groups of compounds. The first group consists of the primary metabolites which includes sugars (constituents of structural and nutritional elements), amino acids (constituents of structural elements and enzymes), lipids (constituents of membranes and nutritional elements) and nucleotides (constituents of genes). These metabolites are needed for growth of the plant (Payne et al., 1991). The second group consists of the secondary metabolites which includes five types of compounds: polyketides, isoprenoids (terpenoids), alkaloids, phenylpropanoids and flavonoids (polyphenols) (Verpoorte, 2000). They are responsible for metabolic and/or growth regulation, lignification, colouring of plant parts and protecting the plant against pathogen attack. Secondary metabolites are important constituents as they possess pharmaceutical properties (Kintzios and Barberaki, 2004, Payne et al., 1991). Thus these compounds are responsible for any possible anticancer activity.

Scientists have discovered many anticancer compounds from plants. A classic example is the discovery of a diterpene known as taxol which was isolated from the Pacific yew tree, *Taxus baccata* (Kintzios and Barberaki, 2004). This research began in 1958 when the National Cancer Institute (NCI) (United States of America) screened 35, 000 plants for anticancer activity. Fortunately, a breakthrough was made in 1963 when Drs M. Wall and M.C. Wani of the Research Triangle Institute (North Carolina) found that the extract from the bark of *T. baccata* exhibited anticancer activity (Cragg, 1998). Twenty years later human clinical studies began and

taxol was shown to be active against ovarian cancer which was incurable during the 80's. In order to further develop taxol, the NCI issued a contract to Bristol Myers- Squibb in the United States (Rowinsky et al., 1990). Nowadays taxol is semi-chemically synthesized as paclitaxel by using the needles and twigs from yew species which are cultivated under agricultural conditions. This drug has been approved by the Food and Drug Administration (FDA) for treating ovarian, breast, lung and other types of cancers. It is sold under the trade name Taxol (Kintzios and Barberaki, 2004). Table 2 shows other plant-derived anticancer compounds that have been commercialized.

Table 2: Plant-derived anticancer compounds that have been commercialized.

Plant	Family	Location	Traditional use/s	Parts used	Commercial products	References
Camptotheca acuminata **(Camptotheca)**	Nyssaceae	Asia, Southern China and Tibet.	Used to treat stomach and liver cancer as well as leukemia.	Bark, wood and young leaves.	Three semi-synthetic drugs have been derived from camptothecin. These have been approved by the FDA: 1) Topotecan is used to treat advanced ovarian cancer. It is marketed under the trade name Hycamtin. 2) Irinotecan HCI is used to treat metastatic cancer of the colon or rectum. This drug was approved in June 1996. It is sold under the trade name Camptosar. 3) 9-nitro camptothecin is used to treat pancreatic cancer. It is sold under the trade name Rubitecan.	(Kintzios and Barberaki, 2004)
Podophyllum peltatum **(Mandrake American)**	Berberidaceae	Canada and North America.	North American Indians used the plant as an emetic and vermifuge.	Root and resin.	Etoposide is one of the most active drugs for the treatment of small cell lung cancer and testicular carcinoma. It is also active against esophageal, gastric, prostatic, ovarian and non-small cell lung cancer as well as chronic and acute leukemias. Etoposide is used as etoposide phosphate. It is sold under the trade name Etopophos.	(Schacter, 1996, Kintzios and Barberaki, 2004)

Table 2 (continued): Plant-derived anticancer compounds that have been commercialized.

Plant	Family	Location	Traditional use/s	Parts used	Commercial products	References
***Vinca rosea* Linn. (Periwinkle)**	Apocynaceae	East Indies, Madagascar and America.	Used to treat skin disorders, cramps, diabetes, high blood pressure, asthma, constipation and menstrual problems.	Leaves, stems and flower buds.	Two Vinca alkaloids are used in the treatment of cancer: 1) Vincristine is used to treat childhood's leukemia, Hodgkin's disease and other lymphomas. 2) Vinblastine is used to treat testicular cancer, breast cancer, Kaposi's sarcoma, Hodgkin's disease and other lymphomas.	(Canellos, 1992, Kintzios and Barberaki, 2004, Samuelsson, 1992)
***Taxus baccata* (Yew)**	Taxaceae and Coniferae	Europe, North Africa and Western Asia.	Played a role in religious practices as temples were built around Yew trees to serve as places of worship.	Stem segments, needles (1–2 cm long) and roots.	Taxol is semi-chemically synthesized as paclitaxel. This drug is used to treat ovarian, breast, lung and other cancers. It is sold under the trade name Taxol.	(Kintzios and Barberaki, 2004)

1.12 Local anticancer plants

South Africa has a variety of anticancer plants. Examples are presented in Table 3.

Table 3: South African plants that have shown to exhibit anticancer activity.

Plant	Traditional uses	Active compound/ extract	Cancer line/s	References
Sutherlandia frutescens (cancer bush or kankerbos)	Wounds, fevers, chicken pox, stomach problems, eye troubles and cancer.	L-canavanine	MIA PaCa-2 (Pancreatic cancer).	(Crooks and Rosenthal, 1996, Swaffar et al., 1994, Thomson, 2002, Van Wyk, 1997, Xaba and Notten, 2003)
Aloe ferox (Cape aloe or bitter aloe)	Skin and hair treatments, constipation, hypertension, stress, arthritis, conjunctivitis, toothaches, sinusitis and stomach pains.	Aloe-emodin	SJ-N-KP (Neuroblastoma), Hep G2 and Hep 3B (liver cancer cell lines).	(Crouch et al., 2006, Kuo et al., 2002, Pecere et al., 2000, Pujol, 1990, Street and Prinsloo, 2013, Watt and Breyer-Brandwijk, 1962)
Withania somnifera	Wounds, abscesses, inflammation, haemorrhoids, rheumatism and syphilis.	Withaferin A	MCF-7 and MDA-MB-231 (breast cancer cell lines).	(Jayaprakasam et al., 2003, Stan et al., 2008, Welman, 2011)
Tulbaghia violacea (Wild garlic)	Oesophageal cancer.	Methyl-α-D-glucopyranoside	MCF7 and HeLa (cervical cancer).	(Bungu et al., 2006, Lyantagaye, 2013, Van Wyk and Gericke, 2000a, Van Wyk, 1997)
Prunus africana	Benign prostatic hyperplasia.	Ethanolic bark extract	PC3 and LNCaP (Prostate cancer cell lines).	(Edgar et al., 2007, Shenouda et al., 2007, Vinceti et al., 2013)

1.13 *Ceratotheca triloba*

1.13.1 Taxonomy of *C. triloba*

C. triloba is a South African annual plant that is found in the summer rainfall areas of South Africa, mainly the grasslands. The plant is commonly called South African Foxglove, Wild foxglove, Vingerhoedblom, Ludvonca (Swazi), Udonqa (Swazi, Zulu), Undoncalwabathwa or Udonqabathwa (Zulu). There are only four known species of Ceratotheca that are found in Southern Africa (Smithies, 2000). The genus name 'Ceratotheca' means a horned capsule which is derived from the Greek words *kerato* (horned) and *theke* (a case). The species name *triloba* is derived from Latin, meaning three-lobed, alluding to leaves (Hutchings, 1996). The plant was first named *Sporledera triloba* Bernh. in 1842 and has undergone several name changes since then (Table 4). According to the current classification system it belongs to the family Pedaliaceae (Table 5) (Wunderlin and Hansen, 2002). This family of plants is characterized by having mucilaginous hairs which give the stems and leaves a slimy or clammy feel. The fruits have hooks or horns. *C. triloba* germinates optimally in disturbed areas like roadsides, where they grow, flower and seed before winter. The height of the plant depends on the water uptake during summer. The leaves are soft, green and about 50 mm long; they are divided into three lobes with a bluntly serrated margin. The plant has pink flowers with red stems or white flowers with yellow-green stems (Figure 10A). The flowers are 50 mm long with 5 lobes. The bottom lobe is longer than the others and has streaks of delicate lines running down the throat of the flower. The small seeds are black and are located in 30 mm long fruits which have very sharp horns at the tips (Figure 10B). The green fruits turn brown and dry and split open to release the flat pear shaped seeds. The stems and leaves of the plant are covered with fine white hairs. *C. triloba* is slightly sticky and when crushed it produces a strong unpleasant smell (Van Der Walt, 2001).

Table 4: History of *C. triloba* (Bernh.) E. Mey. ex Hook.f.

SYNONYM	FULL CITATION
Ceratotheca lamiifolia (Engl.) Engl.	*Ceratotheca lamiifolia* (Engler) Engler, Bot. Jahrb. Syst. 19: 156. 1894. BASIONYM: *Sesamum lamiifolium* Engler 1888.
Sesamum lamiifolium Engl.	*Sesamum lamiifolium* Engler, Bot. Jahrb. Syst. 10: 256, t. 8. 1888. TYPE: SOUTH AFRICA:
Sporledera kraussiana Bernh.	*Sporledera kraussiana* Bernhardi, Linnaea 16: 41. 1842. TYPE: SOUTH AFRICA:
Sporledera triloba Bernh.	*Sporledera triloba* Bernhardi, Linnaea 16: 42. 1842. TYPE: SOUTH AFRICA:
Volkameria lamiifolia (Engl.) Kuntze	*Volkameria lamiifolia* (Engler) Kuntze, Revis. Gen. Pl. 2: 482. 1891. BASIONYM: *Sesamum lamiifolium* Engler 1888.

(Wunderlin and Hansen, 2002)

Table 5: Classification for kingdom plantae.

Kingdom Plantae –Plants
Subkingdom Tracheobionta -Vascular plants
Superdivision Spermatophyta -Seed plants
Division Magnoliophyta -Flowering plants
Class Magnoliopsida –Dicotyledons
Subclass Asteridae -Daisy superorder
Order Scrophulariales -figwort order
Family Pedaliaceae - Sesame family
Genus Ceratotheca Endl. - ceratotheca P
Species - *Ceratotheca triloba* (Bernh.) E. Mey. ex Hook. f.

(Wunderlin and Hansen, 2002)

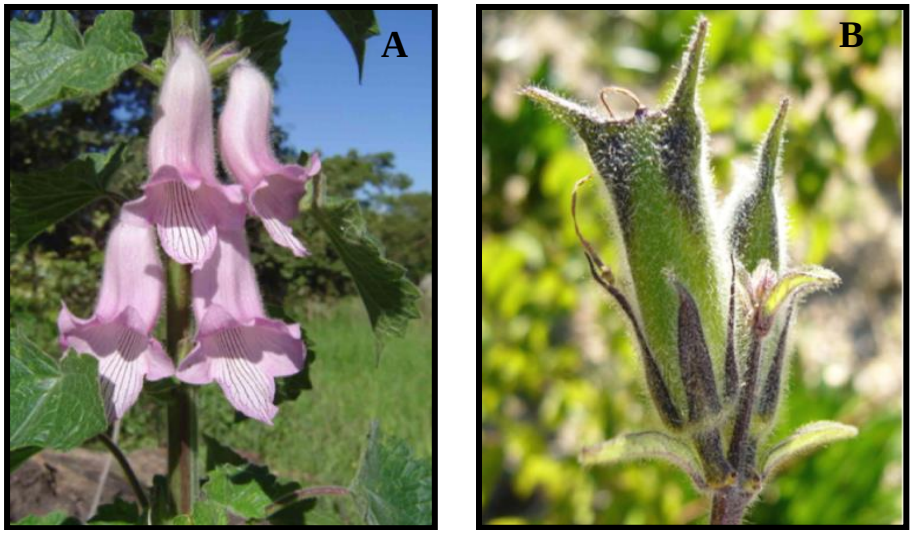

Figure 10: *C. triloba* plant (A) and seed pods (B) (Van Der Walt, 2001).

1.13.2 Traditional uses of *C. triloba*

C. triloba has been used by many traditional cultures. The whole plant was soaked in water to serve as a substitute for soap or shampoo. The plant has been used to treat painful menstruation, stomach cramps, nausea, fever and diarrhea (Tredgold, 1986). Also, infusions of *C. triloba* leaves were prepared and administered as an abortifacient (Pooley, 1998, Roberts, 1990, Van Wyk and Gericke, 2000a, Watt and Breyer-Brandwijk, 1962).

1.13.3 Published biological activities and chemistry of *C. triloba*

Some of the biological activities of *C. triloba* have been documented. The plant has no angiotensin 1-converting enzymes (Ramesar et al., 2008). The leaf extract of the plant has been shown to inhibit α-amylases and thus it has anti-diabetic potential (Odhav et al., 2010). Recently, Mohanlall and Odhav, (2013) reported other biological activities of *C. triloba*. The root and leaf extracts exhibited anti-bacterial activity against *Staphylococcus aureus*, *Micrococcus luteus*, *Escherichia coli*, *Salmonella typhimurium* and *Bacillus cereus*. In addition, partially purified fractions obtained from the root extract exhibited anti-bacterial activity against the same bacterial cultures. These fractions also showed to have anti-oxidant activity and were not toxic to brine shrimp larva.

Mohanlall et al. (2011) identified three anthraquinones (9,10-anthracenedione; 1-hydroxy-4-methylanthraquinone and 5,8-dimethoxy-2,3,10,10a- tetrahydro-1H,4aH-phenanthrene-4,9-dione) and one steroid (androst-5-ene-3, 17, 19-triol) from the partially purified fractions (Figure 11). Reports have shown that these types of compounds possess anticancer activity (Baguley, 1991, Dhingra et al., 2011, Monneret, 2001, Preobrazhenskaya et al., 2006). Since these compounds are valuable, we decided to cultivate cell suspension cultures of *C. triloba* to over produce them by using methyl jasmonate elicitation (Naicker et al., 2011). However, a low quantity of 1-hydroxy-4-methylanthaquinone was produced. Therefore, hairy root cultures of *C. triloba* were induced by *Agrobacterium rhizogenes* transformation. These cultures produced a higher yield of anthraquinones than cell suspension cultures and the roots of the field plant (Naicker, 2012). Also, the following compounds from the hairy root extract were identified: one acridone derivative (5-methoxy-2-nitro-10H-acridin-9-one), one naphthoquinone derivative (2H-naphto[2,3-b]pyran-5,10-dione,3,4-dihydro-2,2-dimethyl-) and seven anthraquinone derivatives (5,8-dimethoxy-2,3,10,10a-tetrahydro-1H,4aH-phenanthrene-4,9-dione; 9,10- anthracenedione, 2-methyl-; 1-hydroxy-4-methylanthraquinone; 9,10- anthracenedione, 2-ethyl-; 1,5-diaminoanthraquinone; phenanthrene, 3,6-dimethoxy- 9-methyl-; 9,10-anthracenedione, 1,4-dimethyl-) (Figure 12). Due to the chemistry of the *C. triloba* plant it has a great potential of contributing towards the treatment of cancer.

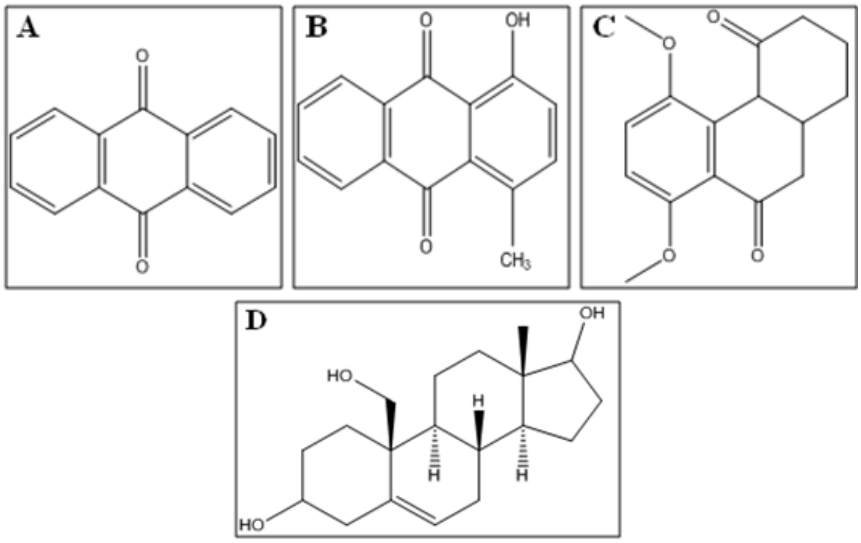

Figure 11: Compounds isolated from *C. triloba* root extract. 9, 10-anthracenedione (A), 1-hydroxy-4-methylanthraquinone (B), 5, 8-dimethoxy-2, 3, 10, 10a-tetrahydro-1H, 4aH-phenanthrene-4, 9-dione (C), androst-5-ene-3, 17, 19-triol (D) (Mohanlall et al., 2011).

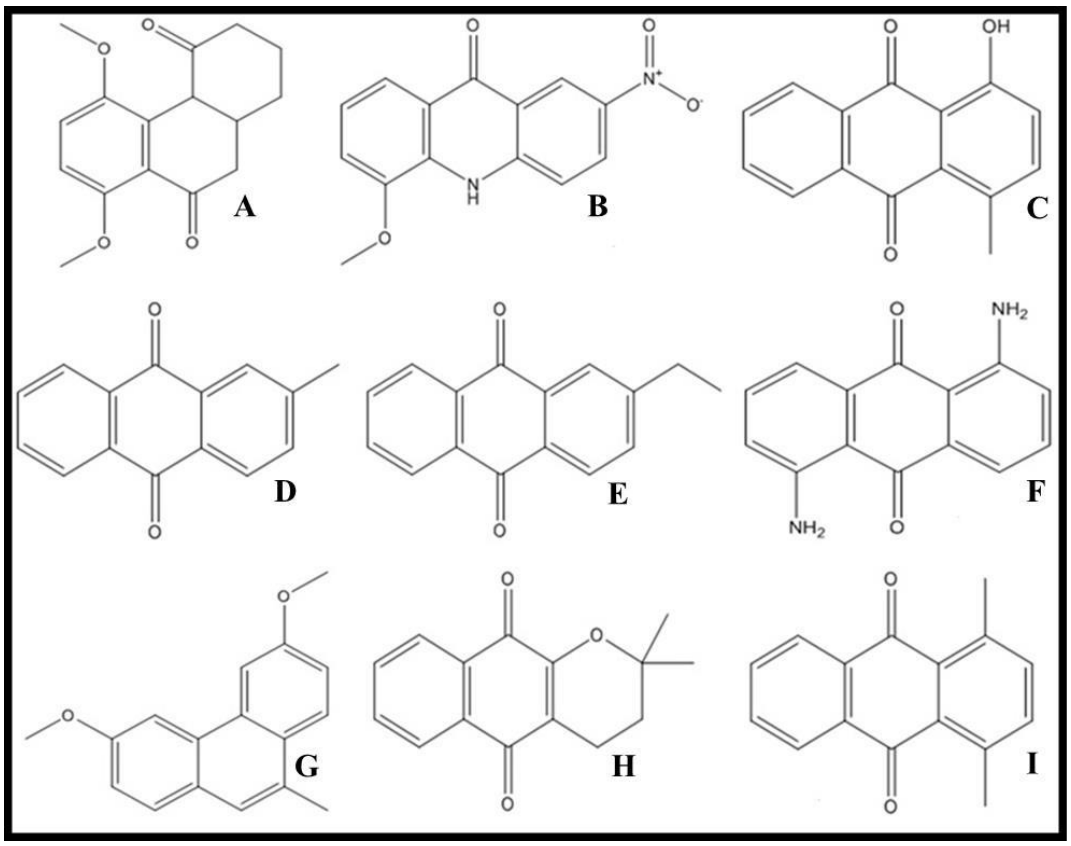

Figure 12: Compounds isolated from *C. triloba* hairy root extract. 5,8-dimethoxy-2,3,10,10a-tetrahydro-1H,4aH-phenanthrene-4,9-dione (A), 5-methoxy-2-nitro-10H-acridin-9-one (B), 1-hydroxy-4-methylanthraquinone (C), 9,10-anthracenedione, 2- methyl- (D), 9,10-anthracenedione, 2-ethyl- (E), 1,5-diaminoanthraquinone (F), phenanthrene, 3,6-dimethoxy-9-methyl- (G), 2H-naphto[2,3-b]pyran- 5,10-dione, 3,4-dihydro-2,2-dimethyl- (H), 9,10 anthracenedione, 1,4- dimethyl- (I) (Naicker, 2012).

1.14 Problem statement

The medical journal, Lancet published that "South Africa could see an increase of 78% in the number of cancer cases by 2030" (Morhason-Bello et al., 2013). Current anticancer drugs are associated with serious side effects and resistance (National Cancer Institute, 2014b, Michael, 2002, Xing-Jie et al., 2010). As a result there is a great need to discover new drugs to fight cancer. Therefore, this project will investigate the anticancer activity of the active fractions isolated from an indigenous plant and subsequently the identity of anticancer compounds found in the active fractions will be determined. The main reasons for this approach are that plants have

the ability to kill cancer cells and sometimes offer protection to normal cells. They also have immunomodulatory properties (Larkin, 1983, Parry, 2015, Saxe, 1987, Umadevi et al., 2013). Thus, our chances of finding effective anticancer compounds are higher.

1.15 Research questions, aims and objectives

Studies conducted in our lab revealed that anthraquinones (9,10-anthracenedione, 1-hydroxy-4-methylanthraquinone and 5,8-dimethoxy-2,3,10,10a-tetrahydro-1H,4aH-phenanthrene-4,9-dione) isolated from the root extract of *C. triloba* inhibited the human topoisomerase II enzyme from converting supercoiled DNA to linear DNA (Mohanlall, 2010). In addition the fractions CT01 (5,8-dimethoxy-2,3,10,10a-tetrahydro-1H,4aH-phenanthrene-4,9-dione, 9,10-anthracenedione, 2-methyl- and 1-hydroxy-4-methylanthraquinone) and CT02 (9,10- anthracenedione, 2-ethyl-) which were isolated from the hairy root extract also inhibited topoisomerase II (research will be published in the future) (Naicker, 2012). The inhibition of topoisomerase II is shown to lead to the activation of signal molecules that are responsible for initiating cell death of cancer cells (Li et al., 2010, Mo and Beck, 1999, Yaoxian et al., 2013). Currently, topoisomerase II inhibitors such as ametantrone, mitoxantrone, doxorubicin, daunorubicin and carminomycin are employed in cancer therapy (Baguley, 1991, Monneret, 2001, Preobrazhenskaya et al., 2006). These facts encouraged us to conduct a preliminary study to investigate if the constituents of *C. triloba* were active against cancer cells. According to the results obtained, it was evident that the root extract, hairy root extract and fractions CT01 and CT02 killed the DU-145 prostate cancer cells (Naicker, 2012).

Hence, thus far we have determined the mechanism of action of the anthraquinones isolated from *C. triloba* and we know that they can kill cancer cells. However, the anticancer activity of *C. triloba* needs to be further investigated for the following reasons: the effect of the root and leaf extracts on cancer cells needs to be determined for isolation of any other anticancer compounds that may be present in the plant. The possible apoptosis pathways that maybe induced by the anthraquinones or other compounds need to be determined because cancer cells are profoundly sensitive to apoptosis (Kerr et al., 1972, Lowe and Lin, 2000). Lastly, these compounds need to be characterized to reveal or validate their identity.

Therefore, the aim of this study was to further investigate the anticancer activity of *C. triloba* and determine the classes of compounds that contributed towards its activity.

This was achieved by the following objectives which were to:

i) Prepare extracts of the leaves and roots of *C. triloba* by using polarity based extraction.

ii) Evaluate the growth inhibitory potential of *C. triloba* extracts on three cancer cell lines (A375 [melanoma], MDA-MB-231[breast] and WHCO1 [oesophageal]) by using the MTT assay.

iii) Investigate different mobile phases for optimum separation of the compounds of the active extract by using thin layer chromatography and subsequently fractionate the compounds of this extract by using column chromatography.

iv) Evaluate the growth inhibitory potential of the fractions on two melanoma cell lines (A375 and UACC-62).

v) Determine the IC_{50} and TGI (total growth inhibition) values of the active fractions on the melanoma cell lines.

vi) Evaluate the apoptosis inducing effects of the active fractions against the melanoma cell lines by using the FITC annexin V assay, PE active caspase 3 assay and BD MitoScreen assay.

vii) Determine the chemical structures of the compounds in the active fractions by using EI-LC-MS.

2. MATERIALS AND METHODS

2.1 Plant material

2.1.1 Collection of plant material

C. triloba was collected from the wild in Durban, Kwa-Zulu Natal, South Africa. The plants were authenticated by Professor H. Baijnath at the School of Life Sciences, University of Kwa-Zulu Natal (UKZN) and a voucher specimen was deposited in the Ward Herbarium at UKZN (Westville campus).

2.1.2 Preparation of the plant material

The roots and leaves were washed under running tap water and dried in an oven for 2-4 days at 40ºC until they could easily be broken by hand. Thereafter, the plant material was grounded to a powder using a Wareing blender.

2.1.3 Extraction of the plant material

Two types of extractions were performed:

i) *Organic extraction*- the ground material was sequentially extracted by using non-polar and polar solvents. The extraction process was initiated by agitation of the ground material (470 g [roots], 281.50 g [leaves]) in 1L of hexane on a shaker at 80 rpm for 24 hours at room temperature. The hexane extract was then filtered and this procedure was repeated four more times. Thereafter, the same used plant material was extracted with DCM, DCM: methanol (1:1) and then methanol as described above. All organic extracts were concentrated by using a roto-evaporator (Heidolph Laborota 400 efficient) with the water bath set at a temperature of 50°C and the flask rotated at 60 rpm. The concentrated extracts were transferred to glass bottles which were covered in foil to prevent the compounds from being degraded by light. The extracts were then dried for 2-3 days under a fume hood and stored at room temperature (27ºC).

ii) *Aqueous extraction*- the grounded material (207.49 g [roots]) was agitated in 1 L of distilled water on a shaker at 80 rpm for 24 hours at room temperature. The aqueous extract was filtered and placed in a bio-freezer at -70ºC for 24 hours. This extract was then freeze dried to a powder and stored at room temperature in a glass bottle covered in foil. The aqueous extraction was only performed on roots as the leaves of the plant were limited.

The percentage yield of the extracts was determined by using the following equation:

%Yield of extract = (mass of extract/mass of plant material) X 100

2.2 Cell culture

2.2.1 Cell lines

The A375, MDA-MB-231 and WHCO1 cell lines were provided by Dr Catherine Kaschula from the International Centre for Genetic Engineering and Biotechnology (ICGEB) at the University of Cape Town (UCT). The UACC-62 cell line was provided by Natasha Kolesnikova from the Biosciences unit at the Council of Scientific and Industrial Research (CSIR)**.** A375 is a melanoma cell line that was derived from a malignant melanoma of a 54 year old female (Fok et al., 2006). MDA-MB-231 is a breast adenocarcinoma cell line that was derived by pleural effusion of a 51 year old Caucasian female with metastatic breast adenocarcinoma (Cailleau et al., 1974). WHCO1 is a human esophageal cancer cell line and is of South African origin. It was derived from a primary esophageal squamous cell carcinoma biopsy (Veale and Thornley, 1989). UACC-62 is a melanoma cell line that was derived from a malignant melanoma of human origin (Shoemaker, 2006).

2.2.2 Regeneration of cells

All cell lines were received in cryovials which were placed in a 37ºC water bath to allow the cells to rapidly thaw. The cells were then transferred to 10 cm cell culture plates (Sigma-Aldrich, Inc) which contained 10 ml of complete culture medium (CCM) (Dulbecco's Modified Eagle Medium [DMEM] [Biochrom] that consisted of glucose [4,5 $g.l^{-1}$], L-glutamine [1 mM] and

sodium pyruvate [1 mM] supplemented with foetal bovine serum (FBS) [10 %] [Gibco, Life Technologies] and penicillin-streptomycin solution [1%] [Gibco, Life Technologies]). Thereafter, the plates were incubated at 37°C in a humidified incubator with 5% CO_2.

2.2.3 Cell culture maintenance

The medium was removed from the plates by using vacuum suction and the monolayer of cells was washed with 5 ml of phosphate buffered saline (PBS) (Sigma-Aldrich, Inc). An aliquot of 1 ml of trypsin (Highveld Biological) was added into the plates and the cells were detached by aspirating the trypsin gently with a pipette. Thereafter, the trypsin was deactivated by adding 5 ml of CCM into the plates. The cells were then centrifuged at 1200 rpm for 3 minutes and the supernatant was discarded prior to resuspension of the cells in 2 ml of CCM. Aliquots of the A375 (100 µl), MDA-MB-231 (200 µl), WHCO1 (200 µl) and UACC-62 (500 µl) cell suspensions were transferred into plates containing 10 ml of CCM. The plates were incubated at 37°C in a humidified incubator with 5% CO_2. The cells were viewed under an inverted microscope (Nikon SM2800) on a daily basis to check for contamination and examine cell growth. The cells were sub-cultured every 2-3 days after the plates became 70-80% confluent.

2.2.4 Cryopreservation of cell lines

Cells that were grown to 70-80% confluency (in a 10 cm cell culture plate) were washed with 5 ml of PBS. The cells were then trypsinized and centrifuged as described in section 2.2.3. Thereafter, the supernatant was discarded and the cells were re-suspended in 2 ml of cryopreservation medium (20% FBS, 10% DMSO and 70% DMEM). Aliquots of 1 ml of the cell suspension were transferred to cryovials (Sigma-Aldrich, Inc) which were stored overnight in a -80 ºC freezer. These cryovials were subsequently transferred to a liquid nitrogen tank for long term storage at -180 ºC.

2.2.5 Enumeration of cells

The cells were enumerated using the Neubauer haemocytometer (Weber Scientific Ltd). An aliquot of 100 µl of the cell suspension was mixed with 100 µl of trypan blue (0.2%) (Sigma-Aldrich, Inc) and 10 µl of this mixture was loaded into the chamber of the haemocytometer.

Only the viable cells (translucent) that appeared within or on the boundary of the primary squares (centre square and four corner squares) were counted. The volume of cell suspension that filled one primary square was 0.1 mm^3. The following equation was used to calculate $cells.ml^{-1}$:

$Cells.ml^{-1}$ = (Number of cells from 5 primary squares/5) X 2 X 10 000

Thereafter the number cells needed for the total number of wells used in the experiment was calculated according to following equations:

Total amount of cells (A) = Number of cells/ml X volume of cells (ml)

Number of cells required for the experiment (B) = 3 x 10^3 per well X number of wells used

Volume of cells required for experiment (C) = (Total volume of cells X B)/(A)

Volume of media required to dilute the cells = (90 µl* X number of wells)-(C)

* [volume of medium added in each well]

2.3 Evaluation of the growth inhibitory potential of *C. triloba* extracts on three cancer cell lines

2.3.1 Seeding of cells

Cells that were grown to 70-80% confluency (in a 10 cm cell culture plate) were washed with 5 ml of PBS. The cells were trypsinized, centrifuged and re-suspended as described in Section 2.2.3. Thereafter, aliquots of 90 µl (3 x 10^3 $cells.well^{-1}$) of the cell suspension (A375, MDA-MB-231 and WHCO1 cell lines) were seeded into 96 well microtiter plates (Costar, Sigma-Aldrich, Inc). After which 200 µl of distilled water was pipetted into the outer wells of the plates to prevent evaporation of the medium. The plates were then incubated for 24 hours at 37°C in a humidified incubator with 5% CO_2.

2.3.2 Set up of controls

An aliquot of 10 µl of CCM was added to the cells which served as the untreated control. DMSO was diluted to 2.0% in CCM. Then, 10 µl of the DMSO solution (0.2%) was used to treat the cells which served as the solvent control.

2.3.3 Treatment of cells

The extracts were prepared at 12.5 $mg.ml^{-1}$ and 25 $mg.ml^{-1}$ in DMSO. Thereafter, the extracts were further diluted to 250 $\mu g.ml^{-1}$ and 500 $\mu g.ml^{-1}$ in CCM. Aliquots of 10 µl of the extracts (25 $\mu g.ml^{-1}$ and 50 $\mu g.ml^{-1}$) were then used to treat the cells. Subsequently, the plates were incubated for 48 hours.

2.3.4 Microscopic examination of the cells

Treated and untreated A375, MDA-MB-231 and WHCO1 cells were examined for signs of apoptosis (such as cytoplasmic shrinkage and rounding) under an inverted microscope (Nikon SM2800) at 100 x magnification.

2.3.5 Measurement of growth inhibition by using the MTT assay

2.3.5.1 Description

The MTT [3-(4,5-dimethylthiazol-2-yl)-2,5-diphenyltetrazolium bromide] assay is based on the activity of cellular reductases (NADH and NADPH) that are present in viable cells. These enzymes cleave the tetrazolium ring of MTT (Figure 13). Consequently, this yellow dye gets reduced to purple formazan crystals which can be dissolved in DMSO or SDS. The resulting purple solution can be measured spectrophotometrically. Thus the increase or decrease in the number of cells depends on the quantity of formazan produced which in turn can denote the degree of growth inhibition exhibited by the test drug (Berridge and Tan, 1993, Maioli et al., 2009, Mossman, 1983).

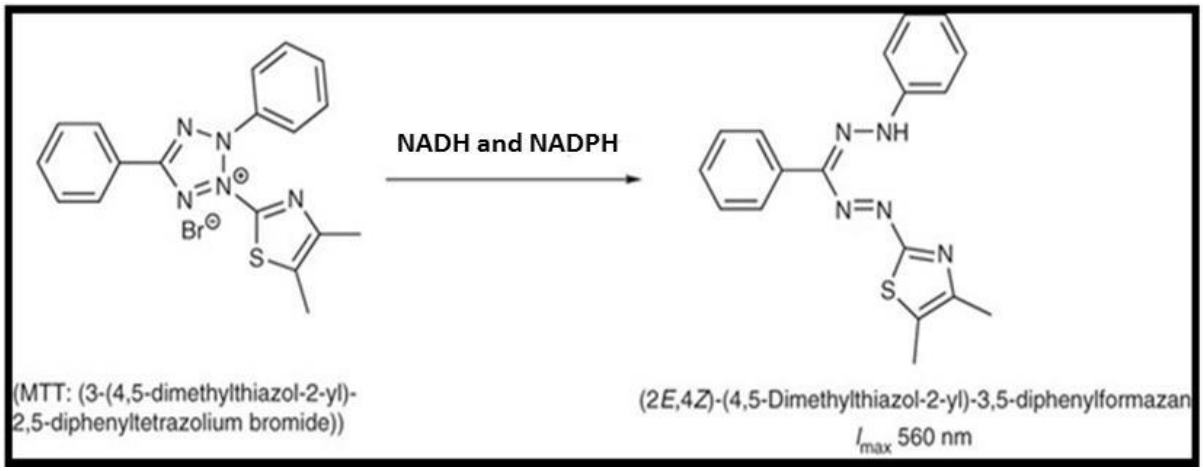

Figure 13: Reduction of MTT (3-(4,5-dimethylthiazol-2-yl)-2,5-diphenyltetrazolium bromide) to a purple formazan (4,5-Dimethylthiazol-2-yl]-3,5-diphenylformazan) product by cellular reductase enzymes, NADH and NADPH (Ebada et al., 2008).

2.3.5.2 MTT assay protocol

The MTT assay was performed according to the procedure described in the Roche cell proliferation assay manual. After the 48 hour treatment, 10 µl of a 5 $mg.ml^{-1}$ MTT (Molecular probes, life technologies) solution was added to the cells and the microtiter plates were incubated for 4 hours at 37°C in a humidified incubator with 5% CO_2. Thereafter, 100 µl of 10% SDS in 0.01 M HCL was added to the cells to dissolve the formazan crystals. The plates were then incubated overnight. The absorbance of the formazan solutions was read at 595 nm by using an ELISA plate reader (Digital Analogue Systems, Italy). The data was transferred to Microsoft Excel and the percentage growth inhibition (%GI) exhibited by the test drug was determined according to the following equation:

%GI = (Absorbance of cells treated with DMSO – Absorbance of cells treated with the test drug)/ (Absorbance of cells treated with DMSO)

2.4 Investigation of the different mobile phases for optimizing the separation of the compounds of the hexane root extract

In order to optimize the separation of the compounds of the hexane root extract for column chromatography, thin layer chromatography (TLC) was done to view which mobile phases

could best separate the compounds of this extract. Aliquots of 10 µl of the hexane root extract were loaded onto six pieces of silica gel TLC plates (1 cm in width and 10 cm in length) (Merck) which were developed in the following mobile phases: hexane: ethyl acetate: ethanol (1:8:1), ethanol: hexane (9:1), ethanol: petroleum ether (1:9), hexane: dichloromethane (3:7), hexane: dichloromethane (1:9) and hexane. Thereafter the TLC plates were sprayed with a vanillin solution (300 mg vanillin in 84 ml of ethanol and 3 ml of H_2SO_4) (Sigma-Aldrich, Inc) and heated with a blow dryer for 2 minutes to reveal the bands.

The separation of the compounds of the hexane root extract was further optimized by using different ratios of hexane: DCM (a polarity based separation method) (Table 6). Eight pieces of TLC plates (1 cm in width and 10 cm in length) were loaded with 10 µl of the hexane root extract. These plates were developed in hexane and one of the plates was sprayed and heated as described above. The seven remaining plates were re-ran in hexane: DCM at a ratio of 10:90 and one of the plates was sprayed and heated. Then the six remaining TLC plates were consecutively processed as described in Table 6. By using this method, the polarity of the mobile phase was gradually increased to facilitate the separation of the compounds of the hexane root extract. A similar principle was applied in the column.

Table 6: Hexane: DCM ratios used to separate compounds from the hexane root extract.

Ratio of hexane: DCM	Number of TLC plates developed	Number of TLC plates sprayed with vanillin and heated
1:0	8	1
10:90	7	1
88:12	6	1
85:15	5	1
60:40	4	1
40:60	3	1
20:80	2	1
0:1	1	1

2.5 Column chromatography of the hexane root extract

The column chromatography set up is illustrated in Figure 14. The lower part of a glass column (30 mm in width and 80 cm in length) was stocked with cotton wool by using a glass rod. An aliquot of 300 ml of hexane and 60 g of silica gel 60 (0.063-0.200 mm, 70-230 mesh ASTM) (Merck) was mixed to form a slurry which was poured into the column. The tap was left open for collection of the excess hexane into a beaker. An aliquot of 50 ml of hexane was left in the column to prevent the formation of air bubbles. Thereafter, 900 mg of the hexane root extract was mixed with 50 ml of hexane and poured gently into the column. The compounds of the extract were separated and eluted by gradually increasing the polarity of the mobile phase in the column. This was done by using the following mobile phases: hexane : DCM (60 : 40, 40 : 60), DCM, DCM : ethyl acetate (90 : 10, 70 : 30, 60 : 40, 50 : 50, 50 : 60, 30: 60, 20 : 80), ethyl acetate and ethyl acetate: methanol (80 : 20, 70 : 30, 50 : 50). Thus, hexane: DCM (60:40) was poured first into the column and the tap was opened for elution of the band/s into test tubes which had a capacity of 20 ml. The next mobile phase was added when no more bands eluted from the column while the hexane: DCM (60:40) mobile phase was used. This procedure was repeated with the remaining mobile phases. The contents in each test tube represented a fraction that consisted of one or several band/s. Each fraction was given a number, for example: 1. In order to visualize the bands of the fractions, an aliquot of 10 µl of the fractions were loaded onto TLC plates which were developed in the appropriate mobile phases (Table 7). The plates were then sprayed and heated as described in Section 2.4. All fractions were not analysed by TLC because if the colour of the solution was repeated in many test tubes; this suggested that similar fractions was present in the respective test tubes.

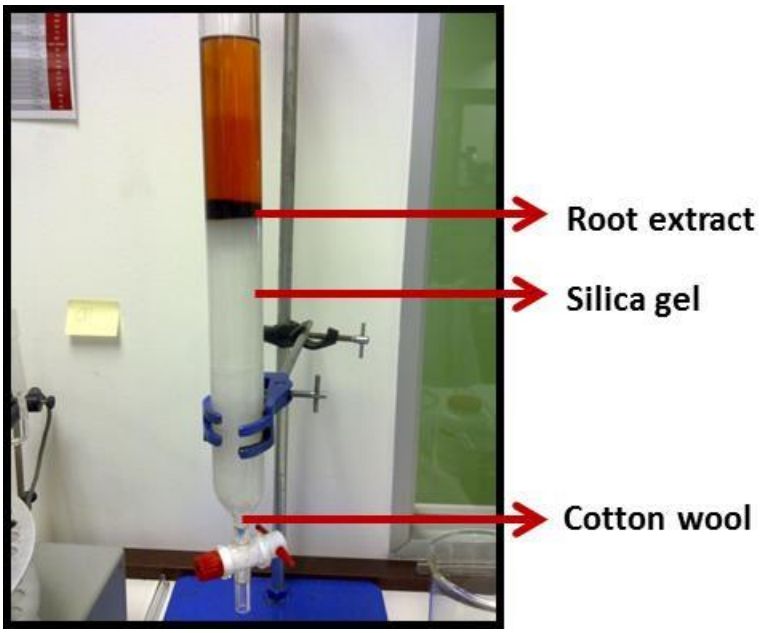

Figure 14: Column chromatography setup displaying a silica gel column loaded with the hexane root extract.

Table 7: Recombination of fractions 13-90 developed in different mobile phases.

TLC plate	Fractions	Mobile phase	Solvent ratio
A	13, 16, 17, 19, 22, 23, 24, 25	hexane: DCM	60:40
B	31, 34, 36, 40, 41, 43, 45, 47	hexane: DCM	60:40
C	48, 50, 53, 54, 57, 58, 60, 66	DCM: ethyl acetate	90:10
D	66, 68, 69, 71, 72, 73	DCM: ethyl acetate	60: 40
E	75, 76, 80	DCM: ethyl acetate	60: 40
F	81, 82, 84, 86, 87, 88, 89, 90	Ethyl acetate: methanol	70: 30

2.6 Evaluation of the growth inhibitory potential of the fractions on two melanoma cell lines

2.6.1 Seeding of cells

The A375 (3 x 10^3 cells.well^{-1}) and UACC-62 (4.7 x10^3 cells.well^{-1}) cells were seeded into 96 well microtiter plates as described in Section 2.3.1

2.6.2 Set up of controls

The untreated and DMSO controls were prepared according to Section 2.3.2

2.6.3 Treatment of cells

The fractions were prepared at 6.25 mg.ml^{-1} and 12.5 mg.ml^{-1} in DMSO. Thereafter, 2 µl of each of the fractions was added to 98 µl of CCM. An aliquot of 10 µl of the fractions was then added to the cells. Thus, the cells were treated with final concentrations of 12.5 µg. ml^{-1} and 25 µg. ml^{-1}. Subsequently the plates were incubated for 48 hours.

2.6.4 Measurement of growth inhibition using the MTT assay

The MTT assay was performed according to Section 2.3.5.2 and the %GI exhibited by the fractions on the melanoma cells was determined (Section 2.3.5.2).

2.7 Determination of the IC_{50} and TGI (total growth inhibition) values of the active fractions

2.7.1 Seeding of cells

The A375 (3 x10^3 cells.per^{-1}) and UACC-62 (4.7 x10^3 cells.per^{-1}) cells were seeded into 96 well microtiter plates as described in Section 2.3.1.

2.7.2 Set up of controls

The untreated and DMSO controls were prepared according to Section 2.3.2. Dose responsive curves of the standards (camptothecin and doxorubicin) (Sigma-Aldrich, Inc) were then generated to determine the IC_{50} and TGI values. Standards at 6.25 $mg.ml^{-1}$, 12.5 $mg.ml^{-1}$ or 25 $mg.ml^{-1}$ in DMSO were prepared. Subsequently, the standards were serially diluted in DMSO and further diluted in CCM. Then, an aliquot of 10 µl of the standards was used to treat the cells which served as positive controls. The concentration range depended on the cell line and standard that was being tested as each cell line had a different degree of sensitivity to each standard (Appendix 1).

2.7.3 Treatment of cells

Dose responsive curves of the active fractions (F2, F4, F5 and F8) were also prepared. Therefore these fractions were prepared at 6.25 $mg.ml^{-1}$, 12.5 $mg.ml^{-1}$ or 25 $mg.ml^{-1}$ in DMSO. Subsquently, the fractions were serially diluted in DMSO (Appendix 1). Thereafter, 2 µl of each of the fractions was added to 98 µl of CCM. An aliquot of 10 µl of the fractions was then added to the cells. The concentration range depended on the cell line and fraction that was being tested as each cell line had a different degree of sensitivity to each fraction (Appendix 1). Subsequently the plates were incubated for 48 hours.

2.7.4 Measurement of growth inhibition by using the MTT assay

The MTT assay was performed according to Section 2.3.5.2. The data was transferred to Microsoft Excel and the %GI exhibited by the standards and fractions (at a range of concentrations) on the melanoma cells was determined (Section 2.3.5.2).

2.7.5 Calculation of IC_{50} and TGI values

The %GI values were used to construct dose responsive curves on Microsoft Excel for determination of the TGI values. Also, the %GI values were transferred to GraphPad Prism 4 to construct the logarithmic form of the dose response curves for calculation of the IC_{50} values.

2.8 Evaluation of the apoptosis inducing effects of the active fractions against two melanoma cell lines

2.8.1 Preparation of cells

Plate cultures that were 70-80% confluent were used to prepare 75 cm^2 flask cultures which were used to bulk up cells for conducting apoptosis assays. The cells were washed, trypsinized, centrifuged and re-suspended (Section 2.2.3). Aliquots of the A375 (300 µl) and UACC-62 (1500 µl) cell suspension cultures were transferred into 75 cm^2 flasks (Sigma-Aldrich, Inc) containing 20 ml of CCM. The flasks were then incubated for 2-3 days at 37°C in a humidified incubator with 5% CO_2. Thereafter, the 75 cm^2 flasks cultures that were 70-80% confluent were used to prepare 25 cm^2 flask cultures. The cells were washed, trypsinized, centrifuged and re-suspended (Section 2.2.3). Aliquots of 1 ml (5 x 10^5 cells) of the A375 and UACC-62 cell suspension cultures were transferred into 25 cm^2 flasks (Sigma-Aldrich, Inc) containing 8 ml of CCM. These flasks were then incubated for 24 hours.

2.8.2 Set up of controls

Appropriate controls were set up to apply compensation to the flow cytometre data that was obtained from apoptosis assays (Table 8 and 9). Aliquots of 1ml of CCM were added to the cells which served as the untreated/unstained and untreated/stained controls. Thereafter the standards (camptothecin and doxorubicin) were prepared at 3 $mg.ml^{-1}$ and/or 12.5 $mg.ml^{-1}$ in DMSO. The standards were then further diluted to 60 $\mu g.ml^{-1}$ and 250 $\mu g.ml^{-1}$ in CCM. An aliquot of 1 ml of the standards (6 $\mu g.ml^{-1}$ and/or 25 $\mu g.ml^{-1}$) was used to treat the cells which served as the positive controls. In addition, camptothecin (25 $\mu g.ml^{-1}$) treated cells served as the FITC annexin V control and heat shocked (70ºC for 15 minutes) cells served as the PI control (Table 9). Also, DMSO was diluted to 2.0% in CCM. Then 1 ml of the DMSO solution (0.2 %) was used to treat the cells which served as the solvent control. Each assay had a particular set of controls.

Table 8: Treatment of cells which served as controls for the BD MitoScreen assay and PE (phycoerythrin) active caspase 3 assay.

Control	Camptothecin ($6\ \mu g.ml^{-1}$ and/or $25\ \mu g.ml^{-1}$)	Doxorubicin ($6\ \mu g.ml^{-1}$)
Untreated/unstained control		
Untreated /stained control		
Positive control	X	
Positive control		X
DMSO control		

Table 9: Treatment of cells which served as controls for the FITC (Fluorescein isothiocyanate) annexin V assay.

Control	Camptothecin ($6\ \mu g.ml^{-1}$ and/or $25\ \mu g.ml^{-1}$)	Doxorubicin ($6\ \mu g.ml^{-1}$)	Heat shock
Untreated/unstained control			
PI control			X
FITC annexin V control	X		
Positive control	X		
Positive control		X	
DMSO control			

*Cells were heat shocked at 70ºC for 15 minutes.

2.8.3 Treatment of cells

The active fractions (F2, F4, F5 and F8) were prepared at 3 $mg.ml^{-1}$ and 12.5 $mg.ml^{-1}$ in DMSO. Thereafter, the fractions were further diluted to 60 $\mu g.ml^{-1}$ and 250 $\mu g.ml^{-1}$ in CCM. An aliquot of 1ml of the fractions (6 $\mu g.ml^{-1}$ and 25 $\mu g.ml^{-1}$) was then used to treat the cells. Subsequently the plates were incubated for 24 hours at 37°C in a humidified incubator with 5% CO_2.

2.8.4 Microscopic examination of the cells

The A375 and UACC-62 cells (untreated and treated) were examined for signs of apoptosis (such as rounding, cell fragmentation, budding and formation of apoptotic bodies) under an inverted microscope (Nikon SM2800) at 100 x magnification.

2.8.5 Dissociation of cells

After a 24 hour treatment period the growth medium from the flasks was poured into labelled centrifuge tubes (the medium was needed for analysis as it contained detached apoptotic cells) and the cells were washed twice with 2 ml of PBS. Thereafter, 1 ml of the cell dissociation buffer (Gibco, life technologies) was added into the flasks which were incubated for 1-2 minutes at 37°C in a humidified incubator with 5% CO_2. A pipette was used to gently aspirate the buffer for detachment of the cells and 1 ml of CCM was added into the flasks to re-suspend the cells. The contents of the flasks were poured into the respective centrifuge tubes that contained the supernatants. The cells were centrifuged at 1200 rpm for 3 minutes and the supernatants were discarded. The cells were then processed through apoptotic assays.

2.8.6 Examination of the state of the mitochondrial membrane potential (ΔΨ) using the BD MitoScreen assay

2.8.6.1 Description

The cellular oxidation reactions of the mitochondrial respiratory chain facilitate the release of energy which is stored as a negative electrochemical gradient (known as the mitochondrial membrane potential [ΔΨ]) across the mitochondrial membrane. In this case, the ΔΨ is polarized. The integrity of the mitochondrial membrane can be compromised when pro-apoptotic proteins (such as Bid, Bim and Bax) facilitate the permeabilization of the outer mitochondrial membrane (Kim et al., 2006, Crow et al., 2004). This results in the collapse (loss of negative energy) of the ΔΨ and activation of other apoptosis signal molecules. Under these circumstances the ΔΨ becomes depolarized (Desagher et al., 1999, Narita et al., 1998, Basanez et al., 1999, Luo et al., 1998, Pope, 2002). Therefore, depolarization of the ΔΨ is an indication that the cell is undergoing apoptosis.

The state of the ΔΨ can be analysed by performing JC-1 staining. JC-1 (5,5',6,6'-tetrachloro-1,1',3,3'-tetraethylbenzimidazolcarbocyanine iodide) is a lipophilic cationic fluorochrome that can exist as two forms, aggregates (at high concentrations) and monomers (at low concentrations). The JC-1 aggregates show a red fluorescence and are measured by the FL-2 filter while the JC-1 monomers show a green fluorescence and are measured by the FL-1 filter. In viable cells, the JC-1 monomers enter the plasma membrane and then the cytoplasm. The polarized state (negative charge) of the ΔΨ also allows the positively charged JC-1 monomers to enter the mitochondrial matrix. When a critical concentration is exceeded, the JC-1 monomers form J-aggregates (Figure 15). Therefore viable cells show both green and red fluorescence and are detected by both the FL-1 and FL-2 optical filters. In apoptotic cells, JC-1 remains in the cytoplasm in a monomer form as the depolarized state of the ΔΨ prevents the accumulation of the dye in the mitochondria. Therefore apoptotic cells show green fluorescence and are detected by the FL-1 filter (Smiley et al., 1991, Cossarizza et al., 1993, Woollacott and Simpson, 2001, Nuydens et al., 1999).

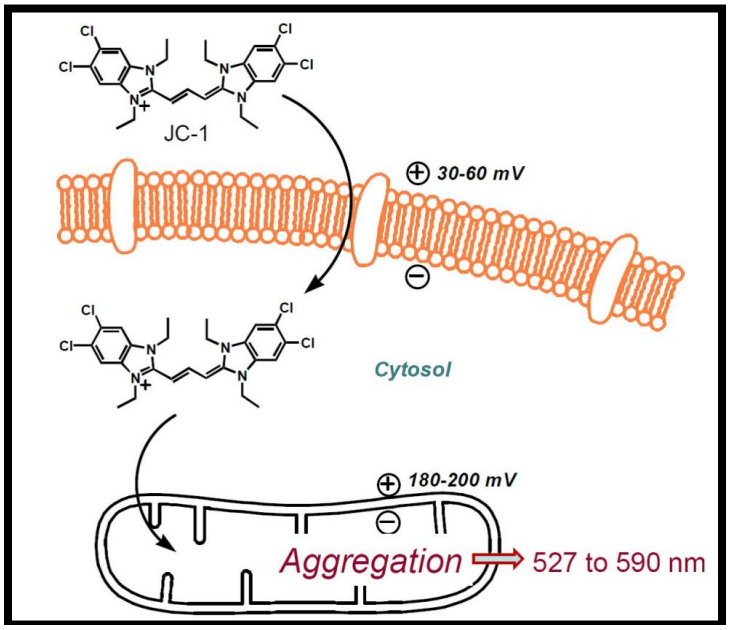

Figure 15: A viable cell absorbing the JC-1 dye into its mitochondrion for the formation of JC-1 aggregates (Dubikovskaya, 2013).

2.8.6.2 BD MitoScreen assay protocol

The BD MitoScreen assay kit (BD Biosciences) was used to examine the state of the ΔΨ in the cells. The cells from the flasks were detached by using the cell dissociation protocol as described in Section 2.8.5. Thereafter, the cells were re-suspended in 2 ml of cold PBS (4ºC) and centrifuged at 1200 rpm for 3 minutes and the supernatants were discarded. These steps were repeated. The cells that served as controls were stained according to Table 10. The cells that were treated with the active fractions were stained with 500 µl of JC-1 working solution. Subsequently the cells were gently vortexed and incubated for 15 minutes at 37°C in a humidified incubator with 5% CO_2. Centrifugation was then applied to the cells at 1200 rpm for 3 minutes and the supernatants were discarded. This was followed by two washing steps. For the first wash step, the cells were re-suspended in 2 ml of JC-1 assay buffer and centrifuged at 1450 rpm for 5 minute and the supernatants were discarded. For the second wash step, the cells were re-suspended in 1 ml of JC-1 assay buffer and processed as described in the first step. Lastly, an aliquot of 250 µl of JC-1 assay buffer was used to resuspend the cells which were then transferred into 5 ml round bottom test tubes for analysis by flow cytometry.

Table 10: Staining of cells which served as controls for the BD MitoScreen assay.

Control	**JC-1 working solution (500 µl)**
Untreated/unstained control	
Untreated/stained control	X
Positive control (Camptothecin at 6 $\mu g.ml^{-1}$ and/or 25 $\mu g.ml^{-1}$)	X
Positive control (Doxorubicin at 6 $\mu g.ml^{-1}$)	X
DMSO control	X

2.8.7 Detection of caspase 3 activity by PE (phycoerythrin) active caspase 3 assay

2.8.7.1 Description

Caspase 3 is a heterodimer that is made up of 17 and 12 kDa subunits. It serves as a marker for cells that are undergoing early apoptosis. Caspase 3 cleaves and activates other caspases and proteins in the cytoplasm (such as Bcl-2) and nucleus (such as PARP) (Alnemri et al., 1996, Fujita and Tsuruo, 1998, Patel et al., 1996). This enzyme is recognized by using a PE-conjugated rabbit anti-activated caspase 3 antibody.

2.8.7.2 PE active caspase 3 assay protocol

The PE active caspase 3 assay kit (BD Biosciences) was used to detect caspase 3 activity. The cells from the flasks were detached by using the cell dissociation protocol as described in Section 2.8.5. Thereafter, the cells were re-suspended in 2 ml of cold PBS (4ºC) and pelleted (centrifugation at 1200 rpm for 3 minutes and the supernatant was discarded), twice. Subsequently, the cells were resuspended in 500 µl of BD cytofix/cytoperm solution, incubated for 20 minutes on ice and pelleted. This was followed by two wash steps whereby the cells were resuspended in 500 µl of BD perm/wash buffer and pelleted, twice. The cells that served as controls were stained according to Table 11. The cells that were treated with the active fractions were stained with 120 µl of BD perm/wash-PE antibody solution. An incubation period of 30 minutes at room temperature was completed and the cells were pelleted. Afterwards, the cells were re-suspended in 1 ml of BD perm/wash buffer and pelleted again. Lastly, an aliquot of 250 µl of BD perm/wash buffer was used to resuspend the cells which were transferred into 5 ml round bottom test tubes for analysis by flow cytometry.

Table 11: Staining of cells which served as controls for the PE active caspase 3 assay.

Control	BD perm/wash-PE antibody solution (20 µl)

Untreated/unstained control	
Untreated/stained control	X
Positive control	X
Positive control	X
DMSO control	X

2.8.8 Detection of early and late apoptosis using FITC (Fluorescein isothiocyanate) annexin V assay

2.8.8.1 Description

The FITC annexin V assay detects the loss of membrane integrity which occurs when the phospholipid phosphatidylserine (PS) flips from the inner to the outer plasma membrane during early apoptosis (Figure 16) (Fadok et al., 1992, Savill et al., 1993). Annexin V is a 35-36 kDa protein that has a high affinity for PS in the presence of Ca^{2+}. Therefore, this protein can bind to early apoptotic cells. Conjugation of annexin V with fluorochromes such as FITC allows for the detection of early apoptotic cells by flow cytometry. However, it is important to take into consideration that the flipped PS precedes to late apoptosis. Therefore, a second stain such as propidium iodide (PI) or 7-Aminoactinomycin D (7-AAD) should be used (Vermes et al., 1995, van Engeland et al., 1997, Schmid et al., 1992). Dual staining allows us to detect and distinguish between viable cells, early apoptotic cells, late apoptotic cells and necrotic cells. This is possible because the cells have a different staining pattern at each stage due to their cell morphology. Viable cells have intact cell membranes and exclude both the annexin V and PI stains while early apoptotic cells have exposed PS at the plasma membrane and stain with annexin V only (Schutte et al., 1998, Vermes et al., 1995). Late apoptotic cells have damaged cell membranes and undergo DNA fragmentation. Therefore, these cells stain with annexin V and PI (Kerr et al., 1972, Shi et al., 2006, Andrade et al., 2010). Eventually, the damaged membrane detaches from the late apoptotic cells which subsequently form rounded residual apoptotic bodies that transition into swollen cells with granular inclusions. This is the final stage of cell death and these cells become necrotic and stain with PI only due to loss of the plasma membrane (Kravtsov et al., 1999).

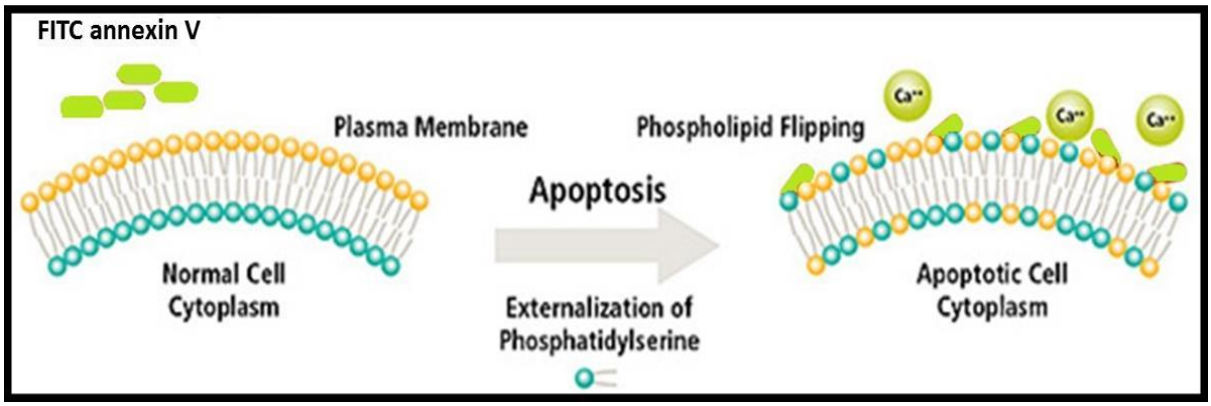

Figure 16: FITC annexin V binds to apoptotic cells with flipped phospholipid phosphatidylserine (Adapted from BD Biosciences, 2015).

2.8.8.2 FITC annexin V assay protocol

The FITC annexin V assay kit (BD Biosciences) was used to detect apoptotic cells. The following protocol was provided by BD Biosciences. The cells from the flasks were detached by using the cell dissociation protocol as described in Section 2.8.5. Thereafter, the cells were re-suspended in 2 ml of cold PBS (4ºC) and centrifuged at 1200 rpm for 3 minutes and the supernatants were discarded. These steps were repeated. An aliquot of 500 µl of 1 X binding buffer was then used to re-suspend the cells and 100 µl of the cell suspensions were transferred into 5 ml round bottom test tubes (BD Biosciences). The cells that served as controls were stained according to Table 12. The cells that were treated with the fractions were stained with 5 µl of FITC annexin V and 5 µl of PI. Subsequently the cells were gently vortexed and incubated for 15 minutes at room temperature in the dark. An aliquot of 200 µl of 1 X binding buffer was then added to the cells which were analysed by flow cytometry within 1 hour.

Table 12: Staining of cells which served as controls for the FITC annexin V assay.

Control	FITC annexin V (5 µl)	PI (5 µl)
Untreated/unstained control		
PI control		X
FITC annexin V control	X	
Positive control (Camptothecin at 6 µg.ml^{-1} and 25 µg.ml^{-1})	X	X
Positive control (Doxorubicin at 6 µg.ml^{-1})	X	X
DMSO control	X	X

2.8.9 Flow cytometer analysis

The BD Accuri C6 flow cytometer was used for this project (Figure 17). This instrument was validated daily to ensure that it was working properly. Assay templates were also set up. These steps were performed according to the BD Accuri C6 flow cytometer software manual. Table 13 shows the instrument and compensation settings that were used for the apoptosis assays. The FlowJo software was used to analyse the data.

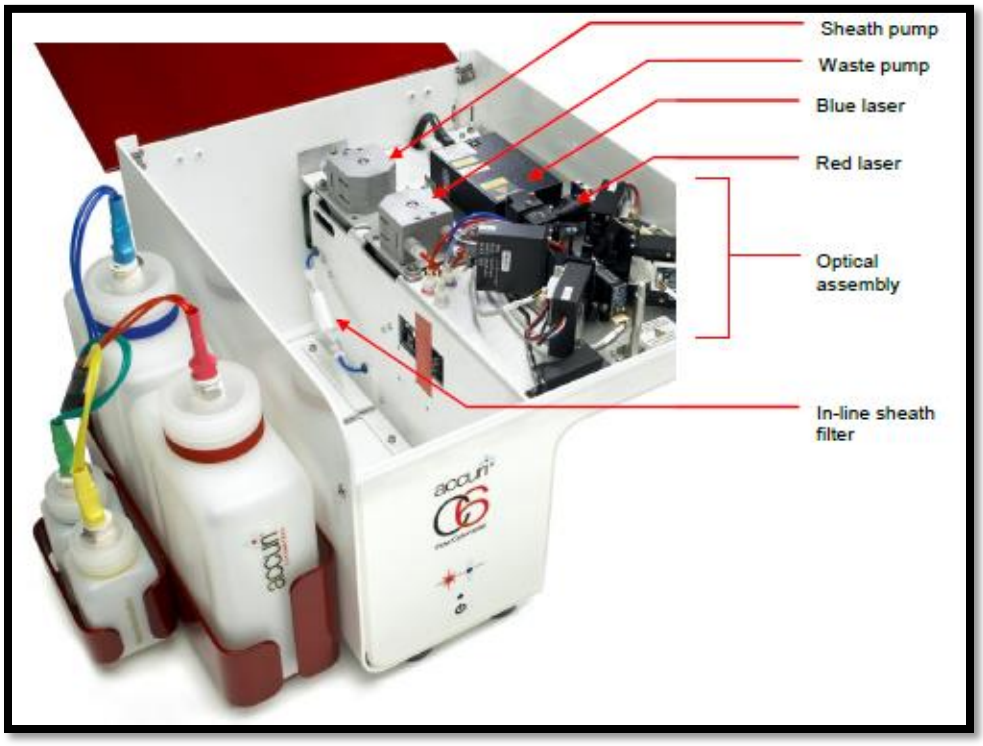

Figure 17: The Accuri C6 flow cytometer consists of the fluidics sub-system (sheath and waste pumps), optical sub-system (lasers and filters) and electronic sub-system (computer) (BD Biosciences, 2012).

Table 13: BD Accuri C6 flow cytometer instrument and compensation settings.

Apoptosis assay	A375		UACC-62		Number of events
	FL-1	FL-2	FL-1	FL-2	
FITC annexin V	12	5	3	17	10 000
BD MitoScreen	3	15	20	15	10 000
PE active caspase	-	-	-	-	200 000

2.9 Statistical analysis

Tests were performed in triplicate. The mean, standard deviation (represented by error bars on the graphs) and standard mean of error (SEM) were calculated. GraphPad InStat was used to conduct the ANOVA test. For the dose response curves, R squared values (the goodness of the graph fit) were calculated by using the GraphPad Prism 4 software. For the apoptosis assays, single tests were performed due to limited reagents in the apoptosis kits. However, appropriate instrument and compensation controls were done to ensure accuracy of the results.

2.10 Electron Ionization-Liquid Chromatography-Mass Spectrometry (EI-LC-MS) analysis of the active fractions

EI-LC-MS analysis was performed by using the Waters Thermabeam (TMD) system which comprised of a 2695 Solvent Delivery System, 2996 photodiode array (PDA) detector, column heater and Thermabeam (TMD) Electron Ionization Mass spectrometry detector. Chromatographic separation was achieved in a Waters Xbridge C_{18} column (150 x 2.1 mm, 3.5

μm) that was kept at 40^0C. The first eluent comprised of water (containing 10 mM Formic acid) (C) and acetonitrile (D) (70:30) at 0.2 $ml.min^{-1}$. The gradient table of the chromatographic process is summarised in Table 14. The TMD detector was operated in positive scan mode (50 – 650 amu) with a gain of 10 collecting 1 spectrum per second. The nebuliser temperature was set at 90^0C, the expansion region temperature at 80^0C and the source temperature at 225^0C. The total volume of post-column eluent was sent to the TMD detector and helium was used as the nebulisation gas at 30 $L.h^{-1}$. The TMD detector was tuned every day prior to starting an analysis run and caffeine was injected as the test compound to ensure functionality of the total system. The injection volume was 5 μl for all fractions.

Table 14: Gradient conditions on the Waters 2695 solvent delivery system.

Time	Flow	% C*	% D#	Curve
0.0	0.20	70	30	6
1.0	0.20	70	30	6
40.0	0.20	0	100	6
48.0	0.20	0	100	4
50.0	0.20	70	30	3
60.0	0.20	70	30	6

* 10 mM Formic acid in water, # acetonitrile.

3. RESULTS

3.1 Extraction of roots and leaves

The percentage yield of the root and leaf extracts of *C. triloba* is shown in Table 15. The hexane and DCM root extracts had the lowest percentage yields (0.51% and 0.52% respectively). These extracts may have contained low concentrations of the various compounds. The DCM: methanol (1:1) leaf extract had the highest percentage yield (21.39%). This extract may have contained high concentrations of the various compounds.

Table 15: Percentage yield of the root and leaf extracts of *C. triloba*.

Part of the plant	Extract	Mass of plant material (g)	Mass of extract (g)	Percentage yield of extract
Root	Hexane	470.0	2.38	0.51
	DCM	470.0	2.43	0.52
	DCM: Methanol (1:1)	470.0	24.47	5.21
	Methanol	470.0	11.94	2.54

	Aqueous	207.49	5.09	2.45
Leaves	Hexane	281.50	9.87	3.50
	DCM	281.50	7.42	2.64
	DCM: Methanol (1:1)	281.50	60.21	21.39
	Methanol	281.50	13.84	4.92

3.2 Evaluation of the growth inhibitory potential of *C. triloba* extracts on three cancer cell lines

3.2.1 Determination of the growth inhibition values

The percentage of growth inhibition (%GI) exhibited by the root and leaf extracts on three cancer cell lines (A375, MDA-MB-231 and WHCO1) is tabulated in Table 16. For some extracts, decreased growth inhibition of the cell lines was observed with increasing concentration of the extract. This could be due to the solubility of the extracts because at high concentrations the extracts become more difficult to dissolve. The hexane root extract exhibited the highest % GI on all three cancer cell lines (81.35%, 65.77% and 78.61% GI at 50 µg.ml^{-1}, respectively). On the other hand, a moderate %GI was detected when the A375 cells were treated with the DCM (50.54% GI at 50 µg.ml^{-1}) and DCM: methanol (1:1) (48.20% at 50 µg.ml^{-1}) root extracts. Similar results were obtained when the MDA-MB-231 cells were treated with the DCM: methanol (1:1) (42.40% GI at 50 µg.ml^{-1}) and aqueous root extracts (49.56% GI at 25 µg.ml^{-1}). In contrast, the leaf extracts exhibited a low %GI on all three cell lines. The leaf extract may lack cancer targeting compounds. Therefore, the hexane root extract was used in future experiments.

Table 16: Percentage of growth inhibition exhibited by the root and leaf extracts on three cancer cell lines.

Part of the plant	Extract	A375 (melanoma)		MDA –MB-231 (breast)		WHCO1 (esophageal)	
		25 µg.ml^{-1} ± SEM	50 µg.ml^{-1} ± SEM	25 µg.ml^{-1} ± SEM	50 µg.ml^{-1} ± SEM	25 µg.ml^{-1} ± SEM	50 µg.ml^{-1}± SEM
Root	Hexane	87.15 ± 0.87	81.35 ± 0.60	63.48 ± 0.98	65.77 ± 0.76	81.35 ± 0.58	78.61 ± 1.02
	DCM	26.37 ± 4.15	50.54 ± 1.76	23.65 ± 1.72	29.93 ± 0.35	29.40 ± 1.07	30.32 ± 0.41
	DCM: Methanol (1:1)	31.28 ± 2.05	48.20 ± 0.80	41.06 ± 0.38	42.40 ± 1.34	22.65 ± 1.14	20.11 ± 1.67
	Methanol	12.23 ± 1.63	14.77 ± 2.48	12.53 ± 0.58	10.29 ± 0.50	-15.07 ± 2.66	-13.41 ± 1.49
	Aqueous	23.60 ± 1.02	29.52 ± 0.98	49.56 ± 1.31	32.94 ± 0.96	38.51 ± 0.63	29.32 ± 1.40
Leaves	Hexane	24.12 ± 1.48	12.11 ± 1.40	21.80 ± 0.23	24.85 ± 1.27	-5.89 ± 0.46	-15.48 ± 1.00
	DCM	27.17 ± 1.90	29.88 ± 5.85	9.82 ± 2.12	6.86 ± 0.23	17.73 ± 2.82	-17.14 ± 0.91
	DCM: Methanol (1:1)	-3.26 ± 1.54	19.03 ± 3.61	2.81 ± 0.50	-14.29 ± 0.19	21.92 ± 3.03	7.68 ± 1.49
	Methanol	13.86 ± 2.68	14.21 ± 1.48	0.50 ± 2.35	3.18 ± 0.60	-28.39 ± 3.94	-9.92 ± 4.07

SEM represents the standard error of mean.

3.2.2 Morphological features of the cells that were treated with the hexane extracts

The morphological features of the untreated or treated cells were observed by microscopic analysis. The untreated or DMSO treated cells remained healthy and attached (Figure 18A, 18B, 19A, 19B, 20A and 20B). The cells treated with the active hexane root extract appeared rounded with cytoplasmic shrinkage (signs of apoptosis which are indicated by the arrows) (Figure 18C, 18D, 19C, 19D, 20C and 20D). In contrast, the cancer cells treated with the hexane leaf extract appeared healthy and attached (Figure 18E, 18F, 19E, 19F, 20E and 20F). This could be due to the lack of cancer targeting compounds. Thus, these results confirmed the growth inhibition of the hexane root extract.

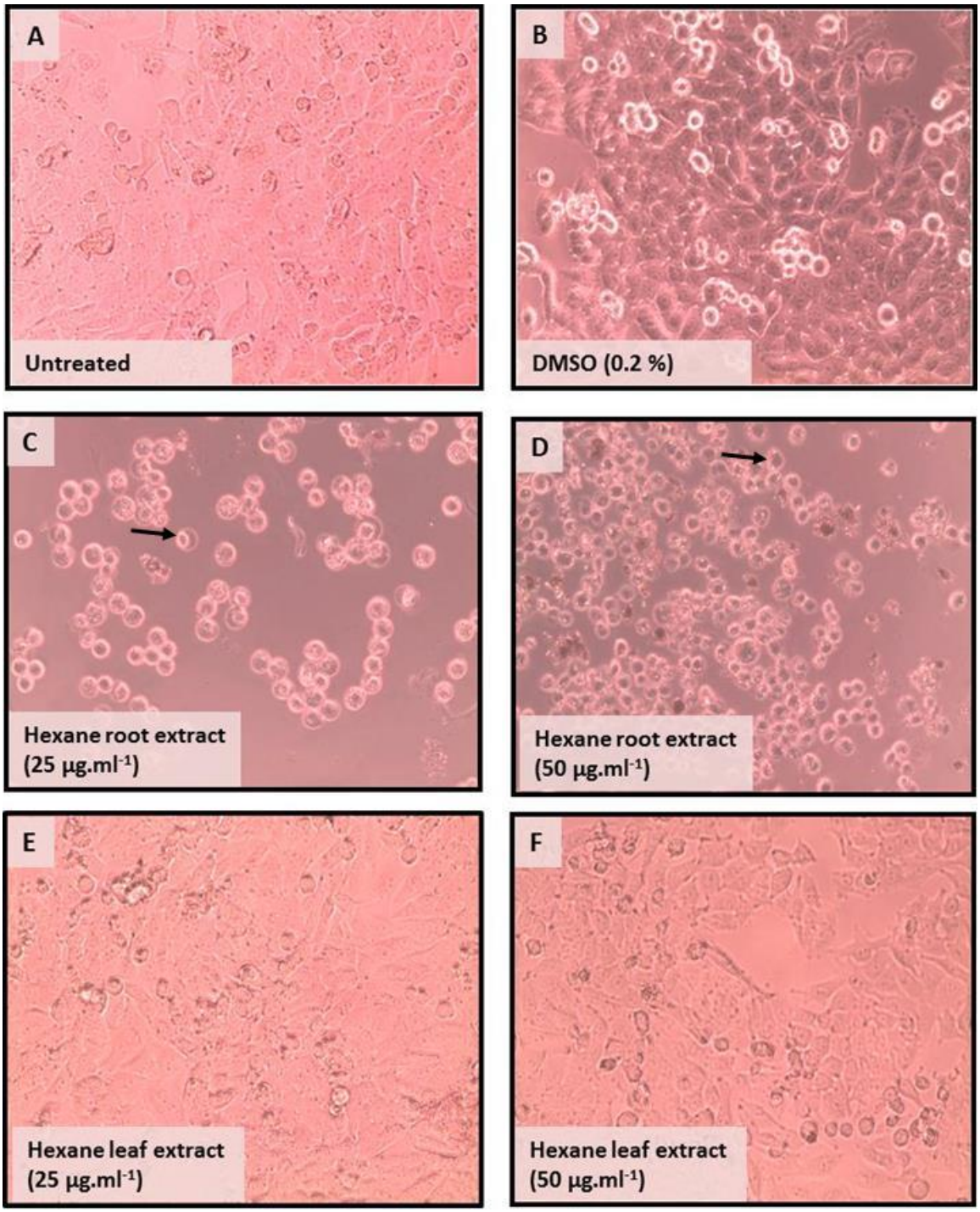

Figure 18: Morphology of untreated A375 cells (A) compared to A375 cells treated with DMSO [0.2 %] (B), hexane root extract [25 µg.ml^{-1}and 50 µg.ml^{-1}] (C-D) and hexane leaf extract [25 µg.ml^{-1}and 50 µg.ml^{-1}] (E-F) (100X magnification).

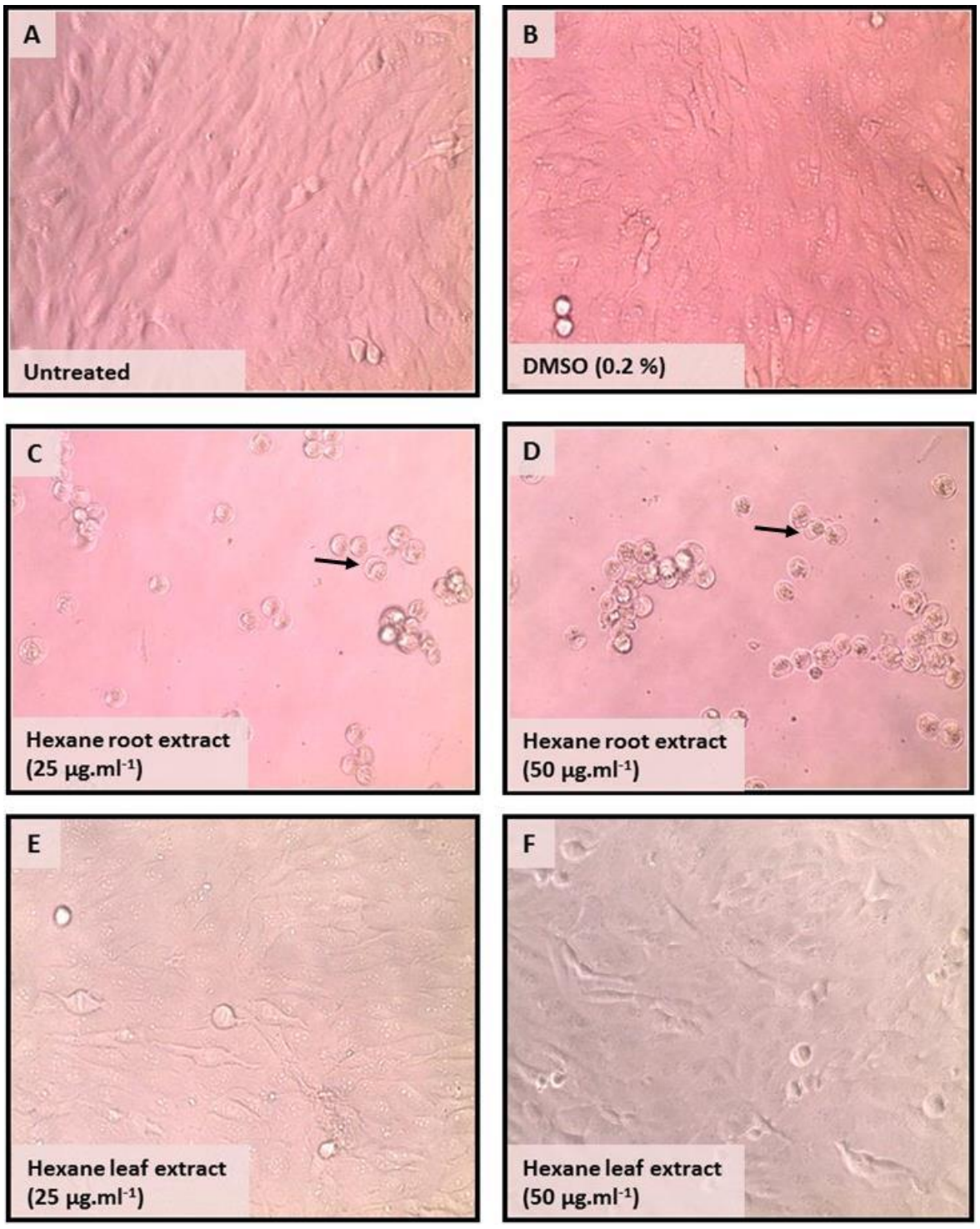

Figure 19: Morphology of untreated MDA-MB-231 cells (A) compared to MDA-MB-231 cells treated with DMSO [0.2 %] (B), hexane root extract [25 µg.ml^{-1}and 50 µg.ml^{-1}] (C-D) and hexane leaf extract [25 µg.ml^{-1}and 50 µg.ml^{-1}] (E-F) (100X magnification).

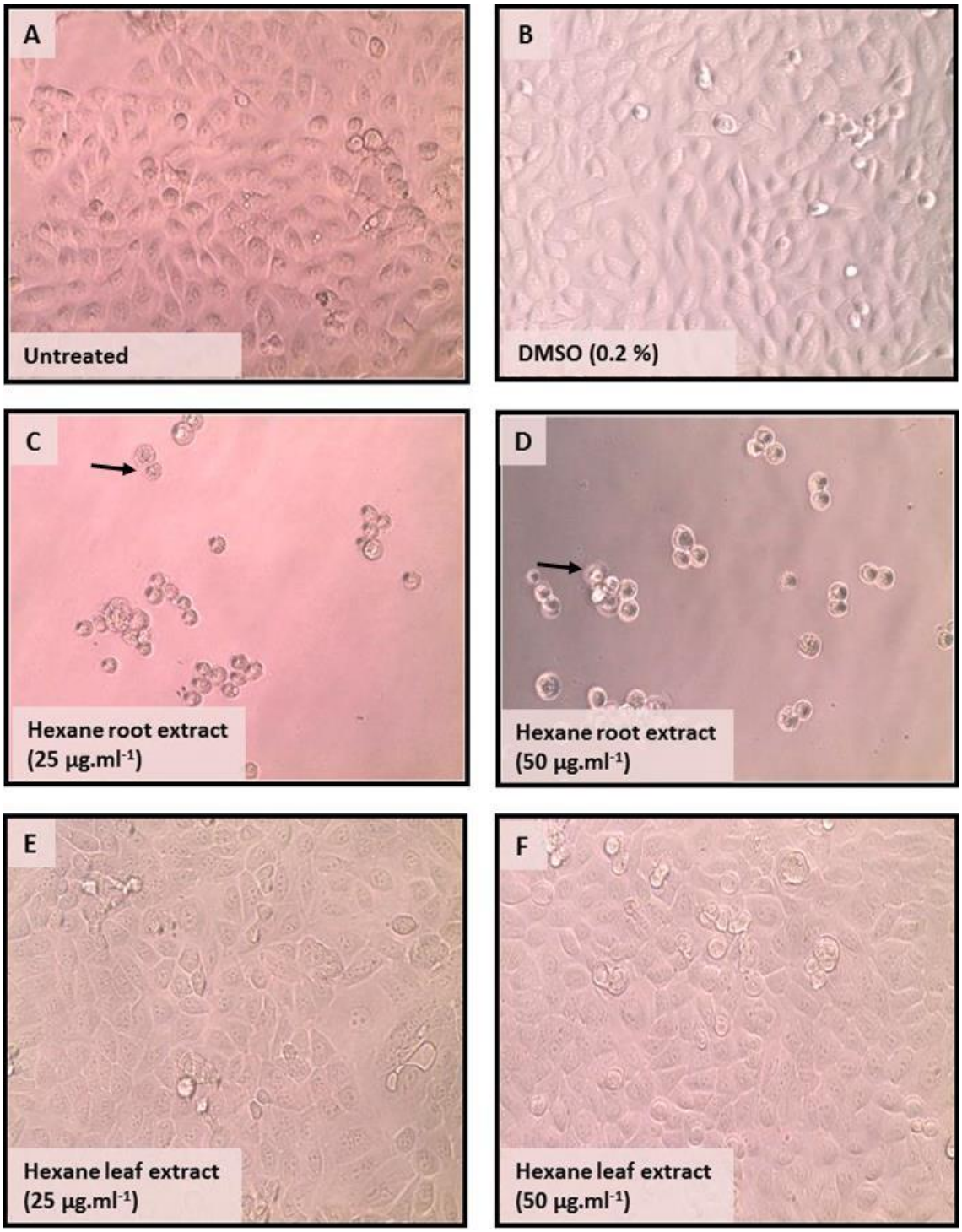

Figure 20: Morphology of untreated WHCO1 cells (A) compared to WHCO1 cells treated with DMSO [0.2 %] (B), hexane root extract [25 µg.ml^{-1}and 50 µg.ml^{-1}] (C-D) and hexane leaf extract [25 µg.ml^{-1}and 50 µg.ml^{-1}] (E-F) (100X magnification).

3.3 Investigation of the different mobile phases for optimizing the separation of the compounds of the hexane root extract

The TLC plates in Figure 21 depict the degree of separation of the compounds after exposing the hexane root extract to different mobile phases. The hexane mobile phase (Lane 6) held back most of the compounds at the baseline and allowed the separation of one band. The hexane: DCM mobile phase at a ratio of 1: 9 (Lane 5) allowed for the separation of two bands and initiated the movement of some compounds from the baseline. The hexane: DCM mobile phase at a ratio of 3: 7 (Lane 4) began the actual separation of the compounds. Subsequently the hexane: DCM mobile phase was chosen for column chromatography as these solvents showed the potential to separate the compounds of the hexane root extract. The other three mobile phases (Lane 1 - ethyl acetate: hexane: ethanol [1:8:1], Lane 2 - hexane: ethanol [9: 1], Lane 3 - ethanol: petroleum ether [1:9]) were not used because these permitted poor separation and allowed the compounds to run too quickly towards the solvent front.

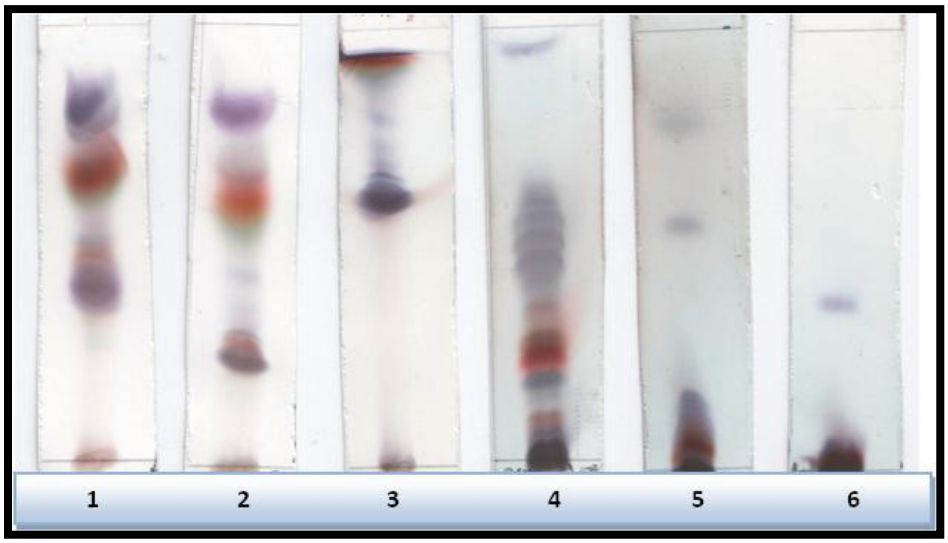

Figure 21: Separation of the compounds of the hexane root extract using different mobile phases. Lane 1- ethyl acetate: hexane: ethanol (1:8:1), Lane 2 - hexane: ethanol (9: 1), Lane 3 - ethanol: petroleum ether (1:9), Lane 4 – hexane: DCM (3: 7), Lane 5 - hexane: DCM (1:9), Lane 6 - hexane.

We then further optimized the separation of the compounds of the hexane root extract. Figure 22 shows the separation of the compounds was achieved by slowly increasing the polarity of the hexane: DCM mobile phase. A similar principle was applied to the column.

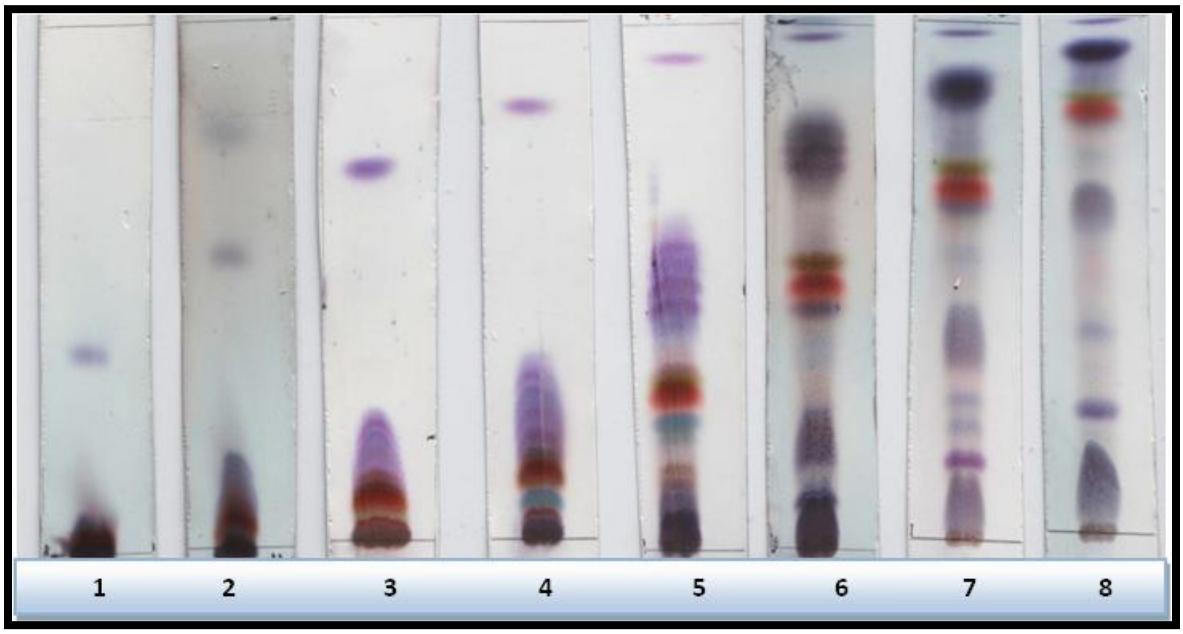

Figure 22: Separation of the compounds of the hexane root extract by using different ratios of hexane: DCM. Lane 1 - 1:0, Lane 2 - 1:9, Lane 3 - 88:12, Lane 4 - 85: 15, Lane 5 - 60:40, Lane 6 - 40:60, Lane 7 - 20:80, Lane 8 - 0:1.

3.4 TLC of the fractions that were collected by column chromatography

Column chromatography was ran twice with the hexane root extract. The fractions that were collected from both column runs were grouped into two sets as shown in Table 17. Set A represented the 91 fractions that were collected from column run 1 while set B represented the 83 fractions that were collected from column run 2 (results not shown) (Figure 23 and Table 18). Thereafter, the fractions with the same or similar band pattern or solution colour (colour of the solvent after the fraction has been dissolved in it) were pooled into two other sets. The fractions that were collected from column run 1 were pooled into 9 fractions (1A-9A) which were represented by Set C. The fractions that were collected from column run 2 were pooled into 8 fractions (1B-8B) which were represented by Set D (Table 17). The fractions from set C and set

D were then ran on TLC plates as shown in Figure 24. Thereafter, the fractions from these two sets were combined according to their band pattern (Figure 24 and Table 19). Subsequently a total of ten combined fractions (F1-F10) were isolated from the hexane root extract. The combined fractions were then ran on TLC plates as shown in Figure 25. The R*f* values and band colours of the these fractions are shown in Table 20. The yields of these fractions are shown in Table 21. Fractions F1, F7 and F9 had the highest percentage yields (232.5 mg, 276.1 mg, 232 mg, respectively) while fraction F3 had the lowest percentage yield (5.9 mg). In addition, fractions F2, F3, F4 and F5 formed crystals when they were concentrated and dried (Figure 26).

Table 17: Fractions that were collected by column chromatography were organized into sets.

Origin of fractions	**Set**
Fractions collected from column run 1	A
Fractions collected from column run 2	B
Fractions collected from column run 1 were pooled into 9 fractions (1A-9A)	C
Fractions collected from column run 2 were pooled into 8 fractions (1B-8B)	D

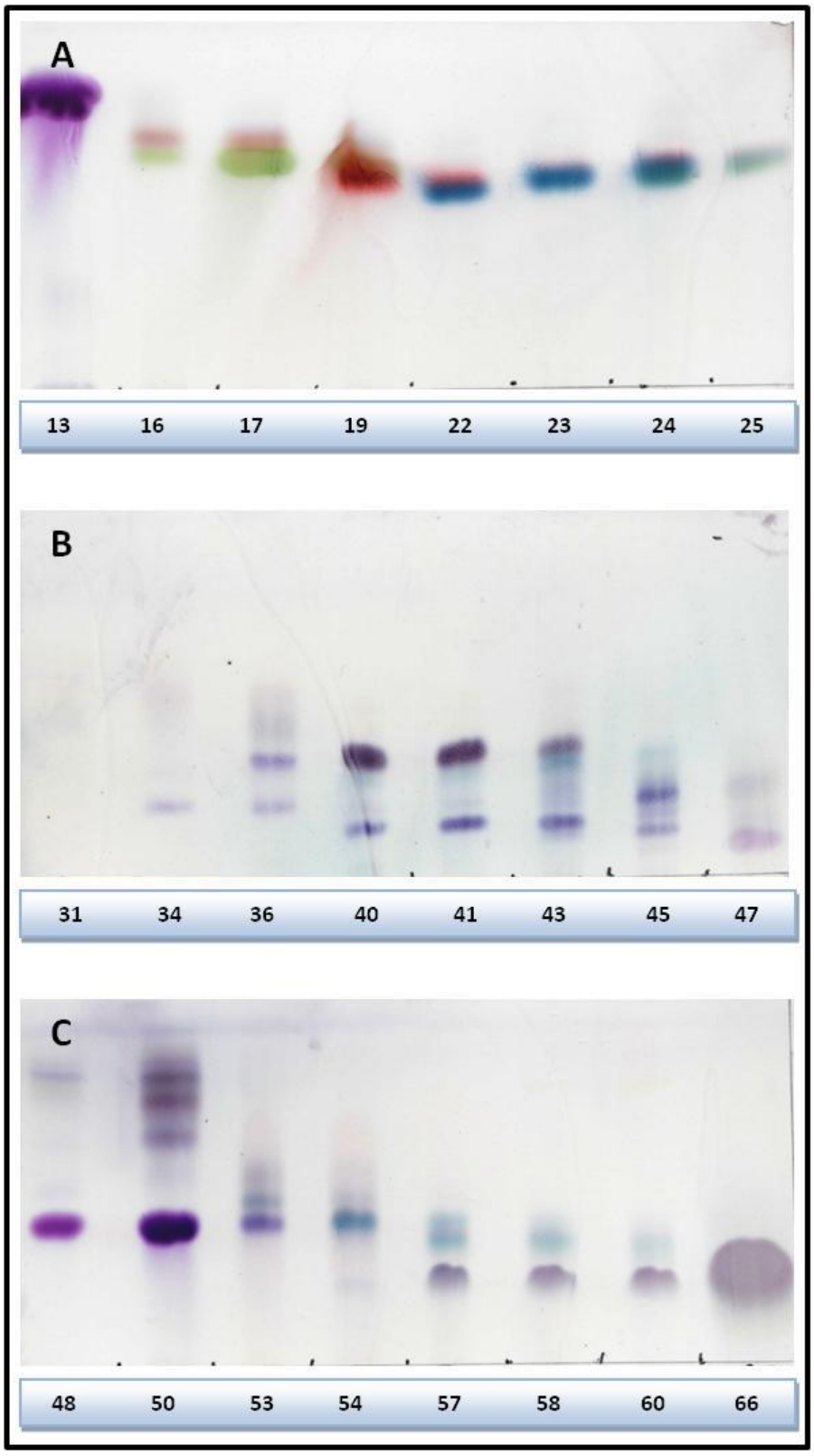
A
13 16 17 19 22 23 24 25
B
31 34 36 40 41 43 45 47
C
48 50 53 54 57 58 60 66

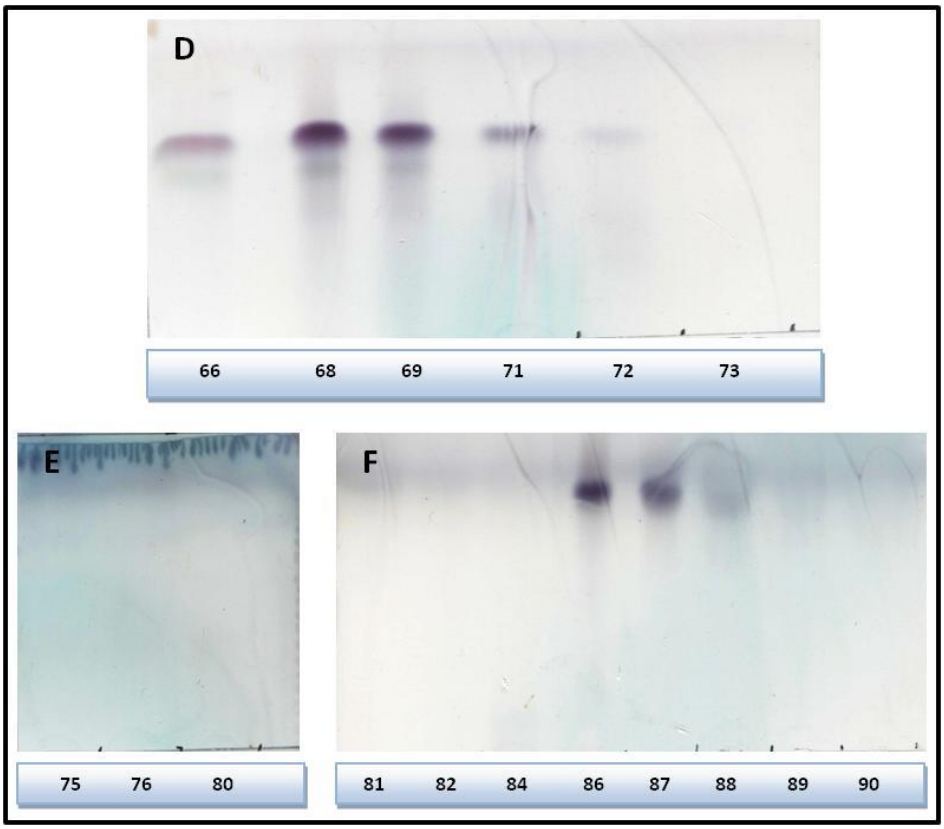

Figure 23: TLC of the fractions (13-90) (A-F) that were collected from column run 1. These fractions were part of set A.

Table 18: Fractions collected from column run 1 by using different mobile phases. These fractions were represented by set A. The same or similar fractions were pooled into 9 fractions (1A-9A) which were represented by set C.

Fraction	Fractions pooled	Solution colour*	Mobile phase	Solvent ratio
1A	1-15	Light yellow	Hexane : DCM	60 : 40
2A	16 - 17	Yellow	Hexane : DCM	60 : 40
	18 - 21	Dark orange	Hexane : DCM	60 : 40
3A	22 - 23	Orange	Hexane : DCM	60 : 40
	24 - 27	Yellow	Hexane : DCM	60 : 40
	28 - 31	Yellow	Hexane : DCM	40 : 60
4A	32 - 34	Light orange	Hexane : DCM	40 : 60
	35 - 43	Orange	Hexane : DCM	40 : 60
5A	44 - 47	Orange	DCM	100
	48 - 49	Orange	DCM : Ethyl acetate	90 : 10
	50 -51	Brownish red	DCM : Ethyl acetate	90 : 10
6A	52 - 55	Dark red	DCM : Ethyl acetate	90 : 10
7A	56 - 58	Reddish orange	DCM : Ethyl acetate	90 : 10
	59 - 60	Orange	DCM : Ethyl acetate	90 : 10
	61 - 66	Orange	DCM : Ethyl acetate	70 : 30
	67 – 72	Orange	DCM : Ethyl acetate	60 : 40
8A	73 - 74	Light orange	DCM : Ethyl acetate	60 : 40
	75	Clear	DCM : Ethyl acetate	50 : 50
	76 - 77	Clear	DCM : Ethyl acetate	50 : 60

***** Colour of the solvent after the fraction has been dissolved in it.

Table 18 continued: Fractions collected from column run 1 by using different mobile phases. These fractions were represented by set A. The same or similar fractions were pooled into 9 fractions (1A-9A) which were represented by set C.

Fraction	Fractions pooled	Solution colour*	Mobile phase	Solvent ratio
8A	78	Clear	DCM : Ethyl acetate	30- 60
	79 - 80	Clear	DCM : Ethyl acetate	20 : 80
	81	Clear	Ethyl acetate	100
	82	Clear	Ethyl acetate : Methanol	80 : 20
9A	83 - 85	Dark purple	Ethyl acetate : Methanol	80 : 20
	86 - 90	Dark purple	Ethyl acetate : Methanol	70 : 30
	91	Dark purple	Ethyl acetate : Methanol	50 : 50

***** Colour of the solvent after the fraction has been dissolved in it.

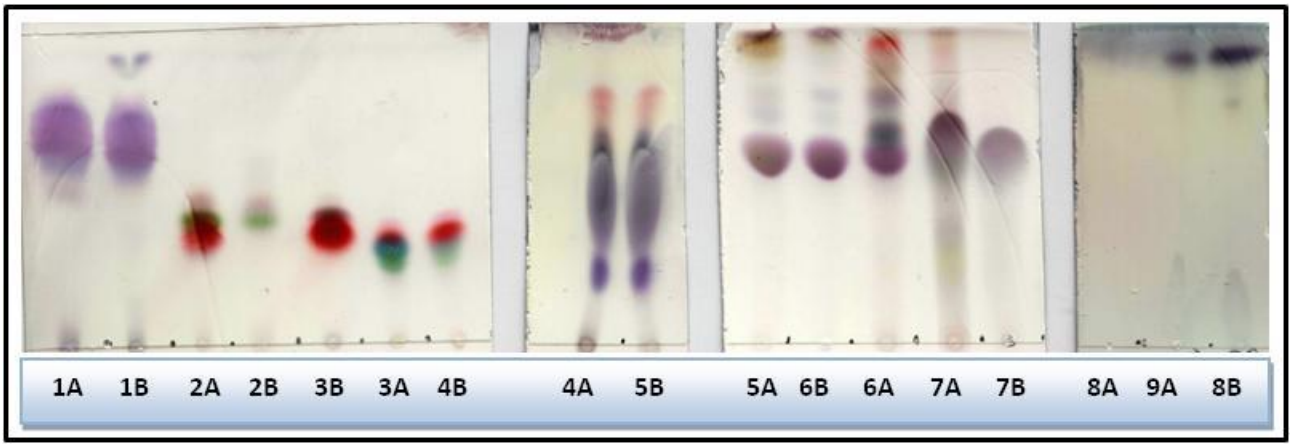

Figure 24: TLC of fractions 1A-9A (originated from column run 1, set C) and 1B-8B (originated from column run 2, set D).

Table 19: Fractions 1A-9A (set C) and 1B-8B (set B) were combined according to their band pattern to produce ten fractions.

Combined fraction	Fractions from set C and D
F1	1A, 1B
F2	2A
F3	2B
F4	3B
F5	3A, 4B
F6	4A, 5B
F7	5A, 6B
F8	6A
F9	7A, 7B
F10	8A, 8B, 9A

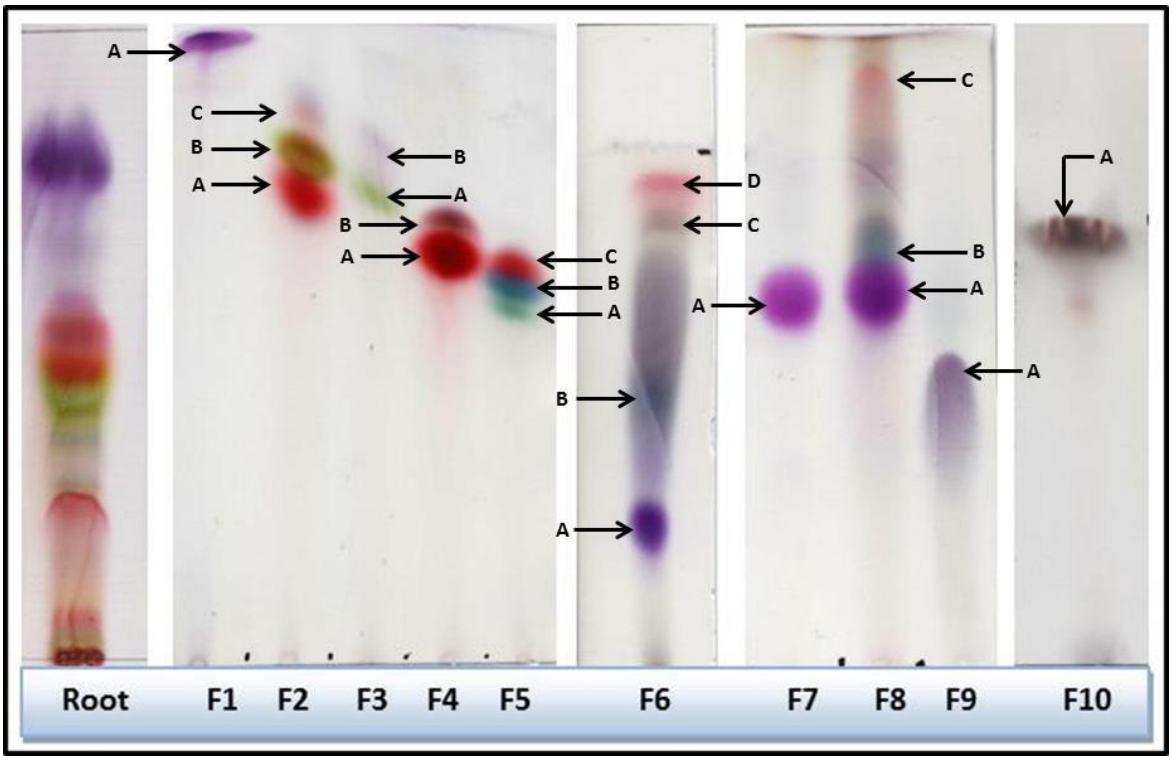

Figure 25: TLC of the hexane root extract and fractions F1-F10.

Table 20: Mobile phases used to develop fractions F1-F10 and the R*f* values and colours of the bands of these fractions.

Fraction	Mobile phase	Band	Colour	R*f* value
F1	Hexane : DCM (60 : 40)	A	Purple	0.98
F2	Hexane : DCM (60 : 40)	A	Red	0.77
		B	Green	0.83
		C	Light red	0.86
F3	Hexane : DCM (60 : 40)	A	Green	0.74
		B	Purple	0.81
F4	Hexane : DCM (60 : 40)	A	Red	0.65
		B	Reddish brown	0.70
F5	Hexane : DCM (60 : 40)	A	Green	0.54
		B	Blue	0.59
		C	Red	0.62
F6	Hexane : DCM (40 : 60)	A	Purple	0.33
		B	Dark green	0.58
		C	Black	0.88
		D	Light red	0.94
F7	DCM : Ethyl acetate (90 : 10)	A	Purple	0.62
F8	DCM : Ethyl acetate (90 : 10)	A	Purple	0.63
		B	Dark green	0.72
		C	Light red	0.95
F9	DCM : Ethyl acetate (90 : 10)	A	Purple	0.49
F10	Ethyl acetate : Methanol (80 : 20)	A	Brownish black	0.73

Table 21: Yield of fractions F1-F10.

Fraction	Mass of fraction (mg)
F1	232.5
F2	96.7
F3	5.9
F4	160
F5	86.2
F6	140.9
F7	276.1
F8	47.7
F9	232
F10	95.3

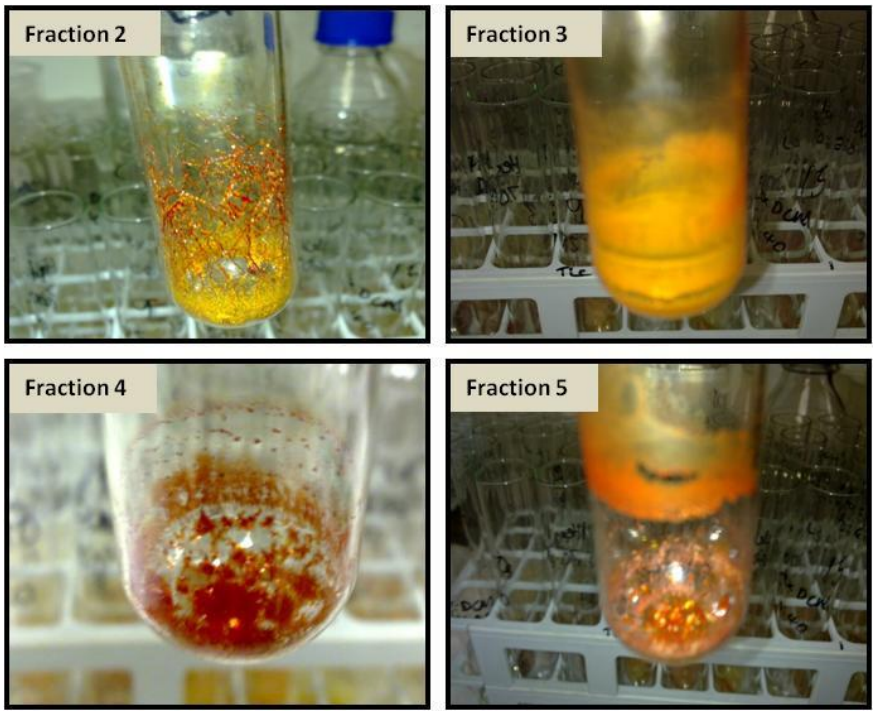

Figure 26: Crystals formed by fractions F2, F3, F4 and F5.

3.5 Evaluation of the growth inhibitory potential of the fractions (F1-F10) on two melanoma cell lines

Since the hexane root extract showed the best activity on the A375 cell line, we decided to determine the %GI of the fractions on this cell line and another melanoma cell line (UACC-62) (Figure 27 and 28). Fractions F2, F4, F5 and F8 exhibited a high %GI on both the A375 (89.85, 89.39, 90.81 and 75.51 %GI at 25 $\mu g.ml^{-1}$, respectively) and UACC-62 (74.54, 97.55, 86.96 and 73.29 %GI at 25 $\mu g.ml^{-1}$, respectively) cell lines. Fraction F7 exhibited a moderate %GI (47.70%) on the A375 cells. The other fractions (F3, F6, F7, F9 and F10) exhibited no growth inhibition or a low %GI on the melanoma cells. Therefore fractions F2, F4, F5 and F8 were further investigated.

The ANOVA test was conducted on the growth inhibitory potential data to determine if there were significant differences between the A375 and UACC-62 melanoma cell line. As shown Figures 27 and 28, some fractions exhibited significantly different growth inhibition values between cell lines while other fractions showed no significant difference of the growth inhibition values between cell lines. The most active fractions (F2, F4, F5 and F8) exhibited similar growth inhibition values at 12 $\mu g.ml^{-1}$ and/or 25 $\mu g.ml^{-1}$. Statistical analysis confirmed that these four fractions had the same cytotoxic effect on both melanoma cell lines.

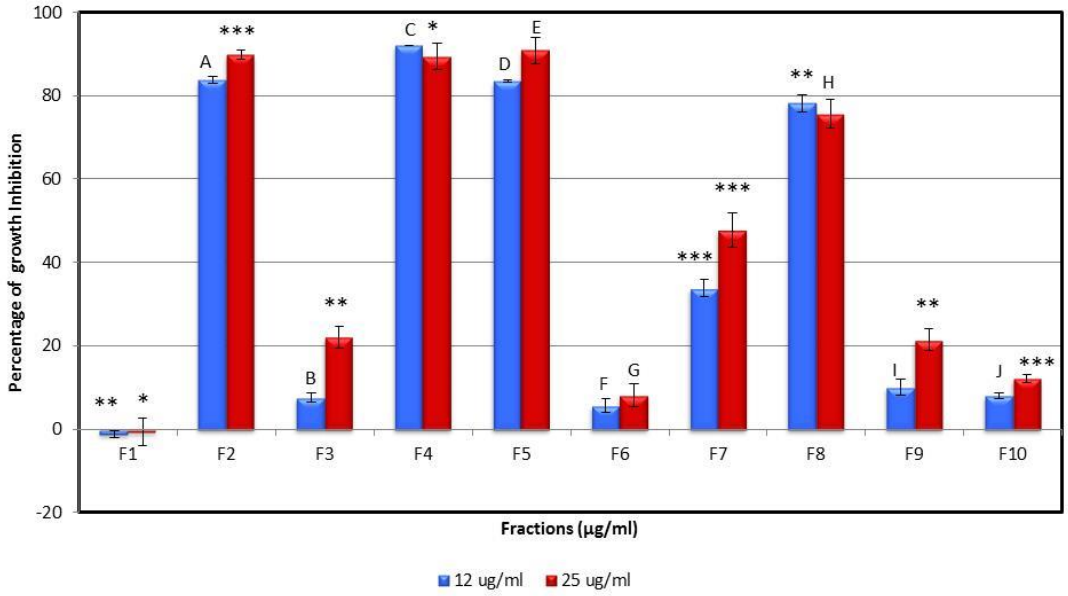

Figure 27: Percentage of growth inhibition (%GI) exhibited by the fractions on the A375 cells. A-J represents no significant different (P> 0.05) between A375 and UACC-62 cells that were treated with respective fractions. * (P < 0.001), * (P < 0.05), ** (P < 0.01) represents significant different between A375 and UACC-62 cells that were treated with respective fractions.**

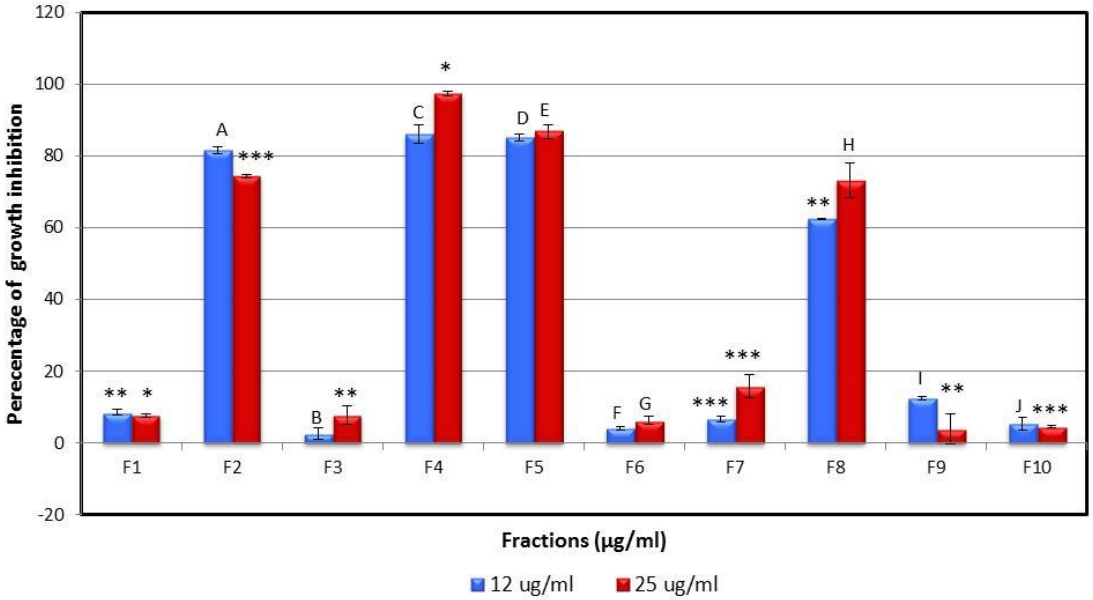

Figure 28: Percentage of growth inhibition (%GI) exhibited by the fractions on the UACC-62 cells. A-J represents no significant different (P> 0.05) between UACC-62 and A375 cells that were treated with respective fractions. * (P < 0.001), * (P < 0.05), ** (P < 0.01) represents significant different between UACC-62 and A375 cells that were treated with respective fractions.**

3.6 Determination of the IC_{50} and total growth inhibition (TGI) values of the active fractions

Figures 29 and 30 illustrates the dose response curves of the melanoma cells treated with the standards (camptothecin and doxorubicin) and active fractions (F2, F4, F5 and F8). This data was used to determine the total growth inhibition (TGI) (concentration of the fraction that inhibits 85-98% of cells) values. In addition, the logarithmic form of the dose response curves was generated for calculation of the IC_{50} (concentration of the fraction that inhibits 50% of cells) values (Appendix 2). The R squared values (between 0.97-0.99) of the logarithmic graphs indicated that the data points fitted accurately on the graph (Tables 22 and 23).

The IC_{50} and TGI values of the fractions were compared to the standards (camptothecin and doxorubicin) as shown in Tables 22 and 23. It was evident that the fractions had higher IC_{50} and TGI values for both melanoma cell lines. However there was an exception to this data as fraction F4 (98.36% of cells were inhibited at 25 $\mu g.ml^{-1}$) had the same TGI value as doxorubicin (95% of cells were inhibited at 25 $\mu g.ml^{-1}$) in terms of the UACC-62 cell line. Therefore, we deciphered that fraction F4 was the most active fraction. The IC_{50} and TGI values for this fraction were 0.70 $\mu g.ml^{-1}$ and 12.50 $\mu g.ml^{-1}$, respectively (A375 cell line) or 0.39 $\mu g.ml^{-1}$ and 25 $\mu g.ml^{-1}$, respectively (UACC-62 cell line). Taken together fraction F4 may contain the most potent anticancer compounds of *C. triloba*.

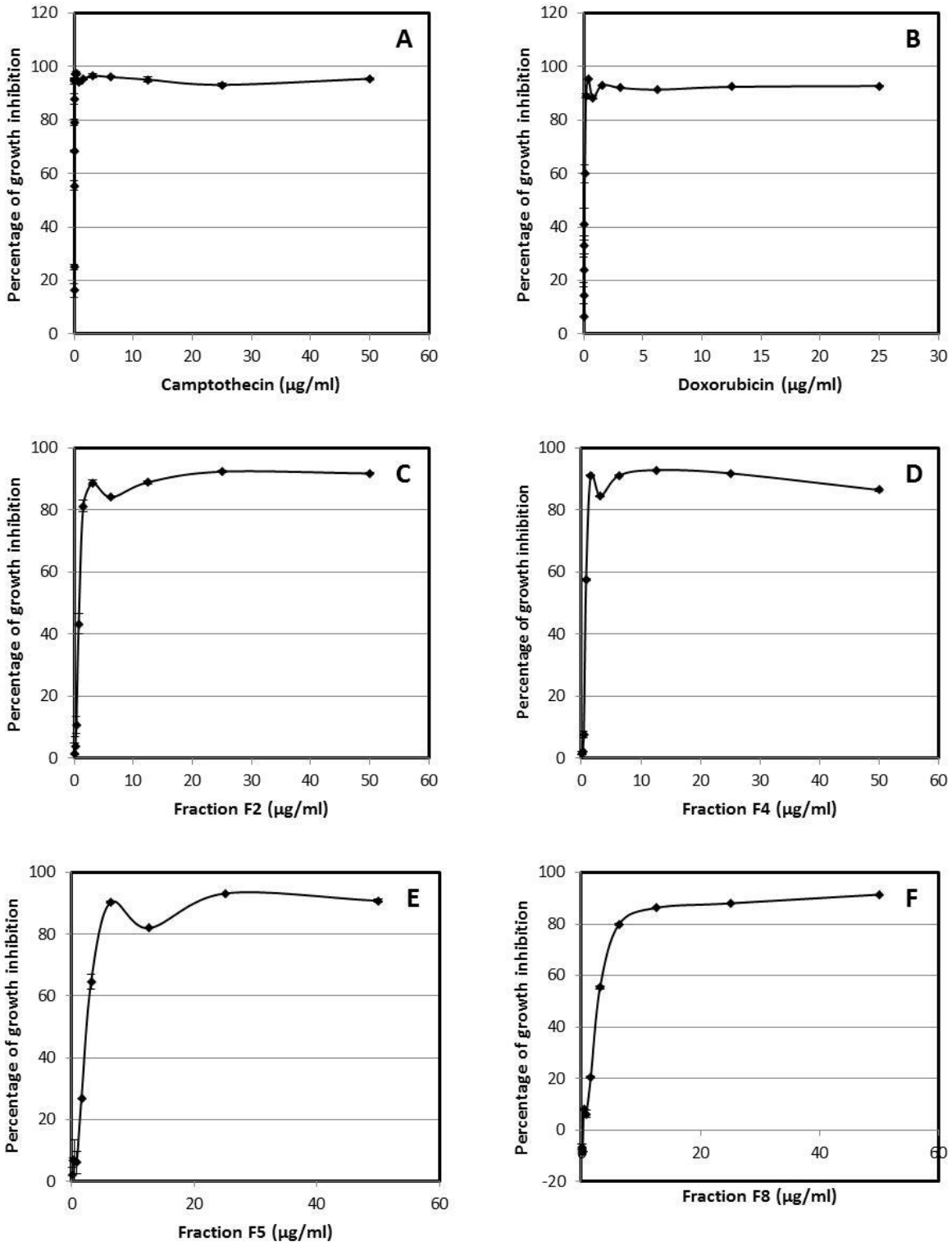

Figure 29: Dose response curves of the A375 cells treated with camptothecin (A), doxorubicin (B) and fractions F2 (C), F4 (D), F5 (E) and F8 (F).

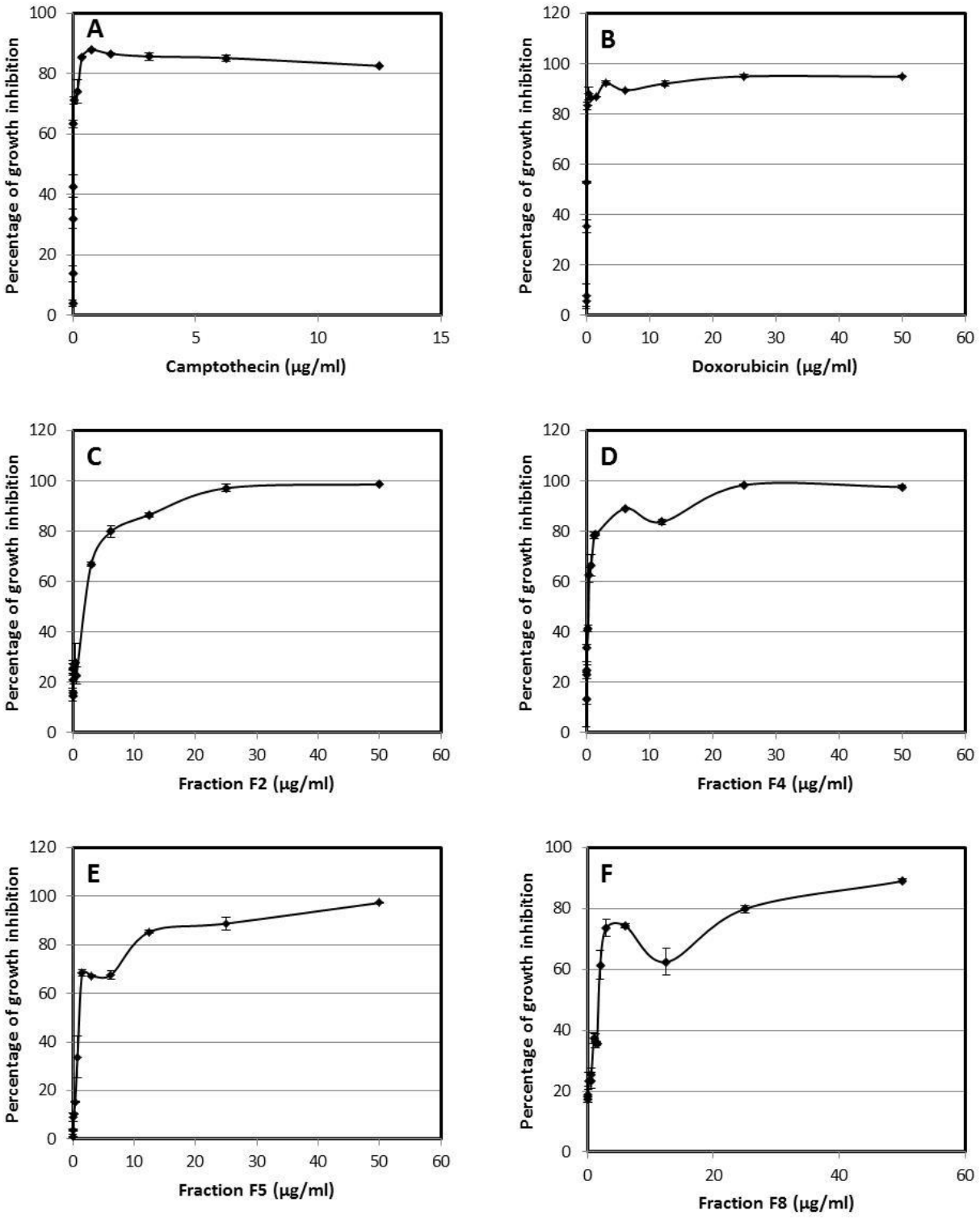

Figure 30: Dose response curves of the UACC-62 cells treated with camptothecin (A), doxorubicin (B) and fractions F2 (C), F4 (D), F5 (E) and F8 (F).

Table 22: IC_{50} and total growth inhibition (TGI) values of the standards and active fractions against the A375 cell line.

Fraction	IC_{50} (µg.ml^{-1})	TGI (µg.ml^{-1})	R Square value (Goodness of fit)
Camptothecin	0.002	0.39	0.991
Doxorubicin	0.06	0.39	0.979
F2	0.80	25.00	0.997
F4	0.70	12.50	0.995
F5	2.28	25.00	0.993
F8	2.46	50.00	0.991

IC_{50} - concentration of the fraction that inhibits 50% of cells

TGI- concentration of the fraction that inhibits 85-98% of cells

Table 23: IC_{50} and total growth inhibition (TGI) values of the standards and active fractions against the UACC-62 cell line.

Fraction	IC_{50} (µg.ml^{-1})	TGI (µg.ml^{-1})	R Square value (Goodness of fit)
Camptothecin	0.01	0.78	0.989
Doxorubicin	0.07	25.00	0.988
F2	2.58	50.00	0.987
F4	0.39	25.00	0.982
F5	1.14	50.00	0.969
F8	1.70	50.00	0.967

IC_{50} - concentration of the fraction that inhibits 50% of cells

TGI- concentration of the fraction that inhibits 85-98% of cells

3.7 Evaluation of the apoptosis inducing effects of the active fractions against two melanoma cell lines

We studied the apoptosis inducing effects of the active fractions (F2, F4, F5 and F8) against two melanoma cell lines (A375 and UACC-62) by using the BD MitoScreen assay, PE active caspase 3 assay and FITC annexin V assay The results from these assays were analysed by flow cytometry.

3.7.1 Examination of the state of the ΔΨ (mitochondrial membrane potential) by using the BD MitoScreen assay

For the BD MitoScreen assay, the data is presented on flow charts as dual parametric dot plots which combine FL-1 (for JC-1 green monomers) and FL-2 (for JC-1 red aggregates) fluorescence (Figure 31-32). The flow charts display the percentage of cells with polarized ΔΨ (quadrant Q2-right upper quadrant) and percentage of cells with depolarized ΔΨ (quadrant Q3-right lower quadrant). In terms of the untreated/unstained control data, the percentage of cells are shown in quadrant Q4 (left lower quadrant) and percentage of auto-fluorescence is shown in quadrant Q3.

Outcomes of flow cytometer analysis are described below:

The A375 cells that were left untreated or exposed to the control treatments were analysed accordingly: The untreated/unstained control contained 100% of cells (Figure 31A). This control was set up to subtract auto-fluorescence from the data that was generated. The untreated/stained control contained 5.85% of cells with depolarized ΔΨ (Figure 31B). This control was also known as the negative control. Plus positive controls were set up by using two standards. Camptothecin (6 $\mu g.ml^{-1}$ and 25 $\mu g.ml^{-1}$) induced depolarization of the ΔΨ in 35.31% and 34.61% of cells, respectively (Figure 31C and 31D). Doxorubicin (6 $\mu g.ml^{-1}$) induced depolarization of the ΔΨ in 1.98% of cells (Figure 31E). Both the negative and positive controls were used to subtract overlapping fluorescence between fluorescence channels. In addition, a DMSO control was set up and it contained 6.89% of cells with depolarized ΔΨ (Figure 31F). The effect of this control was subtracted from the data that was obtained. The following equation was used: % of cells

with depolarized ΔΨ for a specific treatment = % of cells with depolarized cells ΔΨ induced by the treatment -% of cells with depolarized ΔΨ induced by DMSO.

The A375 cells that were treated with the active fractions were analysed accordingly: Essentially we collated the data from the flow charts to obtain a graphical representation which revealed the following facts (Figure 31B-31N and 33). Fractions F2, F4, F5 and F8 (6 $\mu g.ml^{-1}$ and/or 25 $\mu g.ml^{-1}$) induced depolarization of the ΔΨ in the A375 cells. Moreover it was clear that fraction F4 (6 $\mu g.ml^{-1}$ and 25 $\mu g.ml^{-1}$) induced depolarization of the ΔΨ in a higher percentage of cells (44.31% and 78.11%, respectively) than the standards and other fractions. Hence, this fraction was more efficient in inducing depolarization of the ΔΨ in the A375 cells than the standards. This was further elaborated by the fold increase values that are shown in Table 24.

The UACC-62 cells that were left untreated or exposed to the control treatments were analysed accordingly: The untreated/unstained control contained 99.9% of cells (Figure 32A). The untreated/stained control contained 9.53% of cells with depolarized ΔΨ (Figure 32B). Also, positive controls were set up by using two standards. Camptothecin (6 $\mu g.ml^{-1}$ and 25 $\mu g.ml^{-1}$) induced depolarization of the ΔΨ in 29.9% and 38.8% of cells, respectively (Figure 32C-32D). Doxorubicin (6 $\mu g.ml^{-1}$) induced depolarization of the ΔΨ in 24.5 % of cells (Figure 32E). In addition, a DMSO control was set up and it contained 11.5% of cells with depolarized ΔΨ (Figure 32F). These controls were applied to the analysis as described in the previous paragraph.

The UACC-62 cells that were treated with the active fractions were analysed accordingly: Essentially we collated the data from the flow charts to obtain a graphical representation which revealed the following facts (Figure 32B-32N and 34). Fractions F2, F4, F5 and F8 (6 $\mu g.ml^{-1}$ and 25 $\mu g.ml^{-1}$) induced depolarization of the ΔΨ in the UACC-62 cells. Moreover it was clear that fractions F4 (6 $\mu g.ml^{-1}$ and 25 $\mu g.ml^{-1}$) and F2 (6 $\mu g.ml^{-1}$) induced depolarization of the ΔΨ in a higher percentage of cells (42.3%, 87.4% and 60% respectively) than the standards and other fractions. Hence, these two fractions were more efficient in inducing depolarization of the ΔΨ in the UACC-62 cells than the standards. This was further elaborated by the fold increase values that are shown in Table 25.

In summary, the standards and fractions elicited depolarization of the ΔΨ in the A375 and UACC-62 cells. Also, fractions F2 and F4 were the most active fractions in terms of inducing depolarization of the ΔΨ.

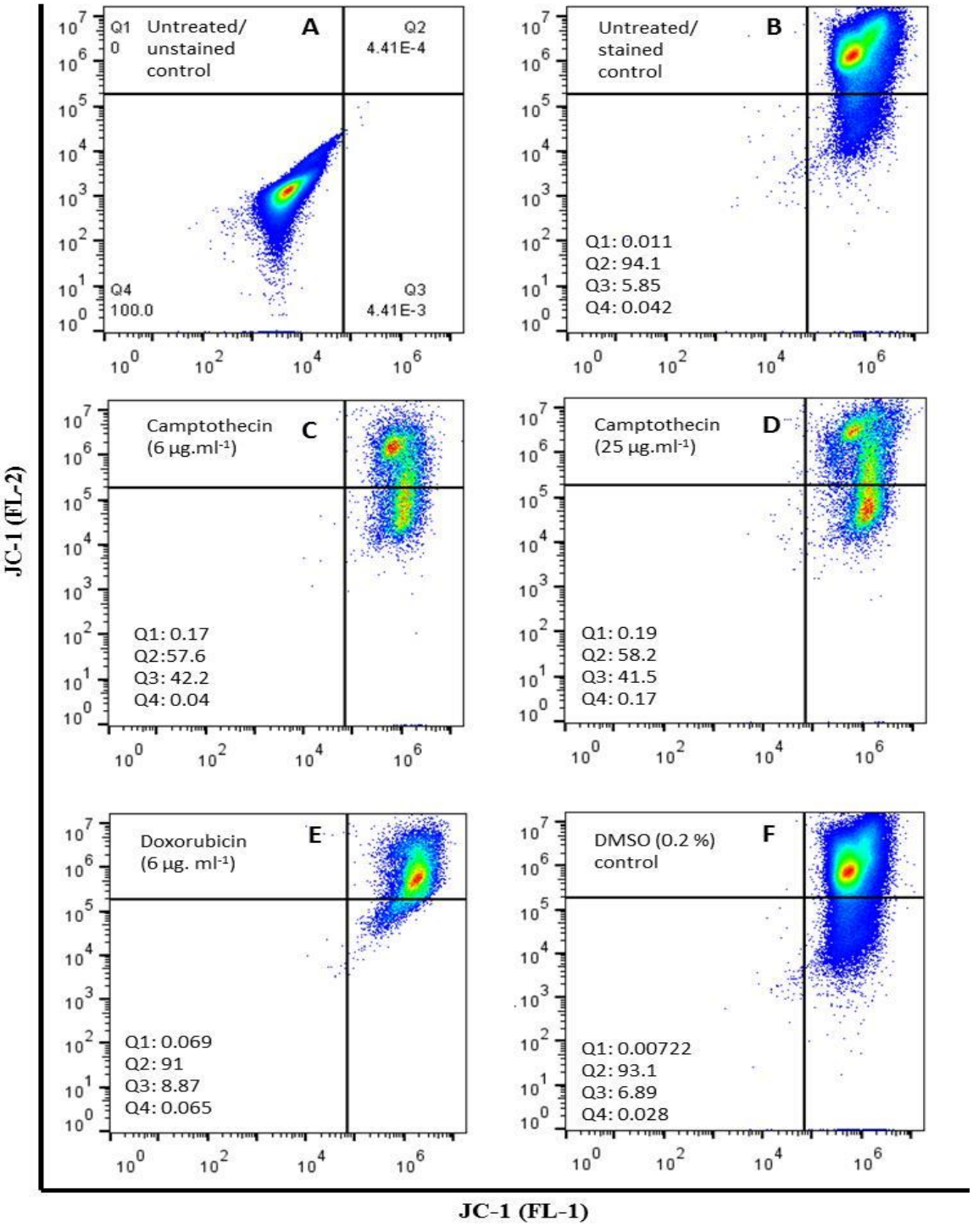

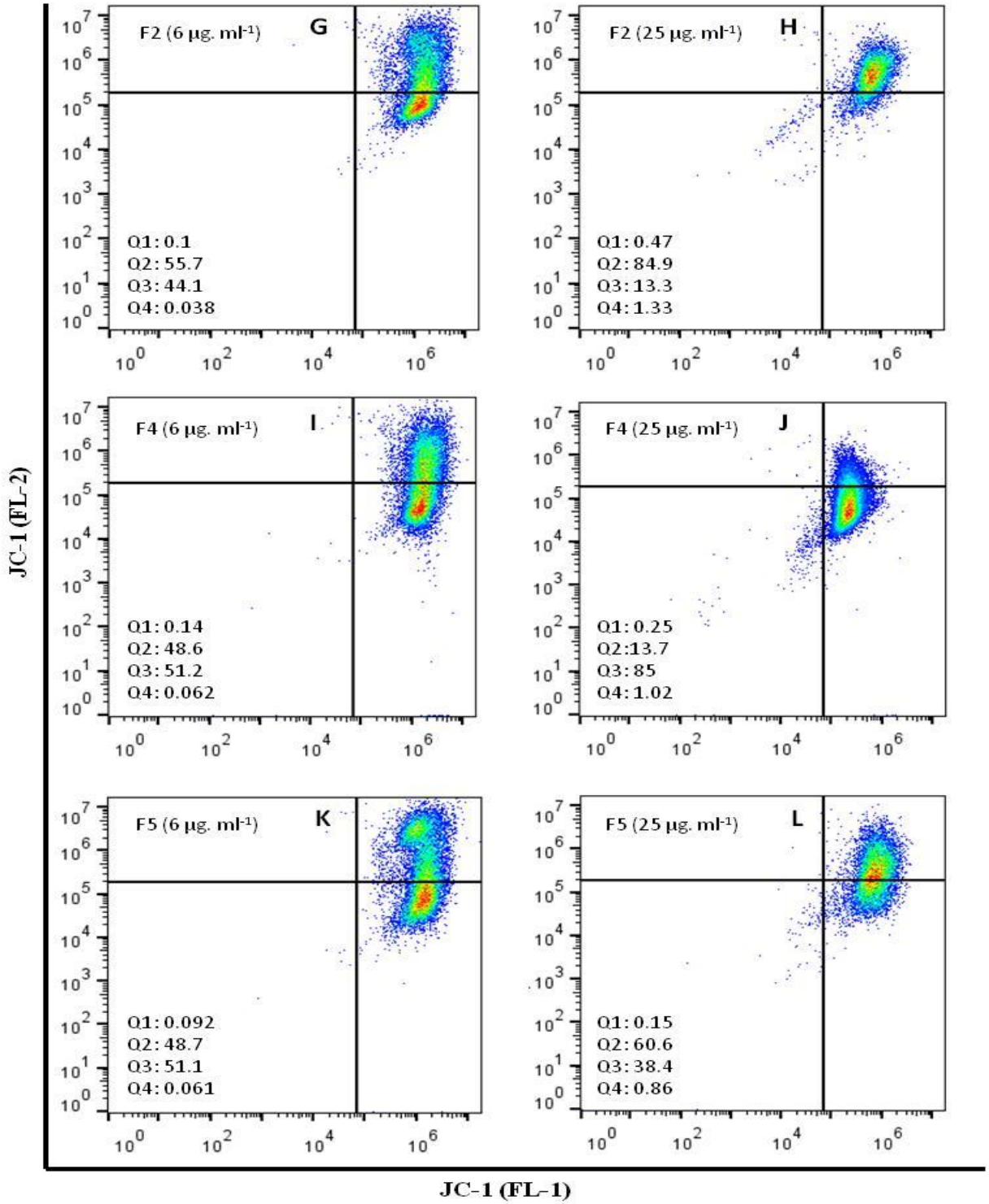
F2 (6 µg. ml-1)
G
Q1: 0.1
Q2: 55.7
Q3: 44.1
Q4: 0.038
F2 (25 µg. ml-1)
H
Q1: 0.47
Q2: 84.9
Q3: 13.3
Q4: 1.33
F4 (6 µg. ml-1)
I
Q1: 0.14
Q2: 48.6
Q3: 51.2
Q4: 0.062
F4 (25 µg. ml-1)
J
Q1: 0.25
Q2:13.7
Q3: 85
Q4: 1.02
F5 (6 µg. ml-1)
K
Q1: 0.092
Q2: 48.7
Q3: 51.1
Q4: 0.061
F5 (25 µg. ml-1)
L
Q1: 0.15
Q2: 60.6
Q3: 38.4
Q4: 0.86
JC-1 (FL-2)
JC-1 (FL-1)

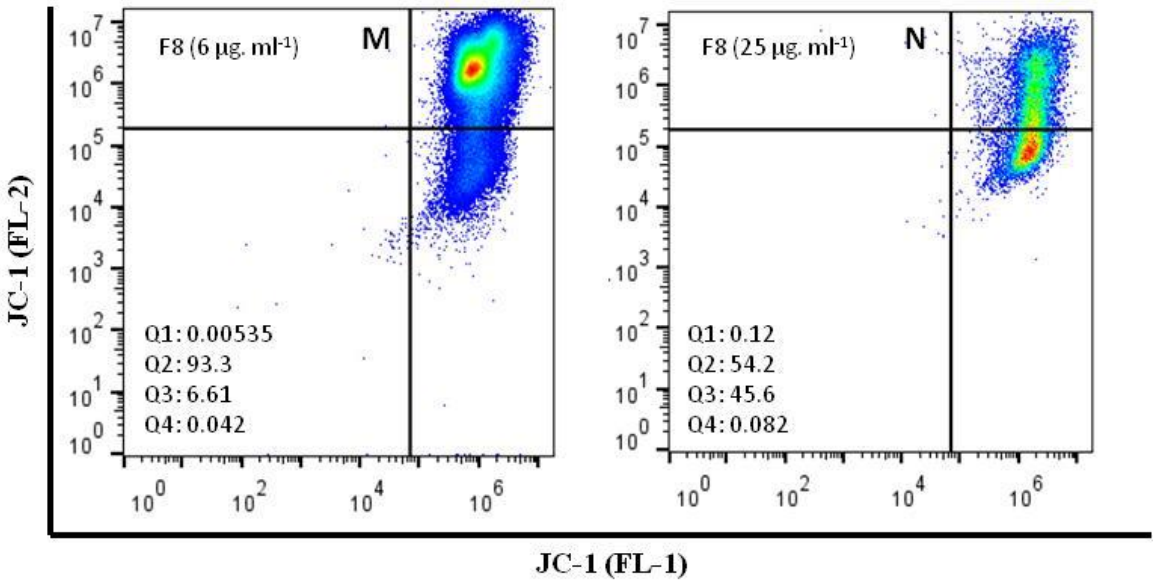

Figure 31: Representation of flow cytometer analysis data from the BD MitoScreen assay which was performed on A375 cells for examination of the state of their ΔΨ. Controls that were set up included the untreated/unstained control (A), untreated/stained control (B), positive controls [cells treated with camptothecin at 6 µg.ml^{-1} and 25 µg.ml^{-1}as well as cells treated with doxorubicin at 6 µg.ml^{-1}] (C-E) and DMSO control [cells treated with 0.2% of solvent] (F). The A375 cells were then treated with fractions F2 [6 µg.ml^{-1} and 25 µg.ml^{-1}] (G-H), F4 [6 µg.ml^{-1} and 25 µg.ml^{-1}] (I-J), F5 [6 µg.ml^{-1} and 25 µg.ml^{-1}] (K-L) and fraction F8 [6 µg.ml^{-1} and 25 µg.ml^{-1}] (M-N). The data is presented in a plot of FL-1 (for JC-1 green monomers) and FL-2 (for JC-1 red aggregates) fluorescence which denotes the percentage of cells with polarized ΔΨ (quadrant Q2) and percentage of cells with depolarized ΔΨ (quadrant Q3). In terms of the untreated/unstained control data, the percentage of cells are shown in quadrant Q4 and percentage of auto-fluorescence is shown in quadrant Q3. Q1-left upper quadrant, Q2- right upper quadrant, Q3- right lower quadrant, Q4- left lower quadrant.

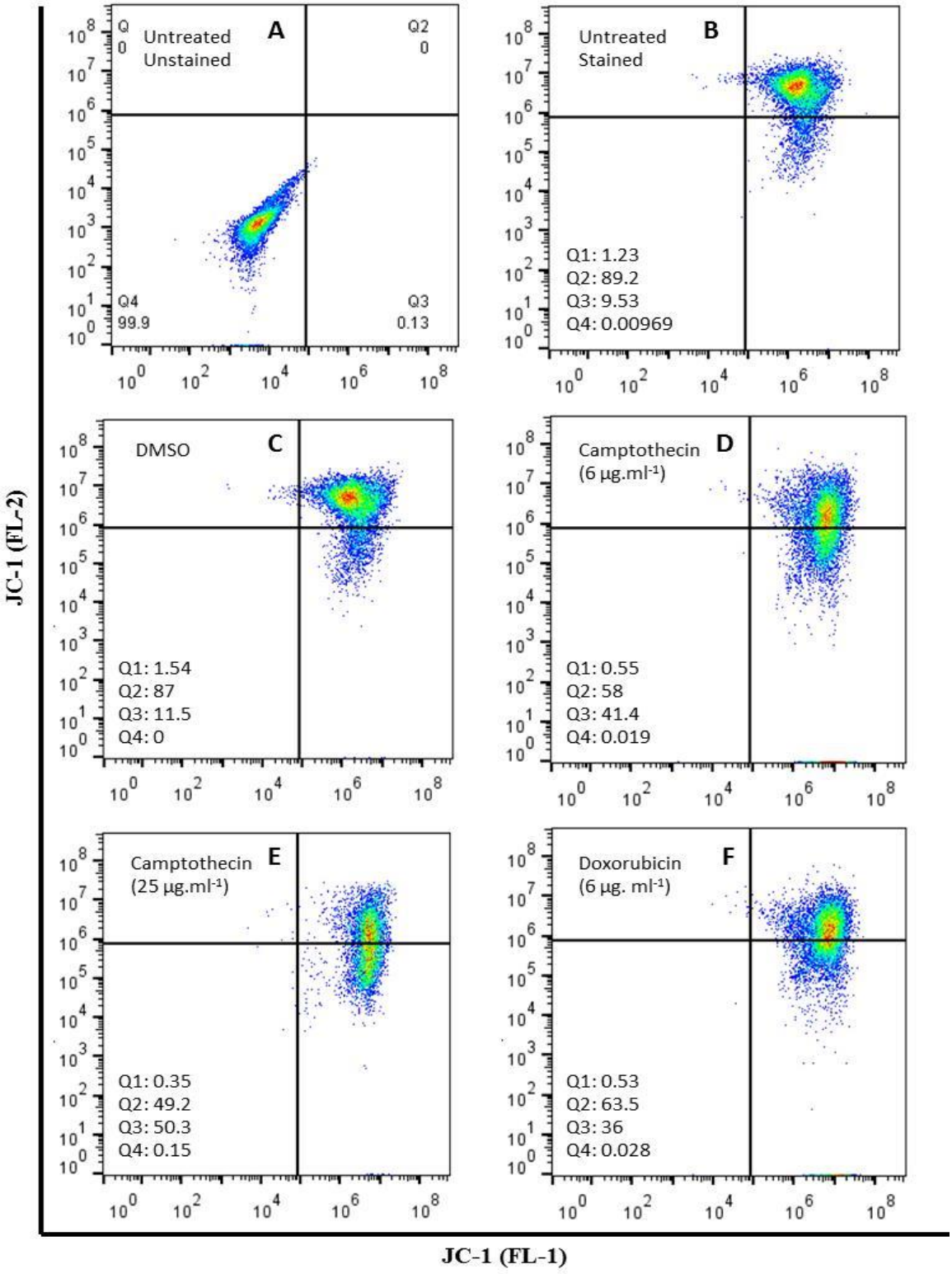
A
Untreated
Unstained
Q1
0
Q2
0
Q4
99.9
Q3
0.13
B
Untreated
Stained
Q1: 1.23
Q2: 89.2
Q3: 9.53
Q4: 0.00969
C
DMSO
Q1: 1.54
Q2: 87
Q3: 11.5
Q4: 0
D
Camptothecin
(6 µg.ml-1)
Q1: 0.55
Q2: 58
Q3: 41.4
Q4: 0.019
E
Camptothecin
(25 µg.ml-1)
Q1: 0.35
Q2: 49.2
Q3: 50.3
Q4: 0.15
F
Doxorubicin
(6 µg. ml-1)
Q1: 0.53
Q2: 63.5
Q3: 36
Q4: 0.028
JC-1 (FL-2)
JC-1 (FL-1)

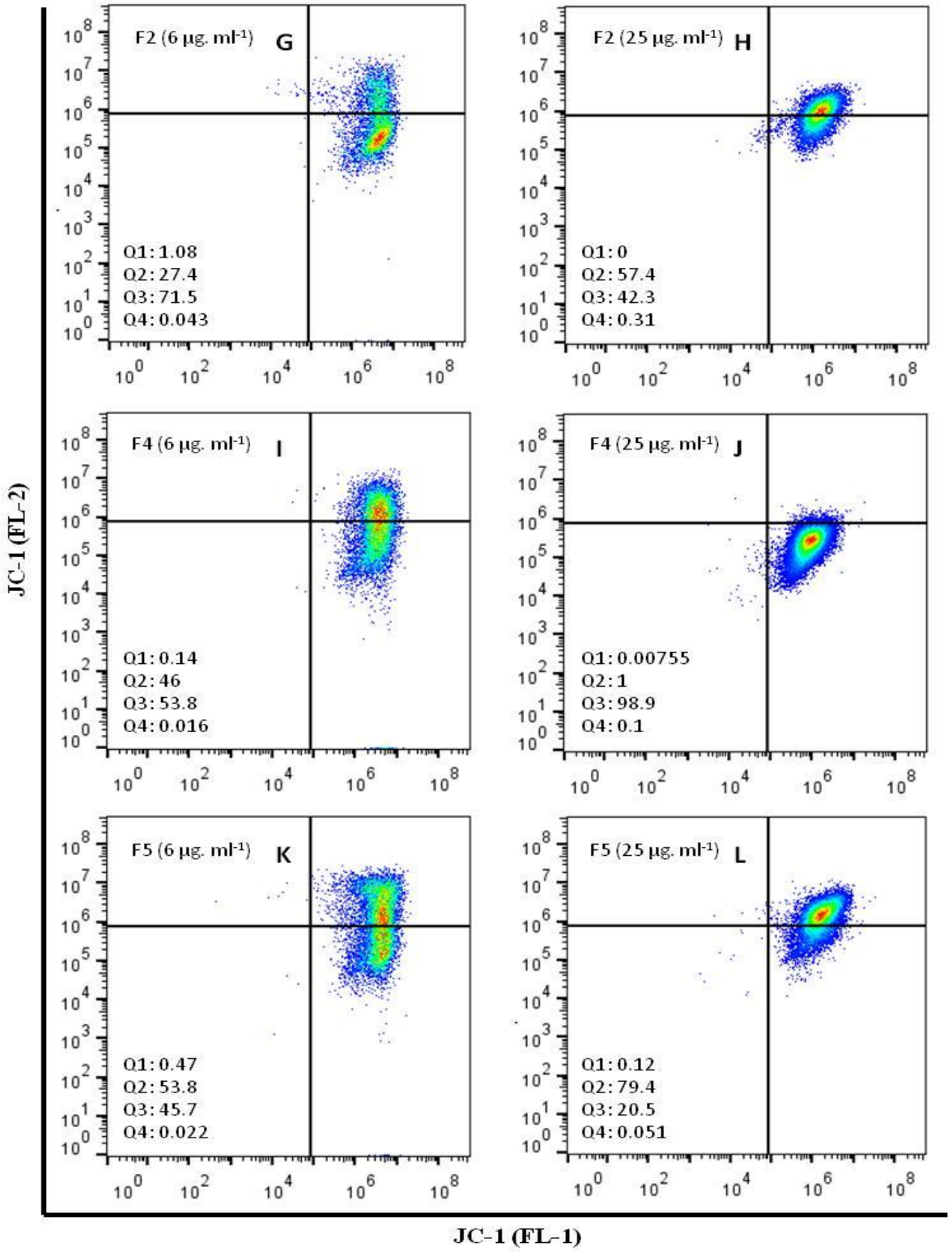
F2 (6 µg. ml-1) G
Q1: 1.08
Q2: 27.4
Q3: 71.5
Q4: 0.043
F2 (25 µg. ml-1) H
Q1: 0
Q2: 57.4
Q3: 42.3
Q4: 0.31
F4 (6 µg. ml-1) I
Q1: 0.14
Q2: 46
Q3: 53.8
Q4: 0.016
F4 (25 µg. ml-1) J
Q1: 0.00755
Q2: 1
Q3: 98.9
Q4: 0.1
F5 (6 µg. ml-1) K
Q1: 0.47
Q2: 53.8
Q3: 45.7
Q4: 0.022
F5 (25 µg. ml-1) L
Q1: 0.12
Q2: 79.4
Q3: 20.5
Q4: 0.051
JC-1 (FL-2)
JC-1 (FL-1)

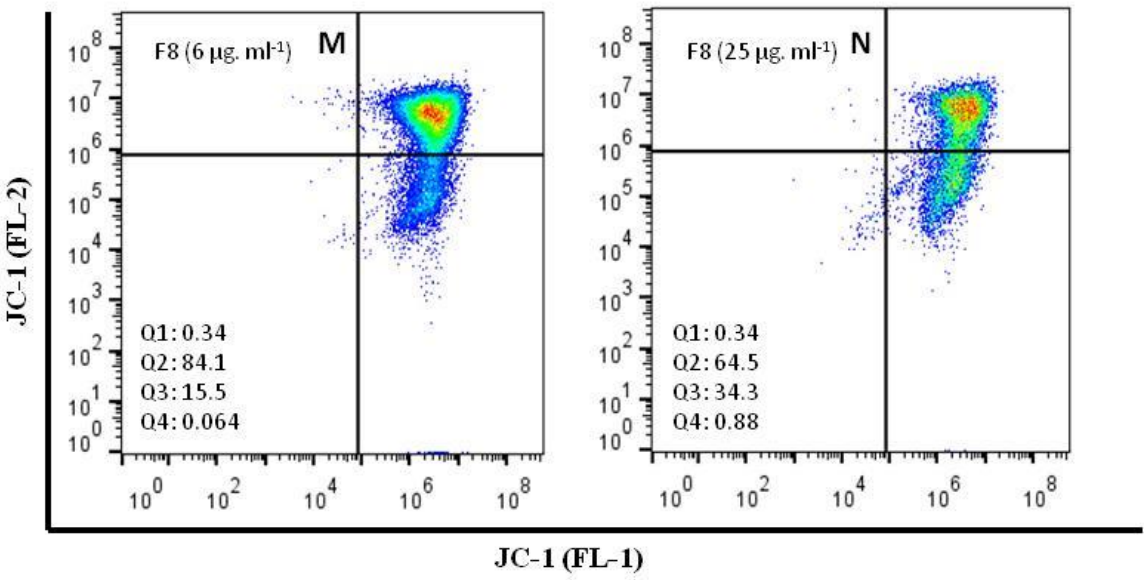

Figure 32: Representation of flow cytometer analysis data from the BD MitoScreen assay which was performed on UACC-62 cells for examination of the state of their ΔΨ. Controls that were set up included the untreated/unstained control (A), untreated/stained control (B), positive controls [cells treated with camptothecin at 6 µg.ml^{-1} and 25 µg.ml^{-1}as well as cells treated with doxorubicin at 6 µg.ml^{-1}] (C-E) and DMSO control [cells treated with 0.2% of solvent] (F). The A375 cells were then treated with fractions F2 [6 µg.ml^{-1} and 25 µg.ml^{-1}] (G-H), F4 [6 µg.ml^{-1} and 25 µg.ml^{-1}] (I-J), F5 [6 µg.ml^{-1} and 25 µg.ml^{-1}] (K-L) and fraction F8 [6 µg.ml^{-1} and 25 µg.ml^{-1}] (M-N). The data is presented in a plot of FL-1 (for JC-1 green monomers) and FL-2 (for JC-1 red aggregates) fluorescence which denotes the percentage of cells with polarized ΔΨ (quadrant Q2) and percentage of cells with depolarized ΔΨ (quadrant Q3). In terms of the untreated/unstained control data, the percentage of cells are shown in quadrant Q4 and percentage of auto-fluorescence is shown in quadrant Q3. Q1-left upper quadrant, Q2- right upper quadrant, Q3- right lower quadrant, Q4- left lower quadrant.

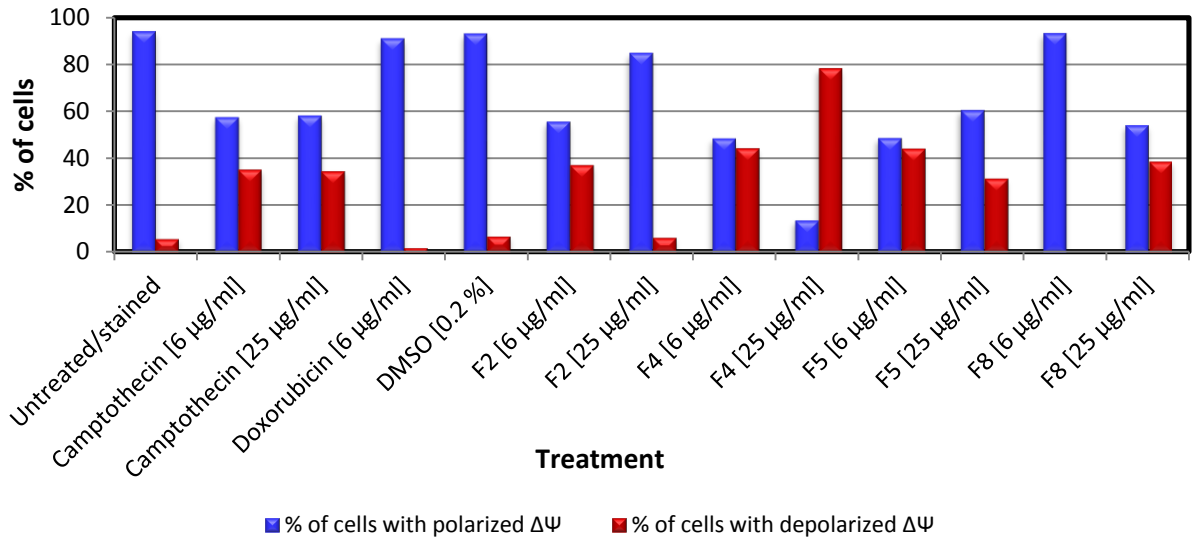

Figure 33: A graphical representation of the flow cytometer analysis data from the BD MitoScreen assay performed on A375 cells for examination of the state of their ΔΨ. Controls that were set up included the untreated/stained control, positive controls [cells treated with camptothecin at 6 µg.ml^{-1} and 25 µg.ml^{-1}as well as cells treated with doxorubicin at 6 µg.ml^{-1}] and DMSO control [cells treated with 0.2% of solvent]. The A375 cells were treated with fractions F2, F4, F5 and F8 [6 µg.ml^{-1} and 25 µg.ml^{-1}]. The percentage of cells with polarized ΔΨ and percentage of cells with depolarized ΔΨ were detected.

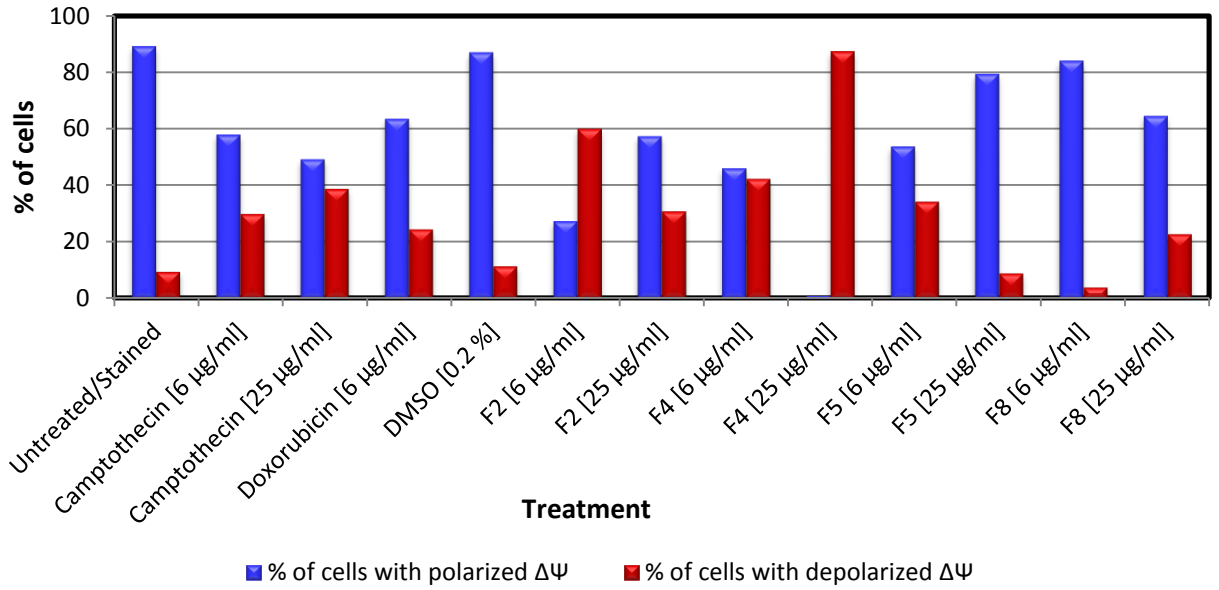

Figure 34: A graphical representation of the flow cytometer analysis data from the BD MitoScreen assay performed on UACC-62 cells for examination of the state of their ΔΨ. Controls that were set up included the untreated/stained control, positive controls [cells treated with camptothecin at 6 µg.ml^{-1} and 25 µg.ml^{-1}as well as cells treated with doxorubicin at 6 µg.ml^{-1}] and DMSO control [cells treated with 0.2% of solvent]. The UACC-62 cells were treated with fractions F2, F4, F5 and F8 [6 µg.ml^{-1} and 25 µg.ml^{-1}]. The percentage of cells with polarized ΔΨ and percentage of cells with depolarized ΔΨ were detected.

Table 24: Fold increase in the percentage of A375 cells that the fractions permitted to have depolarized ΔΨ in relation to the standards.

Fraction	Fold increase in relation to camptothecin		Fold increase in relation to doxorubicin
	6 µg.ml^{-1}	25 µg.ml^{-1}	6 µg.ml^{-1}
F2	1.05	-	18.79
F4	1.25	2.26	22.38
F5	1.25	-	22.33
F8	-	1.12	-

Table 25: Fold increase in the percentage of UACC-62 cells that the fractions permitted to have depolarized ΔΨ in relation to the standards.

Fraction	Fold increase in relation to camptothecin		Fold increase in relation to doxorubicin
	6 µg.ml^{-1}	25 µg.ml^{-1}	6 µg.ml^{-1}
F2	2.01	-	2.45
F4	1.41	2.25	1.73
F5	1.14	-	1.40
F8	-	-	-

3.7.2 Detection of caspase 3 activity by using the PE active caspase 3 assay

For the PE active caspase 3 assay, the flow cytometer analysis data is presented on flow charts as histogram plots which combine cell number and PE active caspase 3 fluorescence. The M1 bi-sector gate represents the percentage of caspase 3 negative cells while the M2 bi-sector gate represents the percentage of caspase 3 positive cells (Figure 35-36). For the untreated/unstained control flow chart the M1 bi-sector gate represents the percentage of cells and M2 bi-sector gate represents the percentage of auto-fluorescence.

Outcomes of flow cytometer analysis are described below:

The A375 cells that were left untreated or exposed to the control treatments were analysed accordingly: The untreated/unstained control contained 1.33% of auto-fluorescence (Figure 35A). This amount was subtracted from the data that was generated. The untreated/stained control contained 10.1% of caspase 3 positive cells (Figure 35B). This control was also known as the negative control. Plus, positive controls were set up by using two standards. Camptothecin (6 $\mu g.ml^{-1}$ and 25 $\mu g.ml^{-1}$) induced 65.36% and 32.26% of caspase 3 positive cells, respectively (Figure 35C-35D). Doxorubicin (6 $\mu g.ml^{-1}$) induced 90.56% of caspase 3 positive cells (Figure 35E). Both the negative and positive controls were used to validate the experiment. In addition, a DMSO control was set up and it contained 9.44% of caspase 3 positive cells (Figure 35F). The effect of this control was subtracted from the data that was obtained.

The A375 cells that were treated with the active fractions were analysed accordingly: Essentially we collated the data from the flow charts to obtain a graphical representation which revealed that fractions F2, F4, F5 and F8 (6 and/or 25 $\mu g.ml^{-1}$) induced a higher percentage of caspase 3 positive cells (approximately 90%) than camptothecin (Figure 35B-35N and 37). This was further elaborated by the fold increase values that are shown in Table 26.

The UACC-62 cells that were left untreated or exposed to the control treatments were analysed accordingly: The untreated/unstained control contained 0.36% of auto-fluorescence (Figure 36A). The untreated/stained control contained 2.47% of caspase 3 positive cells (Figure 36B). Also, positive controls were set up by using two standards. Camptothecin (6 $\mu g.ml^{-1}$ and 25 $\mu g.ml^{-1}$) induced 55.28%, and 54.48% of caspase 3 positive cells, respectively (Figure 36C-36D). Doxorubicin (6 $\mu g.ml^{-1}$) induced 97.28% of caspase 3 positive cells (Figure 36E). In addition, a DMSO control was set up and it contained 2.32% of caspase 3 positive cells (Figure 36F). These controls were applied to the analysis as described in the previous paragraph.

The UACC-62 cells that were treated with the active fractions were analysed accordingly: Essentially we collated the data from the flow charts to obtain a graphical representation which revealed that fractions F2, F4, F5 and F8 (6 and/or 25 $\mu g.ml^{-1}$) induced a higher percentage of caspase 3 positive cells (around 90%) than camptothecin (Figure 36B-36N and 38). This was further elaborated by the fold increase values that are shown in Table 27.

In summary, the standards and fractions elicited caspase 3 activation in the A375 and UACC-62 cells. Also, all four fractions induced a high percentage of caspase 3 positive cells.

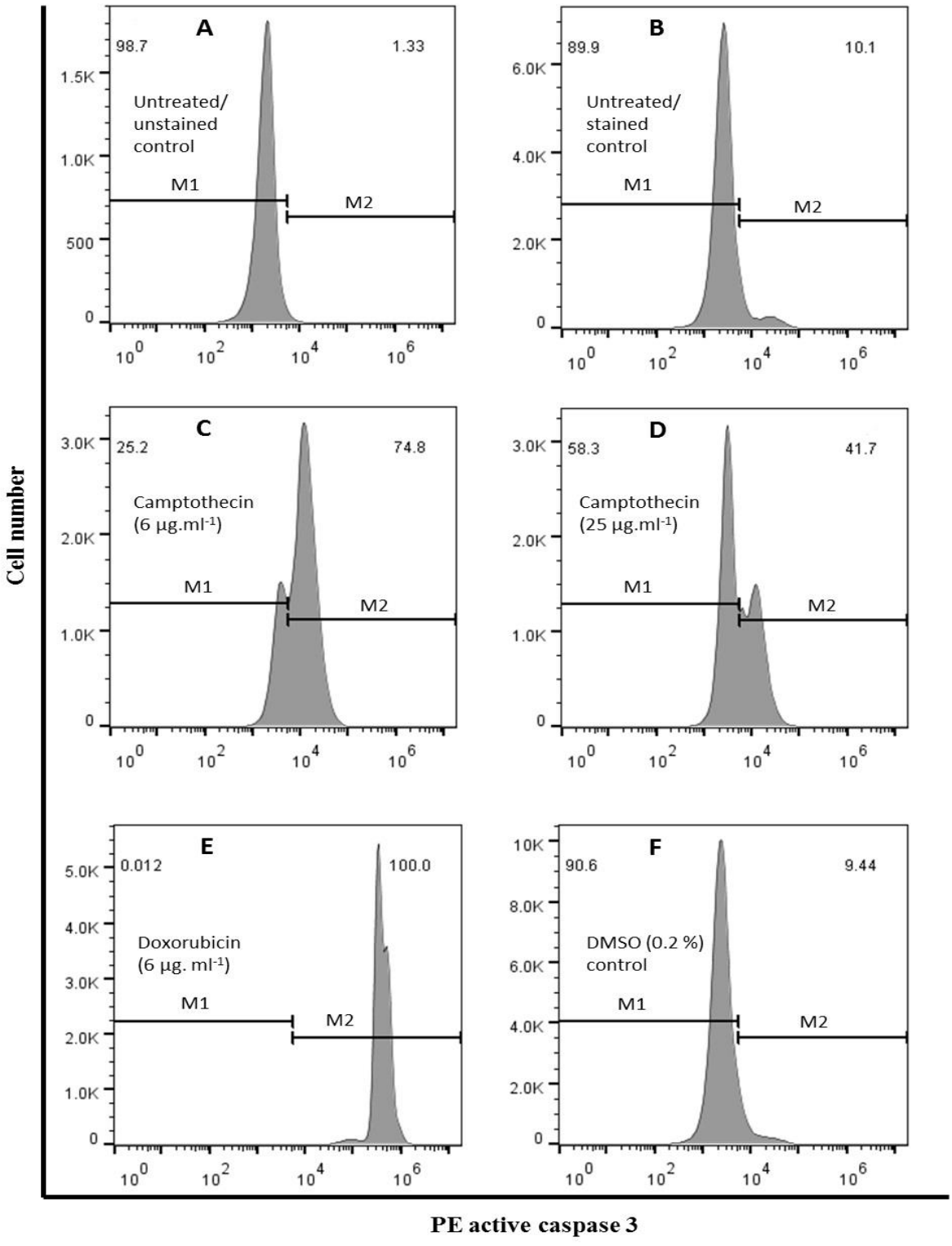
A
98.7
1.33
Untreated/
unstained
control
M1
M2
B
89.9
10.1
Untreated/
stained
control
M1
M2
C
25.2
74.8
Camptothecin
(6 µg.ml-1)
M1
M2
D
58.3
41.7
Camptothecin
(25 µg.ml-1)
M1
M2
E
0.012
100.0
Doxorubicin
(6 µg. ml-1)
M1
M2
F
90.6
9.44
DMSO (0.2 %)
control
M1
M2
Cell number
PE active caspase 3

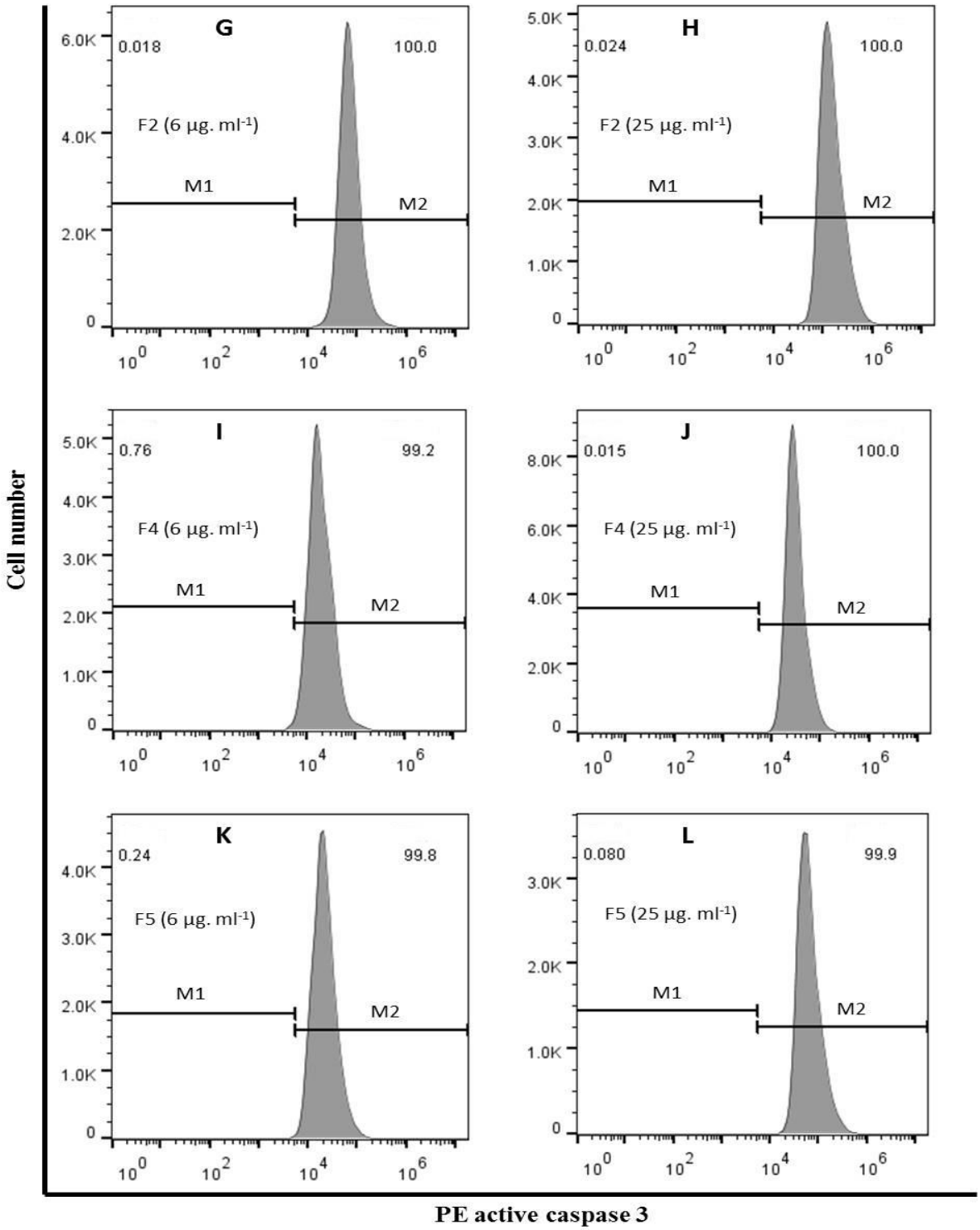
G
0.018
100.0
F2 (6 µg. ml-1)
M1
M2
H
0.024
100.0
F2 (25 µg. ml-1)
M1
M2
I
0.76
99.2
F4 (6 µg. ml-1)
M1
M2
J
0.015
100.0
F4 (25 µg. ml-1)
M1
M2
K
0.24
99.8
F5 (6 µg. ml-1)
M1
M2
L
0.080
99.9
F5 (25 µg. ml-1)
M1
M2
Cell number
PE active caspase 3

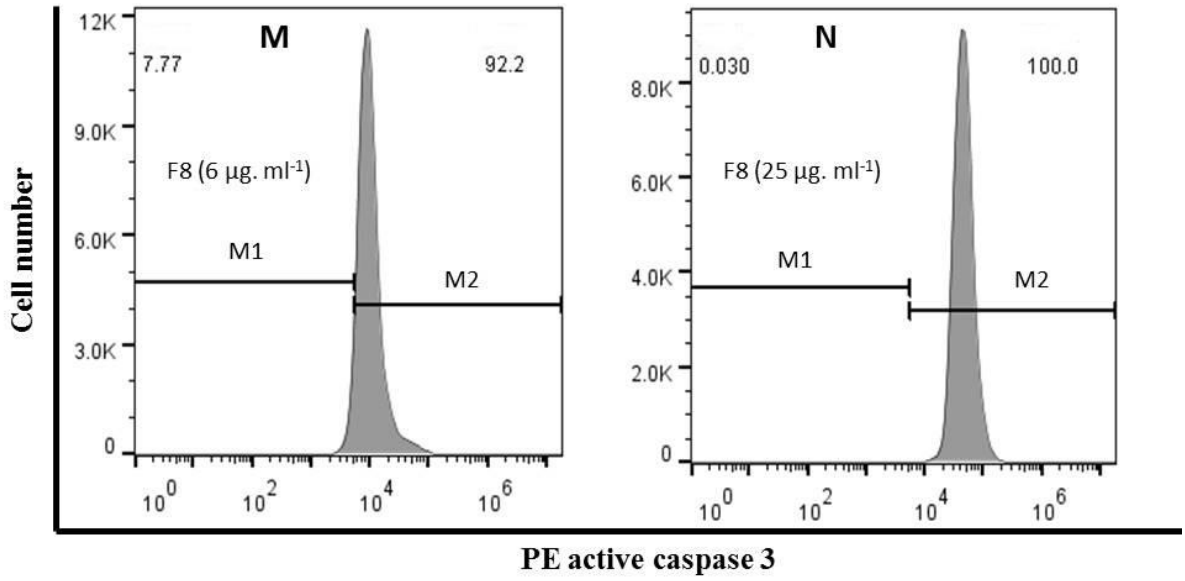

Figure 35: Representation of flow cytometer analysis data from the PE active caspase 3 assay which was performed on A375 cells for detection of caspase 3 activity. Controls that were set up included the untreated/unstained control (A), untreated/stained control (B), positive controls [cells treated with camptothecin at 6 µg.ml^{-1} and 25 µg.ml^{-1}as well as cells treated with doxorubicin at 6 µg.ml^{-1}] (C-E) and DMSO control [cells treated with 0.2% of solvent] (F). The A375 cells were then treated with fractions F2 [6 µg.ml^{-1} and 25 µg.ml^{-1}] (G-H), F4 [6 µg.ml^{-1} and 25 µg.ml^{-1}] (I-J), F5 [6 µg.ml^{-1} and 25 µg.ml^{-1}] (K-L) and fraction F8 [6 µg.ml^{-1} and 25 µg.ml^{-1}] (M-N). The data is presented in a histogram plot which combines cell number and PE active caspase 3 fluorescence. The M1 bi-sector gate represents the percentage of caspase 3 negative cells and M2 bi-sector gate represents the percentage of caspase 3 positive cells. In terms of the untreated/unstained control data, the M1 bi-sector gate represents the percentage of cells and M2 bi-sector gate represents the percentage of auto-fluorescence.

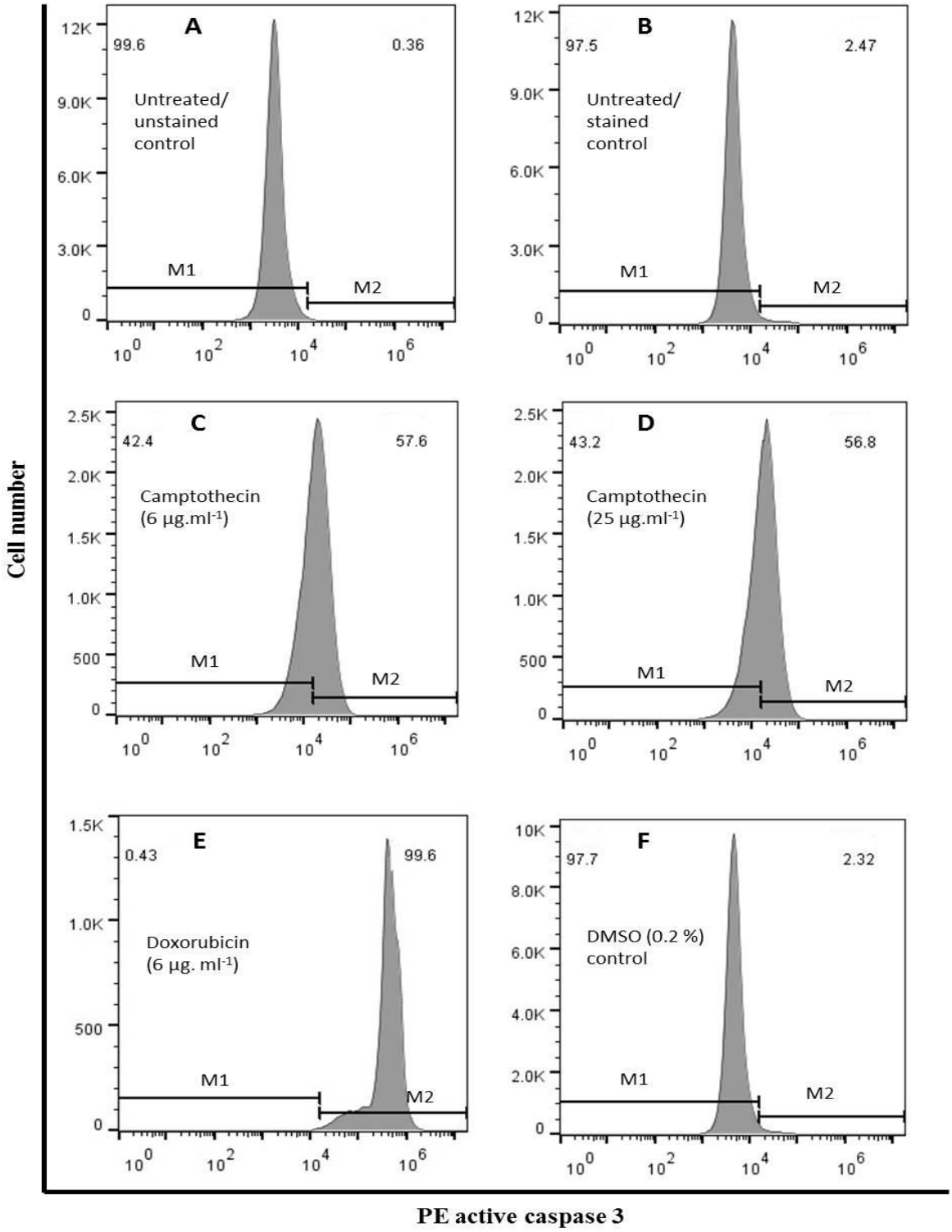
A
99.6
0.36
Untreated/
unstained
control
M1
M2
B
97.5
2.47
Untreated/
stained
control
M1
M2
C
42.4
57.6
Camptothecin
(6 µg.ml-1)
M1
M2
D
43.2
56.8
Camptothecin
(25 µg.ml-1)
M1
M2
E
0.43
99.6
Doxorubicin
(6 µg. ml-1)
M1
M2
F
97.7
2.32
DMSO (0.2 %)
control
M1
M2
Cell number
PE active caspase 3

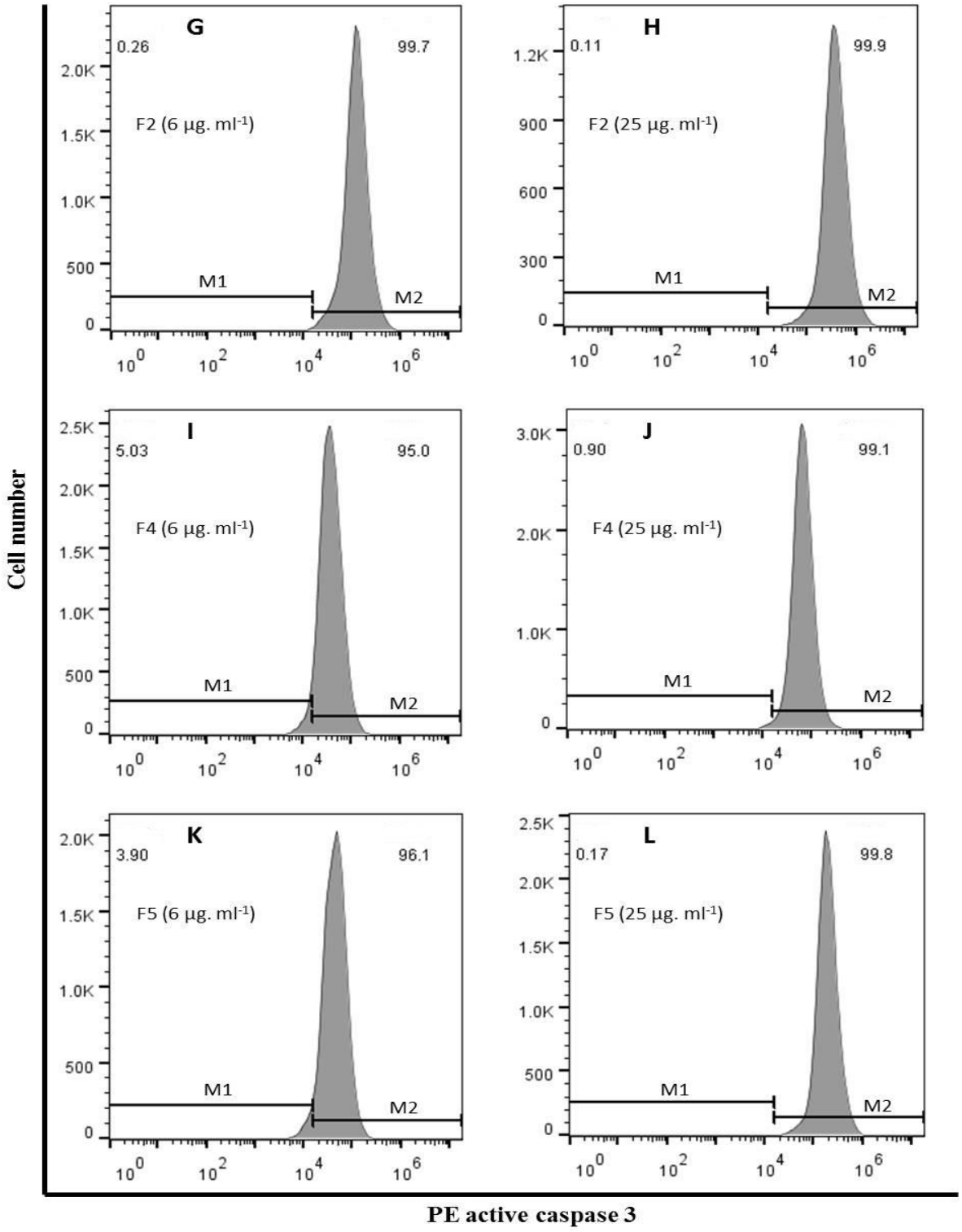
G
0.26
99.7
F2 (6 µg. ml-1)
M1
M2
H
0.11
99.9
F2 (25 µg. ml-1)
M1
M2
I
5.03
95.0
F4 (6 µg. ml-1)
M1
M2
J
0.90
99.1
F4 (25 µg. ml-1)
M1
M2
K
3.90
96.1
F5 (6 µg. ml-1)
M1
M2
L
0.17
99.8
F5 (25 µg. ml-1)
M1
M2
Cell number
PE active caspase 3

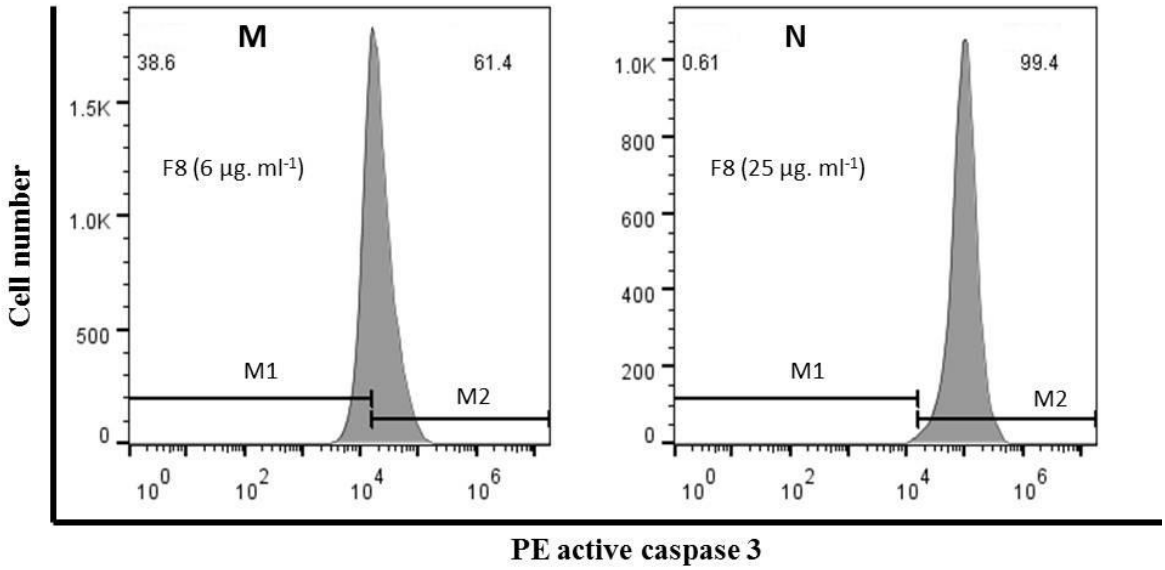

Figure 36: Representation of flow cytometer analysis data from the PE active caspase 3 assay which was performed on UACC-62 cells for detection of caspase 3 activity. Controls that were set up included the untreated/unstained control (A), untreated/stained control (B), positive controls [cells treated with camptothecin at 6 µg.ml^{-1} and 25 µg.ml^{-1}as well as cells treated with doxorubicin at 6 µg.ml^{-1}] (C-E) and DMSO control [cells treated with 0.2% of solvent] (F). The A375 cells were then treated with fractions F2 [6 µg.ml^{-1} and 25 µg.ml^{-1}] (G-H), F4 [6 µg.ml^{-1} and 25 µg.ml^{-1}] (I-J), F5 [6 µg.ml^{-1} and 25 µg.ml^{-1}] (K-L) and fraction F8 [6 µg.ml^{-1} and 25 µg.ml^{-1}] (M-N). The data is presented in a histogram plot which combines cell number and PE active caspase 3 fluorescence. The M1 bi-sector gate represents the percentage of caspase 3 negative cells and M2 bi-sector gate represents the percentage of caspase 3 positive cells. In terms of the untreated/unstained control data, the M1 bi-sector gate represents the percentage of cells and M2 bi-sector gate represents the percentage of auto-fluorescence.

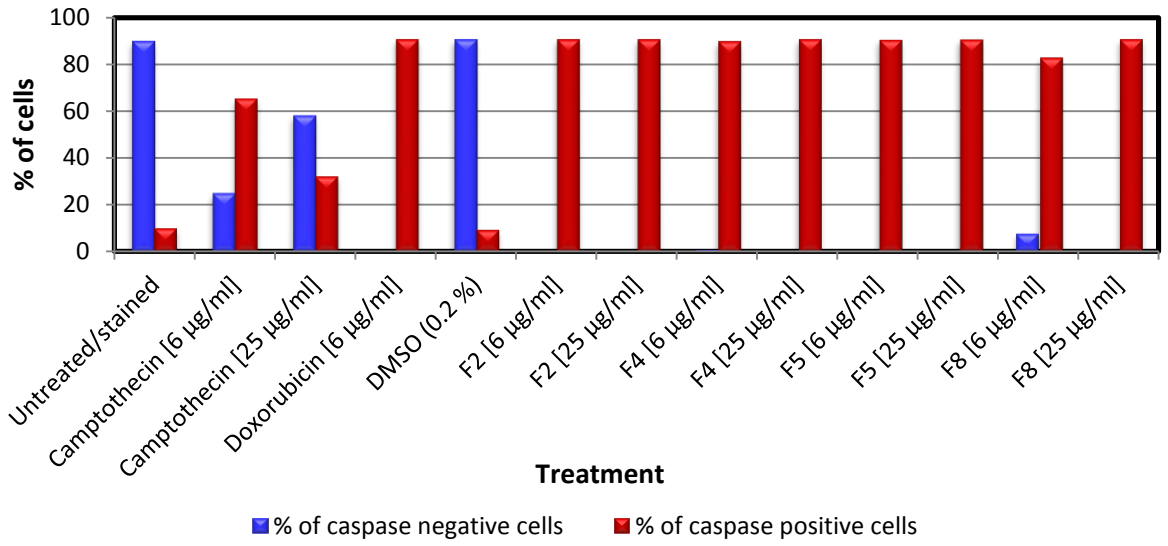

Figure 37: A graphical representation of the flow cytometer analysis data from the PE active caspase 3 assay performed on A375 cells for detection of caspase 3 activity. Controls that were set up included the untreated/stained control, positive controls [cells treated with camptothecin at 6 µg.ml^{-1} and 25 µg.ml^{-1}as well as cells treated with doxorubicin at 6 µg.ml^{-1}] and DMSO control [cells treated with 0.2% of solvent]. The A375 cells were treated with fractions F2, F4, F5 and F8 [6 µg.ml^{-1} and 25 µg.ml^{-1}]. The percentage of caspase 3 negative cells and percentage of caspase 3 positive cells were detected.

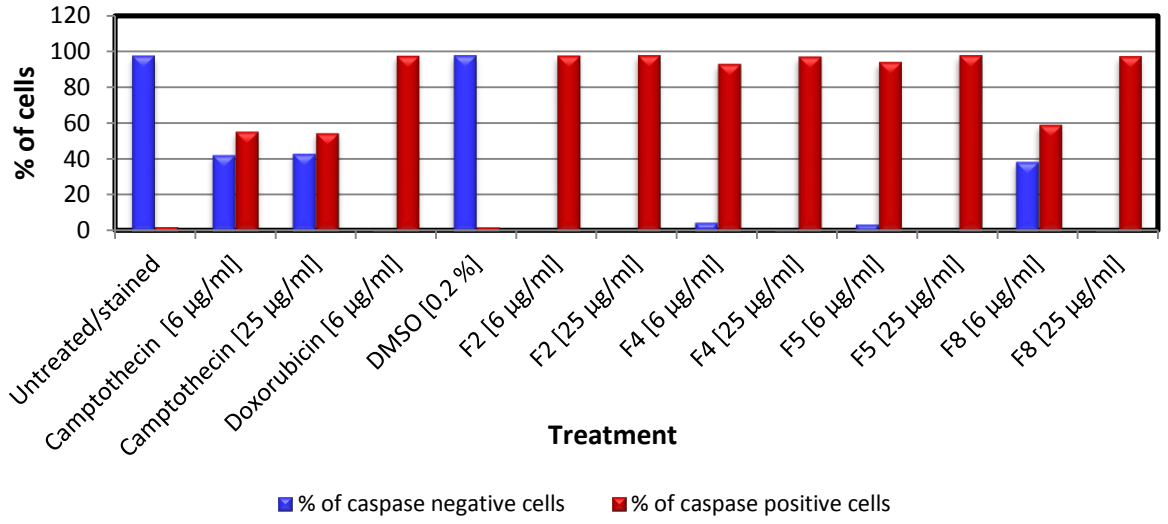

Figure 38: A graphical representation of the flow cytometer analysis data from the PE active caspase 3 assay performed on UACC-62 cells for detection of caspase 3 activity. Controls that were set up included the untreated/stained control, positive controls [cells treated with camptothecin at 6 µg.ml^{-1} and 25 µg.ml^{-1}as well as cells treated with doxorubicin at 6 µg.ml^{-1}] and DMSO control [cells treated with 0.2% of solvent]. The UACC-62 cells were treated with fractions F2, F4, F5 and F8 [6 µg.ml^{-1} and 25 µg.ml^{-1}]. The percentage of caspase 3 negative cells and percentage of caspase 3 positive cells were detected.

Table 26: Caspase 3 induced fold increase in A375 cells in relation to the standards.

Fraction	Fold increase in relation to camptothecin		Fold increase in relation to doxorubicin
	6 µg.ml^{-1}	25 µg.ml^{-1}	6 µg.ml^{-1}
F2	1.39	2.81	-
F4	1.37	2.81	-
F5	1.38	2.80	-
F8	1.27	2.81	-

Table 27: Caspase 3 induced fold increase in UACC-62 cells in relation to the standards.

Fraction	Fold increase in relation to camptothecin		Fold increase in relation to doxorubicin
	6 µg.ml^{-1}	25 µg.ml^{-1}	6 µg.ml^{-1}
F2	1.76	1.79	-
F4	1.68	1.78	-
F5	1.70	1.79	-
F8	1.07	1.78	-

3.7.3 Detection of early and late apoptosis by using the FITC annexin V assay

For the FITC annexin V assay, the data is presented on flow charts as dual parametric dot plots which combine FITC annexin V and PI fluorescence. The flow charts display the percentage of viable cells (quadrant Q4), early apoptotic cells (quadrant Q3), late apoptotic cells (quadrant Q2) and necrotic cells (quadrant Q1) (Figure 39-40). In terms of the untreated/unstained control flow chart quadrant Q4 represents the percentage of cells and quadrant Q3 represents the percentage of auto-fluorescence.

Outcomes of flow cytometer analysis are described below:

The A375 cells that were left untreated or exposed to the control treatments were analysed accordingly: The untreated/unstained control contained 99.9% of cells (Figure 39A). This control was used to subtract auto-fluorescence from the data that was generated. The PI control (cells heated at 70ºC) contained 87% of necrotic cells and the FITC annexin V control (cells treated with 25 $\mu g.ml^{-1}$ of camptothecin) contained 46.14% of early apoptotic cells (Figure 39B and 39C). These controls were used to subtract overlapping fluorescence between fluorescence channels. Also, positive controls were set up by using two standards. Camptothecin (6 $\mu g.ml^{-1}$ and 25 $\mu g.ml^{-1}$) allowed for early apoptotic cells (11.94% and 8.24%, respectively), late apoptotic cells (14.19% and 34.29%, respectively) and necrotic cells (1.53% and 3.52%, respectively) to be detected (Figure 39D and 39E). Doxorubicin (6 $\mu g.ml^{-1}$) only allowed for late apoptotic cells (41.39%) and necrotic cells (52.66%) to be detected (Figure 39F). These standards served as references for apoptosis activity. In addition, a DMSO control was set up and it contained 1.76% of early apoptotic cells, 4.41% of late apoptotic cells and 0.24% of necrotic cells (Figure 39G). The effect of this control was subtracted from the data that was obtained.

The A375 cells that were treated with the active fractions were analysed accordingly: Essentially we collated the data from the flow charts to obtain a graphical representation which revealed the following facts (Figure 39B-39O and 41). Fractions F2, F4, F5 and F8 (6 $\mu g.ml^{-1}$ and/or 25 $\mu g.ml^{-1}$) induced a distribution of cells between all three stages of cell death. Overall there were

two most active fractions in terms of apoptosis activity. Fraction F5 (6 µg.ml^{-1} and 25 µg.ml^{-1}) induced a higher percentage of early apoptotic cells (16.64% and 23.24%, respectively) in comparison to doxorubicin, camptothecin and the other fractions. Fraction F2 (6 µg.ml^{-1} and 25 µg.ml^{-1}) induced a higher percentage of late apoptotic cells (41.39% and 93.39%, respectively) in comparison to camptothecin and the other fractions. Hence, these two fractions were more efficient in inducing apoptosis of the A375 cells than doxorubicin and/or camptothecin. This was further elaborated by the fold increase values that are shown in Table 28.

The UACC-62 cells that were left untreated or exposed to the control treatments were analysed accordingly: The untreated/unstained control contained 100% of cells (Figure 40A). The PI control (cells heated at 70ºC) contained 81% of necrotic cells and the FITC annexin V control (cells treated with 25 µg.ml^{-1} of camptothecin) contained 22.4% of early apoptotic cells (Figure 40B and 40C). Also, positive controls were set up by using two standards. Camptothecin (6 µg.ml^{-1} and 25 µg.ml^{-1}) allowed for early apoptotic cells (17.20% and 8.10%, respectively), late apoptotic cells (1.89% and 0%, respectively) and necrotic cells (1.85% and 2.56%, respectively) to be detected (Figure 40D and 40E). Doxorubicin (6 µg.ml^{-1}) only allowed for late apoptotic cells (48.75%) and necrotic cells (33.50%) to be detected (Figure 40F). In addition, a DMSO control was set up and it contained 10.1% of early apoptotic cells, 7.25% of late apoptotic cells and 1.10% of necrotic cells (Figure 40G). These controls were applied to the analysis as described in the previous paragraph.

The UACC-62 cells that were treated with the active fractions were analysed accordingly: Essentially we collated the data from the flow charts to obtain a graphical representation which revealed the following facts (Figure 40B-40O and 42). Fractions F2, F5 and F8 (6 µg.ml^{-1} and/or 25 µg.ml^{-1}) induced a distribution of cells between all three stages of cell death. However fraction F4 (6 µg.ml^{-1} and 25 µg.ml^{-1}) only induced early apoptotic cells (1.60% and 4.30%, respectively) and necrotic cells (3.15% and 8.03%, respectively). Overall there were two most active fractions in terms of apoptosis activity. Fraction F5 (6 µg.ml^{-1} and 25 µg.ml^{-1}) induced a higher percentage of early apoptotic cells (7.3% and 11.20%, respectively) in comparison to doxorubicin and the other fractions. Fraction F2 (6 µg.ml^{-1} and 25 µg.ml^{-1}) induced a higher percentage of late apoptotic cells (20.15% and 57.65%, respectively) in comparison to

camptothecin and the other fractions. Hence, these fractions were more efficient in inducing apoptosis of the UACC-62 cells than doxorubicin or camptothecin. This was further elaborated by the fold increase values that are shown in Table 29.

In summary, the standards and active fractions induced apoptosis in both the A375 and UACC-62 cells. Also, fractions F5 and F2 were the most active fractions in terms of early and late apoptosis, respectively.

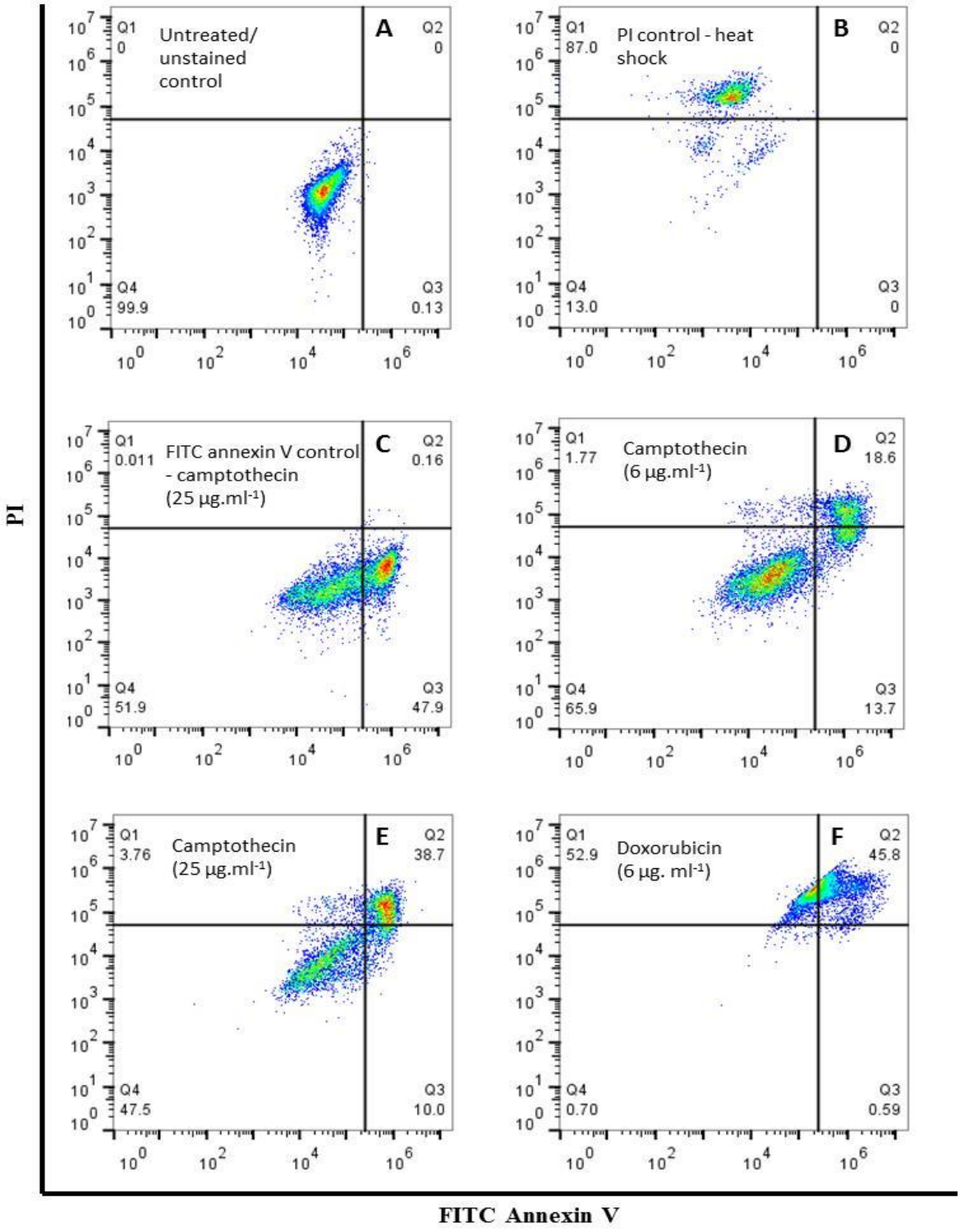
A
Untreated/ unstained control
Q1 0
Q2 0
Q4 99.9
Q3 0.13
B
PI control - heat shock
Q1 87.0
Q2 0
Q4 13.0
Q3 0
C
FITC annexin V control - camptothecin (25 µg.ml-1)
Q1 0.011
Q2 0.16
Q4 51.9
Q3 47.9
D
Camptothecin (6 µg.ml-1)
Q1 1.77
Q2 18.6
Q4 65.9
Q3 13.7
E
Camptothecin (25 µg.ml-1)
Q1 3.76
Q2 38.7
Q4 47.5
Q3 10.0
F
Doxorubicin (6 µg. ml-1)
Q1 52.9
Q2 45.8
Q4 0.70
Q3 0.59
PI
FITC Annexin V

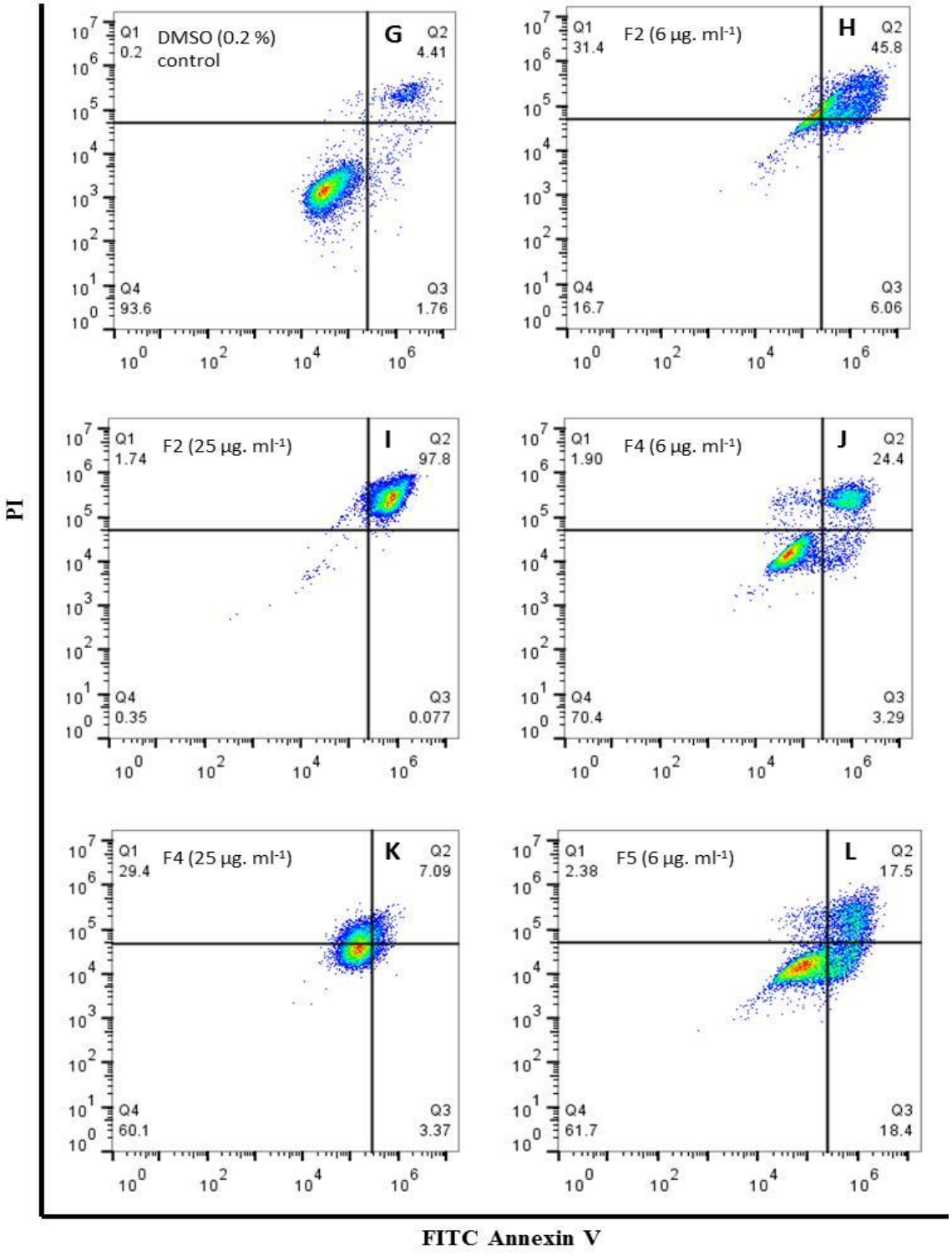
G
DMSO (0.2 %) control
Q1 0.2
Q2 4.41
Q4 93.6
Q3 1.76
H
F2 (6 µg. ml-1)
Q1 31.4
Q2 45.8
Q4 16.7
Q3 6.06
I
F2 (25 µg. ml-1)
Q1 1.74
Q2 97.8
Q4 0.35
Q3 0.077
J
F4 (6 µg. ml-1)
Q1 1.90
Q2 24.4
Q4 70.4
Q3 3.29
K
F4 (25 µg. ml-1)
Q1 29.4
Q2 7.09
Q4 60.1
Q3 3.37
L
F5 (6 µg. ml-1)
Q1 2.38
Q2 17.5
Q4 61.7
Q3 18.4
PI
FITC Annexin V

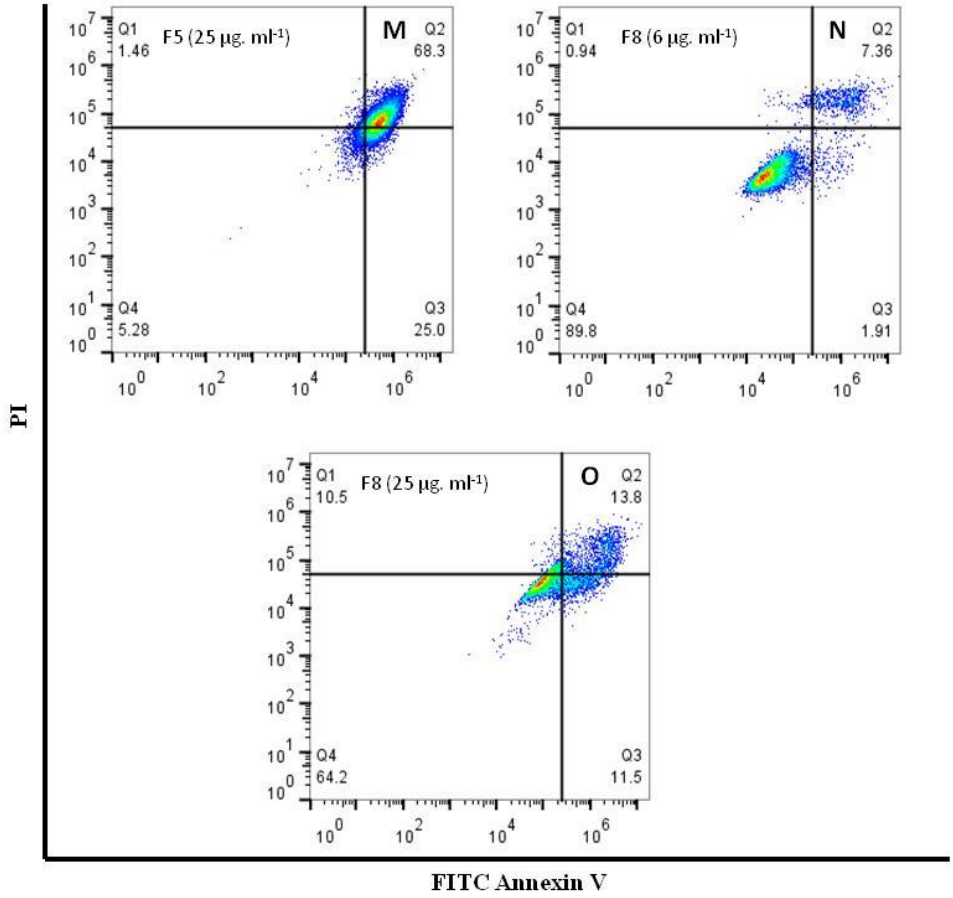

Figure 39: Representation of flow cytometer analysis data from the FITC annexin V assay which was performed on A375 cells for detection of apoptosis. Controls that were set up included the untreated/unstained control (A), PI control [cells treated with heat shock at 70º C for 15 minutes] (B), FITC annexin V control [cells treated with camptothecin at 25 µg.ml^{-1}] (C), positive controls [cells treated with camptothecin at 6 µg.ml^{-1} and 25 µg.ml^{-1}as well as cells treated with doxorubicin at 6 µg.ml^{-1}] (D-F) and DMSO control [0.2%] (G). The A375 cells were then treated with fractions F2 [6 µg.ml^{-1} and 25 µg.ml^{-1}] (H-I), F4 [6 µg.ml^{-1} and 25 µg.ml^{-1}] (J-K), F5 [6 µg.ml^{-1} and 25 µg.ml^{-1}] (L-M) and F8 [6 µg.ml^{-1} and 25 µg.ml^{-1}] (N-O). The data is presented in a plot of FITC annexin V and PI fluorescence which denotes the percentage of viable cells (quadrant Q4) early apoptotic cells (quadrant Q3: FITC annexin V + and PI -), late apoptotic cells (quadrant Q2: FITC annexin V + and PI +) and necrotic cells (quadrant Q1: FITC annexin V- PI +). In terms of the untreated/unstained control data, the percentage of cells are shown in quadrant Q4 and percentage of auto-fluorescence is shown in quadrant Q3.

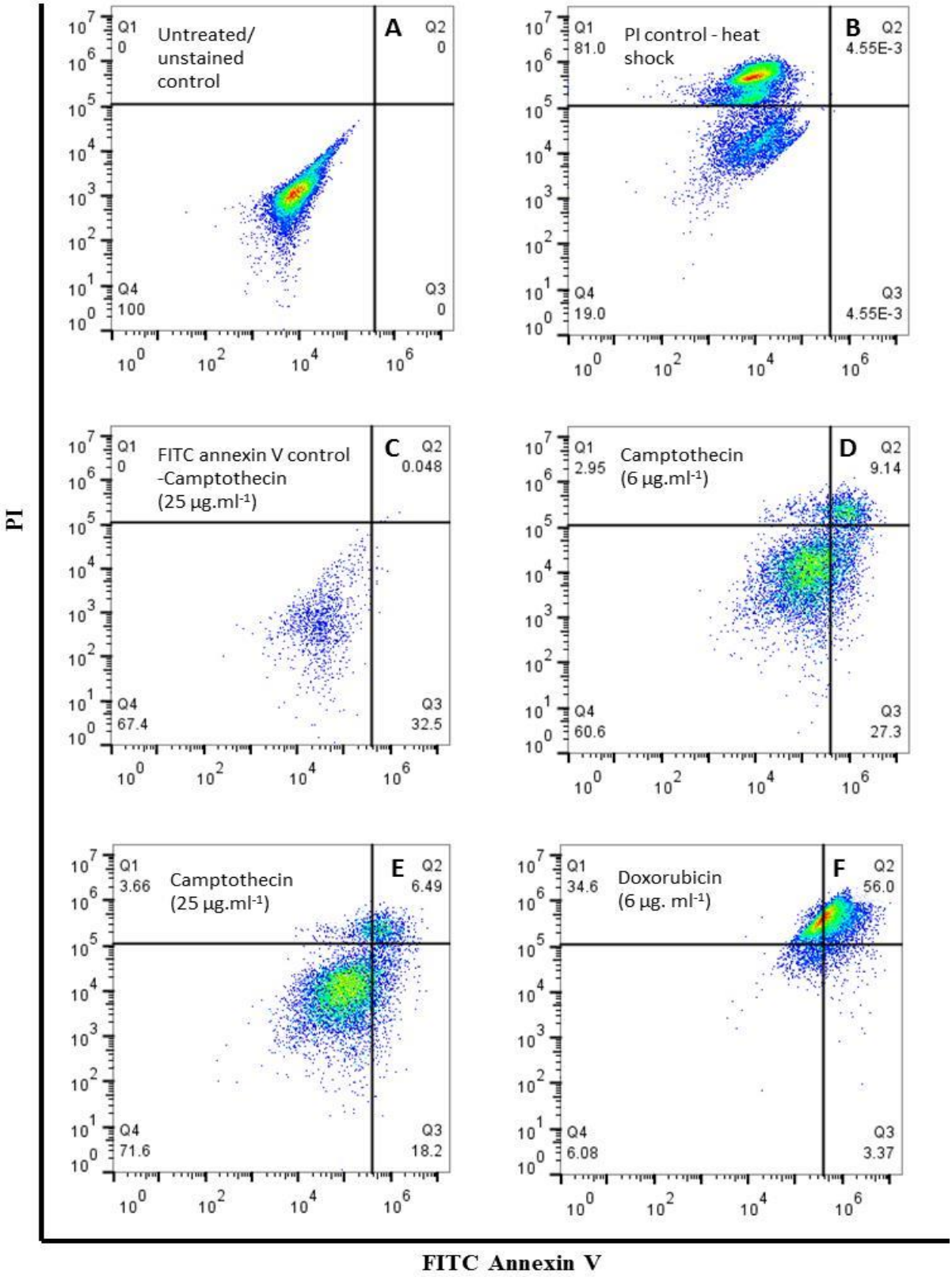
A
Untreated/ unstained control
Q1 0
Q2 0
Q4 100
Q3 0
B
PI control - heat shock
Q1 81.0
Q2 4.55E-3
Q4 19.0
Q3 4.55E-3
C
FITC annexin V control -Camptothecin (25 µg.ml-1)
Q1 0
Q2 0.048
Q4 67.4
Q3 32.5
D
Camptothecin (6 µg.ml-1)
Q1 2.95
Q2 9.14
Q4 60.6
Q3 27.3
E
Camptothecin (25 µg.ml-1)
Q1 3.66
Q2 6.49
Q4 71.6
Q3 18.2
F
Doxorubicin (6 µg. ml-1)
Q1 34.6
Q2 56.0
Q4 6.08
Q3 3.37
PI
FITC Annexin V

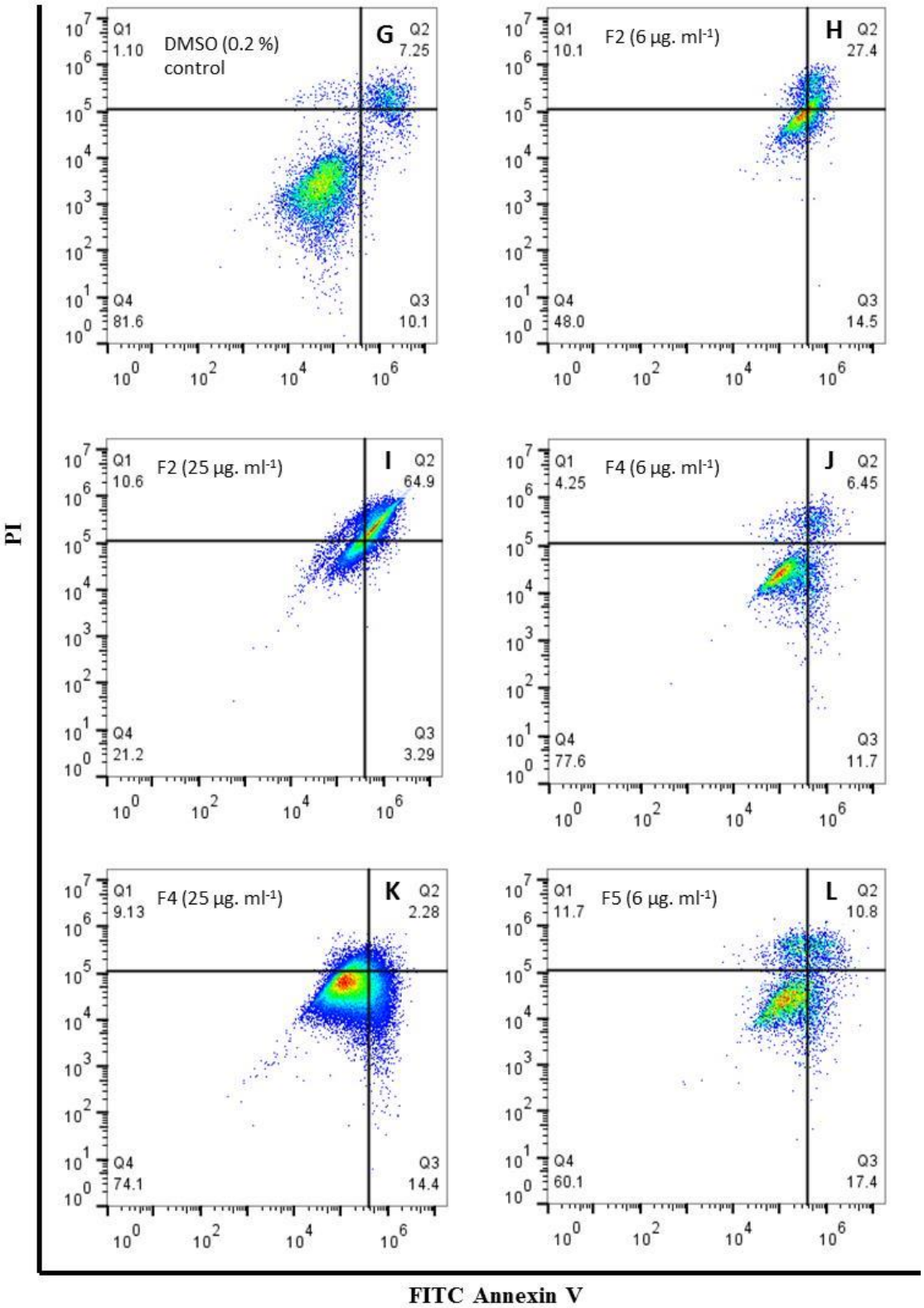
G
DMSO (0.2 %) control
Q1 1.10
Q2 7.25
Q4 81.6
Q3 10.1
H
F2 (6 µg. ml-1)
Q1 10.1
Q2 27.4
Q4 48.0
Q3 14.5
I
F2 (25 µg. ml-1)
Q1 10.6
Q2 64.9
Q4 21.2
Q3 3.29
J
F4 (6 µg. ml-1)
Q1 4.25
Q2 6.45
Q4 77.6
Q3 11.7
K
F4 (25 µg. ml-1)
Q1 9.13
Q2 2.28
Q4 74.1
Q3 14.4
L
F5 (6 µg. ml-1)
Q1 11.7
Q2 10.8
Q4 60.1
Q3 17.4
PI
FITC Annexin V

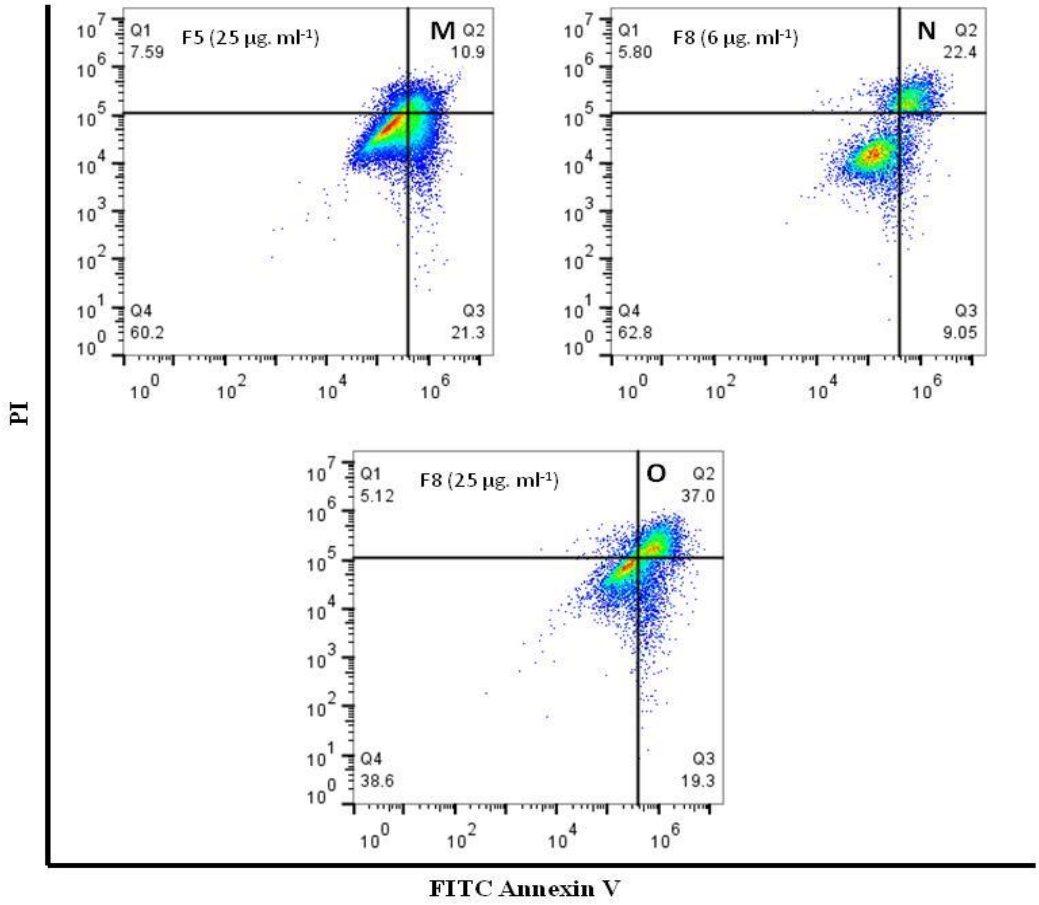

Figure 40: Representation of flow cytometer analysis data from the FITC annexin V assay which was performed on UACC-62 cells for detection of apoptosis. Controls that were set up included the untreated/unstained control (A), PI control [cells treated with heat shock at 70º C for 15 minutes] (B), FITC annexin V control [cells treated with camptothecin at 25 µg.ml^{-1}] (C), positive controls [cells treated with camptothecin at 6 µg.ml^{-1} and 25 µg.ml^{-1}as well as cells treated with doxorubicin at 6 µg.ml^{-1}] (D-F) and DMSO control [0.2%] (G). The A375 cells were then treated with fractions F2 [6 µg.ml^{-1} and 25 µg.ml^{-1}] (H-I), F4 [6 µg.ml^{-1} and 25 µg.ml^{-1}] (J-K), F5 [6 µg.ml^{-1} and 25 µg.ml^{-1}] (L-M) and F8 [6 µg.ml^{-1} and 25 µg.ml^{-1}] (N-O). The data is presented in a plot of FITC annexin V and PI fluorescence which denotes the percentage of viable cells (quadrant Q4) early apoptotic cells (quadrant Q3: FITC annexin V + and PI -), late apoptotic cells (quadrant Q2: FITC annexin V + and PI +) and necrotic cells (quadrant Q1: FITC annexin V- PI +). In terms of the untreated/unstained control data, the percentage of cells are shown in quadrant Q4 and percentage of auto-fluorescence is shown in quadrant Q3.

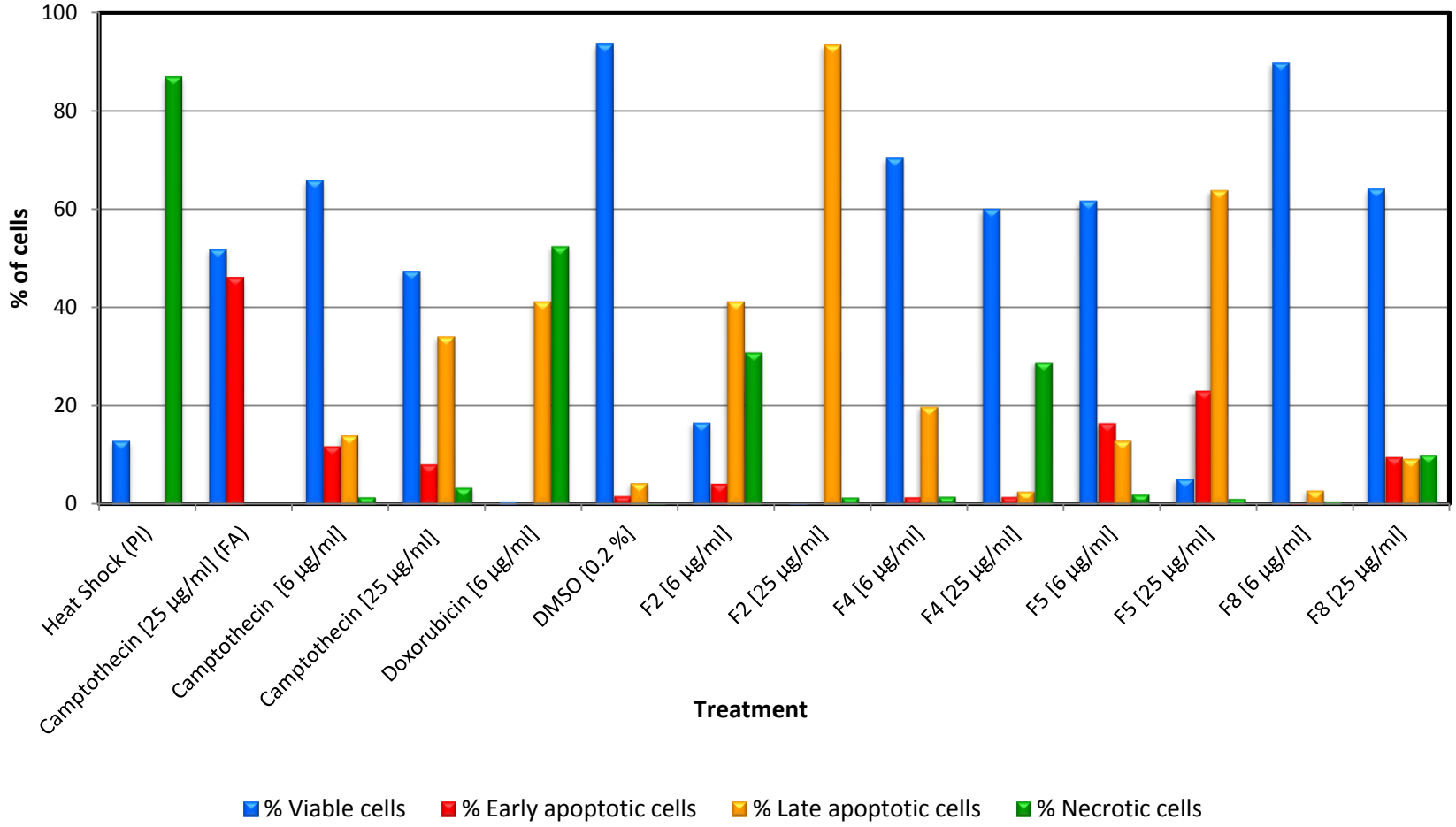

Figure 41: A graphical representation of the flow cytometer analysis data from the FITC annexin V assay which was performed on A375 cells for detection of apoptosis. Controls that were set up included the PI control (PI) [cells treated with heat shock at 70º C for 15 minutes], FITC annexin V control (FA) [cells treated with camptothecin at 25 µg.ml^{-1}], positive controls [cells treated with camptothecin at 6 µg.ml^{-1} and 25 µg.ml^{-1}as well as cells treated with doxorubicin at 6 µg.ml^{-1}] and DMSO control [cells treated with 0.2% of solvent]. The A375 cells were treated with fractions F2, F4, F5 and F8 [6 µg.ml^{-1} and 25 µg.ml^{-1}]. The percentage of viable cells, early apoptotic cells, late apoptotic cells and necrotic cells were detected.

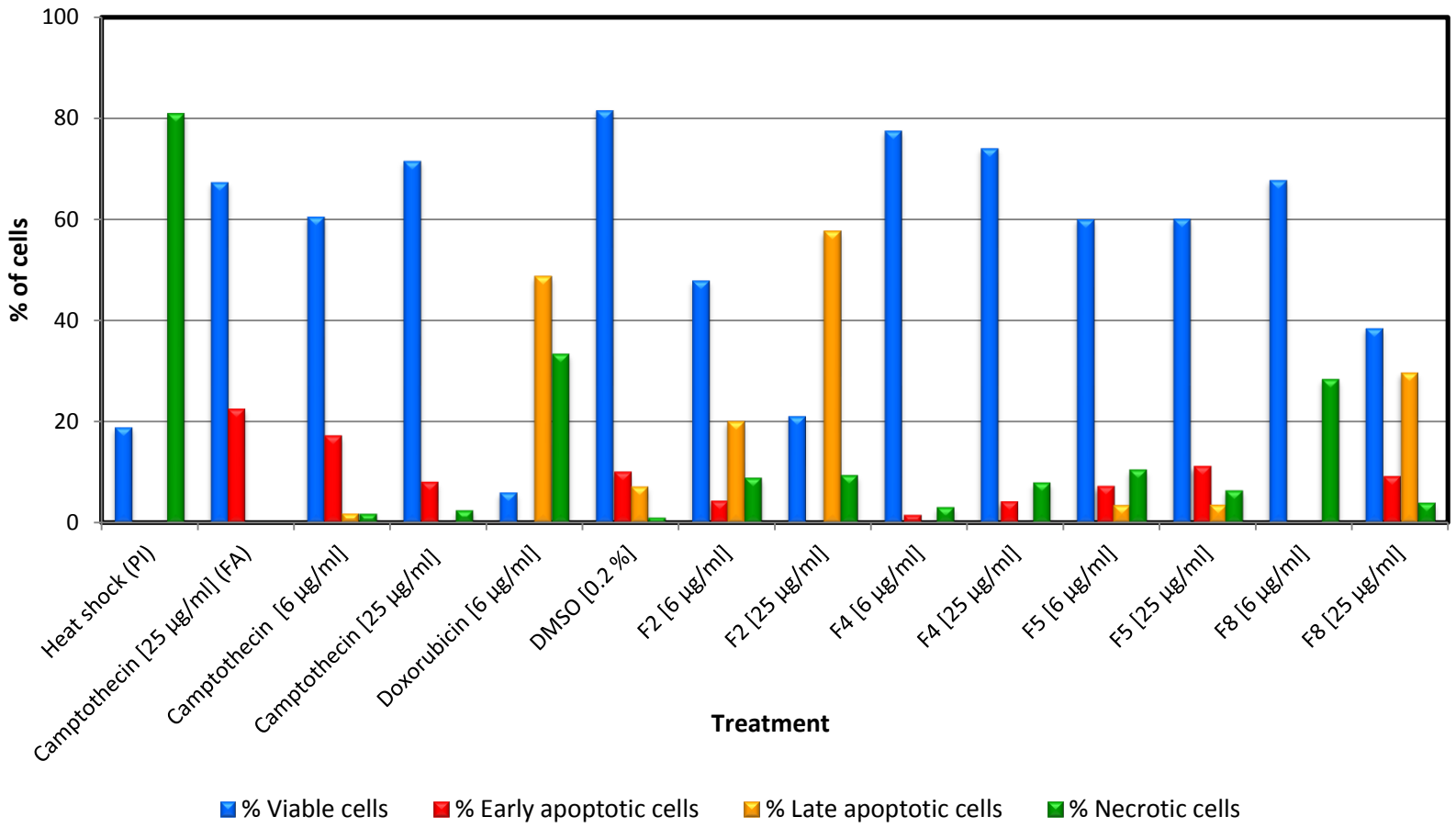

Figure 42: A graphical representation of the flow cytometer analysis data from the FITC annexin V assay which was performed on UACC-62 cells for detection of apoptosis. Controls that were set up included the PI control (PI) [cells treated with heat shock at 70º C for 15 minutes], FITC annexin V control (FA) [cells treated with camptothecin at 25 µg.ml^{-1}], positive controls [cells treated with camptothecin at 6 µg.ml^{-1} and 25 µg.ml^{-1}as well as cells treated with doxorubicin at 6 µg.ml^{-1}] and DMSO control [cells treated with 0.2% of solvent]. The UACC-62 cells were treated with fractions F2, F4, F5 and F8 [6 µg.ml^{-1} and 25 µg.ml^{-1}]. The percentage of viable cells, early apoptotic cells, late apoptotic cells and necrotic cells were detected.

Table 28: Fold increase in the percentage of A375 cells that the fractions allowed to enter apoptosis in relation to the standards.

Fraction	Fold increase in relation to camptothecin (early apoptosis)		Fold increase in relation to camptothecin (late apoptosis)		Fold increase in relation to doxorubicin (early apoptosis)	Fold increase in relation to doxorubicin (late apoptosis)
	6 µg.ml^{-1}	25 µg.ml^{-1}	6 µg.ml^{-1}	25 µg.ml^{-1}	6 µg.ml^{-1}	6 µg.ml^{-1}
F2	-	-	2.92	2.72	4.3	-
F4	-	-	1.41	-	1.53	-
F5	1.39	2.82	-	1.86	16.64	-
F8	-	-	-	-	0.15	-

Table 29: Fold increase in the percentage of UACC-62 cells that the fractions allowed to enter apoptosis in relation to the standards.

Fraction	Fold increase in relation to camptothecin (early apoptosis)		Fold increase in relation to camptothecin (late apoptosis)		Fold increase in relation to doxorubicin (early apoptosis)	Fold increase in relation to doxorubicin (late apoptosis)
	6 µg.ml^{-1}	25 µg.ml^{-1}	6 µg.ml^{-1}	25 µg.ml^{-1}	6 µg.ml^{-1}	6 µg.ml^{-1}
F2	-	-	10.66	57.65	4.40	-
F4	-	-	-	-	1.60	-
F5	-	1.38	1.88	3.65	7.30	-
F8	-	1.14	-	29.75	-	-

3.7.4 Morphological features of the melanoma cells that were treated with the active fractions

The morphological features of the untreated or treated melanoma cells were observed by microscopic analysis (Figure 43-44). For the A375 cells, most of these cells remained healthy and attached when they were untreated or treated with DMSO (Figure 43A and 43B). On the other hand, camptothecin (6 µg.ml^{-1} and 25 µg.ml^{-1}) caused rounding of some cells and allowed the rest of the cells to remain attached (Figure 43C-43D). Doxorubicin induced budding (indicated by the arrow) of the cells (Figure 43E). Fractions F2, F4, F5 and F8 (6 µg.ml^{-1} and/or 25 µg.ml^{-1}) also caused rounding of the cells (Figure 43F-43M). Moreover fractions F2 and F4 (25 µg.ml^{-1}) permitted clustering of the cells (Figure 43G and 43I). Fraction F8 (6 µg.ml^{-1}) caused rounding of some cells and allowed the rest of the cells to remain attached (Figure 43L). According to other studies budding and rounding are signs of apoptosis (Archana et al., 2013, Domnina et al., 2002).

For the UACC-62 cells most of these cells remained healthy and attached when they were untreated or treated with DMSO (Figure 44A-44B). On the other hand, camptothecin (6 µg.ml^{-1} and 25 µg.ml^{-1}) and doxorubicin (6 µg.ml^{-1}) caused rounding of the cells (Figure 44C-44E). Fractions F2, F4 and F5 (6 µg.ml^{-1} and 25 µg.ml^{-1}) also caused rounding of the cells (Figure 44F-44K). In addition, fraction F2 (6 µg.ml^{-1}) allowed apoptotic bodies to form (indicated by the arrow) (Figure 44F). Fraction F8 (6 µg.ml^{-1} and 25 µg.ml^{-1}) caused rounding of very few cells and allowed most of the cells to remain attached (Figure F44L-44M). Hence, these results confirmed that the fractions induced the melanoma cells to undergo apoptosis.

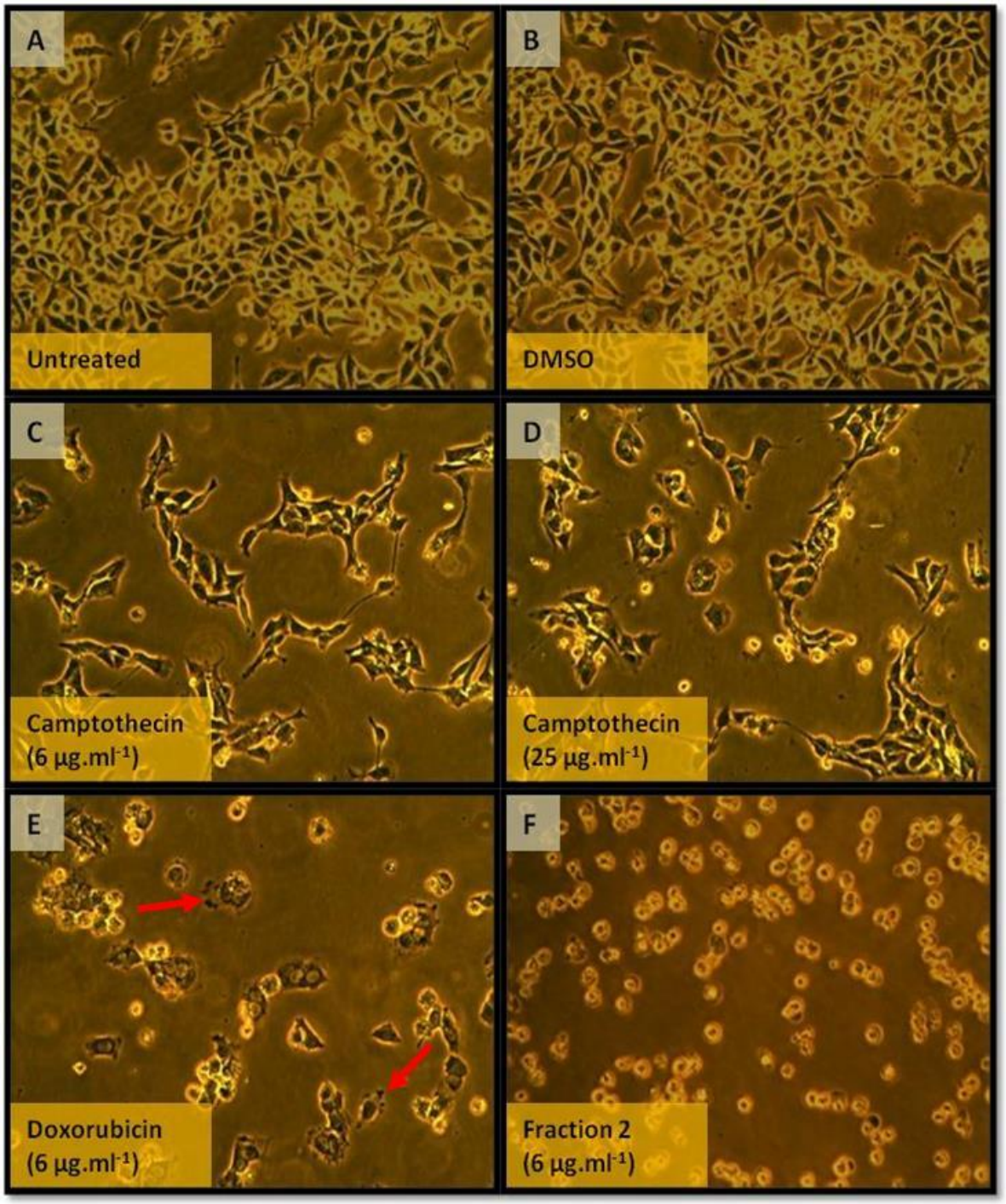
A
Untreated
B
DMSO
C
Camptothecin
(6 µg.ml-1)
D
Camptothecin
(25 µg.ml-1)
E
Doxorubicin
(6 µg.ml-1)
F
Fraction 2
(6 µg.ml-1)

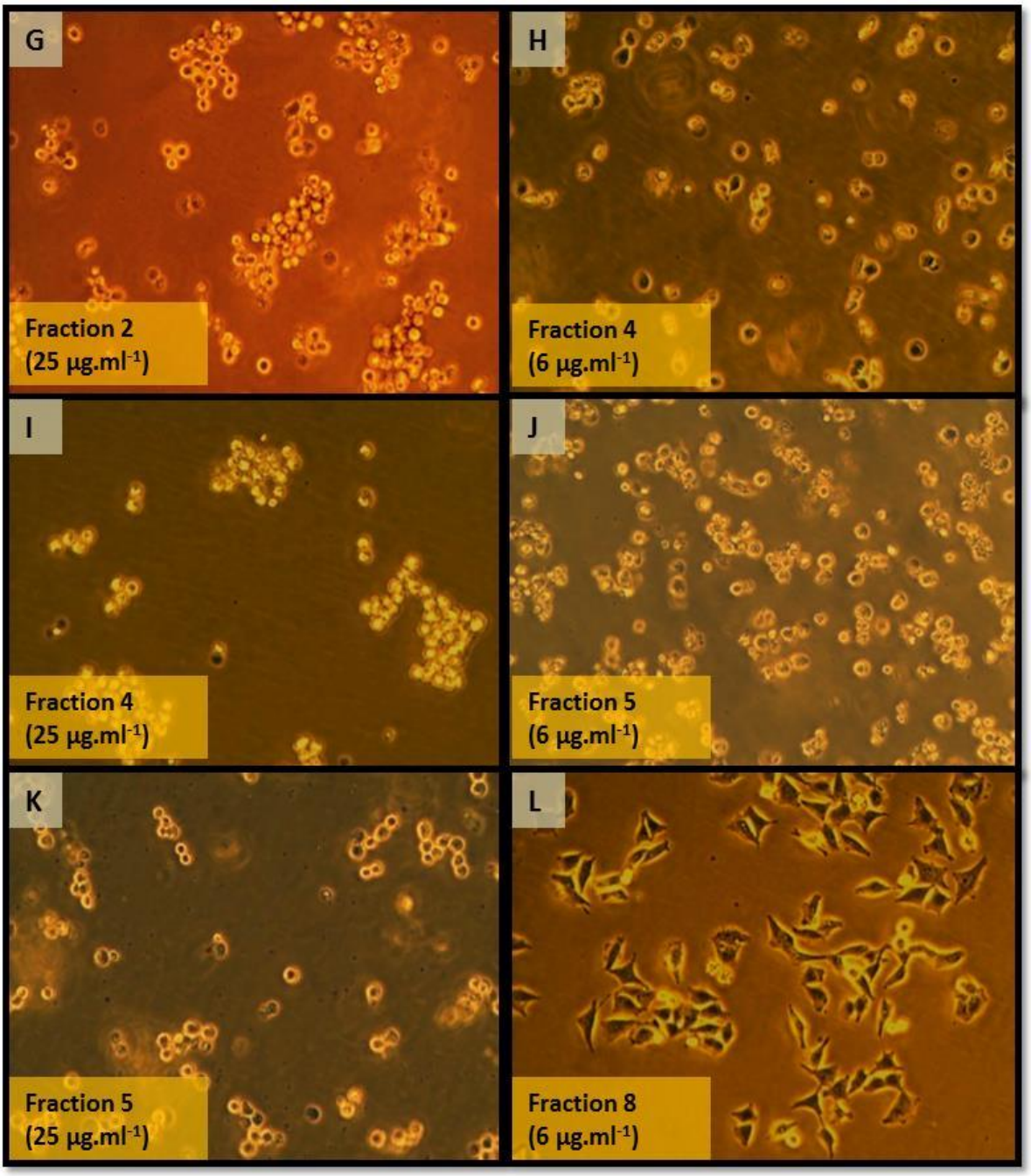
G
Fraction 2
(25 µg.ml-1)
H
Fraction 4
(6 µg.ml-1)
I
Fraction 4
(25 µg.ml-1)
J
Fraction 5
(6 µg.ml-1)
K
Fraction 5
(25 µg.ml-1)
L
Fraction 8
(6 µg.ml-1)

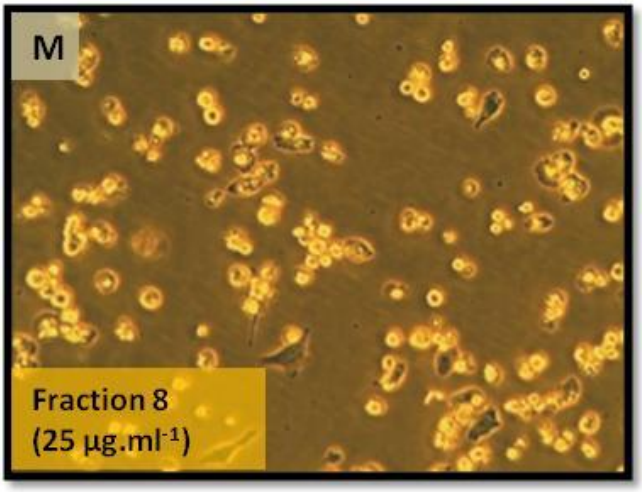

Figure 43: Micrographs (100X magnification) of A375 cells that were untreated (A) or treated with DMSO [0.2%] (B), camptothecin [6 µg.ml^{-1} and 25 µg.ml^{-1}] (C-D), doxorubicin [6 µg.ml^{-1}] (E), fraction F2 [6 µg.ml^{-1} and 25 µg.ml^{-1}] (F-G), F4 [6 µg.ml^{-1} and 25 µg.ml^{-1}] (H-I), F5 [6 µg.ml^{-1} and 25 µg.ml^{-1}] (J-K) and F8 [6 µg.ml^{-1} and 25 µg.ml^{-1}] (L-M).

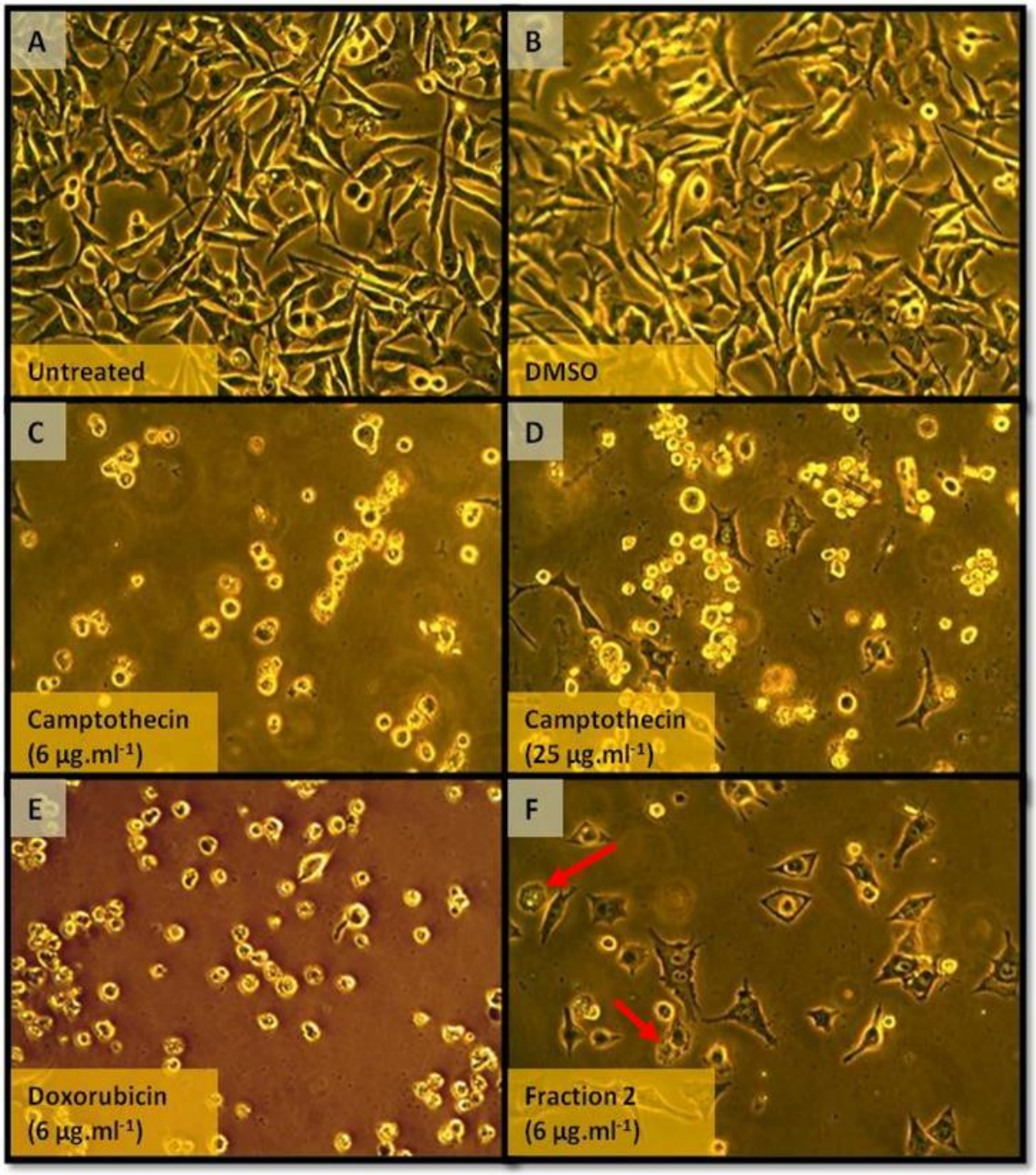
A
Untreated
B
DMSO
C
Camptothecin
(6 µg.ml-1)
D
Camptothecin
(25 µg.ml-1)
E
Doxorubicin
(6 µg.ml-1)
F
Fraction 2
(6 µg.ml-1)

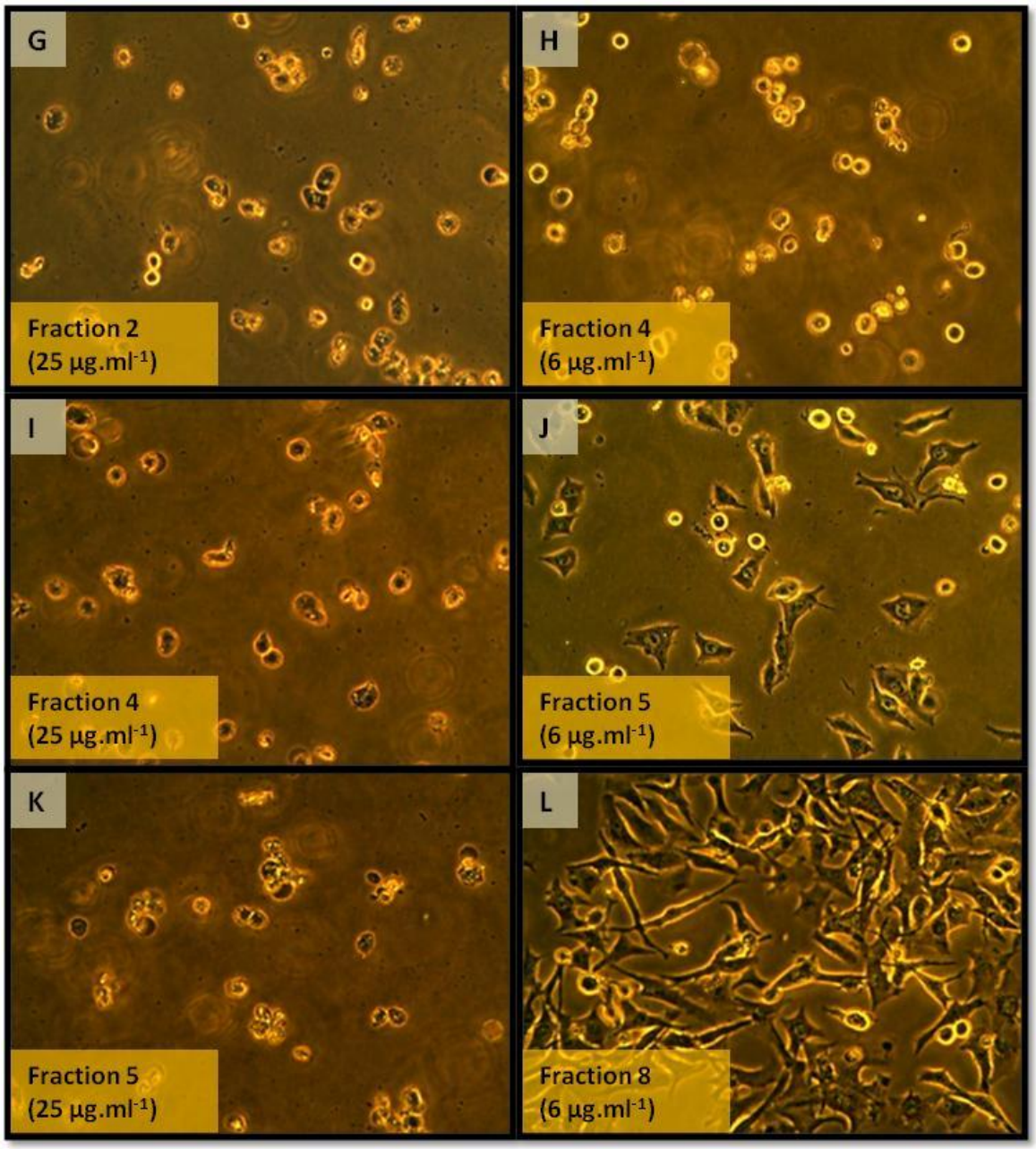
G
Fraction 2
(25 µg.ml-1)
H
Fraction 4
(6 µg.ml-1)
I
Fraction 4
(25 µg.ml-1)
J
Fraction 5
(6 µg.ml-1)
K
Fraction 5
(25 µg.ml-1)
L
Fraction 8
(6 µg.ml-1)

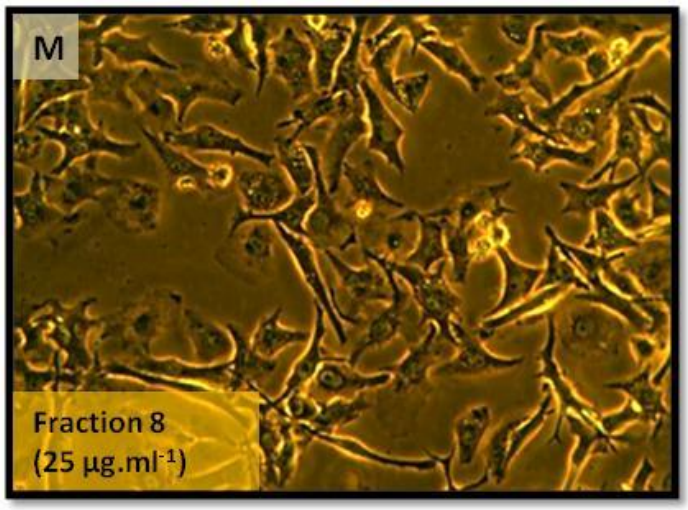

Figure 44: Micrographs (100X magnification) of UACC-62 cells that were untreated (A) or treated with DMSO [0.2%] (B), camptothecin [6 µg.ml^{-1} and 25 µg.ml^{-1}] (C-D), doxorubicin [6 µg.ml^{-1}] (E), fraction F2 [6 µg.ml^{-1} and 25 µg.ml^{-1}] (F-G), F4 [6 µg.ml^{-1} and 25 µg.ml^{-1}] (H-I), F5 [6 µg.ml^{-1} and 25 µg.ml^{-1}] (J-K) and F8 [6 µg.ml^{-1} and 25 µg.ml^{-1}] (L-M).

3.8 EI-LC-MS analysis of the active fractions from *C. triloba* root extract

Preparative High Performance Liquid Chromatography (PHPLC) was used to separate the compounds present in the four active fractions (F2, F4, F5 and F8). The chromatograms in Figure 45-48 display the separation of the compounds. It was evident that the retention times of some of the compounds were very close. Thus the compounds present in the fractions were structurally related. Due to this reason we were unable to separate all of the compounds in the fractions.

The compounds were then structurally elucidated by MS analysis. The mass spectra of the isolated compounds (from PHPLC) were compared to library templates to obtain their structures. For example, the mass spectrum of compound F2A was matched to the mass spectrum of benzothiophen-3(2H)-one, 2-(2-trifluoromethylbenzylideno)- (Figure 49). The library matches for the rest of the compounds are presented in Appendix 3. According to MS analysis a total of 19 compounds were identified from the four fractions that displayed anticancer activity. The structures of these compounds are illustrated in Figure 50-53.

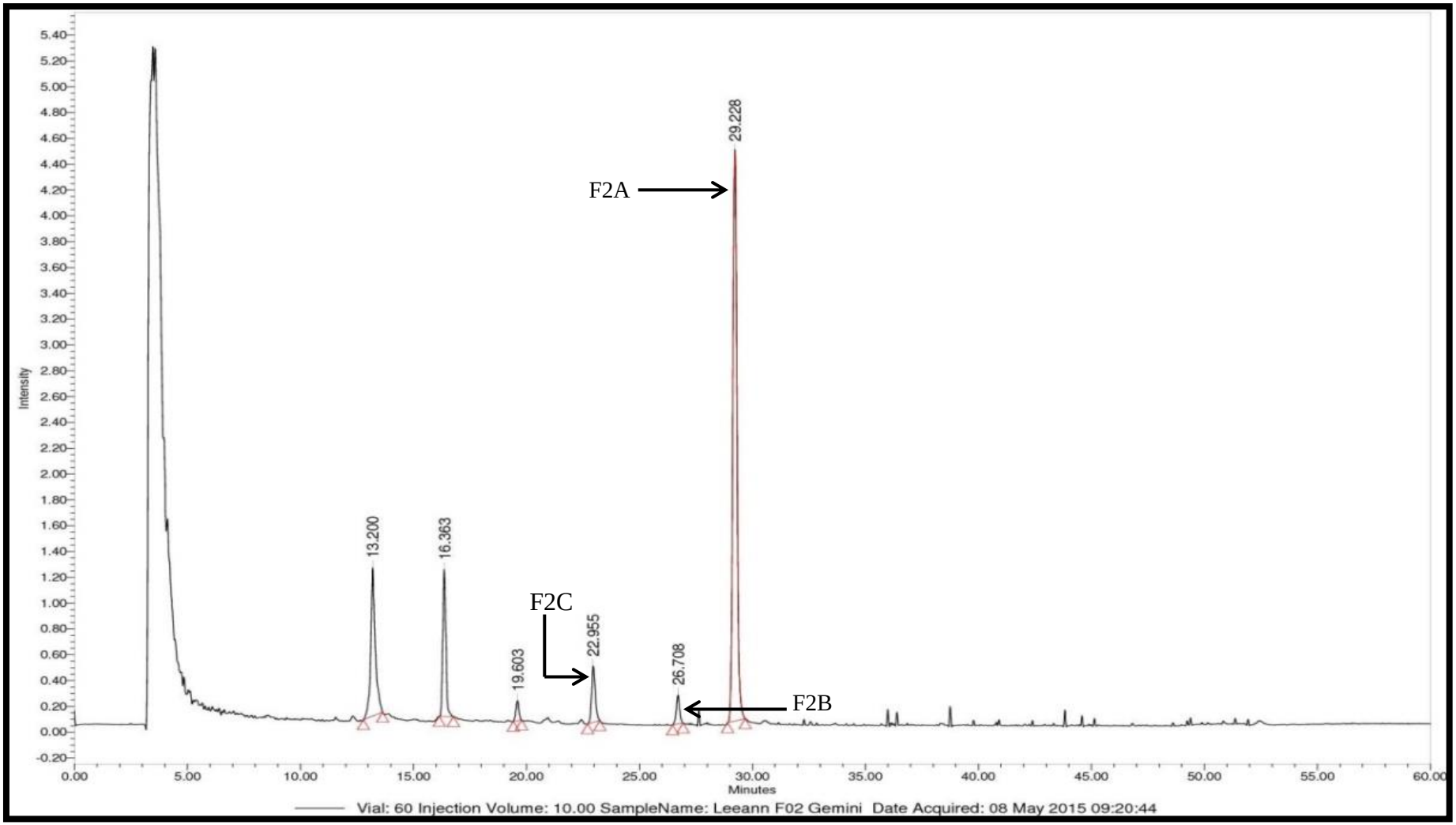

Figure 45: Chromatogram of fraction F2 showing the presence of three distinct compounds of interest at varying retention times. F2A-Retention time (Rt) = 29.228, F2B-Rt = 26.708, F2C-Rt = 22.955.

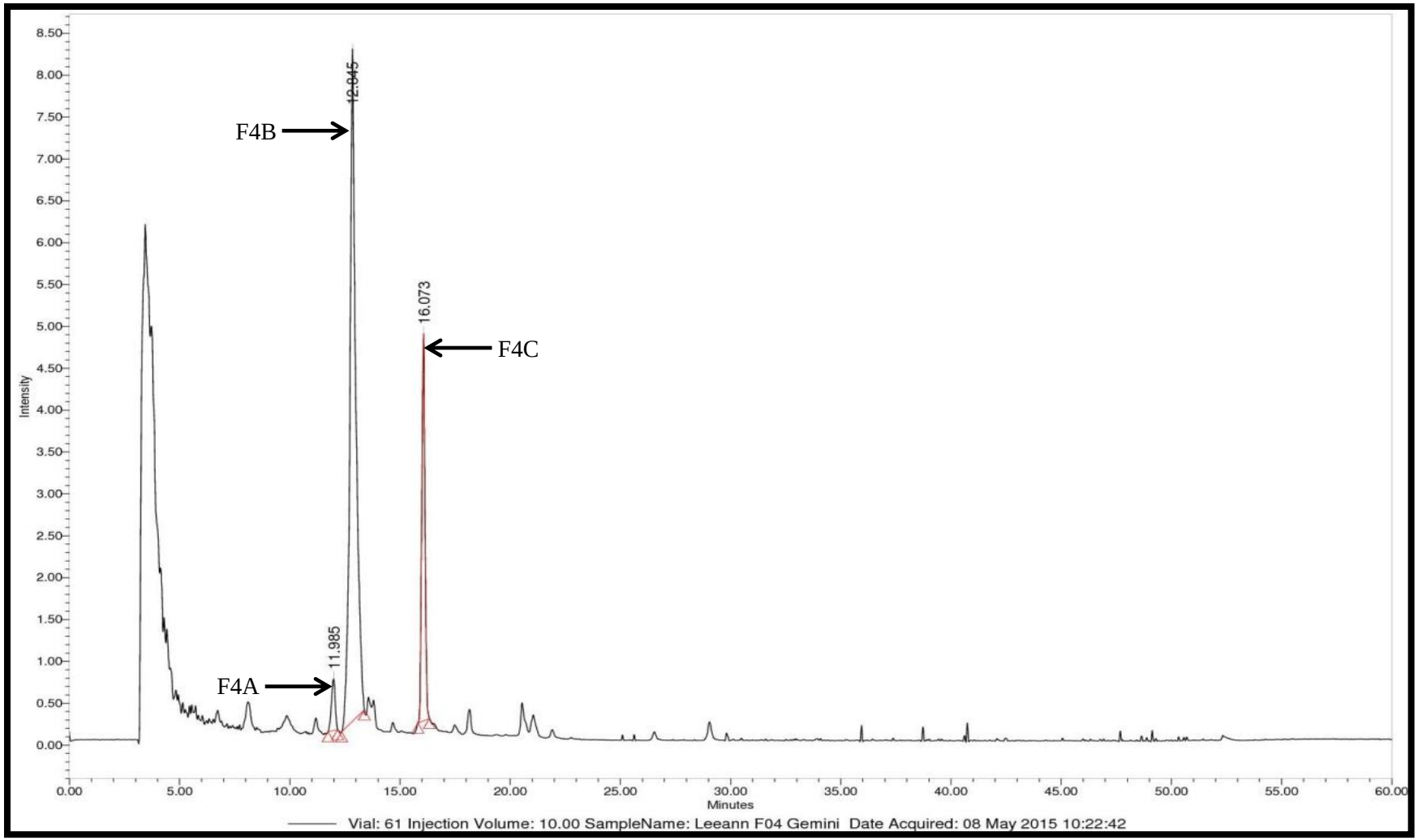

Figure 46: Chromatogram of fraction F4 showing the presence of three distinct compounds of interest at varying retention times. F4A-Retention time (Rt) = 11.985, F4B-Rt = 12.845, F4C-Rt = 16.073.

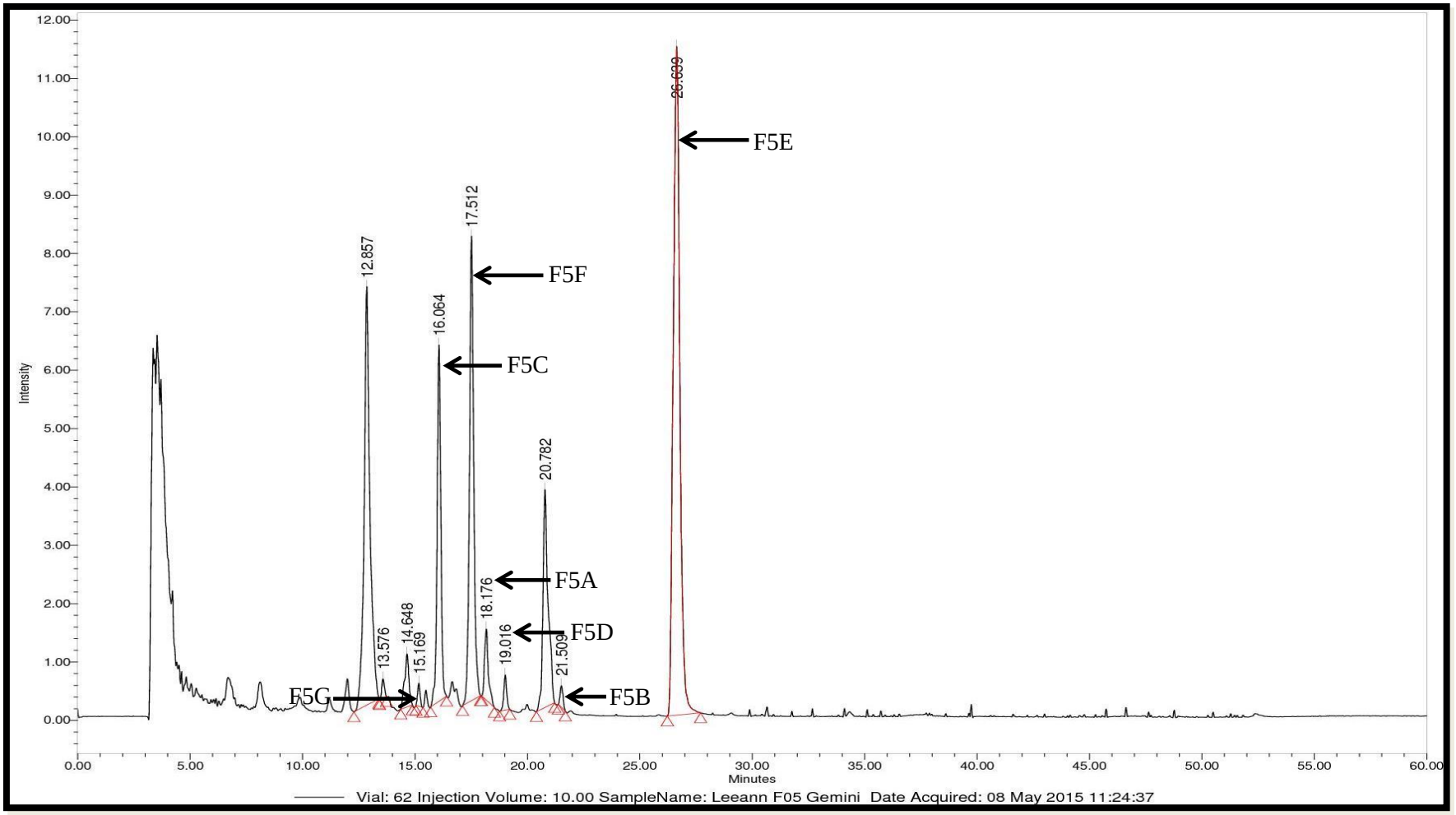

Figure 47: Chromatogram of fraction F5 showing the presence of seven distinct compounds of interest at varying retention times. F5A-Retention time (Rt) =18.176, F5B-Rt = 21.509, F5C-Rt = 16.064, F5D-Rt = 19.016, F5E-Rt = 26.689, F5F-Rt = 17.512, F5G-Rt = 15.169.

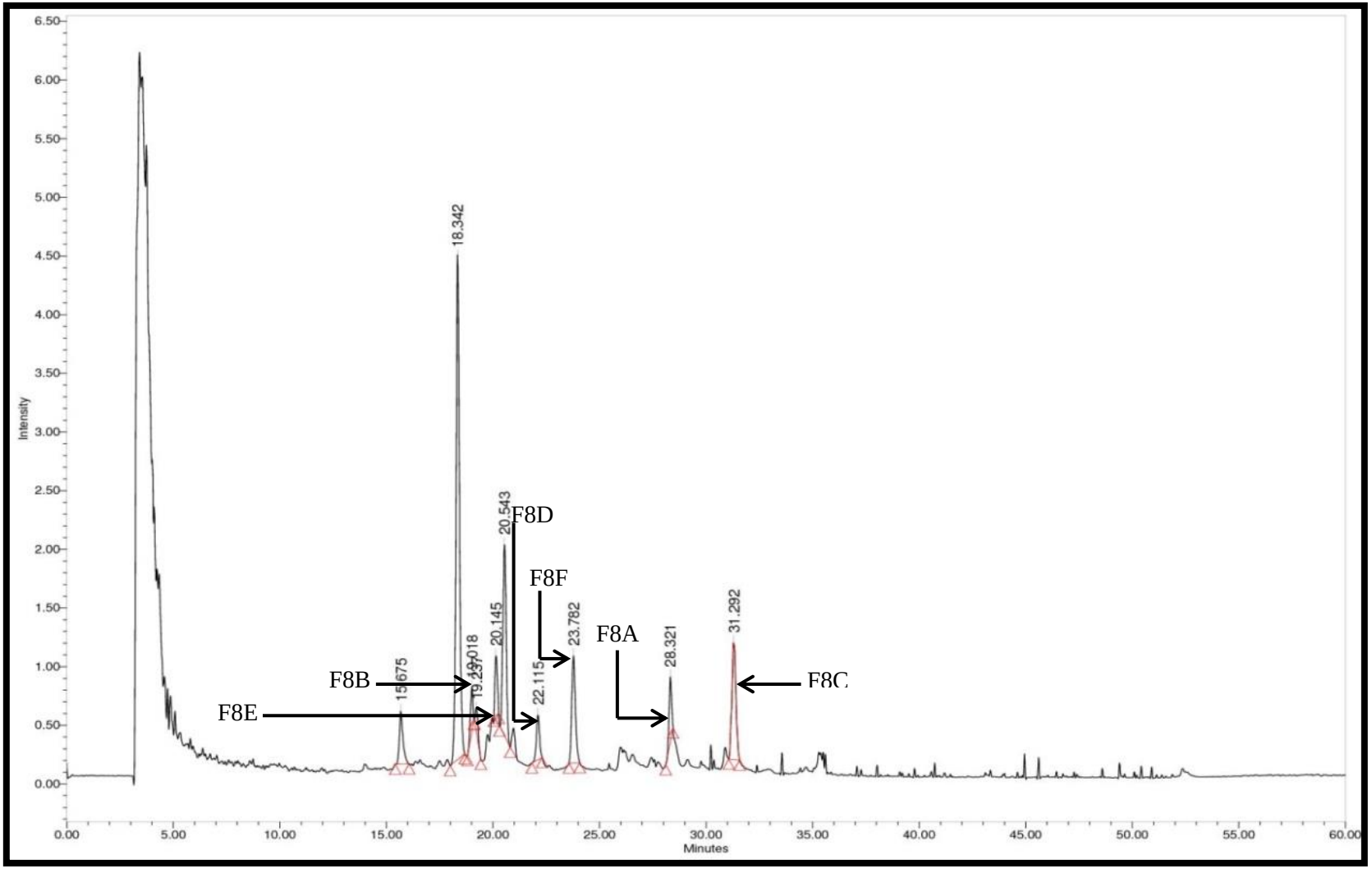

Figure 48: Chromatogram of fraction F8 showing the presence of six distinct compounds of interest at varying retention times. F8A-Retention time (Rt) =28.321, F8B-Rt = 19.237, F8C-Rt = 31.292, F8D-Rt = 22.115, F8E-Rt = 20.145, F8F-Rt = 23.782.

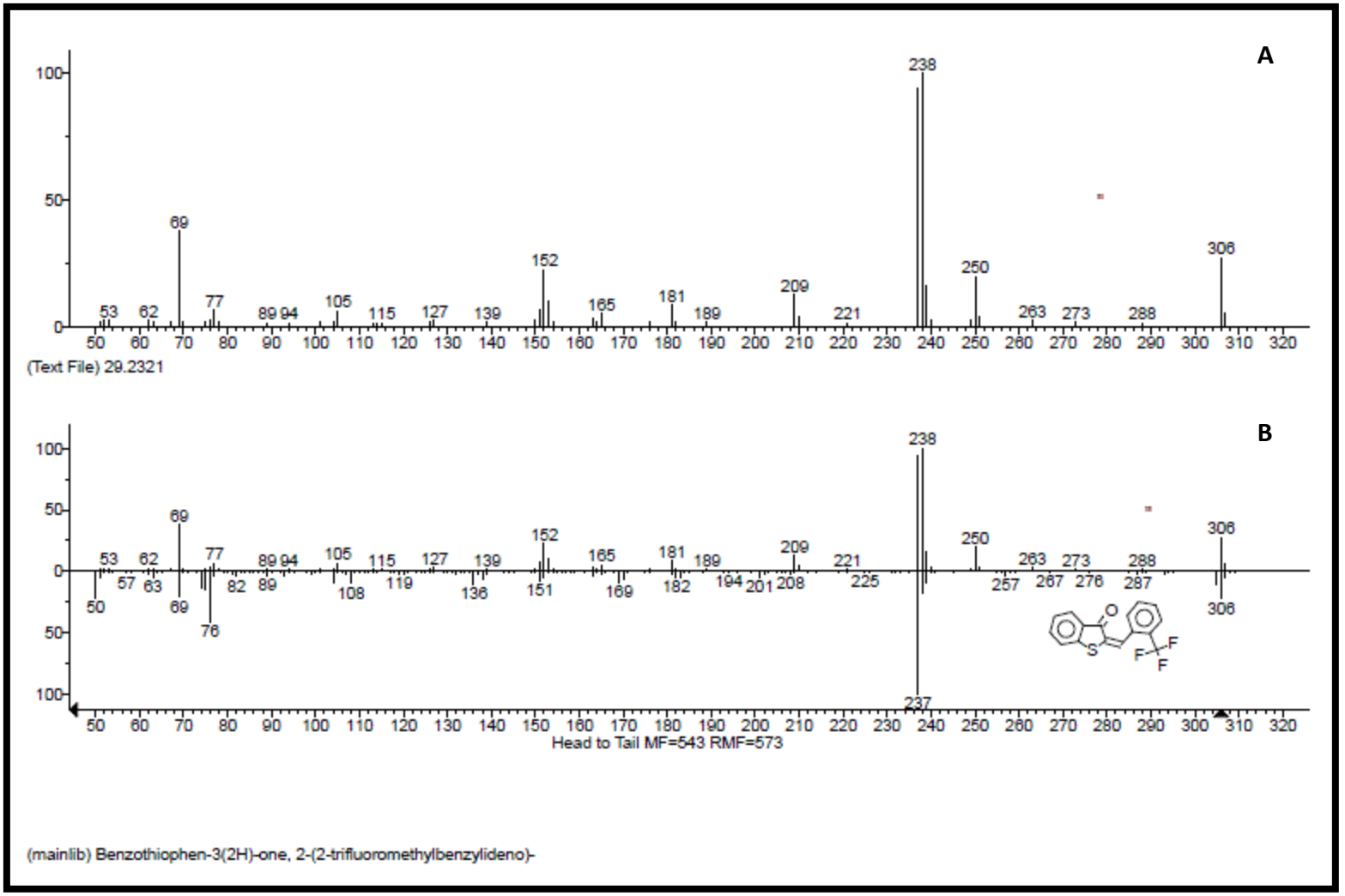

Figure 49: Mass spectrum of compound F2A isolated from *C. triloba* root extract (A) matched the library template of benzothiophen-3(2H)-one, 2-(2-trifluoromethylbenzylideno)-(B).

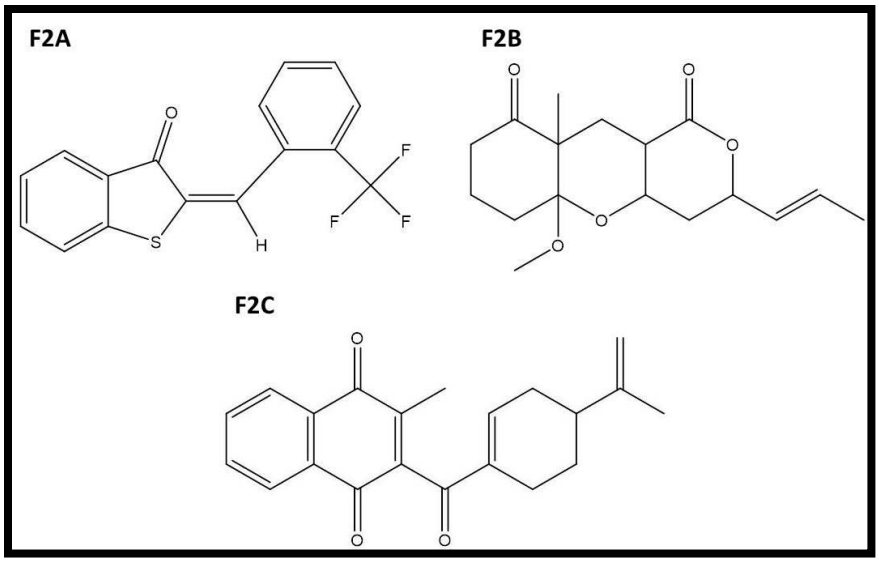

Figure 50: Compounds isolated from fraction F2. F2A-benzothiophen-3(2H)-one, 2-(2-trifluoromethylbenzylideno)-, F2B-pyrano[4,3-b]benzopyran-1,9-dione, 5a-methoxy-9a-methyl-3-(1-propenyl)perhydro, F2C-1,4-naphthoquinone, 3-methyl-2-[(4-isopropenyl-1-cyclohexenyl)formyl]-.

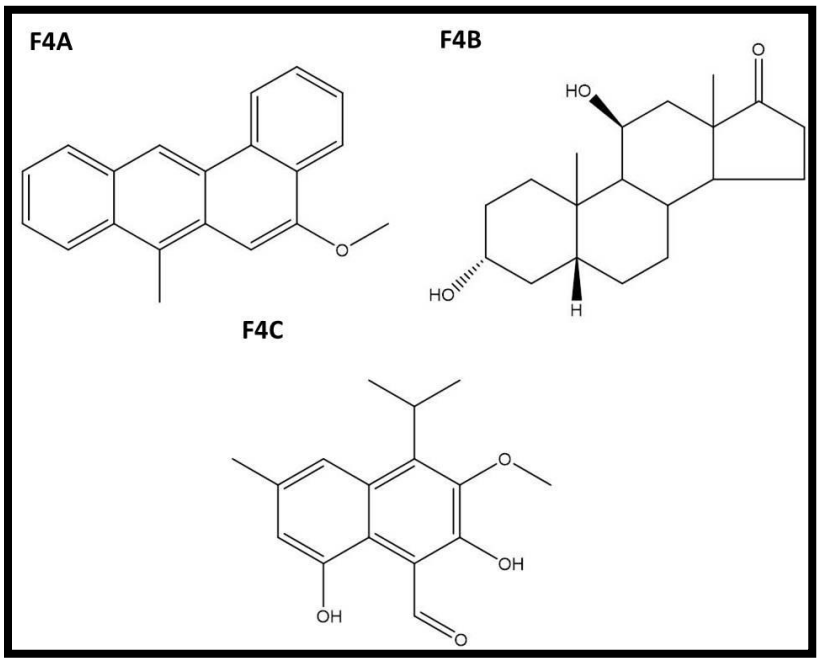

Figure 51: Compounds isolated from fraction F4. F4A-5-methoxy-7-methylbenz(a)anthracene, F4B-androstan-17-one, 3,11-dihydroxy-, (3α,5β,11β)-, F4C-1-naphthalenecarboxaldehyde, 2,8-dihydroxy-3-methoxy-6-methyl-4-(1-methylethyl)-.

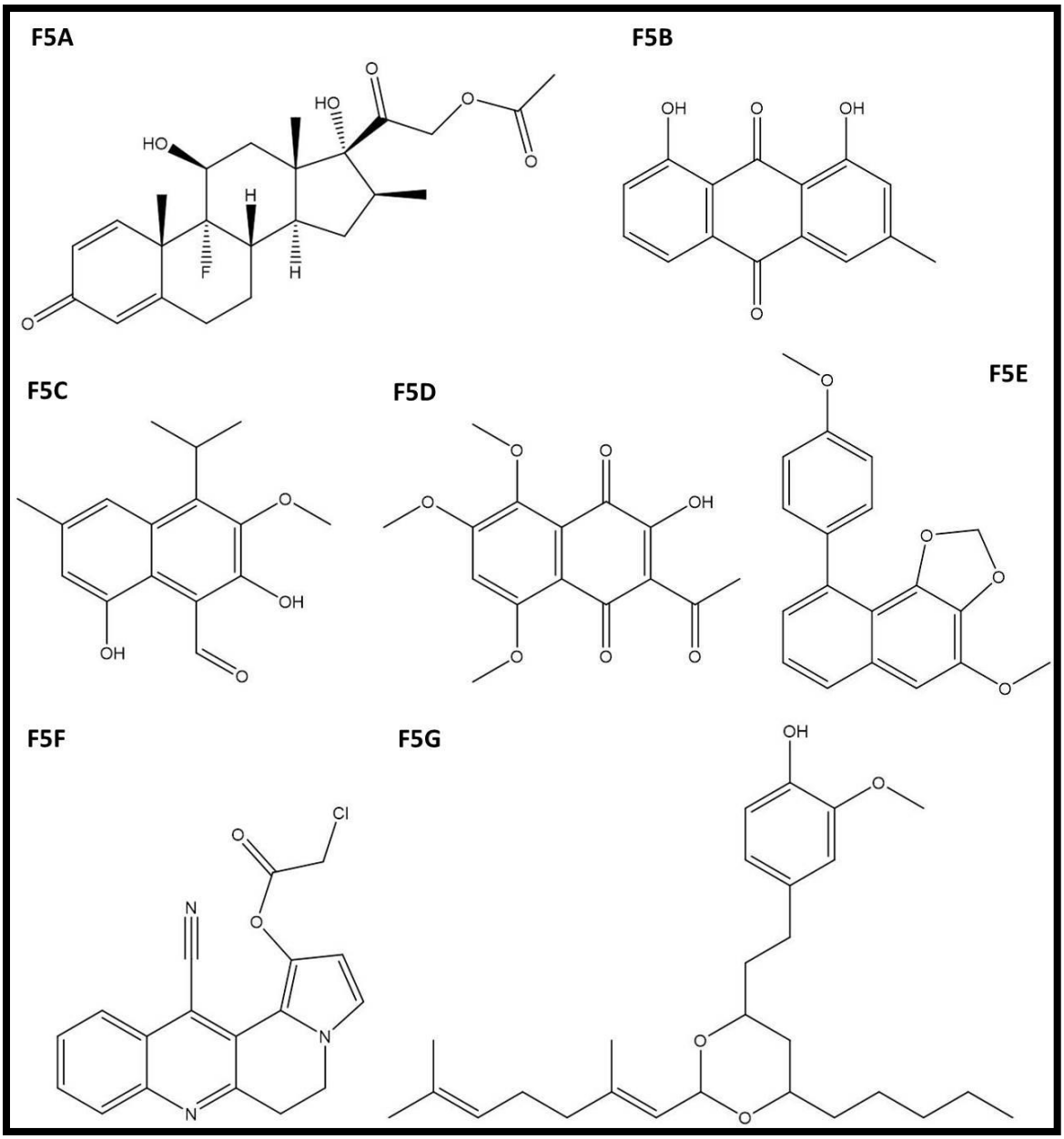

Figure 52: Compounds isolated from fraction F5. F4A-betamethasone acetate, F5B-9,10-anthracenedione, 1,8-dihydroxy-3-methyl, F5C-1-naphthalenecarboxaldehyde, 2,8-dihydroxy-3-methoxy-6-methyl-4-(1-methylethyl)-, F5D-1,4-naphthoquinone, 2-acetyl-3-hydroxy-5,6,8-trimethoxy, F5E-4-methoxy-9-(4-methoxyphenyl)-2H-naphtho[1,2-d][1,3]dioxole, F5F-9-cyano-2,15-diazatetracyclo[8.7.0.0(3,8).0(11,15)]heptadeca-1,3,5,7,9,11,13-heptaen-12-yl 2-chloroacetate, F5G-(E)-4-(2-(2-(2,6-dimethylhepta-1,5-dien-1-yl)-6-pentyl-1,3-dioxan-4-yl)ethyl)-2-methoxyphenol.

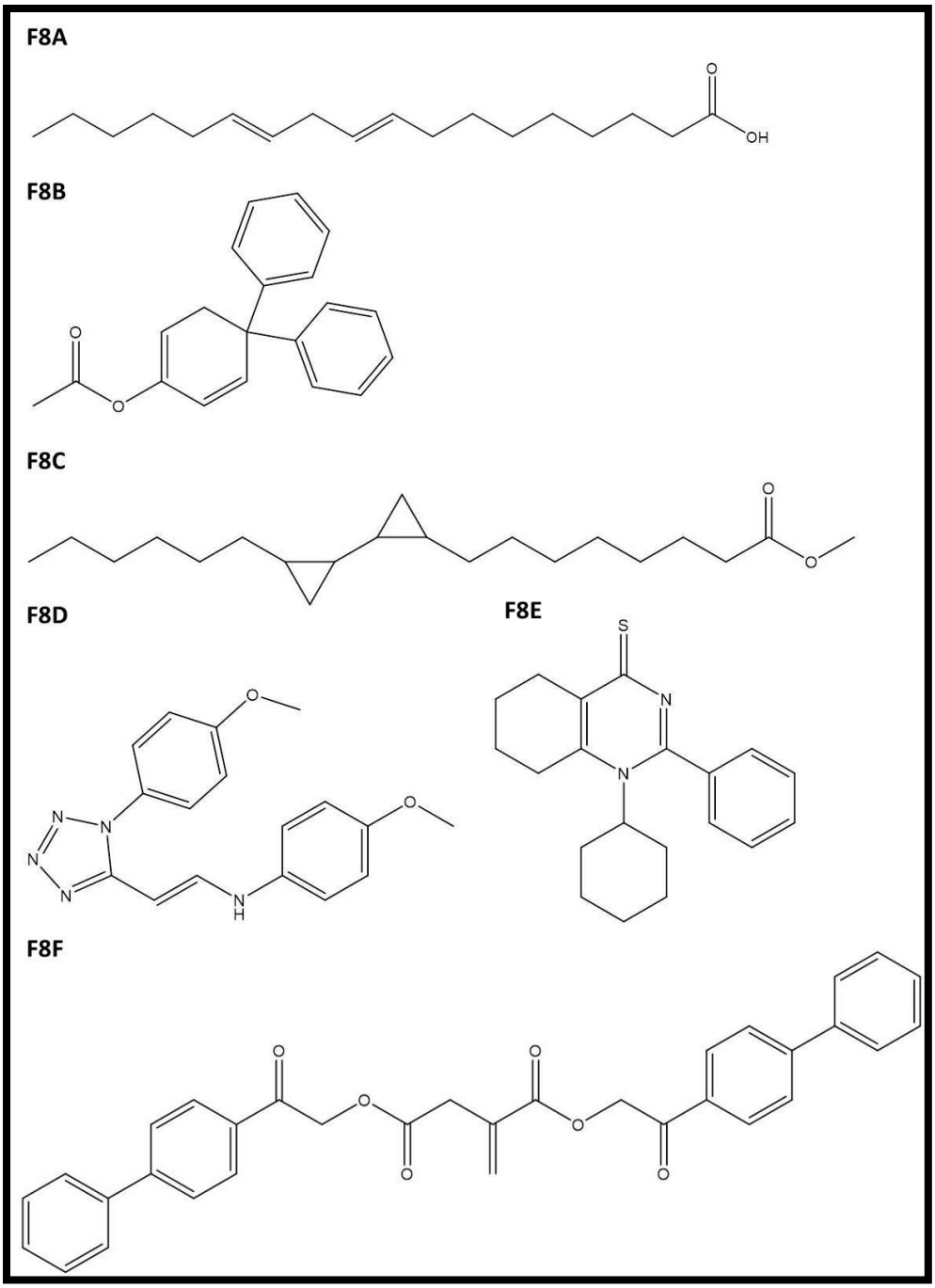

Figure 53: Compounds isolated from fraction F8. F8A-(9E,12E)-octadeca-9,12-dienoic acid, F8B-1,5-cyclohexadien-1-ol, 4,4-diphenyl-, acetate, F8C-[1,1'-bicyclopropyl]-2-octanoic acid, 2'-hexyl-, methyl ester, F8D- benzenamine, 4-methoxy-N-[2-[1-(4-methoxyphenyl)-5-tetrazolyl]ethenyl]-, F8E-4(1H)-quinazolinethione, 1-cyclohexyl-5,6,7,8-tetrahydro-2-phenyl, F8F-2-methylenesuccinic acid, bis-(2-biphenyl-4-yl-2-oxoethyl ester).

4. DISCUSSION

Medicinal plants have played an important role in the discovery of new drugs for the treatment of various diseases such as malaria, Alzheimer's disease, Parkinson's disease, chronic obstructive pulmonary disease, liver diseases and cancer (Veeresham, 2012). The process of drug discovery involves a multifaceted approach that combines the use of botanical, phytochemical, biological and molecular techniques (Balunas and Kinghorn, 2005). Over the years the plant biotechnology group at the Durban University of Technology has used these techniques to determine the pharmacological properties and active constituents of several indigenous plants (Hurinanthan, 2013, Mellem, 2013, Mohanlall, 2010). One of the plants that was studied was *Ceratotheca triloba*. The scientists in our group have reported that the anthraquinones from this plant can inhibit the human topoisomerase II enzyme (target for anticancer drugs) and kill cancer cells (Mohanlall, 2010, Naicker, 2012). However, the *C. triloba* plant has not been extensively studied for its anticancer activity. Therefore, this study was undertaken to further investigate the anticancer activity of *C. triloba* and determine the classes of compounds that contributed towards its activity.

Non-polar to polar solvents (hexane, DCM, DCM: methanol, methanol and water) were used for the extraction of *C. triloba* roots and leaves. According to literature, the use of solvents with different polarities can allow for the retrieval of the different groups of secondary metabolites from plants. For instance, hexane was used to extract prenylated polyketides from the leaves of *Harrisonia abyssinica* (Balde et al., 1999). Hexane was also used to extract terpenoids from the leaves of *Psidium guajava* (Meckes et al., 1996). DCM allowed for terpenoids to be acquired from *Cedrela odorata* stems (Rashed, 2014). A combination of DCM: methanol (1:1) allows for lipids to be extracted from plants (Cos et al., 2006). Methanol was used to extract phenylpropanoid glycosides and a flavonoid from the bark of *Tynanthus panurensis* (Plaza et al., 2005). Methanol was also used to extract benzophenanthridine alkaloids from the leaves, roots and flowers of *Hylomecon hylomeconoides* and *H. vernale* (Kang et al., 2003). The aqueous extraction of *Phyllanthus niruri* leaves allowed for alkaloids and flavonoids to be acquired (Nwanjo, 2006). Therefore, we decided to use a polarity based extraction method so that the

different groups of secondary metabolites could be extracted from *C. triloba* and then be screened on the human cancer cell lines for exhibition of growth inhibition.

The percentage of growth inhibition (%GI) exhibited by *C. triloba* root and leaf extracts on the three cancer cell lines (A375 [melanoma], MDA-MB-231 [breast], and WHC01 [esophageal]) is tabulated in Table 16. Interestingly anthraquinones were isolated from the hexane root extract of *C. triloba* by Mohanlall et al. (2011). This class of compounds could have contributed towards the activity of the hexane root extract as studies have shown that anthraquinones are active against cancer cells. For instance, chrysophanol was found to be active against the MCF-7 (breast) and A375 cancer cell lines (Zhang et al., 2012a). Also emodin (1,3,8-trihydroxy-6-methylanthraquinone) was active against esophageal cancer cells, EC-109 (Wang et al., 2010). Bromo-1-hydroxy-9,10-anthraquinone inhibited the growth of the MCF-7 and MDA-MB-231 cancer cell lines (Abu et al., 2013). Since anthraquinones are important molecules for targeting cancer we chose to further research the anticancer activity of the hexane root extract.

Column chromatography permitted fractionation of the active hexane root extract. This method allowed us to narrow down a large pool of compounds (plant extract) into smaller pools of compounds (fractions). In this way when we screened the fractions for activity, the less active fractions were ruled out while the active fractions were further researched. Certainly, column chromatography did not elute purified compounds (as shown by thin layer chromatograms in Figure 23). This may be due to the co-elution of similar structured compounds from the complex plant extract of *C. triloba*. Hostettmann, (1997) reported that the purification of pharmacological compounds from plants is a difficult and time consuming process. Thus, further research would have to be conducted to achieve the purification of the compounds from *C. triloba*. Separation techniques that can be used to facilitate purification include: mini-column chromatography, preparative thin layer chromatography (PTLC) and preparative high performance liquid chromatography (PHPLC).

Some of the fractions (F2, F3, F4 and F5) isolated from the hexane root extract formed crystals. It has been reported that certain plant derived compounds (such as anthraquinones and naphthoquinones) can form crystals. For instance, 2,6-dihydroxyanthraquinone and 2-hydroxy-6-

methylanthraquinone isolated from the *Rubia cordifolia* extract formed red crystals (Akhtar et al., 2006). In addition, juglone (5-hydroxy-1,4-naphthalenedione) isolated from *Juglans regia* formed yellow crystals (Kale et al., 2013). Thus, the observation of crystals in the fractions may be an indication of the presence of anthraquinones and naphthoquinones.

The percentage growth inhibition of the fractions was determined on two melanoma cell lines. Since the hexane root extract exhibited the highest %GI on the A375 cell line, we chose to continue the study with this cell line and another melanoma cell line (UACC-62). Figure 27 and 28 illustrates the %GI exhibited by the fractions on the two melanoma cell lines. A trend was noticed as fractions F2, F4, F5 and F8 were active on both melanoma cell lines. Thus, it was confirmed that these four fractions contained the active components of the hexane root extract.

Melanoma is a major type of skin cancer that arises from pigment cells called melanocytes (National Cancer Institute, 2015c). According to the World Health Organization (WHO) "one in every three cancers diagnosed is a skin cancer" and "132,000 melanoma skin cancers occur globally each year". It is also important to acknowledge that depletion of the ozone layer enables additional solar UV radiation to penetrate the atmosphere and reach the earth's surface. This phenomenon could lead to an increase in the number of skin cancer cases (World Health Organization, 2015). In terms of treatment, melanoma is extremely resistant to conventional chemotherapy and it can spread to the brain, lung and liver (Gava et al., 2006, Lo et al., 2010). Plus the rate of curing melanoma has not been very high with surgery, radiation or chemotherapy (Hsiao et al., 2012). Therefore, it was essential to investigate the anticancer activity of the fractions on melanoma cells.

The IC_{50} and TGI values are presented in Table 22 and 23. We found that the fractions F2, F5 and F8 were less potent on the melanoma cell lines than the standards (doxorubicin and camptothecin). On the contrary fraction F4 was effective as doxorubicin in terms of exhibiting total growth inhibition of the UACC-62 cells. Therefore, fraction F4 was the most active fraction.

Flow cytometer based assays were conducted for two reasons: firstly to evaluate the apoptosis inducing effects of the active fractions (F2, F4, F5 and F8) and secondly to determine which apoptotic pathways were induced by the fractions. The flow cytometer analysis data revealed that the fractions induced depolarization of the ΔΨ and caspase 3 activity in the A375 and UACC-62 cells (Figure 31, 32, 35 and 36). According to literature these activities form part of the intrinsic and extrinsic (type II) apoptosis pathways.

In the intrinsic pathway, Bid and Bim permeabilizes the outer mitochondrial membrane. Then bax inserts itself into this membrane and induces the release of cytochrome c (mitochondrial intermembrane protein) into the cytosol (Crow et al., 2004, Kim et al., 2006). Subsequently cytochrome c hinders electron flow and causes the impairment of mitochondrial respiratory chain which leads to depolarization of the ΔΨ (Adachi et al., 1997, Cai and Jones, 1998, Lemasters et al., 1999, Mootha et al., 2001). Cytochrome c also participates in the formation of the apoptosome which releases caspase 9. This enzyme in turn activates pro-caspase 3 to caspase 3 (Figure 6) (Acehan et al., 2002, Igney and Krammer, 2002, Luo et al., 1998, Slee et al., 1999).

In the extrinsic pathway (type II), caspase 8 cleaves BID to form truncated BID (tBID) which translocates to the mitochondria and actives pro-apoptotic proteins Bax and Bak (Luo et al., 1998, Pope, 2002). These proteins then facilitate the release of cytochrome c into the cytosol (Belizario et al., 2007, Bonora and Pinton, 2014, Brenner et al., 2000, Jeong and Seol, 2008, Liu et al., 1996b, Narita et al., 1998). Subsequently cytochrome c elicits depolarization of the ΔΨ and participates in the formation of the apoptosome which releases caspase 9. This enzyme in turn activates pro-caspase 3 to caspase 3 (Figure 9) (Acehan et al., 2002, Adachi et al., 1997, Cai and Jones, 1998, Lemasters et al., 1999, Mootha et al., 2001, Slee et al., 1999).

Taken together we can deduce that the fractions (F2, F4, F5 and F8) caused the A375 and UACC-62 cells to undergo apoptosis via the intrinsic or extrinsic (type II) pathway. This can be justified by the following facts: Depolarization of the ΔΨ and caspase 3 activity were induced in the melanoma cells (Figure 31, 32, 35 and 36). According to previous reports depolarization of the ΔΨ and caspase 3 activity form part of a cascade of interactions that facilitate these pathways. This means that these activities cannot happen without the activation of other

apoptotic molecules of the intrinsic or extrinsic (type II) pathway (as describe in the previous paragraphs). Thus, although we did not examine other apoptotic molecules, our results and previous reports provide sufficient evidence to support our argument. However, further research should be conducted to determine which of these two pathways the fractions are capable of inducing.

Moreover the fractions (F2, F4, F5 and F8) induced a high percentage of caspase 3 positive cells (Figure 37 and 38). Reports have shown that caspase 3 cleaves DFF45 (DNA fragmentation factor-45)/ICAD (inhibitor of caspase-activated DNase) which exists in a complex with a 40-kDa endonuclease known as DFF40 (DNA fragmentation factor-40)/CAD (caspase-activated DNase). Subsequently DFF40/CAD is released and it promotes apoptotic DNA fragmentation (Enari et al., 1998, Halenbeck et al., 1998, Liu et al., 1997, Liu et al., 1998). Caspase 3 also activates pro-caspase 6 to caspase 6 which is responsible for degrading lamins, thus promoting nuclear apoptosis (Liu et al., 1996a, Orth et al., 1996). Therefore, caspase 3 probably carried out these tasks to promote apoptosis of the treated melanoma cells.

Interestingly literature has revealed that early and late apoptosis are associated with caspase 3 activity. Researchers, Kekre et al. (2005) reported that both PS exposure and caspase 3 activity occurred during the "induction phase of apoptosis" (early apoptosis). However it is unclear if caspase 3 is involved in bringing about PS exposure in cancer cells as reports only present mechanisms that are responsible for PS exposure in blood and pathogenic cells (Blankenberg and Strauss, 2012, Wood et al., 1996, Zwaal and Schroit, 1997, Zwaal et al., 2005). On the other hand, caspase 3 indirectly activates DNA fragmentation during late apoptosis (Collins et al., 1997, Enari et al., 1998, Halenbeck et al., 1998, Liu et al., 1997, Liu et al., 1998). In our study fraction F4 (25 $\mu g.ml^{-1}$, UACC-62 cells) induced 4.3% of early apoptotic cells, fraction F2 (25 $\mu g.ml^{-1}$, A375 cells) induced 93.39% of late apoptotic cells and fraction F5 (6 $\mu g.ml^{-1}$, A374 cells) induced 16.64% of early apoptotic cells and 13.09% of late apoptotic cells (fraction F8 also induced apoptosis) (Figure 41 and 42). In all three cases, the fractions induced over 80% of caspase 3 positive cells (Figures 37 and 38). Therefore, the fractions permitted early and/or late apoptosis which was associated with caspase 3 activation. This can be further studied by using

time-lapse fluorescence microscopy with live cell imaging (Bouchier-Hayes et al., 2008, Skommer et al., 2010).

The compounds from the four active fractions (F2, F4, F5 and F8) were characterized by EI-LC-MS analysis. After consulting with literature, we confirmed that a total of nine anticancer compounds were found in the root extract of *C. triloba*. These were: benzothiophen-3(2H)-one, 2-(2-trifluoromethylbenzylideno)- (F2A), pyrano[4,3-b]benzopyran-1,9-dione, 5a-methoxy-9a-methyl-3-(1-propenyl)perhydro (F2B), 1,4-naphthoquinone, 3-methyl-2-[(4-isopropenyl-1-cyclohexenyl)formyl]- (F2C), 5-methoxy-7-methylbenz(a)anthracene (F4A), androstan-17-one, 3,11-dihydroxy-, (3α,5β,11β)- (F4B), 9,10-anthracenedione, 1,8-dihydroxy-3-methyl (F5B), 1,4-naphthoquinone, 2-acetyl-3-hydroxy-5,6,8-trimethoxy (F5D), 9-Cyano-2,15-diazatetracyclo[8.7.0.0(3,8).0(11,15)]heptadeca-1,3,5,7,9,11,13-heptaen-12-yl 2-chloroacetate (F5F) and 4(1H)-quinazolinethione, 1-cyclohexyl-5,6,7,8-tetrahydro-2-phenyl (F8E). These compounds fit into the different classes of anticancer compounds based on their core structure. In addition, the active fractions exhibited similar activities (such as growth inhibition and apoptosis activities [depolarization of the mitochondria membrane potential, caspase 3 activation and PS exposure]) as previously studied anticancer compounds. Thus, these nine compounds could have contributed towards the anticancer activity of the active fractions.

Benzothiophen-3(2H)-one, 2-(2-trifluoromethylbenzylideno)- (F2A) belongs to a class of compounds known as benzothiophenones. These compounds have not been extensively studied for their anticancer activity. However, Zhang et al. (2006) filed a patent for an invention that involved the use of benzothiophenones for the treatment of cancer or inflammation. Therefore these compounds do have the ability to kill cancer cells.

Pyrano[4,3-b]benzopyran-1,9-dione, 5a-methoxy-9a-methyl-3-(1-propenyl)perhydro (F2B) belongs to a class of compounds known as benzopyranones (also called coumarins). Studies have shown that these compounds possess anticancer activity. For instance, 2H-l-benzopyran-2-one and 7-hydroxy-2H-l-benzopyran-2-one displayed cytostatic and cytotoxic activities against various human cancer cell lines (A549 [lung], ACHN [renal], H727 [lung], MCF-7 [breast] and HL-60 [leukemia]) (Mohler et al., 1992, Egan et al., 1997, Stanchev et al., 2008, Thornes et al.,

1994). Moreover Zeldis, (2004) filed a patent for an invention that involved the use of benzopyranones for the treatment or prevention of brain cancer or brain metastasis. These compounds are also capable of eliciting apoptosis inducing effects. For example, 2H-l-benzopyran-2-one elicited depolarization of the mitochondrial membrane potential, DNA fragmentation and activation of caspase 3 in HeLa (cervical cancer) cells (Chuang et al., 2007).

1,4-naphthoquinone, 3-methyl-2-[(4-isopropenyl-1-cyclohexenyl)formyl]- (F2C) and 1,4-naphthoquinone, 2-acetyl-3-hydroxy-5,6,8-trimethoxy (F5D) belongs to a class of compounds known as naphthoquinones. Over the years, researchers have reported several anticancer naphthoquinones. We referred to two derivatives. Plumbagin (5-hydroxy- 2-methyl-1, 4-naphthaquinone) can be isolated from the genus known as *Plumbago* (Bhasin et al., 2013). This compound has shown to inhibit various cancer cell lines. Examples include: MDA-MB-231 (breast), CAL27 (oral adenosquamous carcinoma) and U937 (leukemia) (Gaascht et al., 2014, Liu et al., 2015, Manu et al., 2011). Also Xu et al. (2013) reported that plumbagin activated caspase 3 and 9 in several human non-small cell lung cancer cell lines (A549, H292 and H460). Another naphthoquinone, juglone (5-hydroxy-1,4-naphthalenedione) was isolated from *Juglans mandshuria* (Liu et al., 2004). This compound has shown to elicit apoptotic inducing effects such as PS exposure (in HeLa cells) and caspase 3 and 9 activation (in LS-174T cells [colon adenocarcinoma]) (Li et al., 2013, Zhang et al., 2012b).

5-methoxy-7-methylbenz(a)anthracene (F4A) and 9,10-anthracenedione, 1,8-dihydroxy-3-methyl (F5B) belongs to a class of compounds known as anthraquinones. This class of compounds consist of several hundreds of compounds that differ in the nature and positions of substituent groups (Schripsema et al., 1999). Anthraquinone derivatives contain 9,10-anthracenedione as a base structure (Bajaj, 1999). These compounds have been used in the treatment of various cancers. For example, mitoxantrone is used in the treatment of metastatic breast cancer, acute myeloid leukemia and non-Hodgkin's lymphoma (Arlin et al., 1985, Dutcher et al., 1985, Paciucci et al., 1983). Another anthraquinone, doxorubicin is used for the treatment of breast cancer and gynecological and hematological malignancies (Preobrazhenskaya et al., 2006). Moreover, recent studies have reported the anticancer activity of other anthraquinones. Physcion (1,8-dihydroxy-3-methoxy-6-methylanthracene-9,10-dione) from *Rheum tanguticum*

inhibited MDA-MB-231 cells (Hong et al., 2014). 1,3-dihydroxy-9,10-anthraquinone-2-carboxylic acid inhibited MCF-7 cells (Yeap et al., 2015). Rhein (4,5-dihydroxy anthraquinone-2-carboxylic acid) is a natural anthrathraquinone that is found in *Rheum palmatum*, *Rheum tanguticum*, *Cassia angustifolia* and *Cassia fistula* (Duraipandiyan et al., 2012, Hoerhammer et al., 1959, Irshad et al., 2011, Lee et al., 2003) Al-Fatlawi et al. (2014) reported that it induced DNA fragmentation and caspase 3 and 9 activities in several human cancer cell lines (SiHa [cervical cancer], MCF-7 and HepG2).

Androstan-17-one, 3,11-dihydroxy-, (3α,5β,11β)- (F4B) belongs to a class of compounds known as androstanes. The following androstane derivatives have shown to possess anticancer properties. Dehydroepiandrosterone derivatives inhibited KB (nasopharyngeal epidermoid carcinoma) and T47D (human breast cancer) cell lines (Vosooghi et al., 2013). Aminothienoandrostane inhibited HepG2 cells (Elmegeed et al., 2009). Androstane D-Seco-mesyloxy derivatives inhibited MDA-MB-231, HeLa and PC-3 (human prostate cancer) cells (Oklješa et al., 2013). 5α-androstane-3α,17β-diol induced caspase 3 and 8 activities in HL-60 (human promyelocytic leukemia) cells (Jegham et al., 2012). Thus, these steroidal compounds are effective against various cancers.

4(1H)-quinazolinethione, 1-cyclohexyl-5,6,7,8-tetrahydro-2-phenyl (F8E) and 9-Cyano-2,15-diazatetracyclo[8.7.0.0(3,8).0(11,15)]heptadeca-1,3,5,7,9,11,13-heptaen-12-yl 2-chloroacetate (F5F) belongs to a class of compounds known as quinazolines. These compounds are known to have a broad spectrum of biological activity which includes targeting cancer cells (Zahedifard et al., 2015). For instance, 6-[(4-(B-chloro-2-(pyridine-4-yl)quinazoline-4-ylamino)phenyl)-2-amino-4-(4-methoxyphenyl)]-pyridine-3-carbonitrile and 1-(4-(6-chloro-2-(pyridin-4-yl)quinazolin-4-amino)phenyl)-3-(4-nitrophenyl)prop-2-en-1-one inhibited liver cancer cells, HepG2 (Wasfy et al., 2015). In addition, 6-bromo-2-(morpholin-1-yl)-4-anilinoquinazoline induced caspase 3 activity and DNA fragmentation in several leukemia cell lines (L1210, HL-60 and U-937) (Jantova et al., 2008). Other quinazolines, 3-(5-chloro-2-hydroxybenzylideneamino)-2-(5-chloro-2-hydroxyphenyl)-2,3 dihydroquinazolin-41(H)-one and 3-(5-nitro-2-hydroxybenzylideneamino)-2-(5-nitro-2-hydroxyphenyl)-2,3-dihydroquinazolin-4(1H)-one induced budding and chromosomal condensation (which are parts of apoptosis) in MCF-7 cells.

Cellomics High Content Screening (HCS) (automated cellular imaging) revealed that these compounds triggered the release of cytochrome c from the mitochondria into the cytosol. Also, caspase 3, 7, 8 and 9 activities was detected. Zahedifard et al. (2015) deduced that these quinazolines induced apoptosis of the MCF-7 cells through the extrinsic (type II) or intrinsic pathway.

Amongst the compounds that were found in *C. triloba* root extract was an important compound known as betamethasone acetate. This compound is a steroid that has anti-inflammatory and immunosuppressant properties. It is used for the treatment of diseases that involve the blood and lymphatic systems (Bethesda, 2006). Hence, the *C. triloba* plant has great medicinal value.

This is the first study that shows the presence of these compounds in *C. triloba* roots. Mohanlall et al. (2011) previously found 9,10-anthracenedione; 1-hydroxy-4-methylanthraquinone; 5,8-dimethoxy-2,3,10,10a-tetrahydro-1H,4aH-phenanthrene-4,9-dione and androst-5-ene-3, 17, 19-triol. We were unable to find these compounds in the roots of *C. triloba* as derivatization (presence of similar structured compounds) made chromatographic analyse a challenge. Other techniques (such as mini-column chromatography, PTLC and PHPLC) would have to be employed to achieve maximum separation. Nevertheless, our study has revealed that the roots of *C. triloba* serve as a rich source of anticancer compounds. It was important to perform this study as Narang and Desai, (2009) reported that the "identification of cytotoxic compounds led to the development of anticancer therapeutics for several decades". Thus, the compounds characterized in this study could be used towards the development of new anticancer drugs.

5. CONCLUSIONS

C. triloba is an indigenous plant that has been used in traditional medicine to treat painful menstruation, stomach cramps, nausea, fever and diarrhea (Tredgold, 1986). Over the years we have uncovered that this plant has anticancer activity. Studies have found that anthraquinones is the class of compounds that are responsible for its anticancer activity (inhibits human topoisomerase II and kills cancer cells) (Mohanlall, 2010, Naicker, 2012). However, there are certain unanswered questions like: are there any other anticancer compounds present in the plant and do these compounds exhibit apoptotic activity. Thus, in this study the anticancer activity of *C. triloba* was further investigated and the classes of compounds that contributed towards its activity were determined.

Leaf and root extracts were prepared using a polarity based extraction method (the use of non-polar to polar solvents - hexane, DCM, DCM: methanol [1:1], methanol and water). It was clear that the hexane root extract exhibited the highest %GI on all three cancer cell lines (A375 [81.35%], MDA-MB-231 [65.77%] and WHCO1 [78.61%] at 50 µg.ml^{-1}). In addition, the A375 cell line was most susceptible to this extract. Therefore this cell line and another melanoma cell line (UACC-62) were used in the study.

The separation of the compounds of the hexane root extract was optimized on TLC plates by using different ratios of hexane: DCM. The principle behind this method was that the separation of the compounds was achieved by slowly increasing the polarity of the mobile phase. Hence, a similar principle was applied to column chromatography. Subsequently, the fractionation of the hexane root extract was achieved by gradually increasing the polarity of the mobile phase in the column with hexane: DCM, DCM, DCM: ethyl acetate, ethyl acetate and ethyl acetate: methanol. A total of ten combined fractions were collected from the column. Four of these fractions (F2, F4, F5 and F8) displayed a high %GI on the A375 (89.85, 89.39, 90.81 and 75.51 %GI at 25 µg.ml^{-1}, respectively) and UACC-62 (74.54, 97.55, 86.96 and 73.29 %GI at 25 µg.ml^{-1}, respectively) cell lines. Moreover, fraction F4 was the most active fraction as it had the lowest IC_{50} (0.70 µg.ml^{-1} [A375] and 0.39 µg.ml^{-1} [UACC-62]) and TGI (12.50 µg.ml-1[A375] and 25 µg.ml-1 [UACC-62]) values in comparison to the other fractions.

According to the flow cytometer analysis data, fractions F2, F4, F5 and F8 induced depolarization of the mitochondria membrane potential (ΔΨ), caspase 3 activation, early apoptosis (phospholipid phosphatidylserine exposure) and/or late apoptosis in the melanoma cells. The results also revealed that fraction F4 (25 µg.ml-1) induced depolarization of the ΔΨ to a higher percentage of A375 (78.11%) and UACC-62 (87.4%) cells than the other fractions and standards. This fraction also induced caspase 3 activation to a high percentage of A375 (90.56%) and UACC-62 (96.78%) cells. Therefore, fraction F4 was also the most active fraction in terms of apoptosis activity. Based on our results and literature findings, it was deduced that the active fractions induced the intrinsic or extrinsic (type II) apoptosis pathway in the melanoma cells.

Six classes of compounds were isolated from the hexane root extract of *C. triloba*. These were: benzothiophenones (benzothiophen-3(2H)-one, 2-(2-trifluoromethylbenzylideno)- [F2A]), benzopyranones (pyrano[4,3-b]benzopyran-1,9-dione, 5a-methoxy-9a-methyl-3-(1-propenyl)perhydro [F2B]), naphthoquinones (1,4-naphthoquinone, 3-methyl-2-[(4-isopropenyl-1-cyclohexenyl)formyl]- [F2C] and 1,4-naphthoquinone, 2-acetyl-3-hydroxy-5,6,8-trimethoxy [F5D]), anthraquinones (5-methoxy-7-methylbenz(a)anthracene [F4A] and 9,10-anthracenedione, 1,8-dihydroxy-3-methyl [F5B]), androstanes (androstan-17-one, 3,11-dihydroxy-, (3α,5β,11β)- [F4B]) and quinazolines (4(1H)-quinazolinethione, 1-cyclohexyl-5,6,7,8-tetrahydro-2-phenyl [F8E] and 9-Cyano-2,15-diazatetracyclo [8.7.0.0(3,8).0(11,15)] heptadeca-1,3,5,7,9,11,13-heptaen-12-yl 2-chloroacetate [F5F]).

In conclusion, this is the first study that evaluated the growth inhibition potential of the leaf and root extracts of *C. triloba* on a panel of cancer cells. This research indicated that the hexane root extract displayed the best levels of growth inhibition. The active constituents of this extract were isolated into four fractions which elicited apoptosis inducing effects that promoted the extrinsic (type II) or intrinsic apoptotic pathway in the melanoma cells. Furthermore, fraction F4 contained the most active compounds from *C. triloba* as it had the lowest IC_{50} and TGI values (in comparison to the other fractions) and induced depolarization of the ΔΨ in the highest percentage of melanoma cells. It was confirmed that six classes of compounds were accountable for the anticancer activity of these fractions. Thus, the *C. triloba* plant is a rich source of anticancer compounds.

This study represents the initial phase of researching the anticancer activity of the compounds from *C. triloba*. Further studies needs to be conducted as these compounds need to be tested for the ability to inhibit resistant cancer cell lines. In addition, safety tests need be performed to determine the toxicity of these compounds on normal cells. This will involve the use of fibroblast cell lines (such as NIH-3T3 [normal mouse fibroblast] and MRC-5 [human lung fibroblast]), peripheral blood mononuclear cells and cardiomyocytes (Danihelová et al., 2013, Sarzaeem et al., 2013, Philippoussis et al., 2003, Matić et al., 2013, Andersson et al., 1999). Also, mice models need to be developed for evaluating the *in vivo* anticancer activity and toxicity of these compounds.

6. REFERENCES

ABU, N., AKHTAR, M. N., HO, W. Y., YEAP, S. K. & ALITHEEN, N. B. 2013. 3-Bromo-1-Hydroxy-9,10-Anthraquinone (BHAQ) Inhibits Growth and Migration of the Human Breast Cancer Cell Lines MCF-7 and MDA-MB231. *Molecules,* 18**,** 10367-10377.

ACEHAN, D., JIANG, X., MORGAN, D. G., HEUSER, J. E., WANG, X. & AKEY, C. W. 2002. Three-dimensional structure of the apoptosome: implications for assembly, procaspase-9 binding, and activation. *Molecular Cell,* 9**,** 423-432.

ADACHI, S., CROSS, A., BABIOR, B. & GOTTLIEB, R. 1997. Bcl-2 and the outer mitochondrial membrane in the inactivation of cytochrome c during Fas mediated apoptosis. *Journal of Biological Chemistry,* 272**,** 21878 -21882.

ADAM DE BEAUMAIS, T., FAKHOURY, M., MEDARD, Y., AZOUGAGH, S., ZHANG, D., YAKOUBEN, K. & JACQZ-AIGRAIN, E. 2011. Determinants of mercaptopurine toxicity in paediatric acute lymphoblastic leukemia maintenance therapy. *British Journal of Clinical Pharmacology,* 71**,** 575-584.

AKHTAR, M. S., ALI, M., MIR, S. R. & SINGH, O. 2006. New anthraquinones from Rubia cordifolia roots. *Indian Journal of Chemistry,* 45B**,** 1945-1950.

AKSOY, S., HARPUTLUOGLU, H., KILICKAP, S., DEDE, D. S., DIZDAR, O., ALTUNDAG, K. & BARISTA, I. 2007. Rituximab-related viral infections in lymphoma patients. *Leukemia and Lymphoma,* 48**,** 1307-1312.

AL-FATLAWI, A. A., AL-FATLAWI, A. A., ZAFARYAB, M. D., IRSHAD, M. D., AHMAD, I., KAZIM, Z., AHMAD, A. & RIZVI, M. M. A. 2014. Rhein induced cell death and apoptosis through caspase dependent and associated with modulation of p53, bcl-2/bax ratio in human cell lines. *International Journal of Pharmacy and Pharmaceutical Sciences,* 6**,** 515-519.

ALNEMRI, E. S., LIVINGSTO, D. J., NICHOLSON, D. W., SALVESEN, G., THORNBERRY, N. A., WONG, W. W. & YUAN, J. 1996. Human ICE/CED-3 protease nomenclature. *Cell,* 87**,** 171.

AMERICAN CANCER ASSOCIATION. 2014. What are the risks and side effects of cancer surgery? [Online]. Available: http://www.cancer.org/treatment/treatmentsandsideeffects/treatmenttypes/surgery/surgery-risks-and-side-effects. [Accessed: 15 July 2015]

ANDERSSON, B. S., EKSBORG, S., VIDAL, R. F., SUNDBERG, M. & CARLBERG, M. 1999. Anthraquinone-induced cell injury: acute toxicity of carminomycin, epirubicin, idarubicin and mitoxantrone in isolated cardiomyocytes. *Toxicology,* 135**,** 11-20.

ANDRADE, R., CRISOL, L., PRADO, R., BOYANO, M. D., ARLUZEA, J. & ARÉCHAGA, J. 2010. Plasma membrane and nuclear envelope integrity during the blebbing stage of apoptosis: a time-lapse study. *Biology of the Cell,* 102**,** 25–35.

APRAIZ, A., BOYANO, M. D. & ASUMENDI, A. 2011. Cell-Centric View of Apoptosis and Apoptotic Cell Death-Inducing Antitumoral Strategies. *Cancers,* 3**,** 1042-1080.

ARCHANA, M., BASTIAN, YOGESH, T. L. & KUMARASWAMY, K. L. 2013. Various methods available for detection of apoptotic cells--a review. *Indian Journal of Cancer,* 50**,** 274-283.

ARLIN, Z. A., SILVER, R., CASSILETH, P., ARMENTROUT, S., GAMS, R., DAGHESTANI, A., COLEMAN, M., SCHOCH, I. & DUKART, G. 1985. Phase I-II trial of mitoxantrone in acute leukemia. *Cancer treatment reports,* 69**,** 61-64.

BAGULEY, B. C. 1991. DNA intercalating anti-tumour agents. *Anti-Cancer Drug Design,* 6**,** 1-35.

BAHR, C. & GRONER, B. 2004. The insulin like growth factor-1 receptor (IGF-1R) as a drug target: novel approaches to cancer therapy. *Growth Hormone & IGF Research,* 14**,** 287-295.

BAJAJ, Y. P. S. (ed.) 1999. *Biotechnology in Agriculture and Forestry: Medicinal and Aromatic plants,* Berlin: Springer-Verlag.

BALDE, A. M., PIETERS, L., APERS, S., DE BRUYNE, T., VAN DEN HEUVEL, H., CLAEYS, M. & VLIETINCK, A. 1999. Oumarone, Bissaone, and Aissatone, Unusual Prenylated Polyketides from Harrisonia abyssinica. *Journal of Natural Products,* 62**,** 364–366.

BALUNAS, M. J. & KINGHORN, A. D. 2005. Drug discovery from medicinal plants. *Life Sciences,* 78**,** 431-441.

BASANEZ, G., NECHUSHTAN, A., DROZHININ, O., CHANTURIYA, A., CHOE, E., TUTT, S., WOOD, K. A., HSU, Y. T., ZIMMERBERG, J. & YOULE, R. J. 1999. Bax, but not Bcl-XL decreases the lifetime of planar phospholipid bilayer membranes at subnanomolar concentrations. *Proceedings of the National Academy of Sciences of the United States of America,* 96**,** 5492-5497.

BD BIOSCIENCES. 2012. BD Accuri C6 Flow Cytometer Instrument Manual. Version: 7820018 Rev-2.

BD BIOSCIENCES. 2015. Apoptosis [Online]. Available: https://www.bdbiosciences.com/in/research/apoptosis/analysis/cell_death.jsp. [Accessed: 2 August 2015]

BELIZARIO, J. E., ALVES, J., OCCHIUCCI, J. M., GARAY-MALPARTIDA, M. & SESSO, A. 2007. A mechanistic view of mitochondrial death decision pores. *Brazilian journal of medical and biological research,* 40**,** 1011-1024.

BENNETT, V. & GILLIGAN, D. M. 1993. The spectrin-based membrane skeleton and micron-scale organization of the plasma membrane. *Annual Review of Cell and Developmental Biology,* 9**,** 27–66.

BERRIDGE, M. V. & TAN, A. S. 1993. Characterization of the cellular reduction of 3-(4,5-dimethylthiazol-2-yl)-2,5-diphenyltetrazolium bromide (MTT): subcellular localization, substrate dependence, and involvement of mitochondrial electron transport in MTT reduction. *Archives of Biochemistry and Biophysics,* 303**,** 474-482.

BETHESDA, M. D. 2006. Corticosteroids general statement. *In:* MCEVOY, G. K. (ed.) *American Hospital Formulary Service drug information.* American Society of Health-System Pharmacists, 3126-3127.

BHASIN, D., CHETTIAR, S. N., ETTER, J. P., MOK, M. & LI, P. K. 2013. Anticancer activity and SAR studies of substituted 1,4-naphthoquinones. *Bioorganic and Medicinal Chemistry,* 21**,** 4662–4669.

BLAIR, W. S. & SEMLER, B. L. 1991. Self-cleaving proteases. *Current Opinion in Cell Biology,* 3**,** 1039-1045.

BLANKENBERG, F. G. & STRAUSS, H. W. 2012. Recent advances in the molecular imaging of programmed cell death: part I-pathophysiology and radiotracers. *Journal of Nuclear Medicine,* 53**,** 1659-1662.

BOATRIGHT, K. M. & SALVESEN, G. S. 2003. Mechanisms of caspase activation. *Current Opinion in Cell Biology,* 15**,** 725-731.

BODMER, J. L., HOLLER, N., REYNARD, S., VINCIGUERRA, P., SCHNEIDER, P., JUO, P., BLENIS, J. & TSCHOPP, J. 2000. TRAIL receptor-2 signals apoptosis through FADD and caspase-8. *Nature cell biology,* 2**,** 241-243.

BONORA, M. & PINTON, P. 2014. The mitochondrial permeability transition pore and cancer: molecular mechanisms involved in cell death. *Frontiers in Oncology,* 4**,** 1-12.

BOUCHIER-HAYES, L., MUÑOZ-PINEDO, C., CONNELL, S. & GREEN, D. R. 2008. Measuring apoptosis at the single cell level. *Methods,* 44**,** 222-228.

BOWEN, I. D., BOWEN, S. M. & JONES, A. H. 1998. *Mitosis and apoptosis: Matters of life and death,* London, Chapman and Hall.

BRANNON-PEPPAS, L. & BLANCHETTE, J. O. 2004. Nanoparticle and targeted systems for cancer therapy. *Advanced Drug Delivery Reviews,* 56**,** 1649-1659.

BRENNER, C., CADIOU, H., VIEIRA, H. L., ZAMZAMI, N., MARZO, I., XIE, Z., LEBER, B., ANDREWS, D., DUCLOHIER, H., REED, J. C. & KROEMER, G. 2000. Bcl-2 and Bax regulate the channel activity of the mitochondrial adenine nucleotide translocator. *Oncogene,* 19**,** 329-336.

BUNGU, L., FROST, C. L., BRAUNS, S. C. & VAN DE VENTER, M. 2006. Tulbaghia violacea inhibits growth and induces apoptosis in cancer cells in vitro. *African Journal of Biotechnology,* 5**,** 1936-1943.

CAI, J. & JONES, D. P. 1998. Superoxide in apoptosis. Mitochondrial generation triggered by cytochrome c loss. *Journal of Biological Chemistry,* 273**,** 11401-11404.

CAILLEAU, R., YOUNG, R., OLIVE, M. & REEVES, W. J. 1974. Breast tumor cell lines from pleural effusions. *Journal of the National Cancer Institute,* 53**,** 661–674.

CANCER RESEARCH UK. 2014a. Types of cancer [Online]. Available: http://www.cancerresearchuk.org/about-cancer/what-is-cancer/how-cancer-starts/types-of-cancer. [Accessed: 14 July 2015]

CANCER RESEARCH UK. 2014b. Worldwide cancer Factsheet [Online]. Available: http://publications.cancerresearchuk.org/cancerstats/statsworldwide/worldfactsheet.html. [Accessed: 14 July 2015]

CANCER RESEARCH UK. 2014c. Worldwide cancer mortality map [Online]. Available: http://publications.cancerresearchuk.org/cancerstats/statsworldwide/worldmortmap.html. [Accessed: 14 July 2015]

CANELLOS, G. P. 1992. Chemotherapy of Advanced Hodgkin's Disease with MOPP, BVD, or MOPP alternating with ABVD. *New England Journal of Medicine,* 327**,** 1478–1484.

CARSON, K. R., FOCOSI, D., MAJOR, E. O., PETRINI, M., RICHEY, E. A., WEST, D. P. & BENNETT, C. L. 2009. Monoclonal antibody-associated progressive multifocal leucoencephalopathy in patients treated with rituximab, natalizumab, and efalizumab: a Review from the Research on Adverse Drug Events and Reports (RADAR) Project. *The Lancet Oncology,* 10**,** 816-824.

CHAMPOUX, J. J. 2001. DNA topoisomerases: structure, function, and mechanism. *Annual Review of Biochemistry,* 70**,** 369-413.

CHANG, H. M. & BUT, P. P. H. 1986. *Pharmacology and Applications of Chinese Materia Medica,* Singapore, World Scientific Publishing.

CHAUDHARY, S. A., GADHVI, K. V. & CHAUDHARY, A. B. 2010. Comprehensive review on world herb trade and most utilized medicinal plant. *International Journal of Applied Biology and Pharmaceutical Technology,* 1**,** 510-517.

CHEN, Z., NAITO, M., HORI, S., MASHIMA, T., YAMORI, T. & TSURUO, T. 1999. A human IAP family gene, apollon, expressed in human brain cancer cells. *Biochemical and Biophysical Research Communications,* 264**,** 847-854.

CHUANG, J. Y., HUANG, Y. F., LU, H. F., HO, H. C., YANG, J. S., LI, T. M., CHANG, N. W. & CHUNG, J. G. 2007. Coumarin induces cell cycle arrest and apoptosis in human cervical cancer HeLa cells through a mitochondria- and caspase-3 dependent mechanism and NF-kappaB down-regulation. *In Vivo,* 21**,** 1003-1009.

COHEN, G. M. 1997. Caspases: the executioners of apoptosis. *Biochemical Journal,* 326**,** 1-16.

COLLINS, J. A., SCHANDI, C. A., YOUNG, K. K., VESELY, J. & WILLINGHAM, M. C. 1997. Major DNA fragmentation is a late event in apoptosis. *Journal of Histochemistry and Cytochemistry,* 45**,** 923-934.

COS, P., VLIETINCK, A. J., BERGHE, D. V. & MAES, L. 2006. Anti-infective potential of natural products: how to develop a stronger in vitro 'proof-of-concept'. *Journal of Ethnopharmacology,* 106**,** 290-302.

COSSARIZZA, A., BACCARANI-CONTRI, M., KALASHNIKOVA, G. & FRANCESCHI, C. 1993. A new method for the cytofluorimetric analysis of mitochondrial membrane potential using the J-aggregate forming lipophilic cation 5,5',6,6'-tetrachloro- 1,1',3,3' tetraethylbenzimidazolylcarbocyanine iodide (JC-1). *Biochemical and Biophysical Research Communications,* 197**,** 40-45.

COUKELL, A. J. & FAULDS, D. 1997. Epirubicin: An updated review of its pharmacodynamic and pharmacokinetic properties and therapeutic efficacy in the management of breast cancer. *Drugs,* 53**,** 453-482.

CRAGG, G. M. 1998. *Paclitaxel (Taxol): a success story with valuable lessons for Natural Product Drug discovery and development,* New York, John Wiley & Sons, Inc.

CROOKS, P. A. & ROSENTHAL, G. A. 1996. *Use of L-canavanine as a chemotherapeutic agent for the treatment of pancreatic cancer*. United States patent application.

CROUCH, N., SYMMONDS, R., SPRING, W. & DIEDERICHS, N. 2006. Facts sheets for growing popular medicinal plant species. *In:* DIEDERICHS, N. (ed.) *Commercialising Medicinal Plants-A Southern African Guide.* Stellenbosch, South Africa: Sun Press.

CROW, M. T., MANI, K., NAM, Y.-J. & KITSIS, R. N. 2004. The Mitochondrial Death Pathway and Cardiac Myocyte Apoptosis. *Circulation Research,* 95**,** 957-970.

DANIHELOVÁ, M., VEVERKA, M., STURDÍK, E. & JANTOVÁ, S. 2013. Antioxidant action and cytotoxicity on HeLa and NIH-3T3 cells of new quercetin derivatives. *Interdisciplinary Toxicology,* 6**,** 209-216.

DENAULT, J. B. & SALVESEN, G. S. 2002. Caspases: keys in the ignition of cell death. *Chemical Reviews,* 102**,** 4489-4500.

DENECKER, G., OVAERE, P., VANDENABEELE, P. & DECLERCQ, W. 2008. Caspase-14 reveals its secrets. *The Journal of Cell Biology,* 180**,** 451-458.

DESAGHER, S., OSEN-SAND, A., NICHOLS, A., ESKES, R., MONTESSUIT, S., LAUPER, S., MAUNDRELL, K., ANTONSSON, B. & MARTINOU, J. C. 1999. Bid-induced conformational change of Bax is responsible for mitochondrial cytochrome c release during apoptosis. *Journal of Cell Biology,* 144**,** 891-901.

DEWSON, G. & KLUC, R. M. 2010. Bcl-2 family-regulated apoptosis in health and disease. *Cell health and Cytoskeleton,* 2**,** 9-22.

DHINGRA, N., BHARDWAJ, T. R., MEHTA, N., MUKHOPADHYAY, T., KUMAR, A. & KUMAR, M. 2011. Synthesis, antiproliferative activity, acute toxicity and assessment of the antiandrogenic activities of new androstane derivatives. *Archives of Pharmacal Research,* 34**,** 1055-1063.

DIGIOVANNI, J. 1992. Multistage carcinogenesis in mouse skin. *Pharmacology & Therapeutics,* 54**,** 63-128.

DRUKER, B. J. & DAVID, A. 2003. Imatinib as a paradigm of targeted therapies. *Journal of Clinical Oncology,* 21**,** 239s–245s.

DU, C., FANG, M., LI, Y., LI, L. & WANG, X. 2000. SMAC, a mitochondrial protein that promotes cytochrome c-dependent caspase activation by eliminating IAP inhibition. *Cell,* 102**,** 33-42.

DUBIKOVSKAYA, E. 2013. Project 1. Development of new tools for probing mitochondrial activity in cells and living animals [Online]. Available: http://lcbim.epfl.ch/research. [Accessed: 17 July 2015]

DURAIPANDIYAN, V., BASKAR, A. A., IGNACIMUTHU, S., MUTHUKUMAR, C. & AL-HARBI, N. A. 2012. Anticancer activity of Rhein isolated from Cassia fistula L. flower. *Asian Pacific Journal of Tropical Disease,* 2**,** S517-S523.

DUTCHER, J. P., WIERNIK, P. H. & STRAUMAN, J. J. 1985. Mitoxantrone (MITOX) and cytosine arabinoside (ARA-C) in acute non-lymphocytic leukemia (ANLL) and blast crisis of chronic myelogenous leukemia (CML-B). *Proceedings of the American Society of Clinical Oncology,* 4**,** 170.

EBADA, S. S., EDRADA, R. A., LIN, W. & PROKSCH, P. 2008. Methods for isolation, purification and structural elucidation of bioactive secondary metabolites from marine invertebrates. *Nature Protocols,* 3**,** 1820-1831.

EDGAR, A. D., LEVIN, R., CONSTANTINOU, C. E. & DENIS, L. 2007. A critical review of the pharmacology of the plant extract of Pygeum africanum in the treatment of LUTS. *Neurourology and Urodynamics,* 26**,** 458-463.

EGAN, D., JAMES, P., COOKE, D. & O'KENNEDY, R. 1997. Studies on the cytostatic and cytotoxic effects and mode of action of 8-nitro-7-hydroxycoumarin. *Cancer Letters,* 118**,** 201-211.

ELMEGEED, G. A., EL-FAR, M., MAHROUS, H. & TANTAWY, M. A. 2009. Aminothienoandrostane: Novel promising anti-tumor agent. *International Journal of Medicine and Medical Sciences,* 1**,** 126-131.

ELMORE, S. 2007. Apoptosis: a review of programmed cell death. *Toxicologic Pathology,* 35**,** 495–516.

ENARI, M., SAKAHIRA, H., YOKOYAMA, H., OKAWA, K., IWAMATSU, A. & NAGATA, S. 1998. A caspase-activated DNase that degrades DNA during apoptosis, and its inhibitor ICAD. *Nature,* 391**,** 43-50.

ERHABOR, O. & ADIAS, T. C. 2011. From whole blood to component therapy: The economic, supply/demand need for implementation of component therapy in sub-Saharan Africa. *Transfusion Clinique et Biologique,* 18**,** 516–526.

FADOK, V. A., VOELKER, D. R., CAMPBELL, P. A., COHEN, J. J., BRATTON, D. L. & HENSON, P. M. 1992. Exposure of phosphatidylserine on the surface of apoptotic lymphocytes triggers recognition and removal by macrophages. *Journal of Immunology,* 148**,** 2207–2216.

FLOREA, A.-M. & BÜSSELBERG, D. 2011. Cisplatin as an Anti-Tumor Drug: Cellular Mechanisms of Activity, Drug Resistance and Induced Side Effects. *Cancers,* 3**,** 1351-1371.

FOK, J. Y., EKMEKCIOGLU, S. & MEHTA, K. 2006. Implications of tissue transglutaminase expression in malignant melanoma. *Molecular Cancer Therapeutics,* 5**,** 1493-1503.

FORCE, T., KRAUSE, D. S. & VAN ETTEN, R. A. 2007. Molecular mechanisms of cardiotoxicity of tyrosine kinase inhibition. *Nature Reviews Cancer,* 7**,** 332–344.

FUJITA, N. & TSURUO, T. 1998. Involvement of Bcl-2 cleavage in the acceleration of VP-16-induced U937 cell apoptosis. *Biochemical and Biophysical Research Communications,* 246**,** 484-488.

FULDA, S. & DEBATIN, K. M. 2006. Extrinsic versus intrinsic apoptosis pathways in anticancer chemotherapy. *Oncogene,* 25**,** 4798–4811.

FULDA, S., MEYER, E. & DEBATIN, K. M. 2000. Inhibition of TRAIL-induced apoptosis by Bcl-2 overexpression. *Oncogene,* 21**,** 2283-2294.

GAASCHT, F., TEITEN, M. H., CERELLA, C., DICATO, M., BAGREL, D. & DIEDERICH, M. 2014. Plumbagin modulates leukemia cell redox status. *Molecules,* 19**,** 10011-10032.

GASCOIGNE, K. E. & TAYLOR, S. S. 2009. How do anti-mitotic drugs kill cancer cells? *Journal of Cell Science,* 122**,** 2579-2585.

GATENBY, R. A. & GILLIES, R. J. 2004. Why do cancers have high aerobic glycolysis? *Nature Reviews Cancer,* 4**,** 891-899.

GAVA, B., ZORZET, S., SPESSOTTO, P., COCCHIETTO, M. & SAVA, G. 2006. Inhibition of B16 melanoma metastases with the ruthenium complex imidazolium trans-imidazoledimethylsulfoxide-tetrachlororuthenate and down-regulation of tumor cell invasion. *Journal of Pharmacology and Experimental Therapeutics,* 317**,** 284–291.

GIACCONE, G. 2004. The Role of Gefitinib in Lung Cancer Treatment. *Clinical Cancer Research,* 10**,** 4233s.

GOOLSBY, C., PANIAGUA, M., TALLMAN, M. & GARTENHAUS, R. B. 2005. Bcl-2 regulatory pathway is functional in chronic lymphocytic leukaemia. *Cytometry Part B: Clinical Cytometry,* 63**,** 36-46.

GROSS, A., MCDONNELL, J. M. & KORSMEYER, S. J. 1999. BCL-2 family members and the mitochondria in apoptosis. *Genes and Development,* 13**,** 1899-1911.

GUGLIN, M., CUTRO, R. & MISHKIN, J. D. 2008. Trastuzumab-induced cardiomyopathy. *Journal of Cardiac Failure,* 14**,** 437–444.

HALENBECK, R., MACDONALD, H., ROULSTON, A., CHEN, T. T., CONROY, L. & WILLIAMS, L. T. 1998. CPAN, a human nuclease regulated by the caspase-sensitive inhibitor DFF45. *Current Biology,* 8**,** 537–540.

HANSEL, T. T., KROPSHOFER, H., SINGER, T., MITCHELL, J. A. & GEORGE, A. J. 2010. The safety and side effects of monoclonal antibodies. *Nature Reviews Drug Discovery,* 9**,** 325-338.

HOERHAMMER, L., WAGNER, H. & KOEHLER, I. 1959. New investigations on the components of Rheum palmatum L. Part 1: On the analysis of rhein. *Archives of Pharmacal Research,* 292**,** 591-601.

HONG, J. Y., CHUNG, H. J., BAE, S. Y., TRUNG, T. N., BAE, K. & LEE, S. K. 2014. Induction of Cell Cycle Arrest and Apoptosis by Physcion, an Anthraquinone Isolated From Rhubarb (Rhizomes of Rheum tanguticum), in MDA-MB-231 Human Breast Cancer Cells. *Journal of Cancer Prevention,* 19**,** 273-278.

HOSTETTMANN, K. 1997. Strategy for the Biological and Chemical Evaluation of Plant Extracts. Invited lecture presented at the International Conference on Biodiversity and Bioresources: Conservation and Utilization. Phuket, Thailand: IUPAC.

HSIAO, Y. P., YU, C. S., YU, C. C., YANG, J. S., CHIANG, J. H., LU, C. C., HUANG, H. Y., TANG, N. Y., YANG, J. H., HUANG, A. C. & CHUNG, J. G. 2012. Triggering apoptotic death of human malignant melanoma A375.S2 cells by bufalin: involvement of caspase cascade-dependent and independent mitochondrial signaling pathways. *Evidence-Based Complementary and Alternative Medicine,* 2012**,** 1-9.

HURINANTHAN, V. 2013. *Anti-HIV activity of selected South African medicinal plants.* Doctor of Technology, Durban University of Technology.

HUTCHINGS, A. (ed.) 1996. *Zulu Medicinal Plants, an Inventory,* University of Natal Press, Pietermaritzburg.

IGNEY, F. H. & KRAMMER, P. H. 2002. Death and anti-death: tumour resistance to apoptosis. *Nature Reviews Cancer,* 2**,** 277-288.

INTERNATIONAL AGENCY FOR RESEARCH ON CANCER. 2015. Globocan 2012: Estimated Cancer Incidence, Mortality and Prevalence Worldwide in 2012 [Online]. Available: http://globocan.iarc.fr/Pages/fact_sheets_cancer.aspx. [Accessed: 14 July 2015]

IRSHAD, M., SHREAZ, S., MANZOOR, N., KHAN, L. A. & RIZVI, M. M. 2011. Anticandidal activity of Cassia fistula and its effect on ergosterol biosynthesis. *International Journal of Pharma and Bio Sciences,* 49**,** 727-733.

JANTOVA, S., REPICKY, A., PAULOVICOVA, E., LETASIOVA, S. & CIPAK, L. 2008. Antiproliferative activity and apoptosis induced by 6-bromo-2-(morpholin-1-yl)-4-anilinoquinazoline on cells of leukemia lines. *Experimental oncology,* 30**,** 139-142.

JAYAPRAKASAM, B., ZHANG, Y., SEERAM, N. P. & NAIR, M. G. 2003. Growth inhibition of human tumor cell lines by withanolides from Withania somnifera leaves. *Life Sciences,* 74**,** 125-132.

JEAN, G. W. & SHAH, S. R. 2008. Epidermal growth factor receptor monoclonal antibodies for the treatment of metastatic colorectal cancer. *Pharmacotherapy,* 28**,** 742–754.

JEGHAM, H., ROY, J., MALTAIS, R., DESNOYERS, S. & POIRIER, D. 2012. A novel aminosteroid of the 5α-androstane-3α,17β-diol family induces cell cycle arrest and apoptosis in human promyelocytic leukemia HL-60 cells. *Investigational New Drugs,* 30**,** 176-185.

JEONG, S. Y. & SEOL, D. W. 2008. The role of mitochondria in apoptosis. *Biochemistry and Molecular Biology Reports***,** 11-22.

JOHN, S. B. 2001. The molecular biology of cancer. *Molecular aspects of Medicine,* 21**,** 167-223.

JORGEN, W., KAISA, H. & ELLEN, M. H. 2011. Fibroblast growth factors and their receptors in cancer. *Biochemical Journal,* 437**,** 199-213.

KALE, A., GAIKWAD, S., ADSUL, V., DESHPANDE, N. & SALVEKAR, J. 2013. Quantification of a phytotoxin from walnut species by HPTLC method. *International Journal of Pharmacy and Pharmaceutical Sciences,* 5**,** 752-754.

KANEMITSU, H., YAMAUCHI, H., KOMATSU, M., YAMAMOTO, S., OKAZAKI, S., UCHIDA, K. & NAKAYAMA, H. 2009. 6-mercaptopurine (6-MP) induces p53-mediated apoptosis of neural progenitor cells in the developing fetal rodent brain. *Neurotoxicology and Teratology,* 31**,** 198-202.

KANG, J., LEE, M. S. & GORENSTEIN, D. G. 2005. The enhancement of PCR amplification of a random sequence DNA library by DMSO and betaine: Application to in vitro combinatorial selection of aptamers. *Journal of Biochemical and Biophysical Methods,* 64**,** 147-151.

KANG, J. S., LONG, P. H., LIM, H. M., KIM, Y. H. & BLASCHKE, G. 2003. Achiral and chiral determination of benzophenanthridine alkaloids from methanol extracts of hylomecon species by high performance liquid chromatography. *Archives of Pharmacal Research,* 26**,** 114-119.

KAPOOR, L. D. 1990. *Handbook of Ayurvedic Medicinal Plants,* Florida, CRC Press.

KAYE, S. B. 1998. New antimetabolites in cancer chemotherapy and their clinical impact. *British Joumal of Cancer,* 78**,** 1-7.

KEKRE, N., GRIFFIN, C., MCNULTY, J. & PANDEY, S. 2005. Pancratistatin causes early activation of caspase-3 and the flipping of phosphatidyl serine followed by rapid apoptosis specifically in human lymphoma cells. *Cancer Chemotherapy and Pharmacology,* 56**,** 29-38.

KERR, J. F. R., WYLLIE, A. H. & CURRIE, A. R. 1972. Apoptosis: a basic biological phenomenon with wide-ranging implications in tissue kinetics. *British Journal of Cancer,* 26**,** 239-257.

KIM, H., RAFIUDDIN-SHAH, M., TU, H. C., JEFFERS, J. R., ZAMBETTI, G. P., HSIEH, J. J. & CHENG, E. H. 2006. Hierarchical regulation of mitochondrion-dependent apoptosis by BCL-2 subfamilies. *Nature Cell Biology,* 8**,** 1348 –1358.

KINTZIOS, S. E. & BARBERAKI, M. G. (eds.) 2004. *Plants that Fight Cancer,* United States of America: CRC Press.

KOTOPOULIS, S., DIMCEVSKI, G., GILJA, O. H., HOEM, D. & POSTEMA, M. 2013. Treatment of human pancreatic cancer using combined ultrasound, microbubbles, and gemcitabine: a clinical case study. *Medical Physics,* 40.

KRAVTSOV, V. D., DANIEL, T. O. & KOURY, M. J. 1999. Comparative Analysis of Different Methodological Approaches to the in Vitro Study of Drug-Induced Apoptosis. *American Journal of Pathology,* 155**,** 1327–1339.

KUMAR, P. J. & CLARK, M. L. (eds.) 1990. *Clinical medicine,* London: Bailliere Tindall.

KUO, H. M., TSAI, H. C., LIN, Y. L., YANG, J. S., HUANG, A. C., YANG, M. D., HSU, S. C., CHUNG, M. C., GIBSON, W. W. & CHUNG, J. G. 2009. Mitochondrial-dependent caspase activation pathway is involved in baicalein-induced apoptosis in human hepatoma J5 cells. *International Journal of Oncology,* 35**,** 717-724.

KUO, P. L., LIN, T. C. & LIN, C. C. 2002. The antiproliferative activity of aloe-emodin is through p53-dependent and p21-dependent apoptotic pathway in human hepatoma cell lines. *Life Sciences,* 71**,** 1879-1892.

KUWANA, T. & NEWMEYER, D. D. 2003. Bcl-2-family proteins and the role of mitochondria in apoptosis. *Current Opinion in Cell Biology,* 15**,** 1-9.

LARKIN, T. 1983. Herbs are often more toxic than magical. *FDA Consumer,* 17**,** 4–11.

LEE, J. H., KIM, J. M. & KIM, C. 2003. Pharmacokinetic analysis of rhein in Rheum undulatum L. *Journal of Ethnopharmacology,* 84**,** 5-9.

LEE, J. S. & SURH, Y. J. 2005. Nrf2 as a novel molecular target for chemoprevention. *Cancer Letters,* 224**,** 171-184.

LEMASTERS, J., QIAN, T., BRADHAM, C., BRENNER, D., CASCIO, W., TROST, L., NISHIMURA, Y., NIEMINEN, A. & HERMAN, B. 1999. Mitochondrial dysfunction in the pathogenesis of necrotic and apoptotic cell death. *Journal of Bioenergetics and Biomembranes,* 31**,** 305-319.

LETAI, A. 2011. BCL-2 family proteins and the control of mitochondrial apoptosis. *In:* REED, J. C. (ed.) *Apoptosis Physiology and Pathology*. Cambridge: Cambridge University Press.

LI, J. & YUAN, J. 2008. Caspases in apoptosis and beyond. *Oncogene,* 27**,** 6194–6206.

LI, Q., ZHAO, X. L., SUN, J., JIANG, S. G. & GONG, X. F. 2013. Anti-proliferative and apoptosis-inducing activities of juglone in LS-174T cells. *Bangladesh Journal of Pharmacology,* 8**,** 65-72.

LI, Y., LUAN, Y., QI, X., LI, M., GONG, L., XUE, X., WU, X., WU, Y., CHEN, M., XING, G., YAO, J. & REN, J. 2010. Emodin triggers DNA double-strand breaks by stabilizing topoisomerase II-DNA cleavage complexes and by inhibiting ATP hydrolysis of topoisomerase II. *Toxicological Sciences,* 118**,** 435-443.

LIU, L., LI, W., KOIKE, K., ZHANG, S. & NIKAIDO, T. 2004. New alpha-tetralonyl glucosides from the fruit of Juglans mandshurica. *Chemical and Pharmaceutical Bulletin,* 52**,** 566-569.

LIU, X., CAI, W., NIU, M., CHONG, Y., LIU, H., HU, W., WANG, D., GAO, S., SHI, Q., HU, J., ZHOU, X. & YU, R. 2015. Plumbagin induces growth inhibition of human glioma cells by downregulating the expression and activity of FOXM1. *Journal of Neuro-Oncology,* 121**,** 469-477.

LIU, X., KIM, C. N., POHL, J. & WANG, X. 1996a. Purification and characterization of an interleukin-1beta-converting enzyme family protease that activates cysteine protease P32 (CPP32). *Journal of Biological Chemistry,* 271**,** 13371–13376.

LIU, X., KIM, C. N., YANG, J., JEMMERSON, R. & WANG, X. 1996b. Induction of apoptotic program in cell-free extracts: requirement for dATP and cytochrome c. *Cell,* 86**,** 147-157.

LIU, X., LI, P., WIDLAK, P., ZOU, H., LUO, X., GARRARD, W. T. & WANG, X. 1998. The 40-kDa subunit of DNA fragmentation factor induces DNA fragmentation and chromatin condensation during apoptosis. *Proceedings of the National Academy of Sciences of the United States of America,* 95**,** 8461–8466.

LIU, X., ZOU, H., SLAUGHTER, C. & WANG, X. 1997. DFF, a heterodimeric protein that functions downstream of caspase-3 to trigger DNA fragmentation during apoptosis. *Cell,* 89**,** 175–184.

LO, C., LAI, T. Y., YANG, J. H., YANG, J. S., MA, Y. S., WENG, S. W., CHEN, Y. Y., LIN, J. G. & CHUNG, J. G. 2010. Gallic acid induces apoptosis in A375.S2 human melanoma cells through caspase-dependent and -independent pathways. *International Journal of Oncology,* 37**,** 377–385.

LOPES, R. B., GANGESWARAN, R., MCNEISH, I. A., WANG, Y. & LEMOINE, N. R. 2007. Expression of the IAP protein family is dysregulated in pancreatic cancer cells and is important for resistance to chemotherapy. *International Journal of Cancer,* 120**,** 2344-2352.

LOUW, C. A. M., REGNIER, T. J. C. & KORSTEN, L. 2002. Medicinal bulbous plants of South Africa and their traditional relevance in the control of infectious diseases. *Journal of Ethnopharmacology,* 82**,** 147–154.

LOWE, S. W. & LIN, A. W. 2000. Apoptosis in cancer. *Carcinogenesis,* 21**,** 485-495.

LUO, X., BUDIHARDJO, I., ZOU, H., SLAUGHTER, C. & WANG, X. 1998. Bid, a Bcl2 interacting protein, mediates cytochrome c release from mitochondria in response to activation of cell surface death receptors. *Cell,* 94**,** 481-490.

LYANTAGAYE, S. L. 2013. Methyl-α-D-glucopyranoside from Tulbghia violacea extract induces apoptosis in vitro in cancer cells. *Bangladesh Journal of Pharmacology,* 8**,** 93-101.

MADHURI, S. & PANDEY, G. 2008. Some dietary agricultural plants with anticancer properties. *Plant Archives,* 8**,** 13-16.

MAIOLI, E., TORRICELLI, C., FORTINO, V., CARLUCCI, F., TOMMASSINI, V. & PACINI, A. 2009. Critical Appraisal of the MTT Assay in the Presence of Rottlerin and Uncouplers. *Biological Procedures Online,* 11**,** 227-240.

MAJIDI, J., BARAR, J., BARADARAN, B., ABDOLALIZADEH, J. & OMIDI, Y. 2009. Target therapy of cancer: implementation of monoclonal antibodies and nanobodies. *Human Antibodies,* 18**,** 81-100.

MAJOR, E. O. 2010. Progressive multifocal leukoencephalopathy in patients on immunomodulatory therapies. *Annual Review of Medicine,* 61**,** 35–47.

MANTADAKIS, E., COLE, P. D. & KAMEN, B. A. 2005. High-dose methotrexate in acute lymphoblastic leukemia: where is the evidence for its continued use? *Pharmacotherapy,* 25, 748-755.

MANU, K. A., SHANMUGAM, M. K., RAJENDRAN, P., LI, F., RAMACHANDRAN, L., HAY, H. S., KANNAIYAN, R., SWAMY, S. N., VALI, S., KAPOOR, S., RAMESH, B., BIST, P., KOAY, E. S., LIM, L. H., AHN, K. S., KUMAR, A. P. & SETHI, G. 2011. Plumbagin inhibits invasion and migration of breast and gastric cancer cells by downregulating the expression of chemokine receptor CXCR4. *Molecular Cancer,* 10, 107-121.

MARTINON, F. & TSCHOPP, J. 2007. Inflammatory caspases and inflammasomes: master switches of inflammation. *Cell Death and Differentiation,* 14**,** 10-22.

MATIĆ, I. Z., ALJANČIĆ, I., ŽIŽAK, Z., VAJS, V., JADRANIN, M., MILOSAVLJEVIĆ, S. & JURANIĆ, Z. D. 2013. In vitro antitumor actions of extracts from endemic plant Helichrysum zivojinii. *BMC Complementary and Alternative Medicine,* 13**,** 1-12.

MECKES, M., CALZADA, F., TORTORIELLO, J., GONZÁLEZ, J. L. & MARTÍNEZ, M. 1996. Terpenoids Isolated from Psidium guajava Hexane Extract with Depressant Activity on Central Nervous System. *Phytotherapy Research,* 10**,** 600–603.

MELLEM, J. J. 2013. *Isolation and characterization of the leaves of Brachylaena discolor extract as an anti-diabetic agent.* Doctor of Technology, Durban University of Technology.

MICHAEL, M. G. 2002. Mechanisms of Cancer Drug Resistance. *Annual Review of Medicine,* 53**,** 615-627.

MICHEAU, O., SOLARY, E., HAMMANN, A. & DIMANCHE-BOITREL, M. T. 1999. Fas ligand-independent, FADD-mediated activation of the Fas death pathway by anticancer drugs. *Journal of Biological Chemistry,* 274**,** 7987-7992.

MILROSS, C. G., MASON, K. A., HUNTER, N. R., CHUNG, W. K., PETERS, L. J. & MILAS, L. 1996. Relationship of mitotic arrest and apoptosis to antitumor effect of paclitaxel. *Journal of the National Cancer Institute,* 88**,** 1308-1314.

MIQUEL, C., BORRINI, F., GRANDJOUAN, S., AUPÉRIN, A., VIGUIER, J., VELASCO, V., DUVILLARD, P., PRAZ, F. & SABOURIN, J. C. 2005. Role of bax mutations in apoptosis in colorectal cancers with microsatellite instability. *American Journal of Clinical Pathology,* 23**,** 562-570.

MO, Y.-Y. & BECK, W. T. 1999. DNA Damage Signals Induction of Fas Ligand in Tumor Cells. *Molecular Pharmacology,* 55**,** 216-222.

MOHANLALL, V. 2010. *Screening, in-vitro propagation and bioaugmentation of Ceratotheca triloba for the production of secondary metabolites.* Doctor of Technology, Durban University of Technology.

MOHANLALL, V. & ODHAV, B. 2013. Antibacterial, anti-inflammatory and antioxidant activities of anthraquinones from Ceratotheca triloba (Bernh) Hook F. *Journal of Medicinal Plant Research,* 7**,** 877-886.

MOHANLALL, V., STEENKAMP, P. A. & ODHAV, B. 2011. Isolation and characterization of anthraquinone derivatives from Ceratotheca triloba (Bernh.) Hook.f. *Journal of Medicinal Plants Research,* 5**,** 3132-3141.

MOHLER, J. L., GOMELLA, L. G., CRAWFORD, E. D., GLODE, L. M., ZIPPE, C. D., FAIR, W. R. & MARSHALL, M. E. 1992. Phase II evaluation of coumarin (1,2-benzopyrone) in metastatic prostatic carcinoma. *The Prostate,* 20**,** 123-131.

MOLLOY, S. S. & THOMAS, G. 2002. Furin. *In:* DALBEY, R. E. & SIGMAN, D. S. (eds.) *The Enzymes.* San Diego, CA: Academic Press.

MONNERET, C. 2001. Recent developments in the field of antitumour anthracyclines. *European Journal of Medicinal Chemistry,* 36**,** 483-493.

MOOTHA, V. K., WEI, M. C., BUTTLE, K. F., SCORRANO, L., PANOUTSAKOPOULOU, V., MANNELLA, C. A. & KORSMEYER, S. J. 2001. A reversible component of mitochondrial respiratory dysfunction in apoptosis can be rescued by exogenous cytochrome C. *European Molecular Biology Organization Journal,* 20**,** 661 -671.

MORHASON-BELLO, I. O., ODEDINA, F., REBBECK, T. R., HARFORD, J., DANGOU, J. M., DENNY, L. & ADEWOLE, I. F. 2013. Challenges and opportunities in cancer control in Africa: a perspective from the African Organisation for Research and Training in Cancer. *The Lancet Oncology,* 14**,** e142-e151.

MOSSMAN, T. 1983. Rapid colorimetric assay for cellular growth and survival: Application to proliferation and cytotoxicity assays. *Journal of Immunological Methods,* 65**,** 55-63.

NAICKER, L. 2012. *Genetic transformation of Ceratotheca triloba for the production of anthraquinones from hairy root cultures.* Masters of Technology, Durban University of Technology.

NAICKER, L., MOHANLALL, V. & ODHAV, B. 2011. Methyl Jasmonate Induced Over-Production of Anthraquinones from Cell Suspension Cultures of Ceratotheca Triloba (Bernh.) Hook.F. *International Journal of Biotechnology and Biochemistry,* 7**,** 529-541.

NARANG, A. S. & DESAI, D. S. 2009. Anticancer Drug Development. *In:* LU, Y. & MAHATO, R. I. (eds.) *Pharmaceutical Perspectives of Cancer Therapeutics.* Heidelberg, London, New York: Springer Science & Business Media.

NARITA, M., SHIMIZU, S., ITO, T., CHITTENDEN, T., LUTZ, R. J., MATSUDA, H. & TSUJIMOTO, Y. 1998. Bax interacts with the permeability transition pore to induce permeability transition and cytochrome c release in isolated mitochondria. *Proceedings of the National Academy of Sciences of the United States of America*, 95**,** 14681-14686.

NATIONAL CANCER INTSTITUTE. 2014a. Radiation Therapy Side Effects Series [Online]. Available: http://www.cancer.gov/publications/patient-education/radiation-side-effects. [Accessed: 15 July 2015]

NATIONAL CANCER INTSTITUTE. 2014b. Chemotherapy Side Effects Series [Online]. Available: http://www.cancer.gov/publications/patient-education/chemo-side-effects. [Accessed: 15 July 2015]

NATIONAL CANCER INTSTITUTE. 2015a. What is cancer? [Online]. Available: http://www.cancer.gov/about-cancer/what-is-cancer#types-of-cancer. [Accessed: 14 July 2015]

NATIONAL CANCER INTSTITUTE. 2015b. Types of Treatment [Online]. Available: http://www.cancer.gov/about-cancer/treatment/types. [Accessed: 15 July 2015]

NATIONAL CANCER INTSTITUTE. 2015c. Melanoma Treatment (PDQ®), General Information About Melanoma [Online]. Available: http://www.cancer.gov/types/skin/patient/melanoma-treatment-pdq#section/_67. [Accessed: 21 July 2015]

NICHOLSON, D. W. 1999. Caspase structure, proteolytic substrates, and function during apoptotic cell death. *Cell Death and Differentiation,* 6**,** 1028-1042.

NUYDENS, R., NOVALBOS, J., DISPERSYN, G., WEBER, C., BORGERS, M. & GEERTS, H. 1999. A rapid method for the evaluation of compounds with mitochondria-protective properties. *Journal of Neuroscience Methods,* 92**,** 153-159.

NWANJO, H. 2006. Studies On The Effect Of Aqueous Extract Of Phyllanthus Niruri Leaf On Plasma Glucose Level And Some Hepatospecific Markers In Diabetic Wistar Rats. *The Internet Journal of Laboratory Medicine,* 2.

ODHAV, B., KANDASAMY, T., KHUMALO, N. & BAIJNATH, H. 2010. Screening of African traditional vegetables for their alpha-amylase inhibitory effect. *Journal of Medicinal Plants Research,* 4**,** 1502-1507.

OKLJEŠA, A. M., JOVANOVIĆ-ŠANTA, S. S., KLISURIĆ, O. R., SAKAČ, M. N., DJURENDIĆ, E. A., JAKIMOV, D. S., ALEKSIĆ, L. D. & PENOV GAŠI, K. M. 2013. Structural Analysis and Antitumor Activity of Androstane D-Seco-mesyloxy Derivatives. *Journal of the Brazilian Chemical Society,* 24**,** 1613-1622.

ORTH, K., CHINNAIYAN, A. M., GARG, M., FROELICH, C. J. & DIXIT, V. M. 1996. The CED-3/ICE-like protease Mch2 is activated during apoptosis and cleaves the death substrate lamin A. *Journal of Biological Chemistry,* 271**,** 16443–16446.

PACIUCCI, P. A., OHNUMA, T., CUTTNER, J., SILVER, R. T. & HOLLAND, J. F. 1983. Mitoxantrone in patients with acute leukaemia in relapse. *Cancer Research,* 43**,** 3919-3922.

PARRY, L. 2015. How green tea can KILL cancer cells: Compound destroys disease while leaving healthy cells unscathed [Online]. Mail Online. Available: http://www.dailymail.co.uk/health/article-2937811/How-green-tea-KILL-cancer-cells-Compound-destroys-disease-leaving-healthy-cells-unscathed.html. [Accessed 22 July 2015]

PATEL, T., GORES, G. J. & KAUFMANN, S. H. 1996. The role of proteases during apoptosis. *Federation of American Societies for Experimental Biology Journal,* 10**,** 587-597.

PAULUS, H. 2000. Protein splicing and related forms of protein autoprocessing. *Annual Review of Biochemistry,* 69**,** 447-496.

PAYNE, G., BRINGI, V., PRINCE, C. & SHULER, M. 1991. *Plant Cell and Tissue Culture in Liquid Systems,* Munich, Hanser Publishers.

PAYNE, S. & MILES, D. 2008. Mechanisms of anticancer drugs. *In:* GLEESON, M. J. & CLARKE, R. C. (eds.) *Scott-Brown's Otorhinolaryngology: Head and Neck Surgery.* 7th ed.: CRC Press.

PECERE, T., GAZZOLA, M. V., MUCIGNAT, C., PAROLIN, C., VECCHIA, F. D., CAVAGGIONI, A., BASSO, G., DIASPRO, A., SALVATO, B., CARLI, M. & PALÙ, G. 2000. Aloe-emodin is a new type of anticancer agent with selective activity against neuroectodermal tumors. *Cancer Research,* 60**,** 2800-2804.

PEREZ-SOLER, R. & SALTZ, L. 2005. Cutaneous adverse effects with HER1/EGFR-targeted agents: is there a silver lining? *Journal of Clinical Oncology,* 23**,** 5235–5246.

PERLER, F. B., XU, M. Q. & PAULUS, H. 1997. Protein splicing and autoproteolysis mechanisms. *Current Opinion in Cell Biology,* 1**,** 292-299.

PHILIPPOUSSIS, F., ARGUIN, C., MATEO, V., STEFF, A. M. & HUGO, P. 2003. Monoglycerides induce apoptosis in human leukemic cells while sparing normal peripheral blood mononuclear cells. *Blood,* 101**,** 292-294.

PHILLIPS, T. L. & FU, K. K. 1976. Quantification of combined radiation therapy and chemotherapy effects on critical normal tissues. *Cancer,* 37**,** 1186-1200.

PIPERDI, B., LING, Y. H., LIEBES, L., MUGGIA, F. & PEREZ-SOLER, R. 2011. Bortezomib: understanding the mechanism of action. *Molecular Cancer Therapeutics,* 10**,** 2029-2030.

PLAZA, A., MONTORO, P., BENAVIDES, A., PIZZA, C. & PIACENTE, S. 2005. Phenylpropanoid glycosides from Tynanthus panurensis: characterization and LC-MS quantitative analysis. *Journal of Agricultural and Food Chemistry,* 53**,** 2853-2858.

POOLEY, E. (ed.) 1998. *A field guide to wild flowers Kwazulu-Natal and the East Region,* South Africa: Natal Flora Publications Trust, Durban.

POP, C. & SALVESEN, G. S. 2009. Human caspases: activation, specificity and regulation. *Journal of Biological Chemistry,* 284**,** 21777-21781.

POPE, R. M. 2002. Apoptosis as a therapeutic tool in rheumatoid arthritis. *Nature Reviews Immunology,* 2**,** 527-535.

PREOBRAZHENSKAYA, M. N., SHCHEKOTIKHIN, A. E., SHTIL, A. A. & HUANG, H. S. 2006. Antitumor anthraquinone analogues for multidrug resistant tumor cells. *Journal of Medical Sciences,* 26**,** 1-4.

PUJOL, J. (ed.) 1990. *Natura Africa-Herbalist Handbook,* Durban, South Africa: Natural healers foundation.

RAFFO, A. J., PERLMAN, H., CHEN, M. W., DAY, M. L., STREITMAN, J. S. & BUTTYAN, R. 1995. Overexpression of bcl-2 protects prostate cancer cells from apoptosis in vitro and confers resistance to androgen depletion in vivo. *Cancer Research,* 55**,** 4438-4445.

RAI, N. K., TRIPATHI, K., SHARMA, D. & SHUKLA, V. K. 2005. Apoptosis: a basic physiologic process in wound healing. *The International Journal of Lower Extremity Wounds,* 4**,** 138-144.

RAMESAR, S., BAIJNATH, H., GOVENDER, T. & MACKRAJ, I. 2008. Angiotensin I-Converting Enzyme Inhibitor Activity of Nutritive Plants in KwaZulu-Natal. *Journal of Medicinal Food,* 11**,** 331-336.

RASHED, K. 2014. Antioxidant potential of Cedrela odorata stems extracts and Bio active Phytoconstituents. *Hygeia: Journal for drugs and medicines,* 6**,** 25-30.

RASTOGI, R. P., SINHA, R. & SINHA, R. P. 2009. Apoptosis: Molecular mechanisms and pathogenicity. *Experimental and Clinical Sciences, International Online Journal,* 8**,** 155-181.

RIDDICK, D. S., LEE, C., RAMJI, S., CHINJE, E. C., COWEN, R. L., WILLIAMS, K. J., PATTERSON, A. V., STRATFORD, I. J., MORROW, C. S., TOWNSEND, A. J., JOUNAIDI, Y., CHEN, C. S., SU, T., LU, H., SCHWARTZ, P. S. & WAXMAN, D. J. 2005. Cancer chemotherapy and drug metabolism. *Drug Metabolism and Disposition,* 33**,** 1083-1096.

ROBERTS, M. 1990. *Indigenous Healing Plants,* South Africa, Southern Book Publishers.

ROWINSKY, E. K., CAZENAVE, L. A. & DONEHOWER, R. C. 1990. Taxol: a novel investigational antimicrotubule agent. *Journal of the National Cancer Institute,* 82**,** 1247–1259.

SAKAHIRA, H., ENARI, M. & NAGATA, S. 1998. Cleavage of CAD inhibitor in CAD activation and DNA degradation during apoptosis. *Nature,* 391**,** 96-99.

SAMUELSSON, G. 1992. *Drugs of Natural Origin – A textbook of Pharmacognosy,* Swedish Pharmaceutical Press.

SARZAEEM, A., MIRAKABADI, A. Z., MORADHASELI, S. & SAYAD, A. 2013. Comparative study for toxic Effects of Camptothecin in Cancer and Normal Cells. *Journal of Biology and today's world,* 2**,** 188-201.

SAVILL, J., FADOK, V. A., HENSON, P. M. & HASLETT, C. 1993. Phagocyte recognition of cells undergoing apoptosis. *Immunology Today,* 14**,** 131–136.

SAXE, T. G. 1987. Toxicity of medicinal herbal preparations. *American Family Physician,* 35**,** 135–142.

SCHACTER, L. 1996. Etoposide phosphate: what, why, where, and how? *Seminars in Oncology,* 23**,** 1–7.

SCHMID, I., KRALL, W. J., UITTENBOGAART, C. H., BRAUN, J. & GIORGI, J. V. 1992. Dead cell discrimination with 7-amino-actinomycin D in combination with dual color immunofluorescence in single laser flow cytometry. *Cytometry,* 13**,** 204-208.

SCHRIPSEMA, J., RAMOS-VALDIVIA, A. & VERPOORTE, R. 1999. Robustaquinones novel anthraquinones from elicited Cinchona robusta suspension culture. *Phytochemistry,* 51**,** 55-60.

SCHUTTE, B., NUYDENS, R., GEERTS, H. & RAMAEKERS, F. 1998. Annexin V binding assay as a tool to measure apoptosis in differentiated neuronal cells. *Journal of Neuroscience Methods,* 86**,** 63-69.

SHENOUDA, N. S., SAKLA, M. S., NEWTON, L. G., BESCH-WILLIFORD, C., GREENBERG, N. M., MACDONALD, R. S. & LUBAHN, D. B. 2007. Phytosterol Pygeum africanum regulates prostate cancer in vitro and in vivo. *Endocrine,* 31**,** 72-81.

SHI, L. G., ZHANG, G. P. & JIN, H. M. 2006. Inhibition of microvascular endothelial cell apoptosis by angiopoietin-1 and the involvement of cytochrome C. *Chinese Medical Journal,* 119**,** 725-730.

SHI, Y. 2002. Mechanisms of caspase activation and inhibition during apoptosis. *Molecular Cell,* 9**,** 459–470.

SHOEMAKER, R. H. 2006. The NCI60 human tumour cell line anticancer drug screen. *Nature Reviews Cancer,* 6**,** 813-823.

SIVALOKANATHAN, S., ILAYARAJA, M. & BALASUBRAMANIUM, M. P. 2005. Efficacy of terminalia arjuna (Roxb.) on N-nitrosodiethylamine induced hepatocellular carcinoma in rats. *Indian Journal of Experimental Biology,* 43**,** 264-267.

SKOMMER, J., DARZYNKIEWICZ, Z. & WLODKOWIC, D. 2010. Technological advances in real-time tracking of cell death. *Cell Cycle,* 9**,** 2330-2341.

SLEE, E. A., HARTE, M. T., KLUCK, R. M., WOLF, B. B., CASIANO, C. A., NEWMEYER, D. D., WANG, H. G., REED, J. C., NICHOLSON, D. W., ALNEMRI, E. S., GREEN, D. R. & MARTIN, S. J. 1999. Ordering the cytochrome c-initiated caspase cascade: hierarchical activation of caspases-2, -3, -6, -7, -8, and -10 in a caspase-9-dependent manner. *Journal of Cell Biology,* 144**,** 281-292.

SMILEY, S. T., REERS, M., MOTTOLA-HARTSHORN, C., LIN, M., CHEN, A., SMITH, T. W., STEELE, G. D. & CHEN, L. B. 1991. Intracellular heterogeneity in mitochondrial membrane potentials revealed by a J-aggregate forming lipophilic cation JC-1. *Proceedings of the National Academy of Sciences of the United States of America,* 88**,** 3671-3675.

SMITH, A. D., DATA, S. P., SMITH, G. H., CAMPBELL, P. N., BENTLEY, R. & MCKENZIE, H. A. (eds.) 1997. *Oxford Dictionary of Biochemistry and Molecular Biology,* New York: Oxford University Press.

SMITH, B. D. 2011. Imatinib for chronic myeloid leukemia: the impact of its effectiveness and long-term side effects. *Journal of the National Cancer Institute,* 103**,** 527-529.

SMITH, L., WATSON, M. B., O'KANE, S. L., DREW, P. J., LIND, M. J. & CAWKWELL, L. 2006. The analysis of doxorubicin resistance in human breast cancer cells using antibody microarrays. *Molecular Cancer Therapeutics,* 5**,** 2115-2120.

SMITHIES, S. J. 2000. Pedaliaceae. *In:* LEISTNER, O. A. (ed.) *Seed plants of Southern Africa: families and genera.* Pretoria: National Botanical Institute.

STAN, S. D., HAHM, E. R., WARIN, R. & SINGH, S. V. 2008. Withaferin A causes FOXO3a- and Bim-dependent apoptosis and inhibits growth of human breast cancer cells in vivo. *Cancer Research,* 68**,** 7661–7669.

STANCHEV, S., MOMEKOV, G., JENSEN, F. & MANOLOV, I. 2008. Synthesis, computational study and cytotoxic activity of new 4-hydroxycoumarin derivatives. *European Journal of Medicinal Chemistry,* 43**,** 694-706.

STARK, T. D., MTUI, D. J. & BALEMBA, O. B. 2013. Ethnopharmacological Survey of Plants Used in the Traditional Treatment of Gastrointestinal Pain, Inflammation and Diarrhea in Africa: Future Perspectives for Integration into Modern Medicine. *Animals,* 3**,** 158-227.

STREET, R. A. & PRINSLOO, G. 2013. Commercially Important Medicinal Plants of South Africa: A Review. *Journal of Chemistry,* 2013**,** 1-16.

SUBCHAREON, P. 1998. *Handbook of anticancer: Thai traditional medicine: new concept for treated cancer,* Bangkok, Thai Traditional Medicine Institute, 3.

SUSIN, S. A., LORENZO, H. K., ZAMZAMI, N., MARZO, I., SNOW, B. E., BROTHERS, G. M., MANGION, J., JACOTOT, E., COSTANTINI, P., LOEFFLER, M., LAROCHETTE, N., GOODLETT, D. R., AEBERSOLD, R., SIDEROVSKI, D. P., PENNINGER, J. M. & KROEMER, G. 1999. Molecular characterization of mitochondrial apoptosis-inducing factor. *Nature,* 397**,** 441-446.

SWAFFAR, D. S., ANG, C. Y., DESAI, P. B. & ROSENTHAL, G. A. 1994. Inhibition of the growth of human pancreatic cancer cells by the arginine antimetabolite L-canavanine. *Cancer Research,* 54**,** 6045-6048.

SWIFT, L. H. & GOLSTEYN, R. M. 2014. Genotoxic Anti-Cancer Agents and Their Relationship to DNA Damage, Mitosis, and Checkpoint Adaptation in Proliferating Cancer Cells. *International Journal of Molecular Sciences,* 15**,** 3403-3431.

THOMSON, S. 2002. Canavanine toxicity: Is Sutherlandia a healthy herb or potential poison? HIV Positive and AIDS Sufferers Beware: The Remedy may be Worse than the Alleged Disease [Online]. Available: http://www.gaiaresearch.co.za. [Accessed: 21 July 2015].

THORNES, R. D., DALY, L., LYNCH, G., BRESLIN, B., BROWNE, H., BROWNE, H. Y., CORRIGAN, T., DALY, P., EDWARDS, G., GAFFNEY, E., HENLEY, J., HEALY, F., KEANE, F., LENNON, F., MCMURRAY, N., O'LOUGHLIN, S., SHINE, M. & TANNER, A. 1994. Treatment with coumarin to prevent or delay recurrence of malignant melanoma. *Journal of Cancer Research and Clinical Oncology,* 120**,** S32–S34.

TREDGOLD, M. H. (ed.) 1986. *Food of plants of Zimbabwe,* Gweru: Mambo Press, 153.

TSUJIMOTO, Y., FINGER, L. R., YUNIS, J., NOWELL, P. C. & CROCE, C. M. 1984. Cloning of the chromosome breakpoint of neoplastic B cells with the t(14; 18) chromosome translocation. *Science,* 226**,** 1097-1099.

UMADEVI, M., KUMAR, K. P. S., BHOWMIK, D. & DURAIVEL, S. 2013. Traditionally Used Anticancer Herbs In India. *Journal of Medicinal Plants Studies,* 1**,** 56-74.

VAN CRUCHTEN, S. & VAN DEN BROECK, W. 2002. Morphological and biochemical aspects of apoptosis, oncosis and necrosis. *Anatomia, Histologia, Embryologia,* 31**,** 214-223.

VAN DER WALT, L. 2001. Ceratotheca triloba (Bernh.) Hook.f. [Online]. Kirstenbosch: South African National Biodiversity Institute. Available: http://www.plantzafrica.com/plantcd/ceratothectrilob.htm. [Accessed: 18 July 2015]

VAN ENGELAND, M., KUIJPERS, H. J. H., RAMAEKERS, F. C. S., REUTELINGSPERGER, C. P. M. & SCHUTTE, B. 1997. Plasma membrane alterations and cytoskeletal changes in apoptosis. *Experimental Cell Research,* 235**,** 421–430.

VAN WYK, B. E. (ed.) 1997. *Medicinal Plants of South Africa,* Pretoria, South Africa: Briza Publishers.

VAN WYK, B. E. & GERICKE, N. (eds.) 2000a. *People's plants. A guide to useful plants of Southern Africa,* South Africa: Briza Publications.

VAN WYK, B. E. & GERICKE, N. 2000b. *People's Plants: A Guide to Useful Plants of Southern Africa,* South Africa, Briza Publications.

VEALE, R. B. & THORNLEY, A. L. 1989. Increased single class low-affinity EGF receptors expressed by human oesophageal squamous carcinoma cell lines. *South African Journal of Science,* 85**,** 375-379.

VEERESHAM, C. 2012. Natural products derived from plants as a source of drugs. *Journal of Advanced Pharmaceutical Technology and Research,* 3**,** 200–201.

VERMES, I., HAANEN, C., STEFFENS-NAKKEN, H. & REUTELINGSPERGER, C. 1995. A novel assay for apoptosis flow cytometric detection of phosphatidylserine early apoptotic cells using fluorescein labeled expression on Annexin V. *Journal of Immunological Methods,* 184**,** 39-51.

VERMORKEN, J. B., HARPER, P. G. & BUYSE, M. 1999. The role of anthracyclines in epithelial ovarian cancer. *Annals of Oncology,* 10**,** 43-50.

VERPOORTE, R. 2000. *Metabolic Engineering of Plant Secondary Metabolism*, Kluwer Academic Publishers.

VINCETI, B., LOO, J., GAISBERGER, H., VAN ZONNEVELD, M. J., SCHUELER, S., KONRAD, H., KADU, C. A. C. & GEBUREK, T. 2013. Conservation priorities for Prunus africana defined with the aid of spatial analysis of genetic data and climatic variables. *PLoS One,* 8**,** e59987.

VOET, D. & VOET, J. G. 1995. *Biochemistry,* New York, John Wiley.

VOSOOGHI, M., YAHYAVI, H., DIVSALAR, K., SHAMSA, H., KHEIROLLAHI, A., SAFAVI, M., ARDESTANI, S. K., SADEGHI-NESHAT, S., MOHAMMADHOSSEINI, N., EDRAKI, N., KHOSHNEVISZADEH, M., SHAFIEE, A. & FOROUMADI, A. 2013. Synthesis and In vitro cytotoxic activity evaluation of (E)-16-(substituted benzylidene) derivatives of dehydroepiandrosterone. *DARU Journal of Pharmaceutical Sciences,* 21.

VUCIC, D. & FAIRBROTHER, W. J. 2007. The inhibitor of apoptosis proteins as therapeutic targets in cancer. *Clinical Cancer Research,* 13**,** 5995-6000.

WANG, Z. & SUN, Y. 2010. Targeting p53 for Novel Anticancer Therapy. Translational Oncology, 3, 1-12.

WASFY, A. A. F., MOHMED, N. A. & SALMAN, A. A. 2015. Synthesis and anti-cancer properties of novel quinazoline derivatives. *International Journal of Research in Pharmacy and Chemistry,* 5**,** 34-40.

WATT, J. M. & BREYER-BRANDWIJK, M. G. (eds.) 1962. *The medicinal and poisonous plants of Southern and Eastern Africa,* London: Livingstone.

WEI, Y., FAN, T. & YU, M. 2008. Inhibitor of apoptosis proteins and apoptosis. *Acta Biochimica et Biophysica Sinica,* 40**,** 278-288.

WELMAN, M. 2011. Withania somnifera (L.) Dunal [Online]. Pretoria: South African National Biodiversity Institute. Available: http://www.plantzafrica.com/plantwxyz/withaniasomnifera.htm. [Accessed: 21 July 2015].

WETERINGS, E., VERKAIK, N. S., BRUÈGGENWIRTH, H. T., HOEIJMAKERS, J. H. J. & VAN GENT, D. C. 2003. The role of DNA dependent protein kinase in synapsis of DNA ends. *Nucleic Acids Research,* 31**,** 7238-7246.

WONG, R. S. Y. 2011. Apoptosis in cancer: from pathogenesis to treatment. *Journal of Experimental & Clinical Cancer Research,* 30**,** 2-14.

WOOD, B. L., GIBSON, D. F. & TAIT, J. F. 1996. Increased phosphatidylserine exposure in sickle cell disease: flow cytometric measurement and clinical associations. *Blood,* 88**,** 1873–1880.

WOOLLACOTT, A. J. & SIMPSON, P. B. 2001. High throughput fluorescence assays for the measurement of mitochondrial activity in intact human neuroblastoma cells. *Journal of Biomolecular Screening,* 6**,** 413-420.

WORLD HEALTH ORGANIZATION. 2015. Ultraviolet radiation and the INTERSUN Programme, Skin cancers [Online]. Available: http://www.who.int/uv/faq/skincancer/en/index1.html. [Accessed: 21 July 2015]

WUNDERLIN, R. P. & HANSEN, B. F. 2002. Atlas of Florida vascular plants [Online]. Tampa: University of South Florida. Available: http://www.plantatlas.usf.edu/. [Accessed: 23 July 2010]

XABA, P. M. A. & NOTTEN, A. 2003. Sutherlandia frutescens (L.) R.Br. [Online]. Kirstenbosch: South African National Biodiversity Institute. Available: http://www.plantzafrica.com/plantqrs/sutherfrut.htm. [Accessed: 21 July 2015]

XI, S. 2003. Src kinases mediate STAT growth pathways in squamous cell carcinoma of the head and neck. *Journal of Biological Chemistry,* 278**,** 31574-31583.

XING-JIE, L., CHUNYING, C., YULIANG, Z. & PAUL, C. W. 2010. Circumventing Tumor Resistance to Chemotherapy by Nanotechnology. *Methods in Molecular Biology,* 596**,** 467-488.

XU, T. P., SHEN, H., LIU, L. X. & SHU, Y. Q. 2013. Plumbagin from Plumbago Zeylanica L induces apoptosis in human non-small cell lung cancer cell lines through NF- κB inactivation. *Asian Pacific Journal of Cancer Prevention,* 14**,** 2325-2331.

YAN, N. & SHI, Y. 2005. Mechanisms of apoptosis through structural biology. *Annual Review of Cell and Developmental Biology,* 21**,** 35-56.

YAOXIAN, W., HUI, Y., YUNYAN, Z., YANQIN, L., XIN, G. & XIAOKE, W. 2013. Emodin induces apoptosis of human cervical cancer hela cells via intrinsic mitochondrial and extrinsic death receptor pathway. *Cancer Cell International,* 13**,** 1-8.

YEAP, S., AKHTAR, M. N., LIM, K. L., ABU, N., HO, W. Y., ZAREEN, S., ROOHANI, K., KY, H., TAN, S. W., LAJIS, N. & ALITHEEN, N. B. 2015. Synthesis of an anthraquinone derivative (DHAQC) and its effect on induction of G2/M arrest and apoptosis in breast cancer MCF-7 cell line. *Journal of Drug Design, Development and Therapy,* 9**,** 983-992.

YIP, K. W. & REED, J. C. 2008. Bcl-2 family proteins and cancer. *Oncogene,* 27**,** 6398–6406.

ZAHEDIFARD, M., FARAJ, F. L., PAYDAR, M., LOOI, C. Y., HAJREZAEI, M., HASANPOURGHADI, M., KAMALIDEHGHAN, B., MAJID, N. A., ALI, H. M. & ABDULLA, M. A. 2015. Synthesis, characterization and apoptotic activity of quinazolinone Schiff base derivatives toward MCF-7 cells via intrinsic and extrinsic apoptosis pathways. *Scientific Reports,* 5.

ZELDIS, J. B. 2004. *Use of benzopyranones for treating or preventing a primary brain cancer or a brain metastasis*. WO2002US31417 20021003

ZHAI, D., JIN, C., HUANG, Z., SATTERTHWAIT, A. C. & REED, J. C. 2008. Differential regulation of Bax and Bak by anti-apoptotic Bcl-2 family proteins Bcl-B and Mcl-1. *Journal of Biological Chemistry,* 283**,** 9580-9586.

ZHANG, W., LIU, A., LI, Y., ZHAO, X., LV, S., ZHU, W. & JIN, Y. 2012b. Anticancer activity and mechanism of juglone on human cervical carcinoma HeLa cells. *Canadian Journal of Physiology and Pharmacology,* 90**,** 1553-1558.

ZHANG, Z., DAYNARD, T. & KALMAR, G. 2006. *Methods of using benzothiophenone derivatives to treat cancer or inflammation*. United States patent application 60390589.

ZHAO, Y., WU, M., SHEN, Y. & ZHAI, Z. 2001. Analysis of nuclear apoptotic process in a cell-free system. *Cellular and Molecular Life Sciences,* 58**,** 298-306.

ZWAAL, R. F. A., COMFURIUS, P. & BEVERS, E. M. 2005. Surface exposure of phosphatidylserine in pathological cells. *Cellular and Molecular Life Sciences,* 62**,** 971–988.

ZWAAL, R. F. A. & SCHROIT, A. J. 1997. Pathophysiologic implications of membrane phospholipid asymmetry in blood cells. *Blood,* 89**,** 1121–1132.

APPENDIX

Appendix 1: Concentration ranges of the standards and fractions

Table A1: Concentration ranges of the standards and fractions that were used to treat the A375 cells.

Standard/fraction	Concentration range (µg.ml^{-1})
Camptothecin	7.81 x 10^{-4}, 1.56 x 10^{-3}, 3.13 x 10^{-3}, 6.25 x10^{-3}, 1.25 x 10^{-2}, 2.50 x10^{-2}, 5.0 x10^{-2}, 0.10, 0.20, 0.39, 0.78, 1.56, 3.13, 6.25, 12.50, 25.00, 50
Doxorubicin	3.125 x10^{-3}, 6.25 x10^{-3}, 1.25, x10^{-2}, 2.50 x 10^{-2}, 5.0 x10^{-2}, 0.10, 0.20, 0.39, 0.78, 1.56, 3.13, 6.25, 12.50, 25.00
Fraction F2	0.10, 0.20, 0.39, 0.78, 1.56, 3.13, 6.25, 12.50, 25.00, 50.00
Fraction F4	0.10, 0.20, 0.39, 0.78, 1.56, 3.13, 6.25, 12.50, 25.00, 50.00
Fraction F5	0.10, 0.20, 0.39, 0.78, 1.56, 3.13, 6.25, 12.50, 25.00, 50.00
Fraction F8	0.10, 0.20, 0.39, 0.78, 1.56, 3.13, 6.25, 12.50, 25.00, 50.00

Table A2: Concentration ranges of the standards and fractions that were used to treat the UACC-62 cells.

Standard/fraction	Concentration range (µg.ml^{-1})
Camptothecin	7.81 x10^{-4}, 1.56 x 10^{-3}, 6.25 x 10^{-3}, 1.25 x10^{-2}, 2.50 x10^{-2}, 5.0 x 10^{-2}, 0.20, 0.39, 0.78, 1.56, 3.13, 6.25, 12.50
Doxorubicin	1.25 x10^{-2}, 2.50 x 10^{-2}, 5.0 x 10^{-2}, 0.10, 0.20, 0.39, 0.78, 1.56, 3.13, 6.25, 12.50, 25.00, 50
Fraction F2	1.56 x 10^{-3}, 3.13 x10^{-3}, 6.25 x10^{-3}, 3.75 x10^{-2}, 7.50 x10^{-2}, 0.30, 0.50, 0.60, 3, 6.25, 12.50, 25, 50
Fraction F4	2.5 x 10^{-2}, 5.0 x 10^{-2}, 0.075, 0.15, 0.3, 0.5, 0.78, 1.25, 1.5, 6.25, 12.50, 25, 50
Fraction F5	3.13 x 10^{-3}, 5.0 x 10^{-2}, 0.10, 0.20, 0.39, 0.78, 1.56, 3.13, 6.25, 12.50, 25, 50
Fraction F8	3.75 x10^{-2}, 7.50 x 10^{-2}, 0.15, 0.50, 0.60, 1, 1.25, 1.5, 2, 3, 6, 12.50, 25, 50

Appendix 2: Log curves of the melanoma cells treated with the standards and fractions

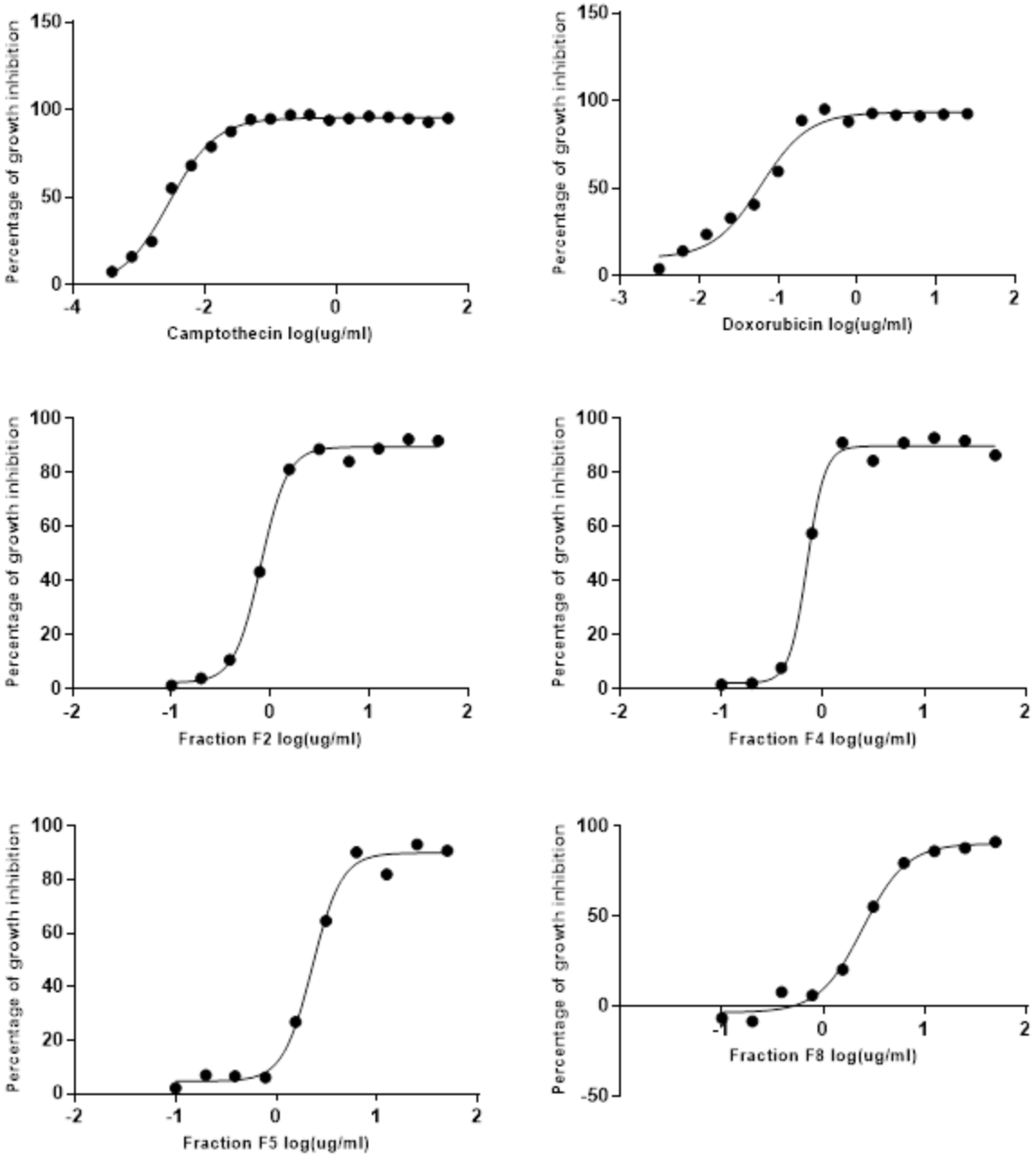

Figure A1: Log curves of the A375 cells treated with camptothecin (A), doxorubicin (B) and fractions F2 (C), F4 (D), F5 (E) and F8 (F).

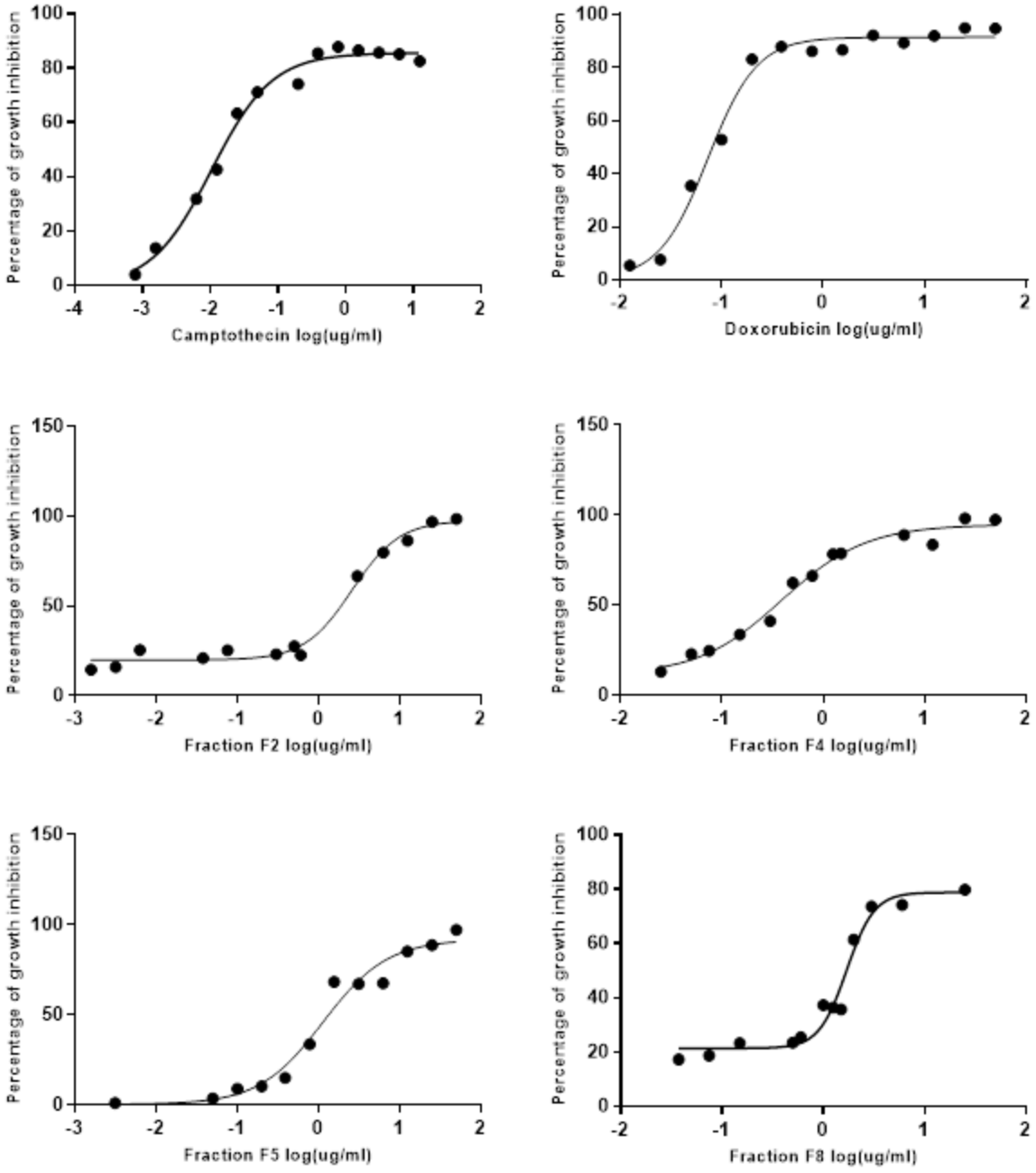

Figure A2: Log curves of the UACC-62 cells treated with camptothecin (A), doxorubicin (B) and fractions F2 (C), F4 (D), F5 (E) and F8 (F).

Appendix 3: MS library matches

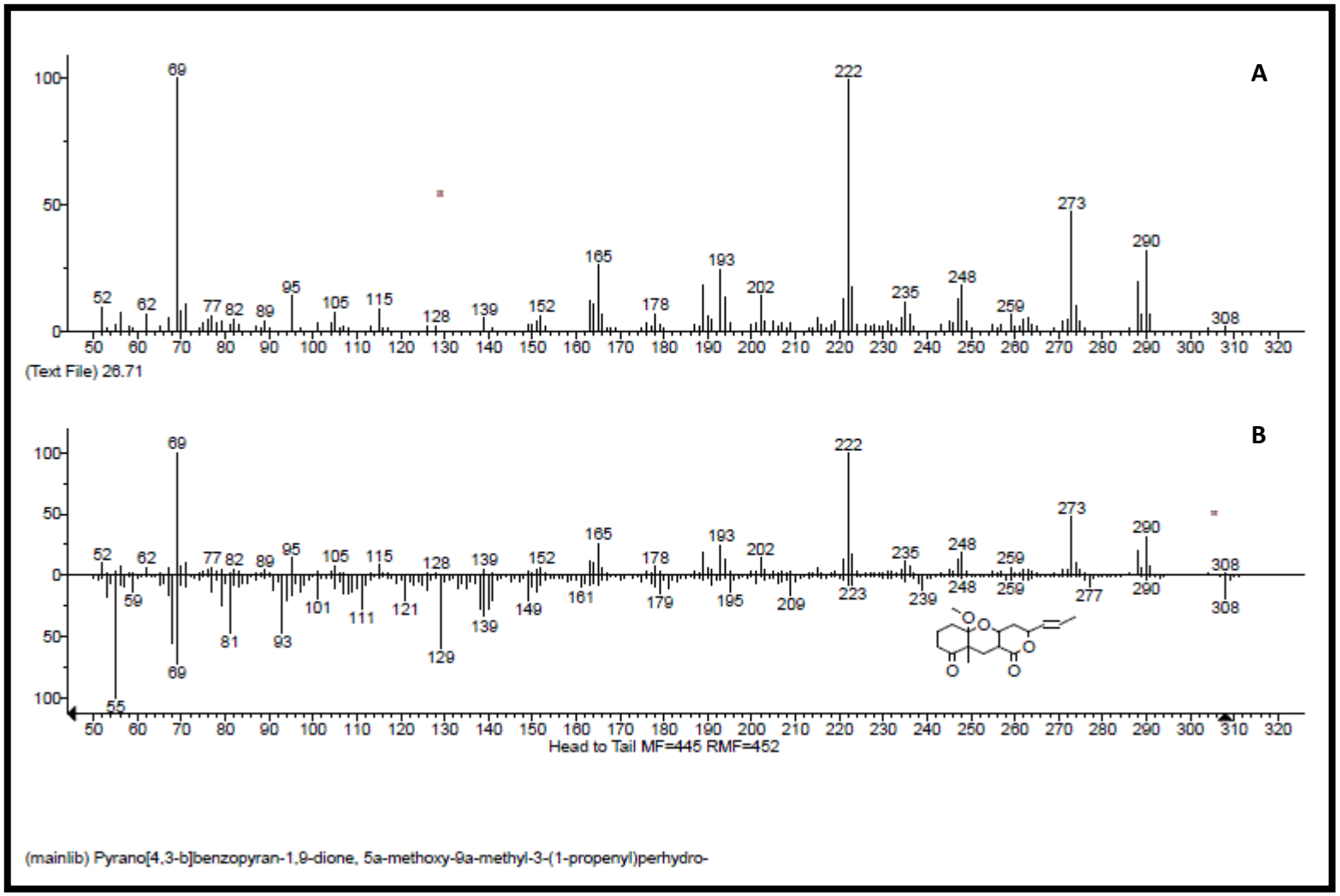

Figure A3: Mass spectrum of compound F2B isolated from *C. triloba* root extract (A) matched the library template of pyrano[4,3-b]benzopyran-1,9-dione, 5a-methoxy-9a-methyl-3-(1-propenyl)perhydro- (B).

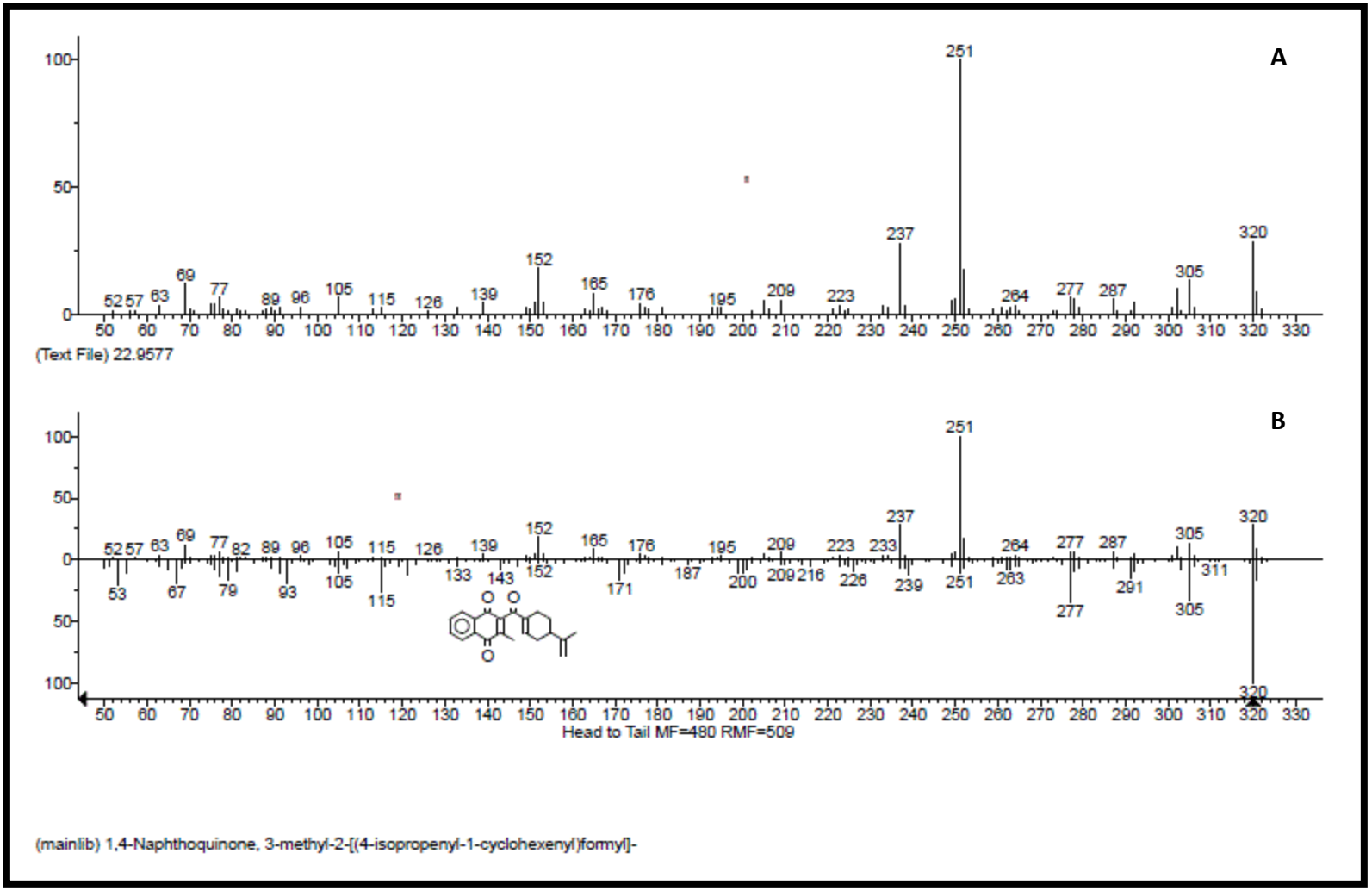

Figure A4: Mass spectrum of compound F2C isolated from *C. triloba* root extract (A) matched the library template of 1,4-naphthoquinone, 3-methyl-2-[(4-isopropenyl-1-cyclohexenyl)formyl]- (B).

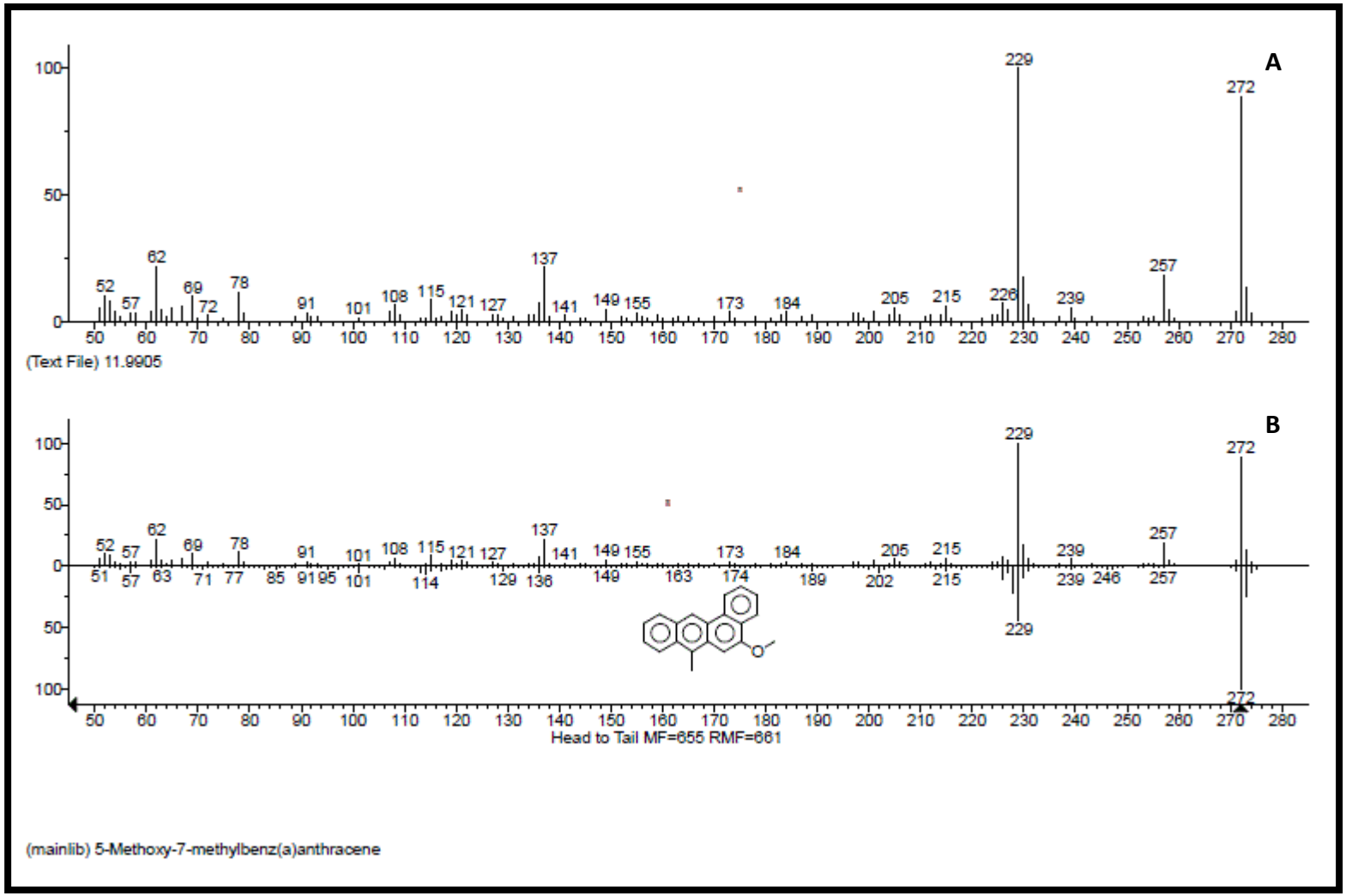

Figure A5: Mass spectrum of compound F4A isolated from *C. triloba* root extract (A) matched the library template of 5-methoxy-7-methylbenz(a)anthracene (B).

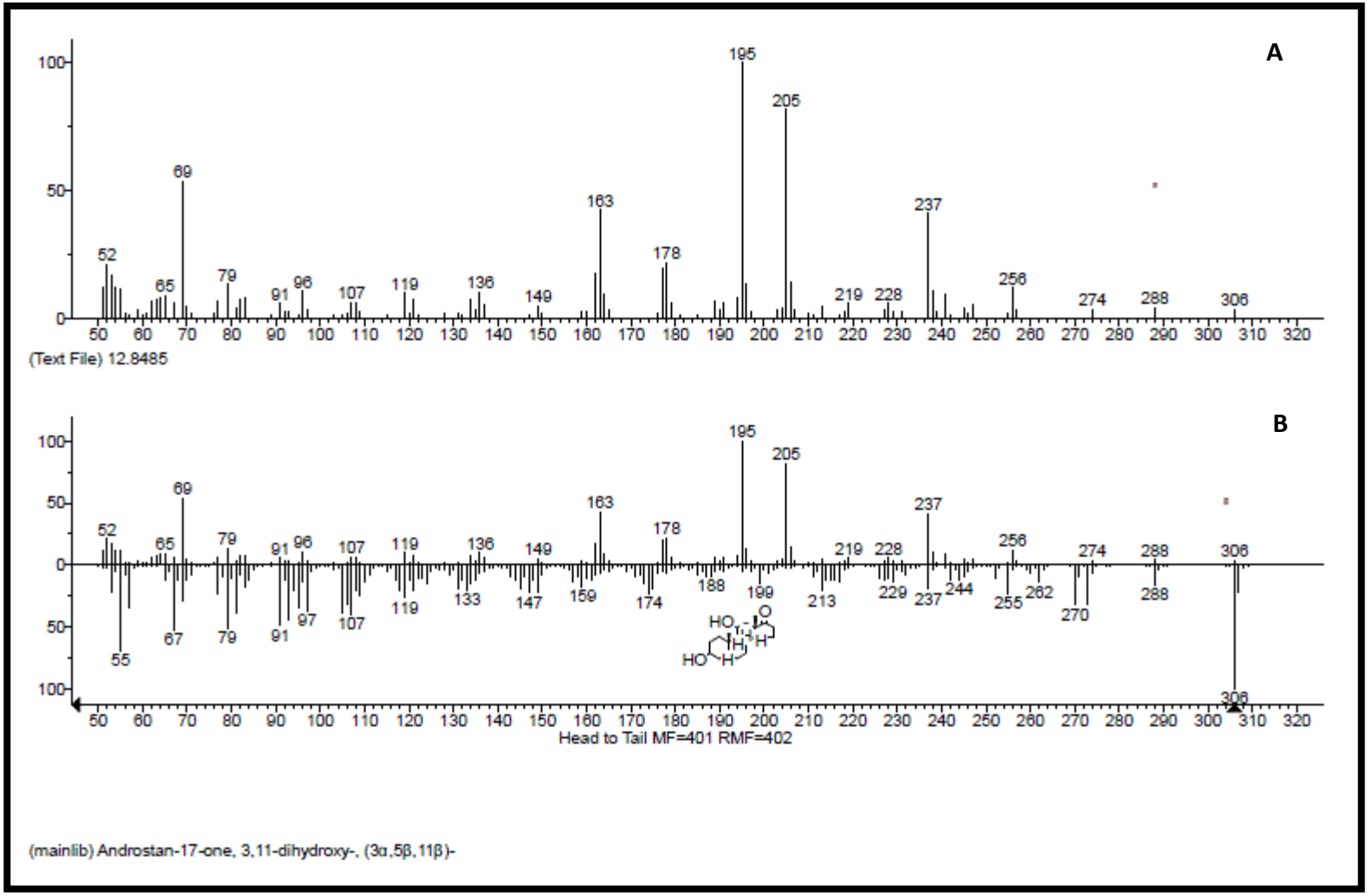

Figure A6: Mass spectrum of compound F4B isolated from *C. triloba* root extract (A) matched the library template of androstan-17-one, 3,11-dihydroxy-, (3α,5β,11β)- (B).

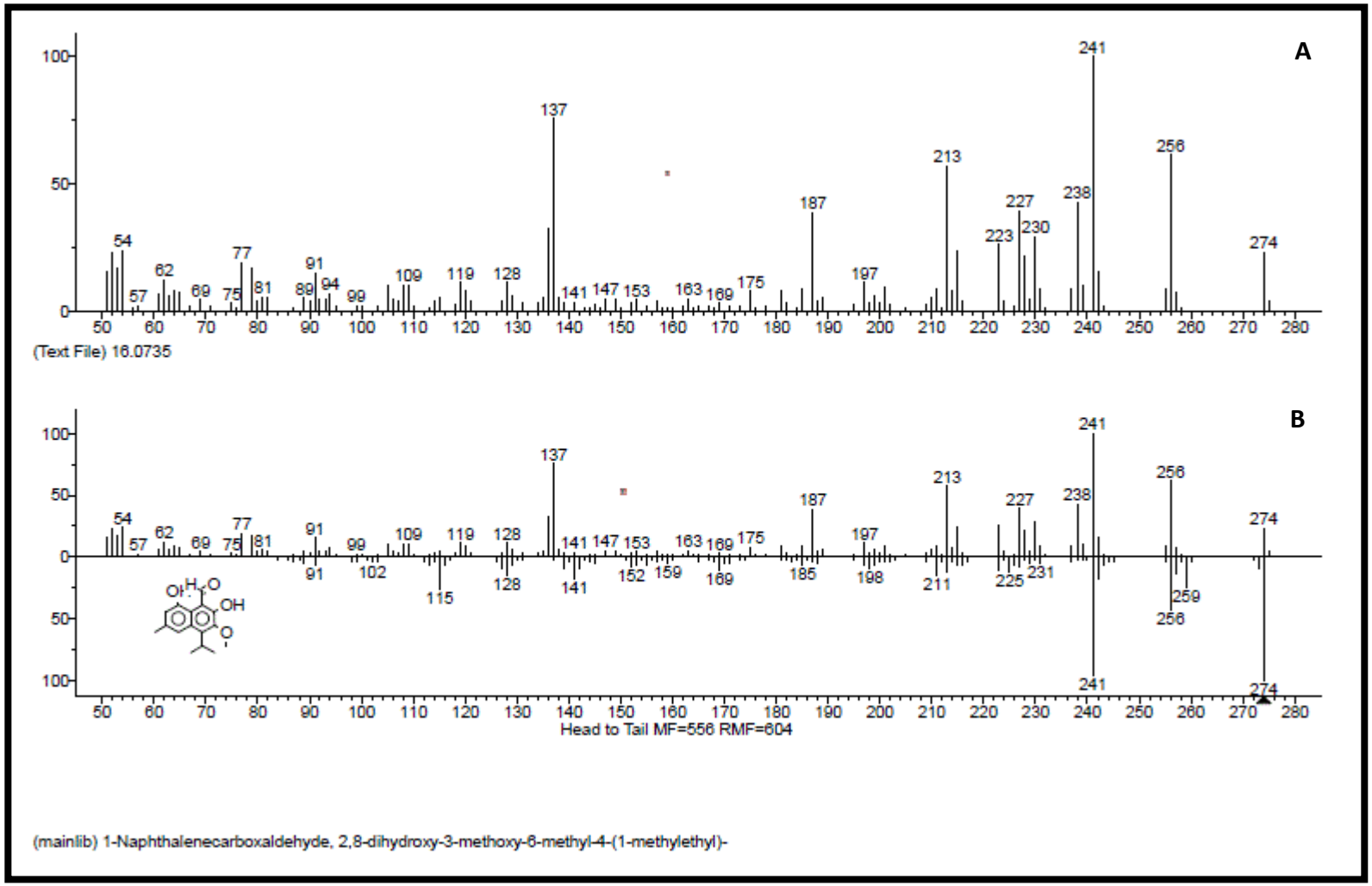

Figure A7: Mass spectrum of compound F4C isolated from *C. triloba* root extract (A) matched the library template of 1-naphthalenecarboxaldehyde, 2,8-dihydroxy-3-methoxy-6-methyl-4-(1-methylethyl)- (B).

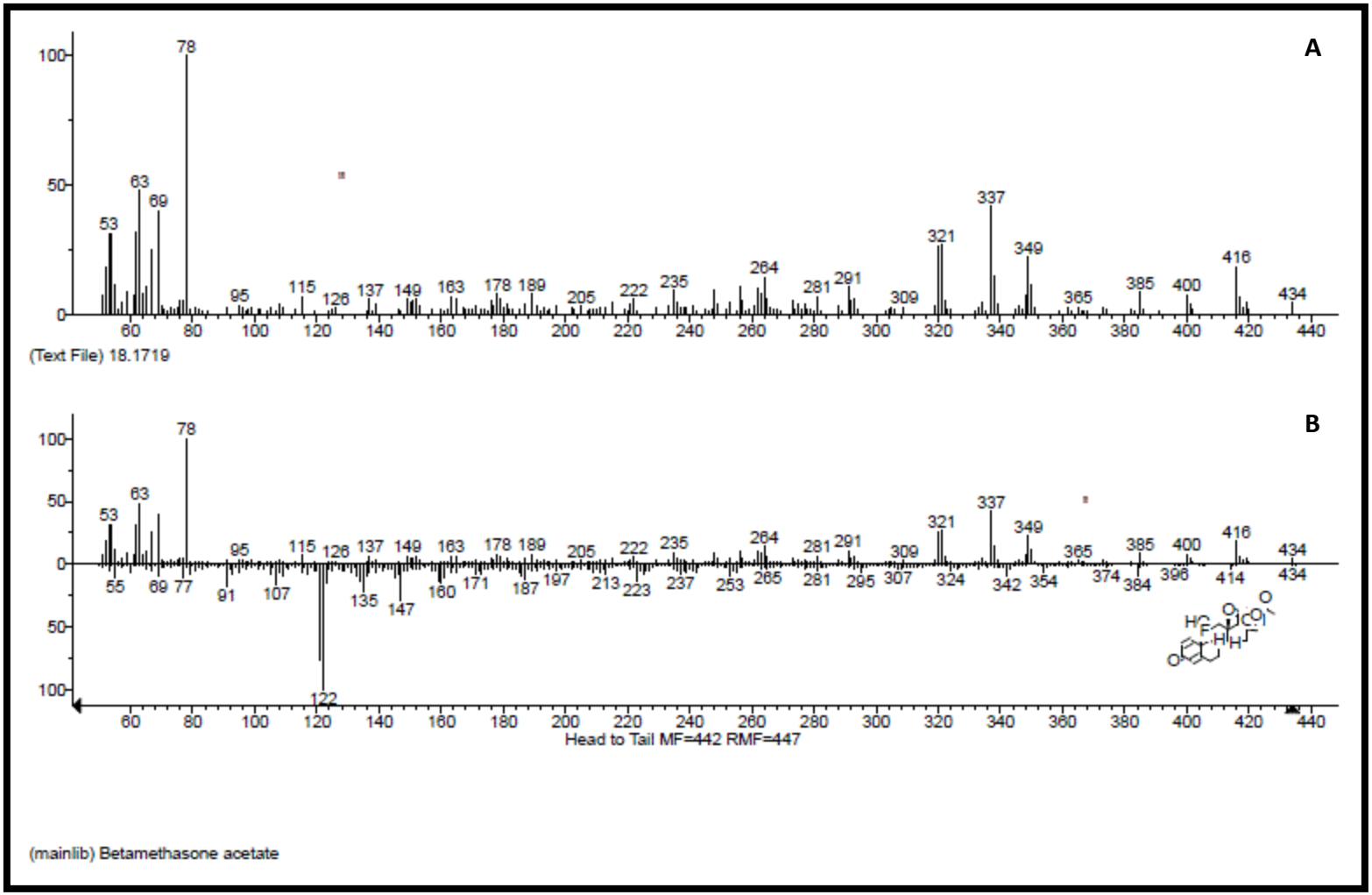

Figure A8: Mass spectrum of compound F5A isolated from *C. triloba* root extract (A) matched the library template of betamethasone acetate (B).

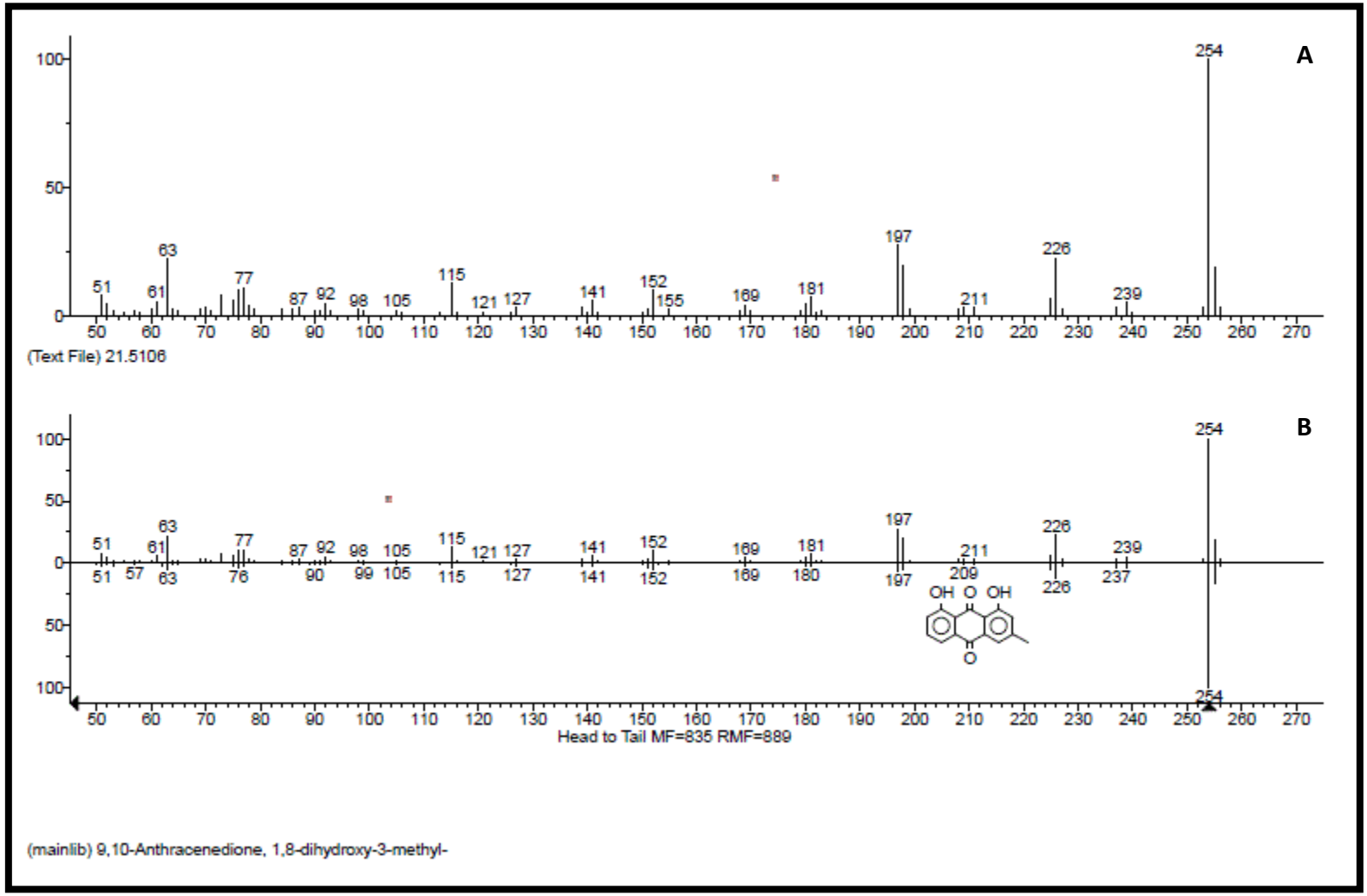

Figure A9: Mass spectrum of compound F5B isolated from *C. triloba* root extract (A) matched the library template of 9,10-anthracenedione, 1,8-dihydroxy-3-methyl (B).

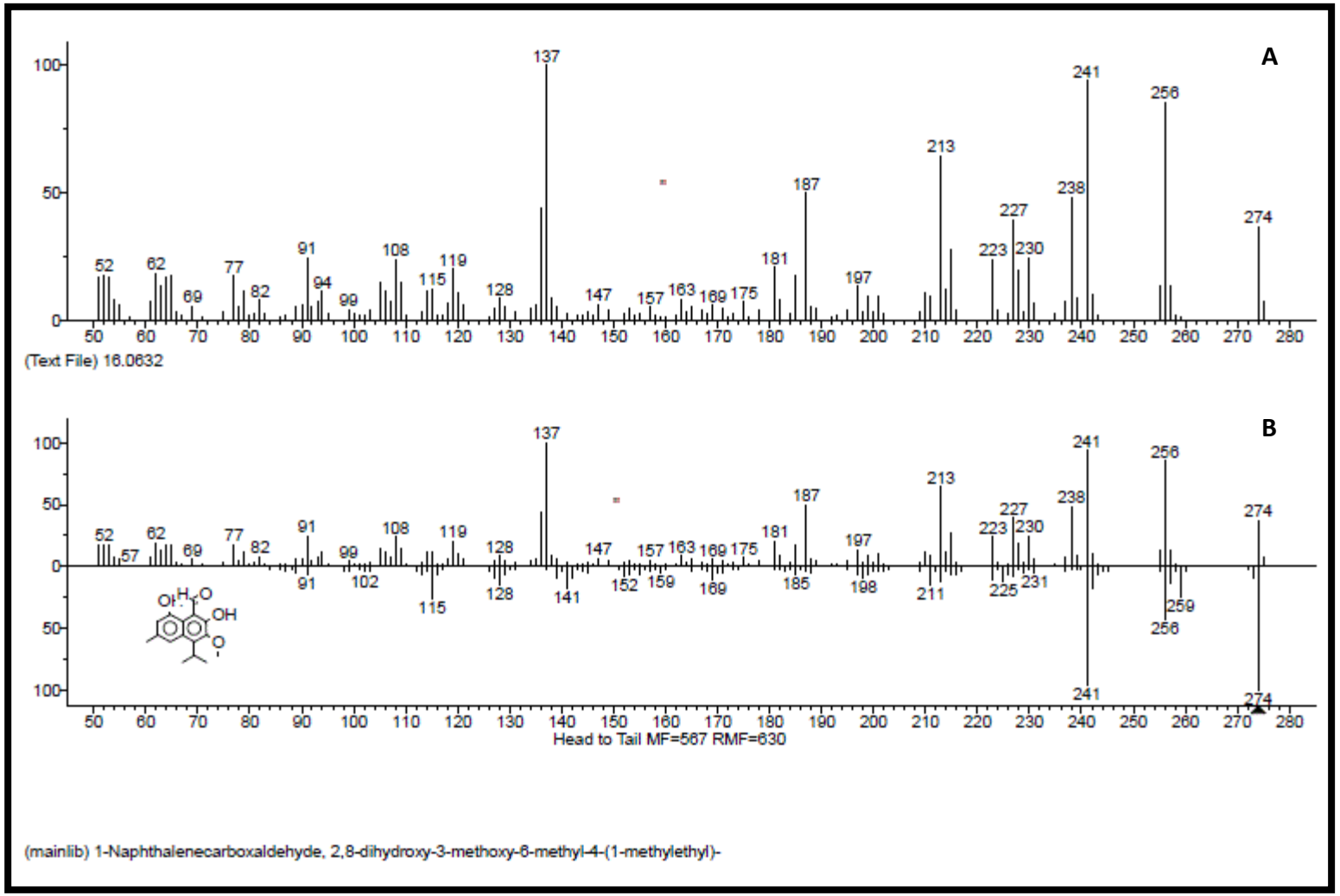

Figure A10: Mass spectrum of compound F5C isolated from *C. triloba* root extract (A) matched the library template of 1-naphthalenecarboxaldehyde, 2,8-dihydroxy-3-methoxy-6-methyl-4-(1-methylethyl)- (B).

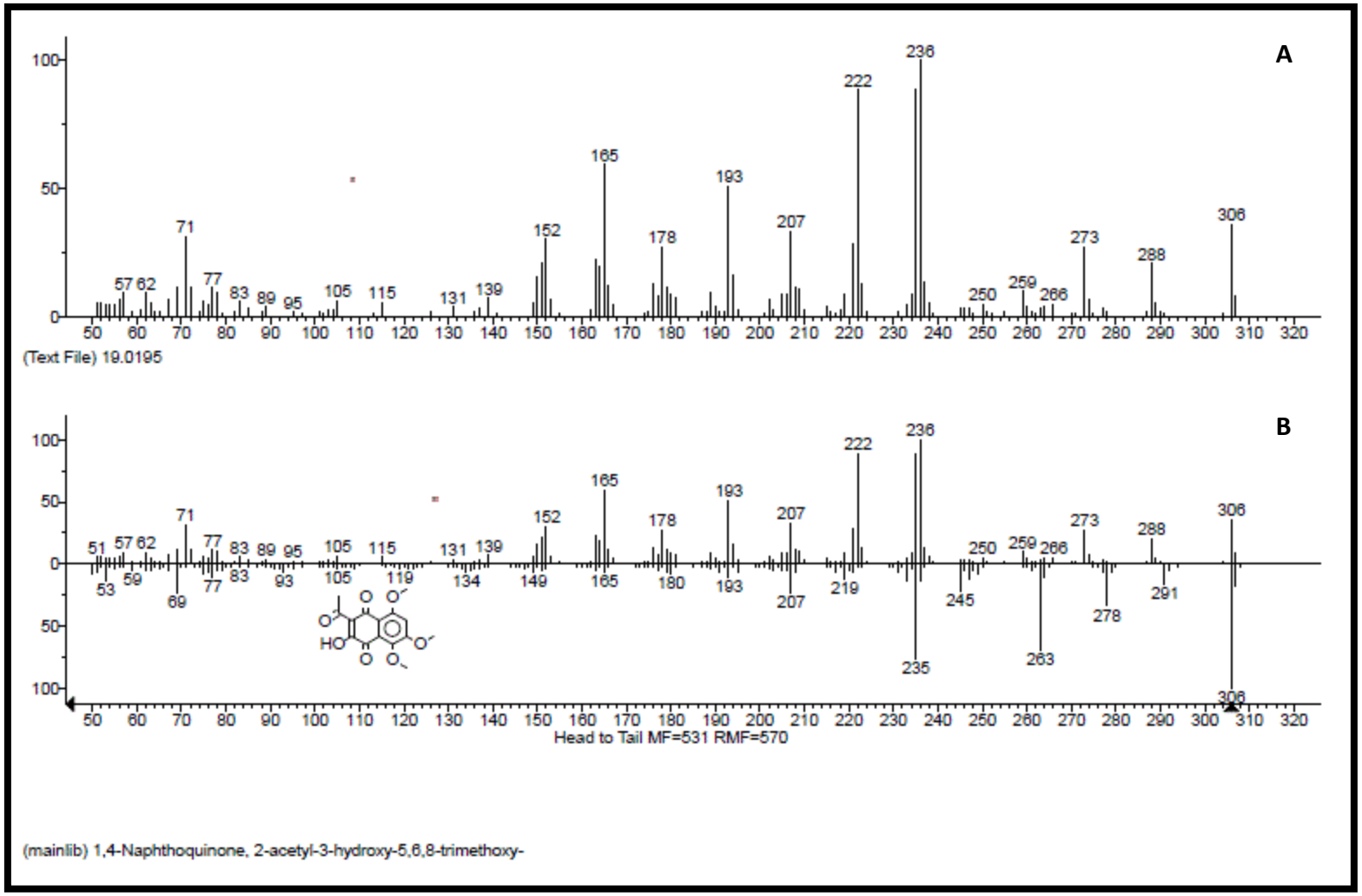

Figure A11: Mass spectrum of compound F5D isolated from *C. triloba* root extract (A) matched the library template of 1,4-naphthoquinone, 2-acetyl-3-hydroxy-5,6,8-trimethoxy (B).

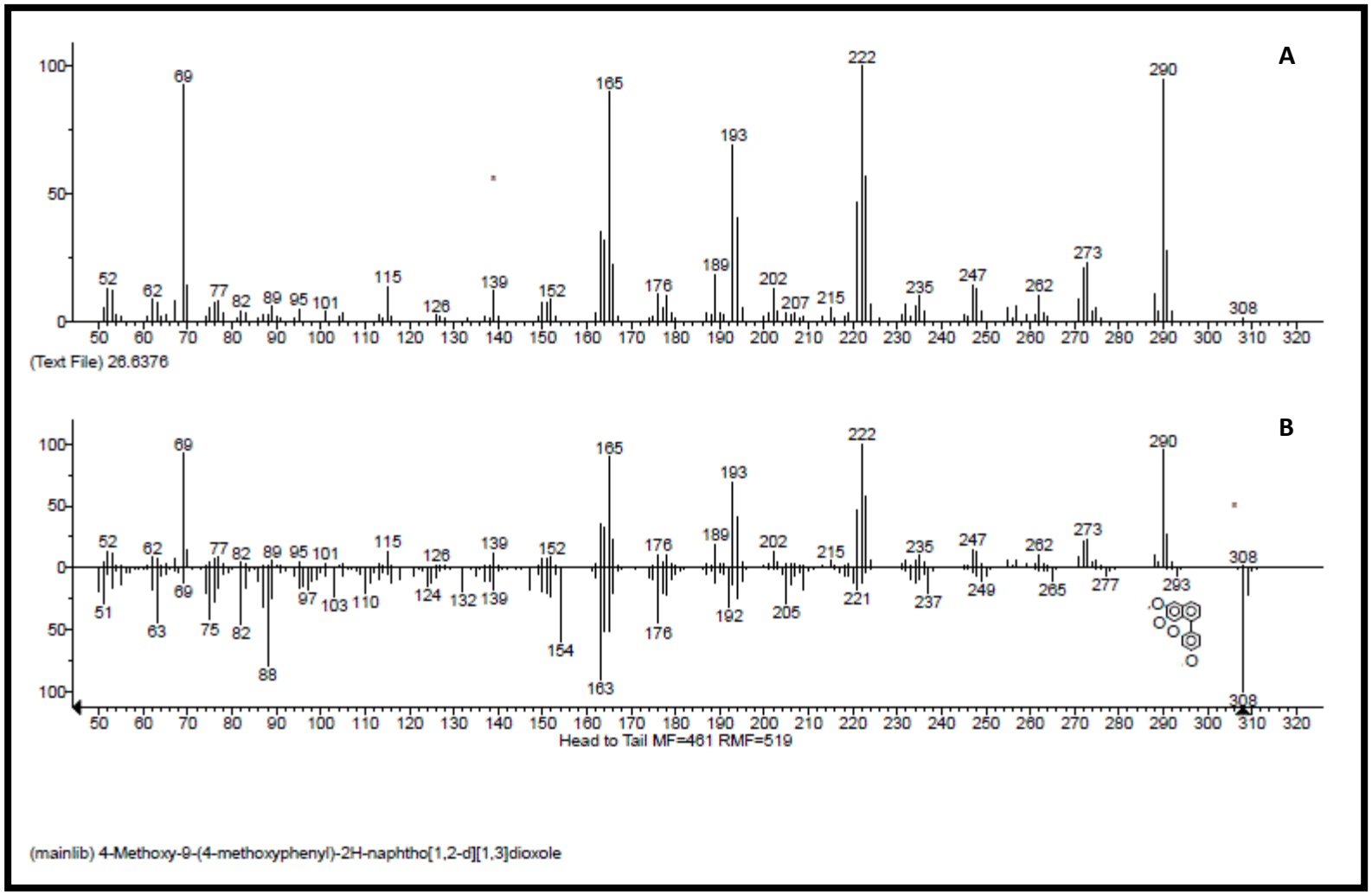

Figure A12: Mass spectrum of compound F5E isolated from *C. triloba* root extract (A) matched the library template of 4-methoxy-9-(4-methoxyphenyl)-2H-naphtho[1,2-d][1,3]dioxole (B).

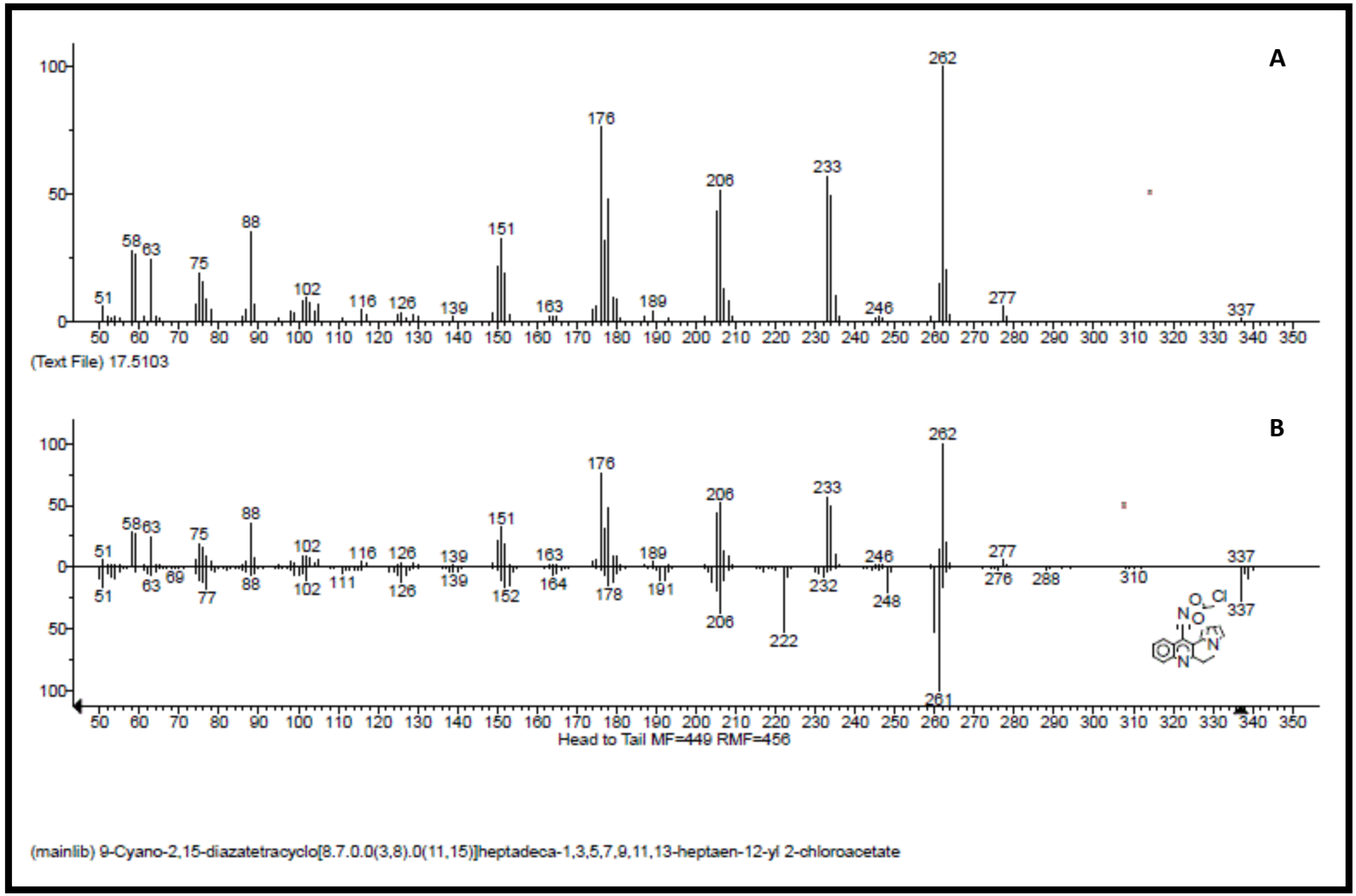

Figure A13: Mass spectrum of compound F5F isolated from *C. triloba* root extract (A) matched the library template of 9-cyano-2,15-diazatetracyclo[8.7.0.0(3,8).0(11,15)]heptadeca-1,3,5,7,9,11,13-heptaen-12-yl 2-chloroacetate (B).

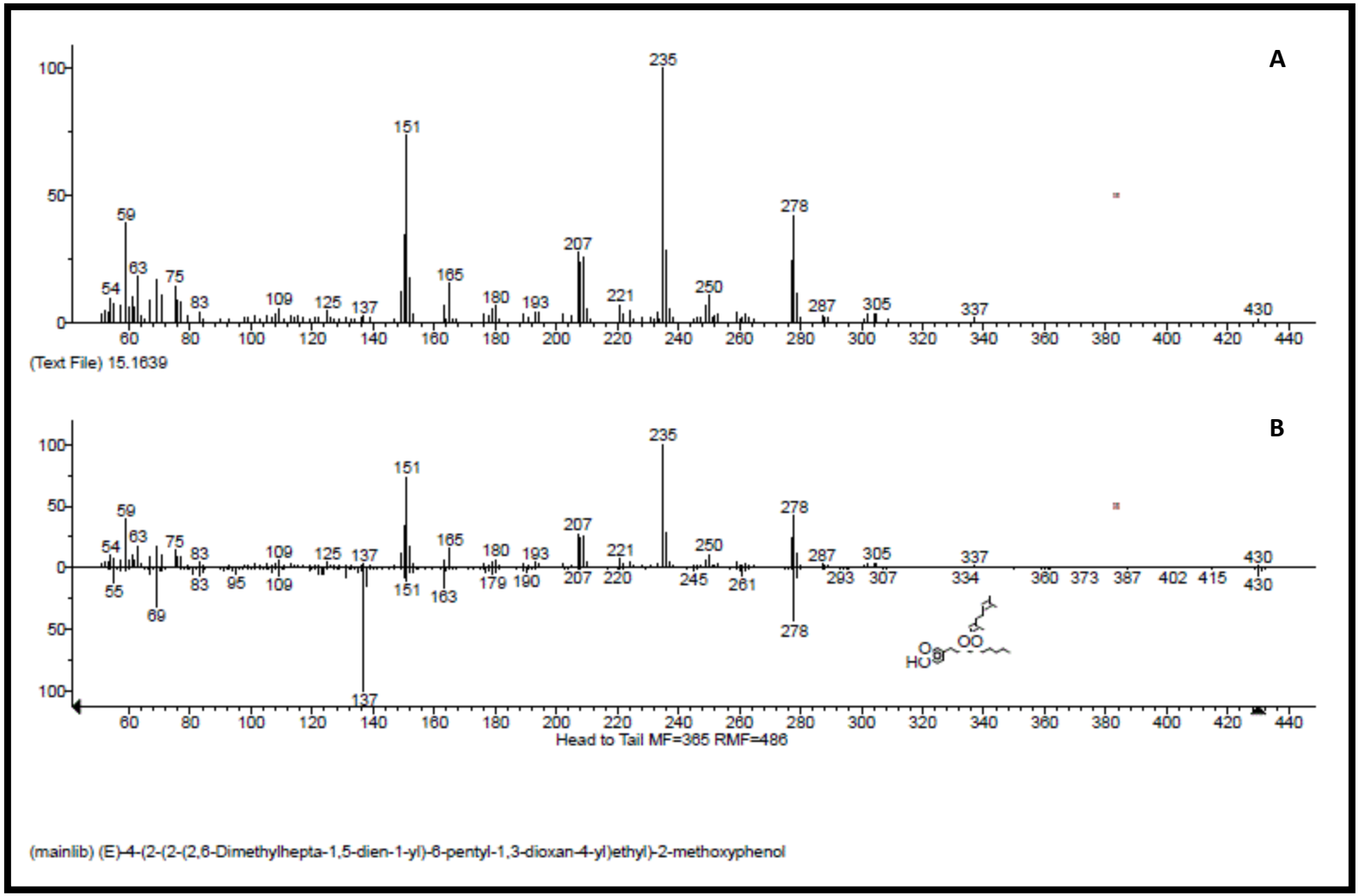

Figure A14: Mass spectrum of compound F5G isolated from *C. triloba* root extract (A) matched the library template of (E)-4-(2-(2-(2,6-dimethylhepta-1,5-dien-1-yl)-6-pentyl-1,3-dioxan-4-yl)ethyl)-2-methoxyphenol (B).

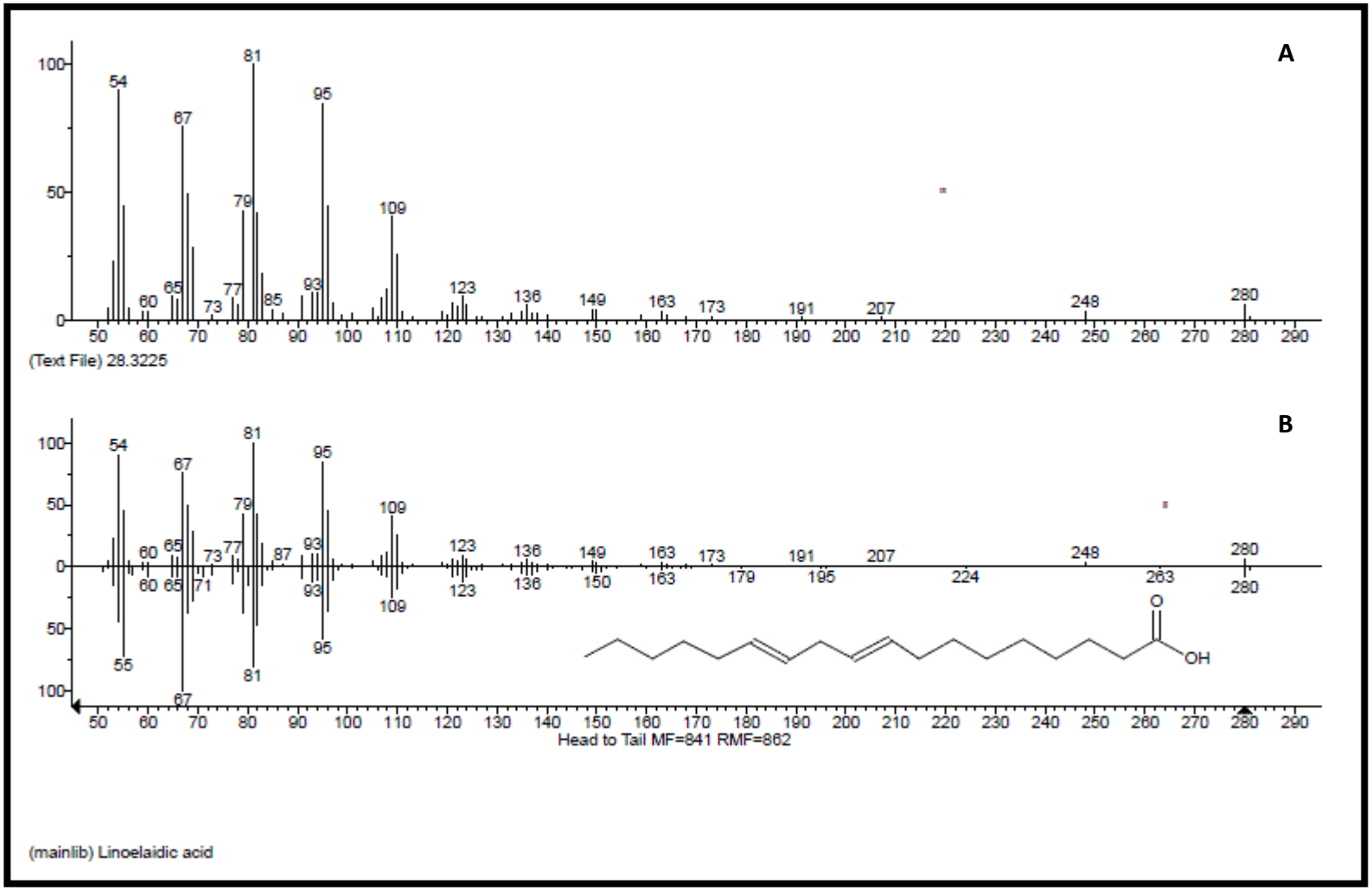

Figure A15: Mass spectrum of compound F8A isolated from *C. triloba* root extract (A) matched the library template of linoelaidic acid (B).

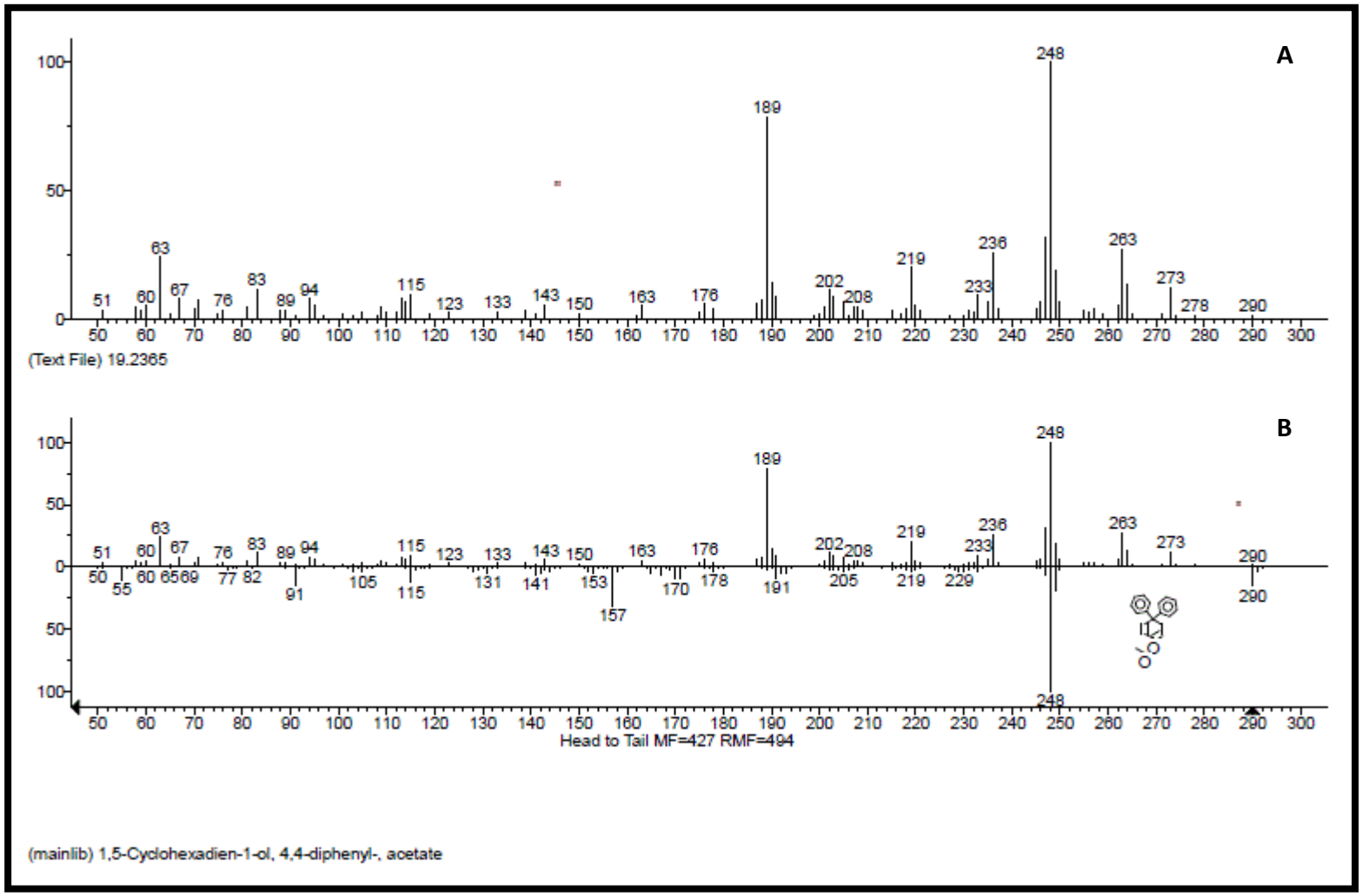

Figure A16: Mass spectrum of compound F8B isolated from *C. triloba* root extract (A) matched the library template of 1,5-cyclohexadien-1-ol, 4,4-diphenyl-, acetate (B).

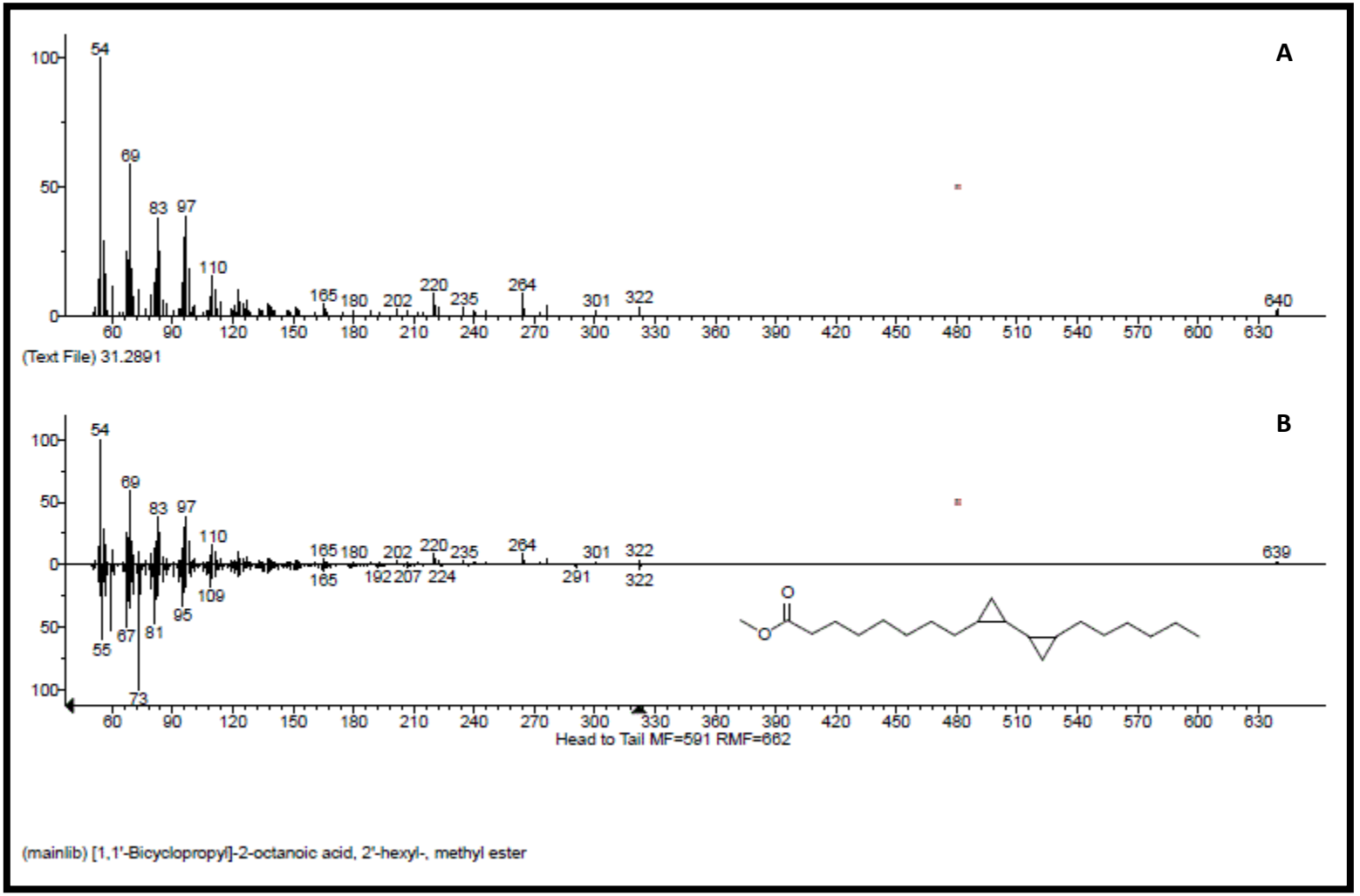

Figure A17: Mass spectrum of compound F8C isolated from *C. triloba* root extract (A) matched the library template of [1,1'-bicyclopropyl]-2-octanoic acid, 2'-hexyl-, methyl ester (B).

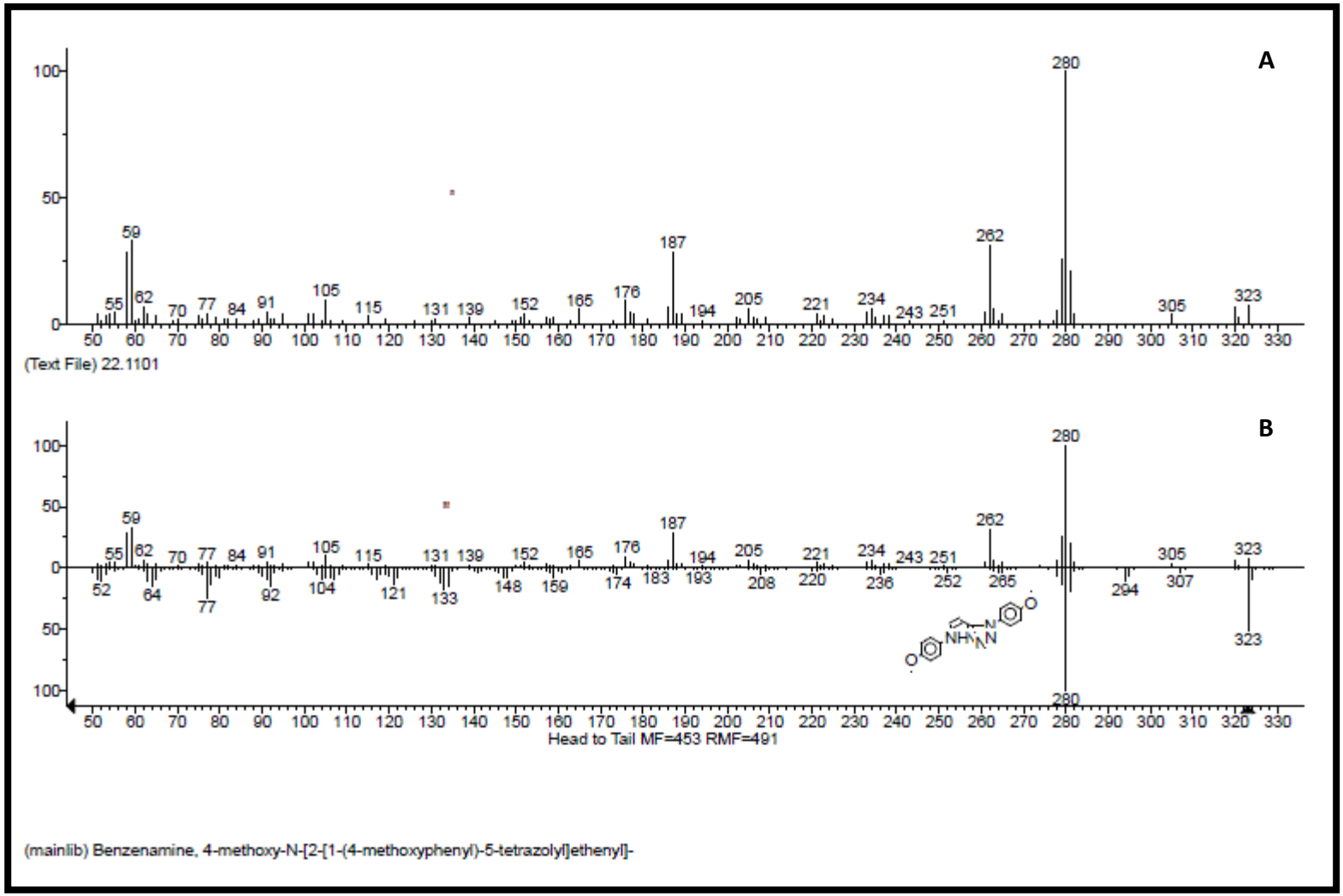

Figure A18: Mass spectrum of compound F8D isolated from *C. triloba* root extract (A) matched the library template of benzenamine, 4-methoxy-N-[2-[1-(4-methoxyphenyl)-5-tetrazolyl]ethenyl]- (B).

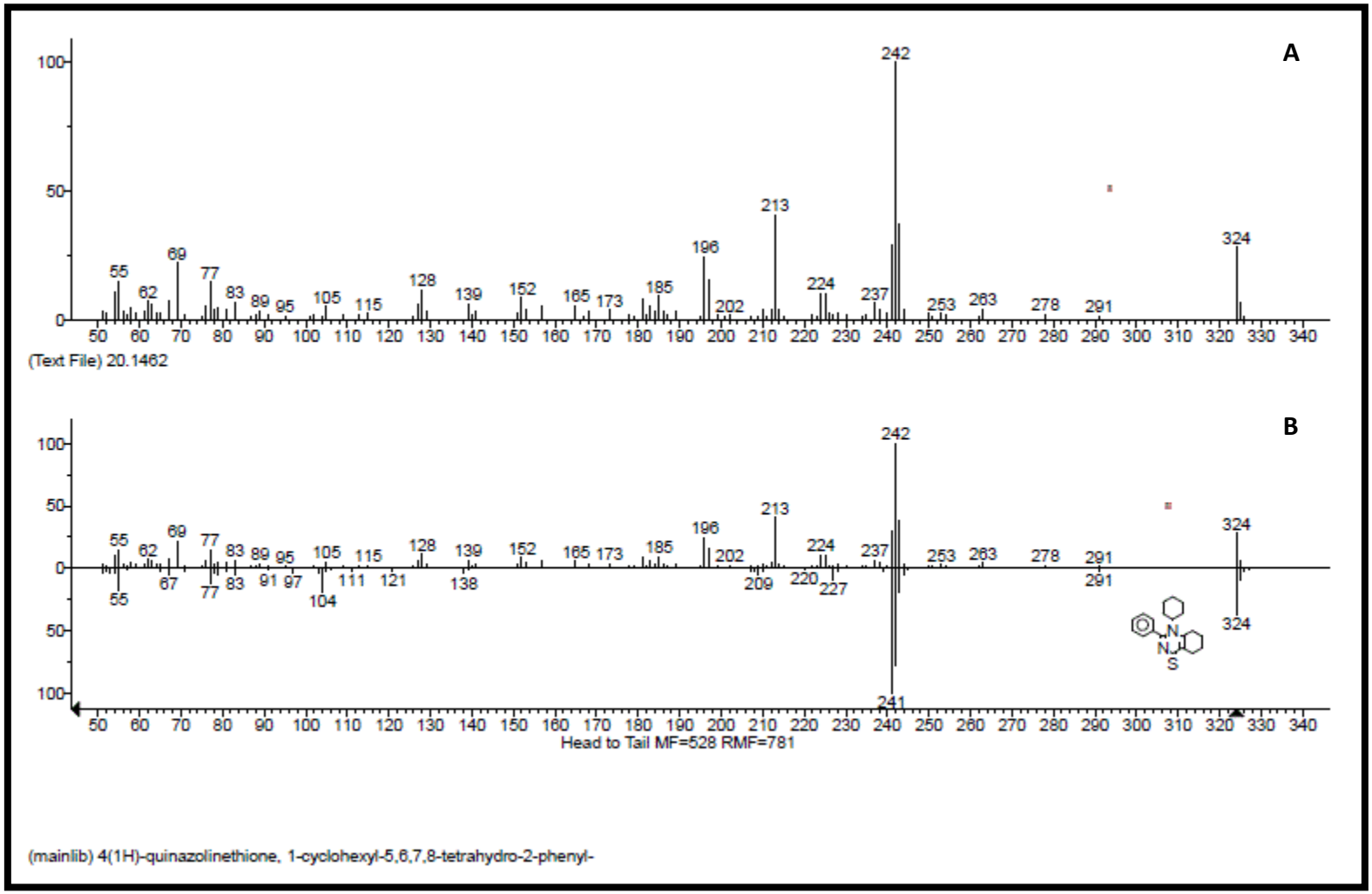

Figure A19: Mass spectrum of compound F8E isolated from *C. triloba* root extract (A) matched the library template of 4(1H)-quinazolinethione, 1-cyclohexyl-5,6,7,8-tetrahydro-2-phenyl (B).

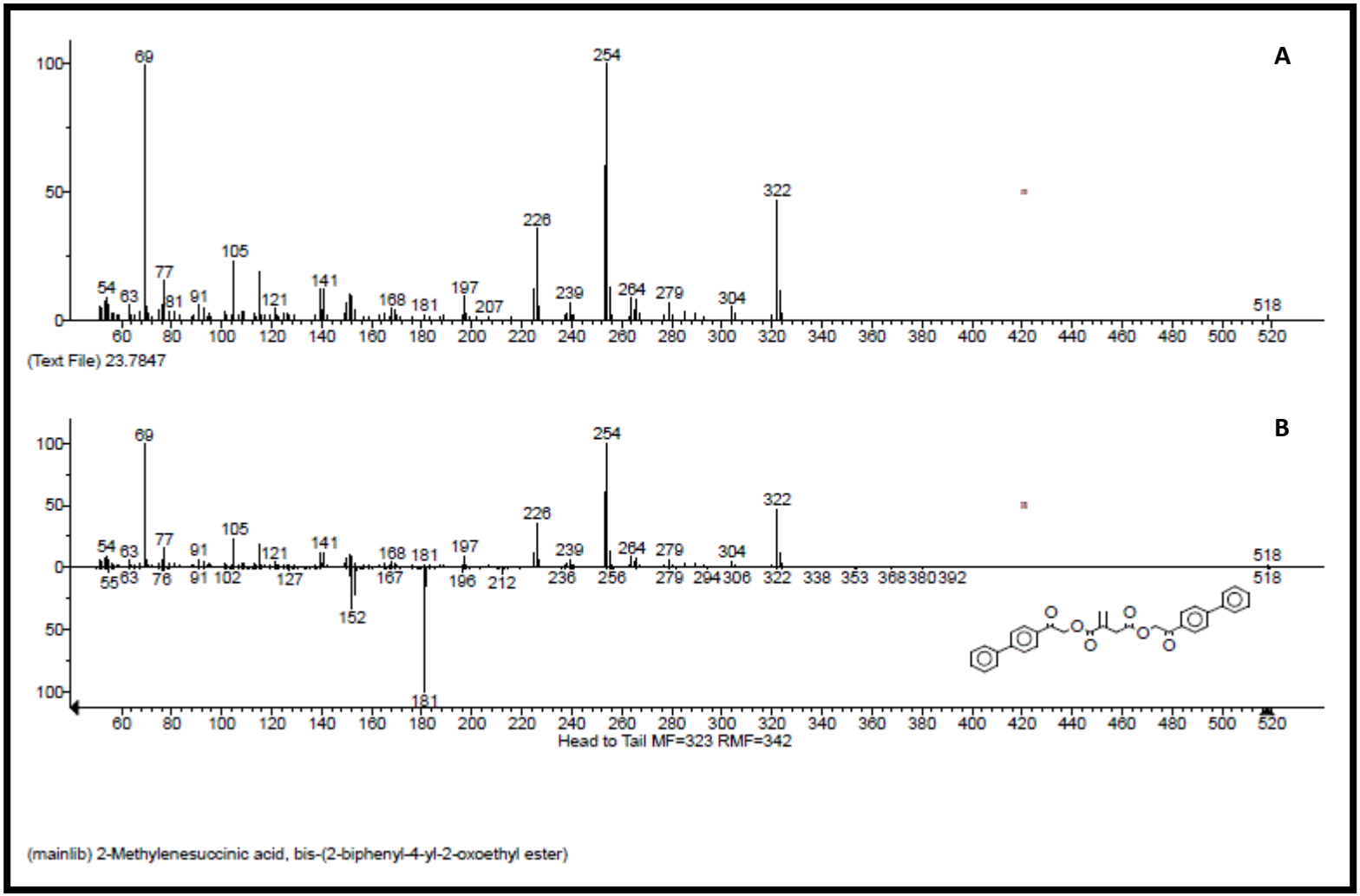

Figure A20: Mass spectrum of compound F8F isolated from *C. triloba* root extract (A) matched the library template of 2-methylenesuccinic acid, bis-(2-biphenyl-4-yl-2-oxoethyl ester) (B).

Appendix 3: Submitted and accepted publications

Anticancer compounds from *Ceratotheca triloba*

Naicker L*, Kaschula C, Steenkamp P, Matsabisa MG, Mohanlall V, Odhav B.

*Durban University of Technology, Department of Biotechnology, Faculty of Applied Sciences, P. O Box 1334, Durban 4001, South Africa. Telephone: +2731 327 5426; Fax: +2731 327 5351.

leeannnaicker@gmail.com

Abstract
C. triloba is a South African annual plant that is found in the summer rainfall areas of South Africa. The plant has been used by many traditional cultures as an abortifacient and to treat painful menstruation, stomach cramps, nausea, fever and diarrhea. Previously, Mohanlall et al. (2011) identified three anthraquinone derivatives (9,10-anthracenedione; 1-hydroxy-4-methylanthraquinone and 5,8-dimethoxy-2,3,10,10a- tetrahydro-1H,4aH-phenanthrene-4,9-dione) and one steroid (androst-5-ene-3, 17, 19-triol) from *C. triloba*. Reports have shown that these types of compounds possess anticancer activity. Thus the aim of this study was to investigate *C. triloba* for other possible anticancer compounds.

Different mobile phases were prepared for optimizing the separation of the compounds of the hexane root extract by TLC. Column chromatography was performed with this extract using six mobile phases (hexane, hexane: DCM, DCM, DCM: ethyl acetate, ethyl acetate and ethyl acetate: methanol). The fractions collected from the column were examined for cytotoxicity on two melanoma cell lines (A375 and UACC-62). The compounds from the active fractions were structurally characterized by EI-LC-MS.

Column chromatography led to the isolation of ten combined fractions. Four of these fractions (F2, F4, F5 and F8) displayed over 60% of cytotoxicity on the melanoma cell lines. Comparison of the EI-LC-MS library structures to literature sources revealed that six classes of compounds (nine anticancer compounds) were found in the hexane root extract of *C. triloba*. These included: These were: benzothiophenones (benzothiophen-3(2H)-one, 2-(2-trifluoromethylbenzylideno)- [F2A]), benzopyranones (pyrano[4,3-b]benzopyran-1,9-dione, 5a-methoxy-9a-methyl-3-(1-propenyl)perhydro [F2B]), naphthoquinones (1,4-naphthoquinone, 3-methyl-2-[(4-isopropenyl-1-cyclohexenyl)formyl]- [F2C] and 1,4-naphthoquinone, 2-acetyl-3-hydroxy-5,6,8-trimethoxy [F5D]), anthraquinones (5-methoxy-7-methylbenz(a)anthracene [F4A] and 9,10-anthracenedione, 1,8-dihydroxy-3-methyl [F5B]), androstanes (androstan-17-one, 3,11-dihydroxy-, (3α,5β,11β)- [F4B]) and quinazolines (4(1H)-quinazolinethione, 1-cyclohexyl-5,6,7,8-tetrahydro-2-phenyl [F8E] and 9-Cyano-2,15-diazatetracyclo [8.7.0.0(3,8).0(11,15)] heptadeca-1,3,5,7,9,11,13-heptaen-12-yl 2-chloroacetate [F5F]). In conclusion, this study revealed that the roots of *C. triloba* serve as a rich source of anticancer compounds. Thus, the compounds characterized in this study could be used towards the development of new anticancer drugs.

Key words: *Ceratotheca triloba*, cancer, cytotoxicity, hexane root extract, thin layer chromatography, column chromatography, anticancer compounds.

1. Introduction

C. triloba is a South African annual plant that is found in the summer rainfall areas of South Africa, mainly the grasslands. There are only four known species of Ceratotheca that are found in Southern Africa[1]. The genus name 'Ceratotheca' means a horned capsule which is derived from the Greek words *kerato* (horned) and *theke* (a case). The species name *triloba* is derived from Latin, meaning three-lobed, alluding to leaves[2]. The plant belongs to the family Pedaliaceae[3]. *C. triloba* has been used by many traditional cultures. The whole plant was soaked in water to serve as a substitute for soap or shampoo. The plant was used to treat painful menstruation, stomach cramps, nausea, fever and diarrhea[4]. Also, infusions of *C. triloba* leaves were prepared and administrated as an abortifacient[5-8].

Some of the biological activities of *C. triloba* have been documented. The plant has no angiotensin 1-converting enzymes[9]. The leaf extract of the plant has shown to inhibit α-

amylases and thus it has anti-diabetic potential[10]. Mohanlall and Odhav, (2013) reported other biological activities of *C. triloba*[11]. The root and leaf extracts exhibited anti-bacterial activity against *Staphylococcus aureus, Micrococcus luteus, Escherichia coli, Salmonella typhimurium* and *Bacillus cereus*. In addition, partially purified fractions were obtained from the root extract and they exhibited anti-bacterial activity against the same bacterial cultures.

According to previous research, Mohanlall et al. (2011) identified three anthraquinones (9,10-anthracenedione; 1-hydroxy-4-methylanthraquinone and 5,8-dimethoxy-2,3,10,10a-tetrahydro-1H,4aH-phenanthrene-4,9-dione) and one steroid (androst-5-ene-3, 17, 19-triol) from the hexane root extract of *C. triloba*[12]. Reports have shown that these types of compounds possess anticancer activity[13-16]. In the search for finding alternative anticancer drugs, we decided to further investigate the plant for other possible anticancer compounds. Fractionation of the hexane root extract by column chromatography led to the isolation of 10 combined fractions. The cytotoxicity of the fractions was determined and the characterization of nine anticancer compounds from the four active fractions was performed by LC-MS analysis.

2. Materials and Methods

2.1 Plant material

C. triloba plants were collected from the wild in Durban, Kwa-Zulu Natal, South Africa. The plants were authenticated by Professor H. Baijnath at the School of Life Sciences, University of Kwa-Zulu Natal, Durban, South Africa. A voucher specimen was deposited in the Ward Herbarium at UKZN (Westville campus).

2.2 Extraction

The roots and leaves were washed under running tap water and dried in an oven for 2-4 days at 40ºC until they broke easily by hand. Thereafter, the plant material was ground to a powder by using a blender. The ground material was extracted in hexane on a shaker at 80 rpm for 24 hours at room temperature. The hexane extract was concentrated by using a roto-evaporator (Heidolph Laborota 400 efficient) with the water bath set at a temperature of 50°C and the flask rotated at 60 rpm. The concentrated extract was transferred to a glass bottle which was covered in foil to prevent the compounds from being degraded by light. The extract was then dried for 2-3 days under a fume hood and stored at room temperature.

2.3 Bioassay

2.3.1 Cell lines

Two melanoma cell lines were used in this study. The A375 cell line was provided by Dr Catherine Kaschula from the International Centre for Genetic Engineering and Biotechnology (ICGEB) at the University of Cape Town (UCT). The UACC-62 cell line was provided by Natasha Kolesnikova from the Biosciences unit at the Council of Scientific and Industrial Research (CSIR).

2.3.2 Sample preparation

The fractions were dissolved in DMSO and further diluted in the culture medium and added to the cells at concentrations of 12.5 $\mu g.ml^{-1}$ and 25 $\mu g.ml^{-1}$. The final concentration of DMSO that was used for all treatments was 0.1 %. Cells treated with DMSO served as a negative control.

2.3.3 Cytotoxicity assay (MTT assay)

Cells were cultured in DMEM supplemented with 10% heat-inactivated FBS, and antibiotics (10,000 U/ml of penicillin, 10 mg/ ml of streptomycin) at 37°C in a humidified incubator containing 5% CO_2 gas. An aliquot of 90 µl of cells (3×10^3) was added to each well of a 96 well plate. After an incubation period of 24 hours the cells were treated with DMSO or the fractions. The cells were incubated for 48 hours. Subsquently, MTT (0.5 mg/ml) was added the and the mixture was incubated for 4 hours. Then 100 µl of 10% SDS in 0.01 M HCL was added to the cells to dissolve the formazan crystals. The plates were incubated overnight. The color intensity was read at 595 nm an ELISA plate reader (Digital Analogue Systems, Italy) to obtain the absorbance density values.

2.4 Thin layer chromatography

Aliquots of 10 µl of the hexane root extract were loaded onto six pieces of silica gel TLC plates (1 cm in width and 10 cm in length) (Merck) which were developed in the following mobile phases: hexane: ethyl acetate: ethanol (1:8:1), ethanol: hexane (9:1), ethanol: petroleum ether (1:9), hexane: dichloromethane (3:7), hexane: dichloromethane (1:9) and hexane. Thereafter, the TLC plates were sprayed with a vanillin solution (300 mg vanillin in 84 ml of ethanol and 3 ml of H_2SO_4) (Sigma-Aldrich, Inc) and heated with a blow dryer for 2 minutes to reveal the bands.

The separation of the compounds of the hexane root extract was further optimized by using different ratios of hexane: DCM (a polarity based separation method) (Table 1). Eight pieces of TLC plates (1 cm in width and 10 cm in length) were loaded with 10 µl of the hexane root extract. These plates were developed in hexane and one of the plates was sprayed and heated as described above. The seven remaining plates were re-ran in hexane: DCM at a ratio of 10:90 and one of the plates was sprayed and heated. Then the six remaining TLC plates were consecutively processed as described in Table 1.

Table 1: Ratios hexane and DCM used to separate the compounds of the hexane root extract by TLC

Ratio of hexane: DCM	Number of TLC plates developed	Number of TLC plates sprayed with vanillin and heated
1:0	8	1
10:90	7	1
88:12	6	1
85:15	5	1
60:40	4	1
40:60	3	1
20:80	2	1
0:1	1	1

2.5 Column chromatography

The lower part of a glass column (30 mm in width and 80 cm in length) was stocked with cotton wool by using a glass rod. An aliquot of 300 ml of hexane and 60 g of silica gel 60 (0.063-0.200 mm, 70-230 mesh ASTM) (Merck) was mixed to form a slurry which was poured into the column. The tap was left open for collection of the excess hexane into a

beaker. An aliquot of 50 ml of hexane was left in the column to prevent the formation of air bubbles. Thereafter, 900 mg of the hexane root extract was mixed with 50 ml of hexane and poured gently into the column. The compounds of the extract were separated and eluted by gradually increasing the polarity of the mobile phase in the column. This was done by using the following mobile phases: hexane : DCM (60 : 40, 40 : 60), DCM, DCM : ethyl acetate (90 : 10, 70 : 30, 60 : 40, 50 : 50, 50 : 60, 30: 60, 20 : 80), ethyl acetate and ethyl acetate: methanol (80 : 20, 70 : 30, 50 : 50). Thus, hexane: DCM (60:40) was poured first into the column and the tap was opened for elution of the band/s into test tubes which had a capacity of 20 ml. The next mobile phase was added when no more bands eluted from the column while the hexane: DCM (60:40) mobile phase was used. This procedure was repeated with the remaining mobile phases. The contents in each test tube represented a fraction that consisted of one or several band/s. Each fraction was given a number, for example: 1. In order to visualize the bands of the fractions, an aliquot of 10 µl of the fractions were loaded onto TLC plates which were developed in the appropriate mobile phases (Table 2). The plates were then sprayed and heated as described in section 4.4. All fractions were not analysed by TLC because if the colour of the solution was repeated in many test tubes; this suggested that similar fractions was present in the respective test tubes.

Table 2: Fractions were loaded onto TLC plates which were developed in the appropriate mobile phases

TLC plate	Fractions	Mobile phase	Solvent ratio
A	13, 16, 17, 19, 22, 23, 24, 25	hexane: DCM	60:40
B	31, 34, 36, 40, 41, 43, 45, 47	hexane: DCM	60:40
C	48, 50, 53, 54, 57, 58, 60, 66	DCM: ethyl acetate	90:10
D	66, 68, 69, 71, 72, 73	DCM: ethyl acetate	60: 40
E	75, 76, 80	DCM: ethyl acetate	60: 40
F	81, 82, 84, 86, 87, 88, 89, 90	Ethyl acetate: methanol	70: 30

2.6 Electron Ionization-Liquid Chromatography-Mass Spectrometry (EI-LC-MS) analysis

EI-LC-MS analysis was performed by using the Waters Thermabeam (TMD) system which comprised of a 2695 Solvent Delivery System, 2996 photodiode array (PDA) detector, column heater and Thermabeam (TMD) Electron Ionization Mass spectrometry detector. Chromatographic separation was achieved in a Waters Xbridge C18 column (150 x 2.1 mm, 3.5 µm) that was kept at 400C. The first eluent comprised of water (containing 10 mM Formic acid) (C) and acetonitrile (D) (70:30) at 0.2 ml.min-1. The gradient table of the chromatographic process is summarised in Table 3. The TMD detector was operated in positive scan mode (50 – 650 amu) with a gain of 10 collecting 1 spectrum per second. The nebuliser temperature was set at 900C, the expansion region temperature at 800C and the source temperature at 2250C. The total volume of post-column eluent was sent to the TMD detector and helium was used as the nebulisation gas at 30 L.h-1. The TMD detector was tuned every day prior to starting an analysis run and caffeine was injected as the test

compound to ensure functionality of the total system. The injection volume was 5 µl for all fractions.

Table 3: Gradient conditions on the Waters 2695 solvent delivery system.

Time	Flow	% C	% D	Curve
0.0	0.20	70	30	6
1.0	0.20	70	30	6
40.0	0.20	0	100	6
48.0	0.20	0	100	4
50.0	0.20	70	30	3
60.0	0.20	70	30	6

Water containing 10 mM Formic acid (C), acetonitrile (D).

3. Results and discussion

3.1 Thin layer chromatography analysis

In order to optimize the seperation of the compounds of the hexane root extract for column chromatography, we performed thin layer chromatography (TLC) to view which mobile phases could best separate the compounds of this extract. The TLC plates in Figure 1 depict the degree of separation of the compounds after exposing the hexane root extract to different mobile phases. The hexane mobile phase (Lane 6) held back most of the compounds at the baseline and allowed the separation of one band. The hexane: DCM mobile phase at a ratio of 1: 9 (Lane 5) allowed for the separation of two bands and initiated the movement of some compounds from the baseline. The hexane: DCM mobile phase at a ratio of 3: 7 (Lane 4) began the actual separation of the compounds. Subsequently the hexane: DCM mobile phase was chosen for column chromatography as these solvents showed the potential to separate the compounds of the hexane root extract. The other three mobile phases (Lane 1 - ethyl acetate: hexane: ethanol [1:8:1], Lane 2 - hexane: ethanol [9: 1], Lane 3 - ethanol: petroleum ether [1:9]) were not used because these permitted poor separation and allowed the compounds to run too quickly towards the solvent front. We further optimized the separation of the compounds of the hexane root extract. Figure 2 shows the separation of the compounds was achieved by slowly increasing the polarity of the hexane: DCM mobile phase. A similar principle was applied to the column.

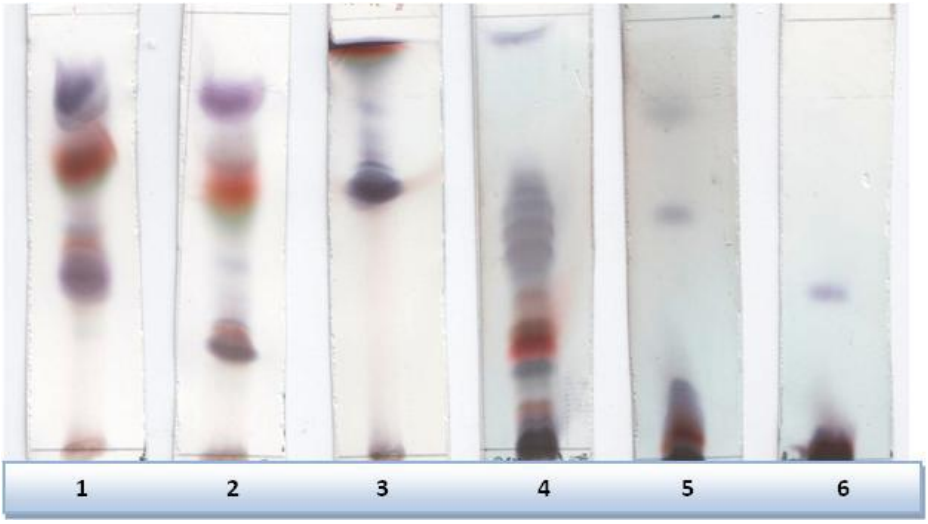

Figure 1: Separation of the compounds of the hexane root extract by using different mobile phases. Lane 1- ethyl acetate: hexane: ethanol (1:8:1), Lane 2 - hexane: ethanol (9: 1), Lane 3 - ethanol: petroleum ether (1:9), Lane 4 – hexane: DCM (3: 7), Lane 5 - hexane: DCM (1:9), Lane 6 - hexane.

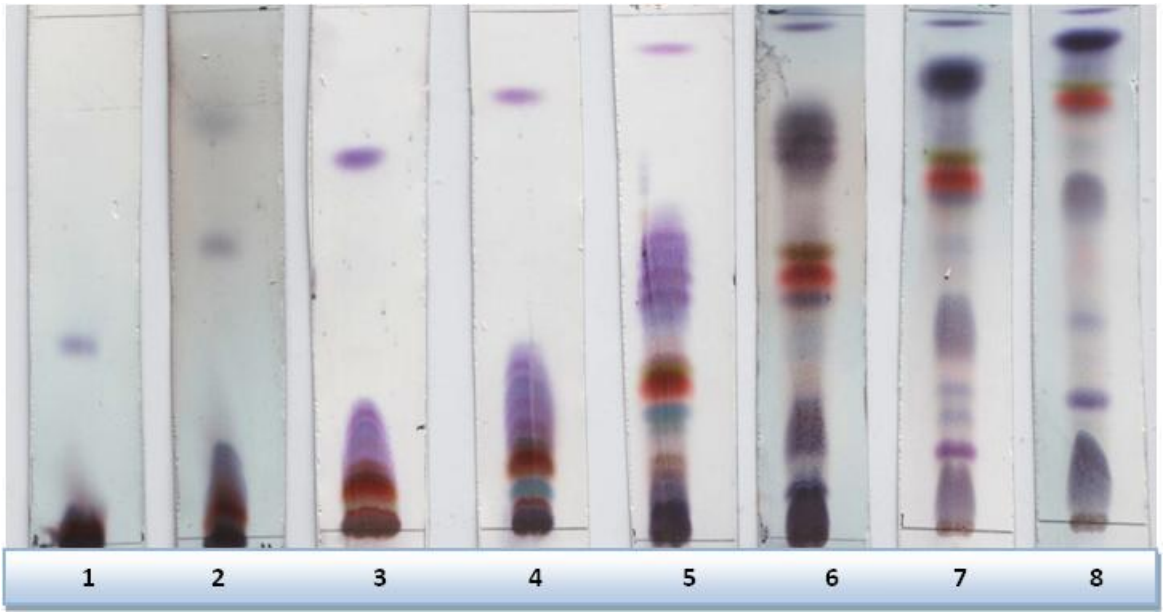

Figure 2: Separation of the compounds of the hexane root extract by using different ratios of hexane: DCM. Lane 1 - 1:0, Lane 2 - 1:9, Lane 3 - 88:12, Lane 4 - 85: 15, Lane 5 - 60:40, Lane 6 - 40:60, Lane 7 - 20:80, Lane 8 - 0:1.

3.3 Fractionation of the root extract by column chromatography

Column chromatography was ran twice with the hexane root extract (results from column run 2 are not shown as the experiment was repeated to bulk up the fractions). The fractions that were collected from both column runs were grouped into two sets as shown in Table 4. Set A represented the 91 fractions that were collected from column run 1 while set B represented the 83 fractions that were collected from column run 2 (results not shown) (Figure 3 and Table 5). Thereafter, the fractions with the same or similar band pattern or solution colour (colour of the solvent after the fraction has been dissolved in it) were pooled into two other sets. The fractions that were collected from column run 1 were pooled into 9 fractions (1A-9A) which were represented by Set C. The fractions that were collected from column run 2 were pooled into 8 fractions (1B-8B) which were represented by Set D (Table 4). The fractions from set C and set D were then ran on TLC plates as shown in Figure 4. Thereafter, the fractions from these two sets were combined according to their band pattern (Figure 4 and Table 6). Subsequently a total of ten combined fractions (F1-F10) were isolated from the hexane root extract. The combined fractions were then ran on TLC plates as shown in Figure 5. The R*f* values and band colours of the these fractions are shown in Table 7. The yields of these fractions are shown in Table 8. Fractions F1, F7 and F9 had the highest percentage yields (approximately 200 mg) while fraction F3 had the lowest percentage yield (5.9 mg).

Column chromatography allowed us to narrow down a large pool of compounds (plant extract) into smaller pools of compounds (fractions). In this way when we screened the fractions for activity, the less active fractions were ruled out while the active fractions were further researched. Certainly, column chromatography did not elute purified compounds (as shown by thin layer chromatograms in Figure 3. This may be due to the co-elution of similar structured compounds from the complex plant extract of *C. triloba*. Hostettmann, (1997) reported that the purification of pharmacological compounds from plants is a difficult and time consuming process[17]. Thus, further research would have to be conducted to achieve the purification of the compounds from *C. triloba*. Separation techniques that can be used to facilitate purification include: mini-column chromatography, preparative thin layer chromatography (PTLC) and preparative high performance liquid chromatography (PHPLC).

Some of the fractions (F2, F3, F4 and F5) isolated from the hexane root extract formed crystals (Figure 6). It has been reported that certain plant derived compounds (such as anthraquinones and naphthoquinones) can form crystals. For instance, 2,6-dihydroxyanthraquinone and 2-hydroxy-6-methylanthraquinone isolated from the *Rubia cordifolia* extract formed red crystals[18]. In addition, juglone (5-hydroxy-1,4-naphthalenedione) isolated from *Juglans regia* formed yellow crystals[19]. Thus, the observation of crystals in the fractions may be an indication of the presence of anthraquinones and naphthoquinones.

Table 4: Fractions that were collected by column chromatography were organized into sets.

Origin of fractions	**Set**
Fractions collected from column run 1	A
Fractions collected from column run 2	B
Fractions collected from column run 1 were pooled into 9 fractions (1A-9A)	C
Fractions collected from column run 2 were pooled into 8 fractions (1B-8B)	D

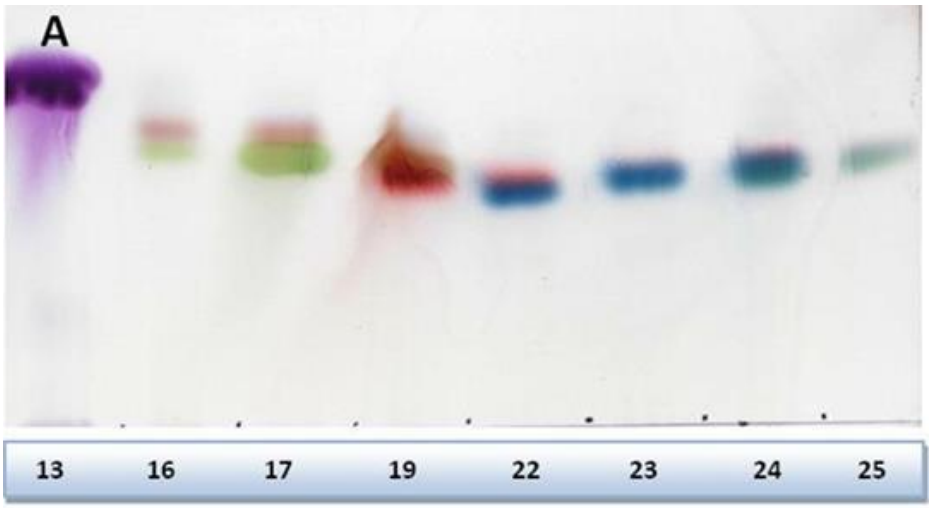
A
13
16
17
19
22
23
24
25

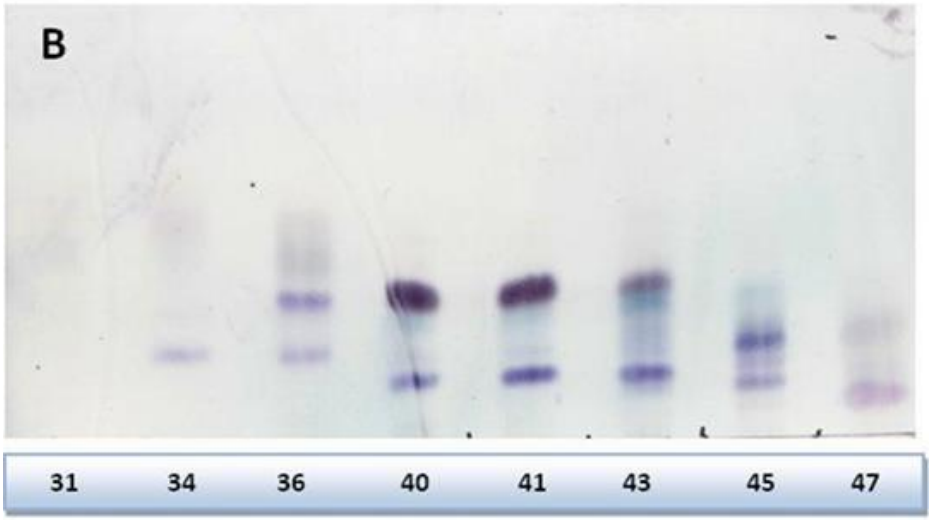
B
31
34
36
40
41
43
45
47

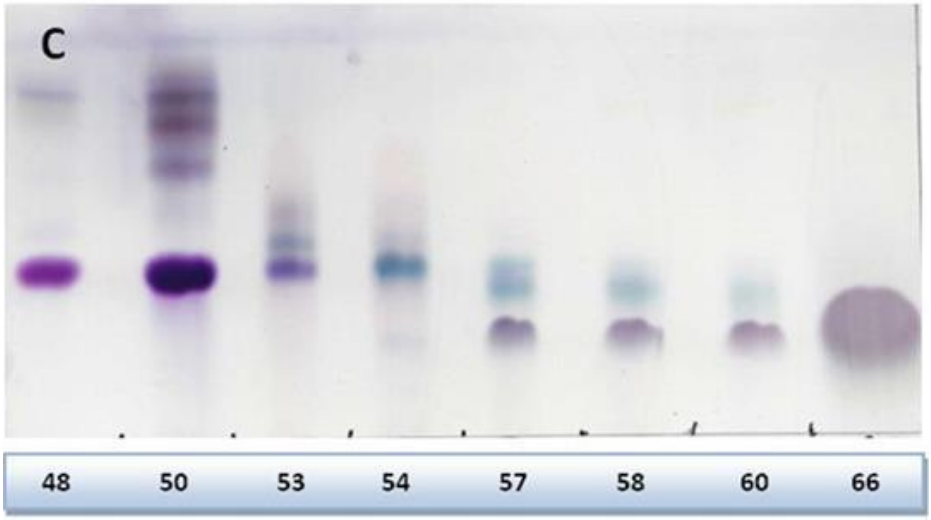
C
48
50
53
54
57
58
60
66

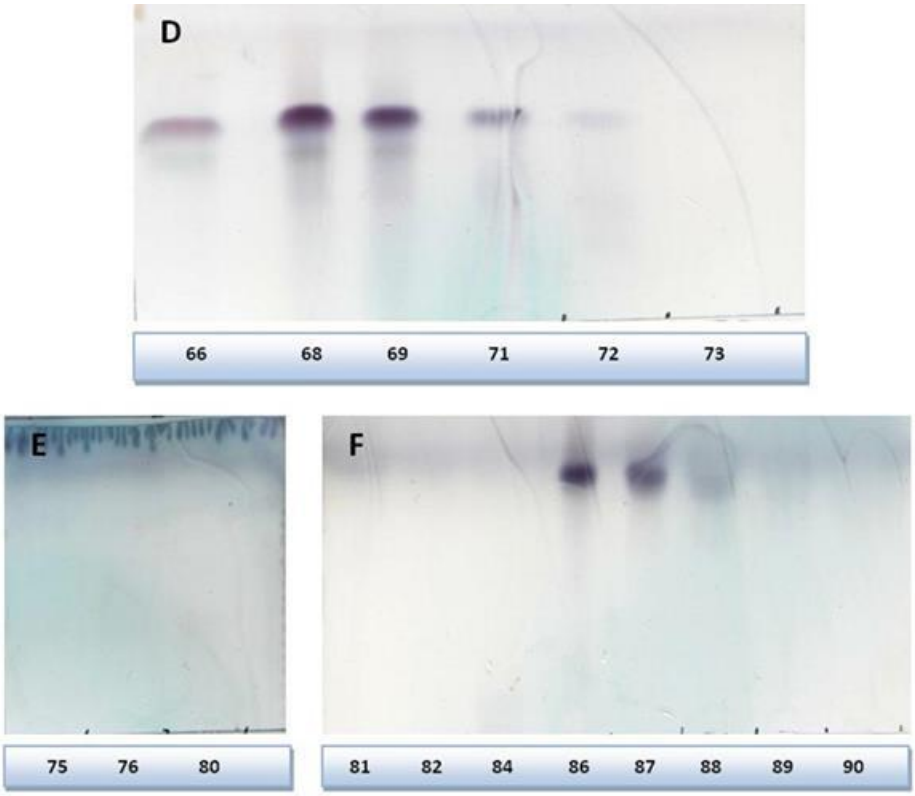

Figure 3: TLC of the fractions (13-90) (A-F) that were collected from column run 1.

Table 5: Fractions collected from column run 1 by using different mobile phases.

Fraction	Fractions pooled	Solution colour*	Mobile phase	Solvent ratio
1A	1-15	Light yellow	Hexane : DCM	60 : 40
2A	16 - 17	Yellow	Hexane : DCM	60 : 40
	18 - 21	Dark orange	Hexane : DCM	60 : 40
3A	22 - 23	Orange	Hexane : DCM	60 : 40
	24 - 27	Yellow	Hexane : DCM	60 : 40
	28 - 31	Yellow	Hexane : DCM	40 : 60
4A	32 - 34	Light orange	Hexane : DCM	40 : 60
	35 - 43	Orange	Hexane : DCM	40 : 60
5A	44 - 47	Orange	DCM	100
	48 - 49	Orange	DCM : Ethyl acetate	90 : 10
	50 -51	Brownish red	DCM : Ethyl acetate	90 : 10
6A	52 - 55	Dark red	DCM : Ethyl acetate	90 : 10
7A	56 - 58	Reddish orange	DCM : Ethyl acetate	90 : 10
	59 - 60	Orange	DCM : Ethyl acetate	90 : 10
	61 - 66	Orange	DCM : Ethyl acetate	70 : 30

	67 – 72	Orange	DCM : Ethyl acetate	60 : 40
8A	73 - 74	Light orange	DCM : Ethyl acetate	60 : 40
	75	Clear	DCM : Ethyl acetate	50 : 50
	76 - 77	Clear	DCM : Ethyl acetate	50 : 60
	78	Clear	DCM : Ethyl acetate	30- 60
	79 - 80	Clear	DCM : Ethyl acetate	20 : 80
	81	Clear	Ethyl acetate	100
	82	Clear	Ethyl acetate : Methanol	80 : 20
9A	83 - 85	Dark purple	Ethyl acetate : Methanol	80 : 20
	86 - 90	Dark purple	Ethyl acetate : Methanol	70 : 30
	91	Dark purple	Ethyl acetate : Methanol	50 : 50

***** Colour of the solvent after the fraction has been dissolved in it.

Note: These fractions were represented by set A. The same or similar fractions were pooled into 9 fractions (1A-9A) which were represented by set C.

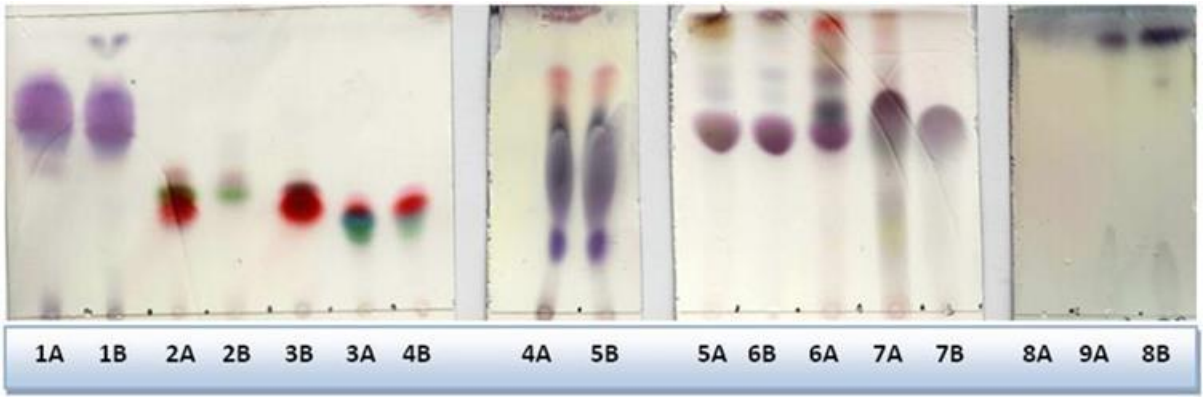

Figure 4: TLC of fractions 1A-9A (originated from column run 1, set C) and 1B-8B (originated from column run 2, set D).

Table 6: Fractions 1A-9A (set C) and 1B-8B (set B) were combined according to their band pattern to produce ten fractions.

Combined fraction	Fractions from set C and D
F1	1A, 1B
F2	2A
F3	2B
F4	3B
F5	3A, 4B
F6	4A, 5B
F7	5A, 6B
F8	6A
F9	7A, 7B
F10	8A, 8B, 9A

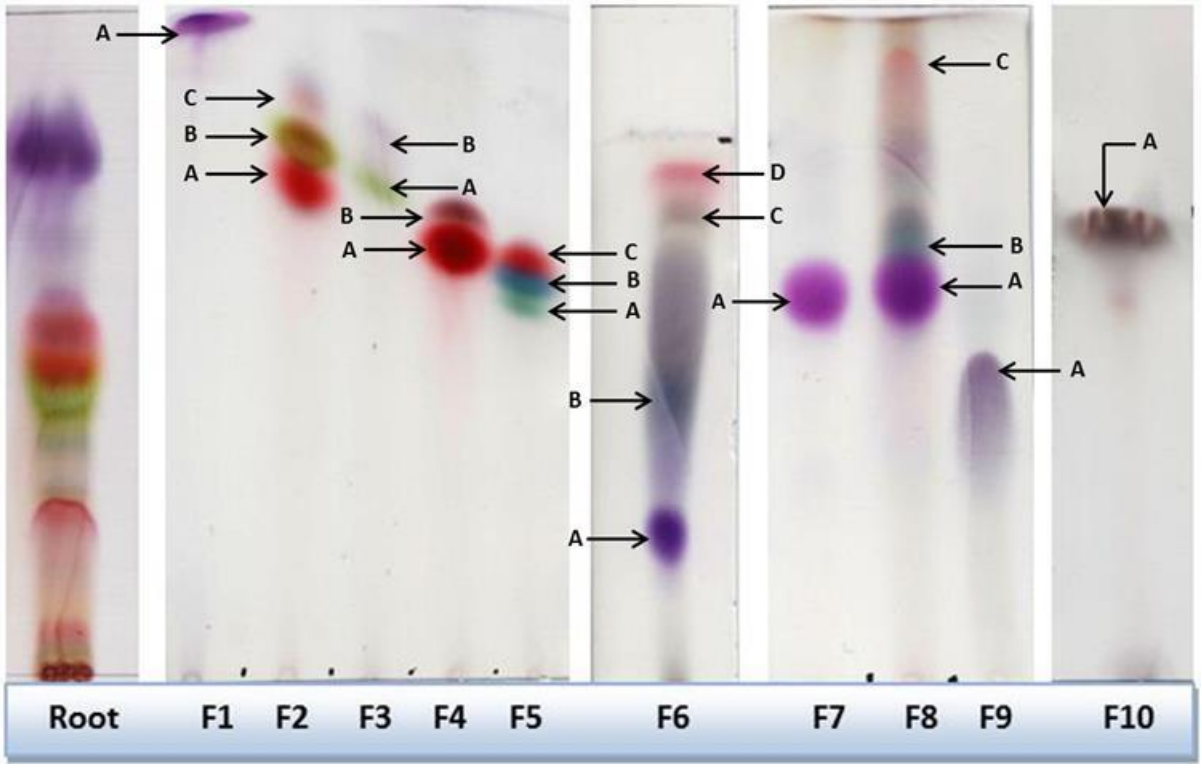

Figure 5: TLC of the hexane root extract and fractions F1-F10.

Table 7: Mobile phases used to develop fractions F1-F10 and the R*f* values and colours of the bands of these fractions.

Fraction	Mobile phase	Band	Colour	R*f* value
F1	Hexane : DCM (60 : 40)	A	Purple	0.98
F2	Hexane : DCM (60 : 40)	A	Red	0.77
		B	Green	0.83
		C	Light red	0.86
F3	Hexane : DCM (60 : 40)	A	Green	0.74
		B	Purple	0.81
F4	Hexane : DCM (60 : 40)	A	Red	0.65
		B	Reddish brown	0.70
F5	Hexane : DCM (60 : 40)	A	Green	0.54
		B	Blue	0.59
		C	Red	0.62
F6	Hexane : DCM (40 : 60)	A	Purple	0.33
		B	Dark green	0.58
		C	Black	0.88
		D	Light red	0.94
F7	DCM : Ethyl acetate (90 : 10)	A	Purple	0.62
F8	DCM : Ethyl acetate (90 : 10)	A	Purple	0.63
		B	Dark green	0.72
		C	Light red	0.95
F9	DCM : Ethyl acetate (90 : 10)	A	Purple	0.49
F10	Ethyl acetate : Methanol (80 : 20)	A	Brownish black	0.73

Table 8: Yield of fractions F1-F10.

Fraction	Mass of fraction (mg)
F1	232.5
F2	96.7
F3	5.9
F4	160
F5	86.2
F6	140.9
F7	276.1
F8	47.7
F9	232
F10	95.3

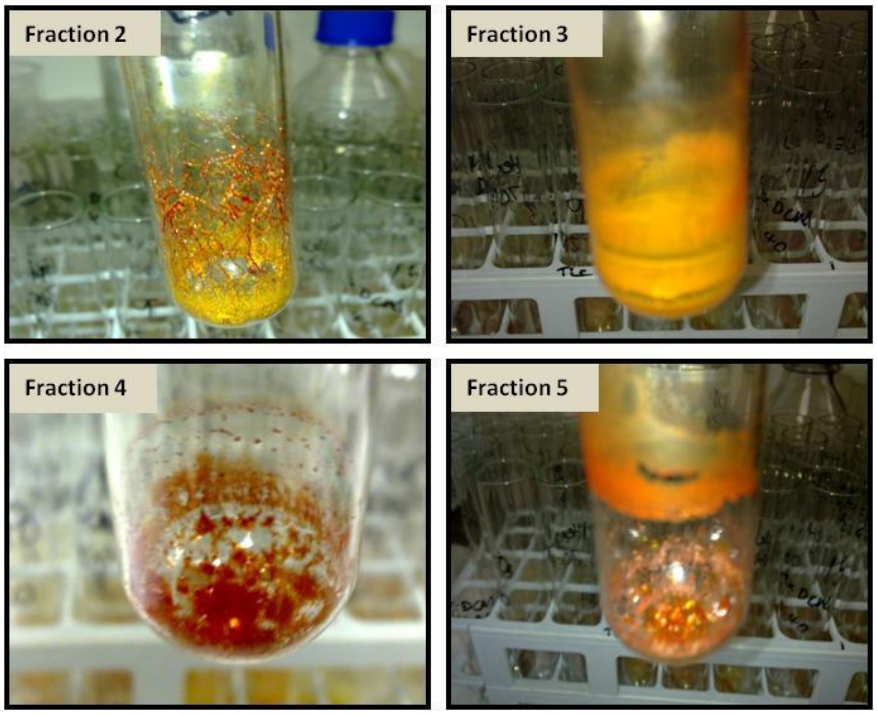

Figure 54: Crystals formed by fractions F2, F3, F4 and F5.

3.2 Cytotoxicity activity

The ten combined fractions were screened on two melanoma cell lines. Fractions F2, F4, F5 and F8 exhibited a high percentage of cytotoxicity on both the A375 (89.85, 89.39, 90.81 and 75.51% at 25 µg.ml^{-1}, respectively) and UACC-62 (74.54, 97.55, 86.96 and 73.29% at 25 µg.ml^{-1}, respectively) cell lines. Fraction F7 exhibited a moderate percentage of cytotoxicity (47.70%) on the A375 cells. The other fractions (F3, F6, F7, F9 and F10) exhibited no cytotoxicity or a low percentage of cytotoxicity on the melanoma cells (Figure 7 and 8). Therefore fractions F2, F4, F5 and F8 were further investigated.

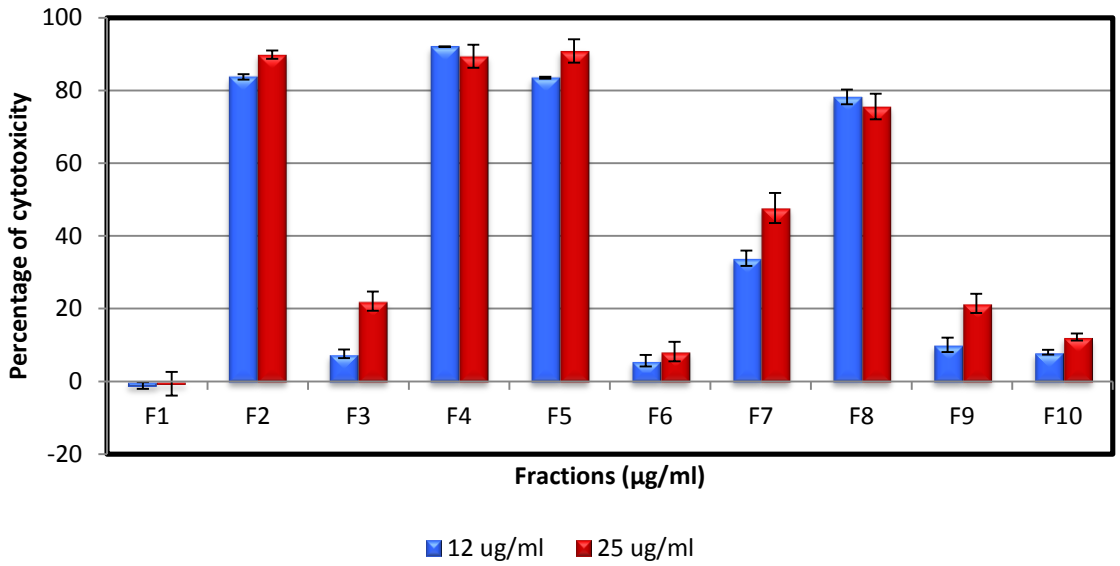

Figure 55: Percentage of cytotoxicity exhibited by the fractions on the A375 cell line.

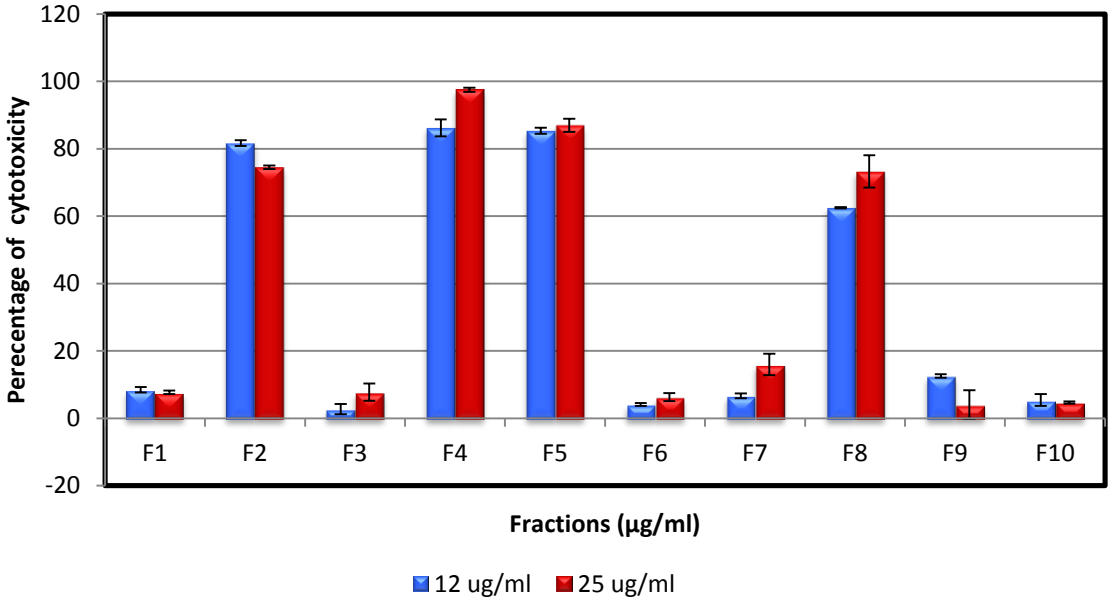

Figure 56: Percentage of cytotoxicity exhibited by the fractions on the UACC-62 cell line.

3.3 EI-LC-MS analysis

Preparative High Performance Liquid Chromatography (PHPLC) was used to separate the compounds present in the four active fractions (F2, F4, F5 and F8). The chromatograms in Figures 9-12 display the separation of the compounds. It was evident that the retention times of some of the compounds were very close. Thus, the compounds present in the fractions were structurally related. Due to this reason we were unable to separate all of the compounds in the fractions. The compounds were structurally elucidated by MS analysis. The mass spectrums of the isolated compounds (from PHPLC) were compared to library templates to obtain their structures (Figure 13-21). Comparison of the structure names to literature sources such as Zhang et al. (2006), Chuang et al. (2007), Xu et al. (2013), Hong et al. (2014), Yeap et al. (2015), Oklješa et al. (2013) and Wasfy et al. (2015) revealed that six classes of compounds (nine anticancer compounds) were found in the root extract of *C. triloba* [20-26]. These were: benzothiophenones (benzothiophen-3(2H)-one, 2-(2-trifluoromethylbenzylideno)- [F2A]), benzopyranones (pyrano[4,3-b]benzopyran-1,9-dione, 5a-methoxy-9a-methyl-3-(1-propenyl)perhydro [F2B]), naphthoquinones (1,4-naphthoquinone, 3-methyl-2-[(4-isopropenyl-1-cyclohexenyl)formyl]- [F2C] and 1,4-naphthoquinone, 2-acetyl-3-hydroxy-5,6,8-trimethoxy [F5D]), anthraquinones (5-methoxy-7-methylbenz(a)anthracene [F4A] and 9,10-anthracenedione, 1,8-dihydroxy-3-methyl [F5B]), androstanes (androstan-17-one, 3,11-dihydroxy-, (3α,5β,11β)- [F4B]) and quinazolines (4(1H)-quinazolinethione, 1-cyclohexyl-5,6,7,8-tetrahydro-2-phenyl [F8E] and 9-Cyano-2,15-diazatetracyclo [8.7.0.0(3,8).0(11,15)] heptadeca-1,3,5,7,9,11,13-heptaen-12-yl 2-chloroacetate [F5F]). The structures of these compounds are illustrated in Figures 22-25.

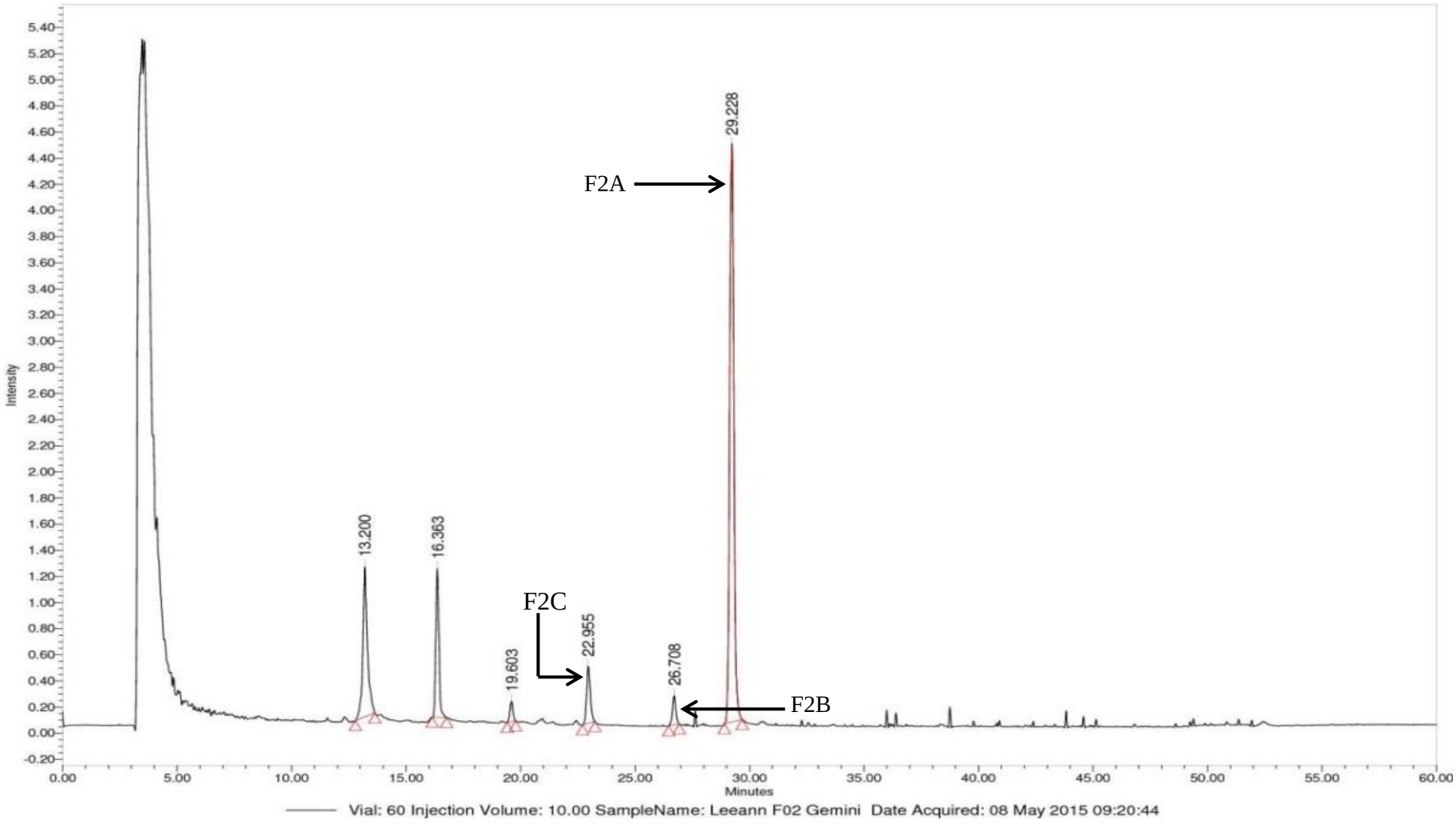

Figure 9: Chromatogram of fraction F2 showing the presence of three distinct compounds of interest at varying retention times. F2A-Retention time (Rt) = 29.228, F2B-Rt = 26.708 and F2C-Rt = 22.955.

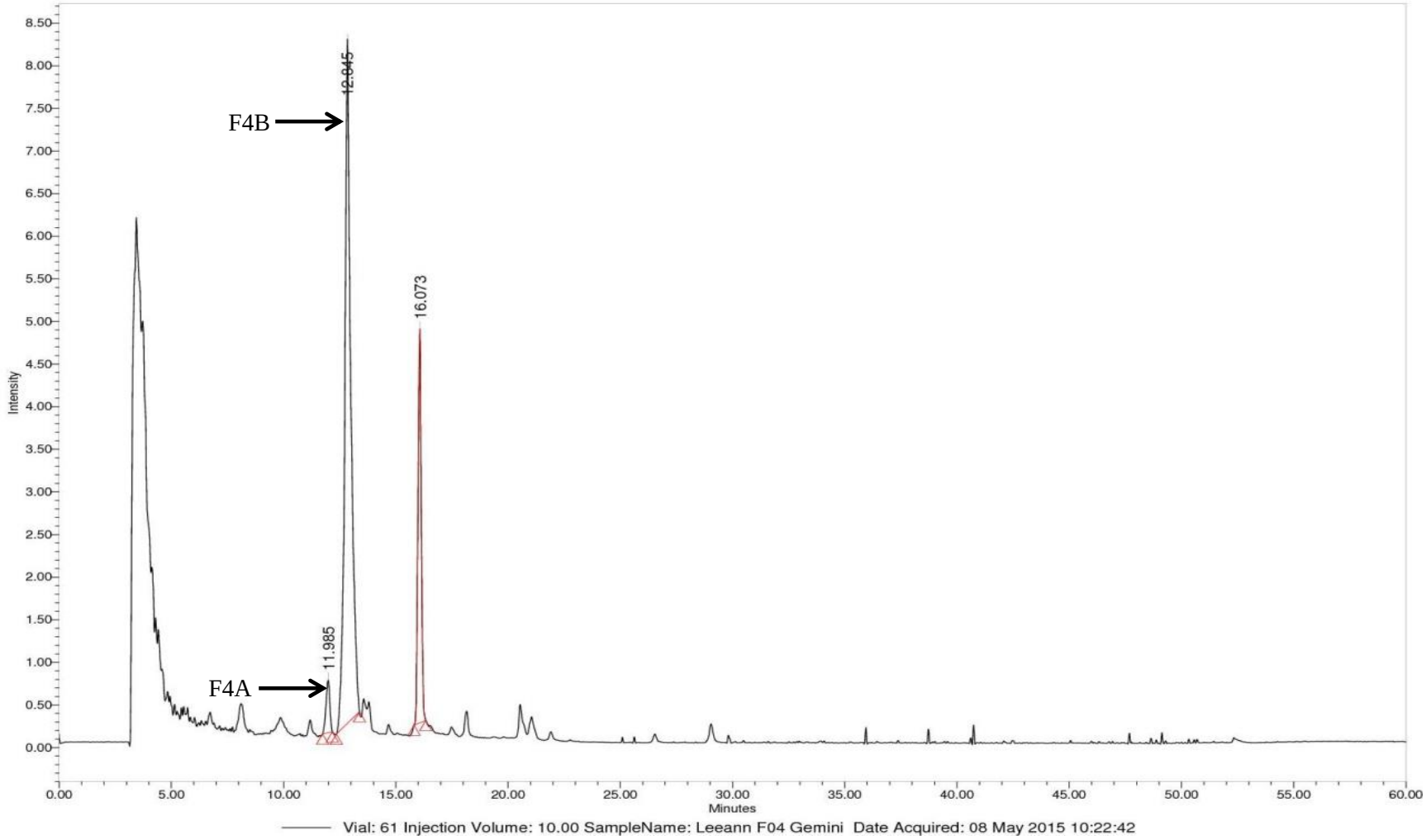

Figure 10: Chromatogram of fraction F4 showing the presence of three distinct compounds of interest at varying retention times. F4A-Rt = 11.985 and F4B-Rt = 12.845.

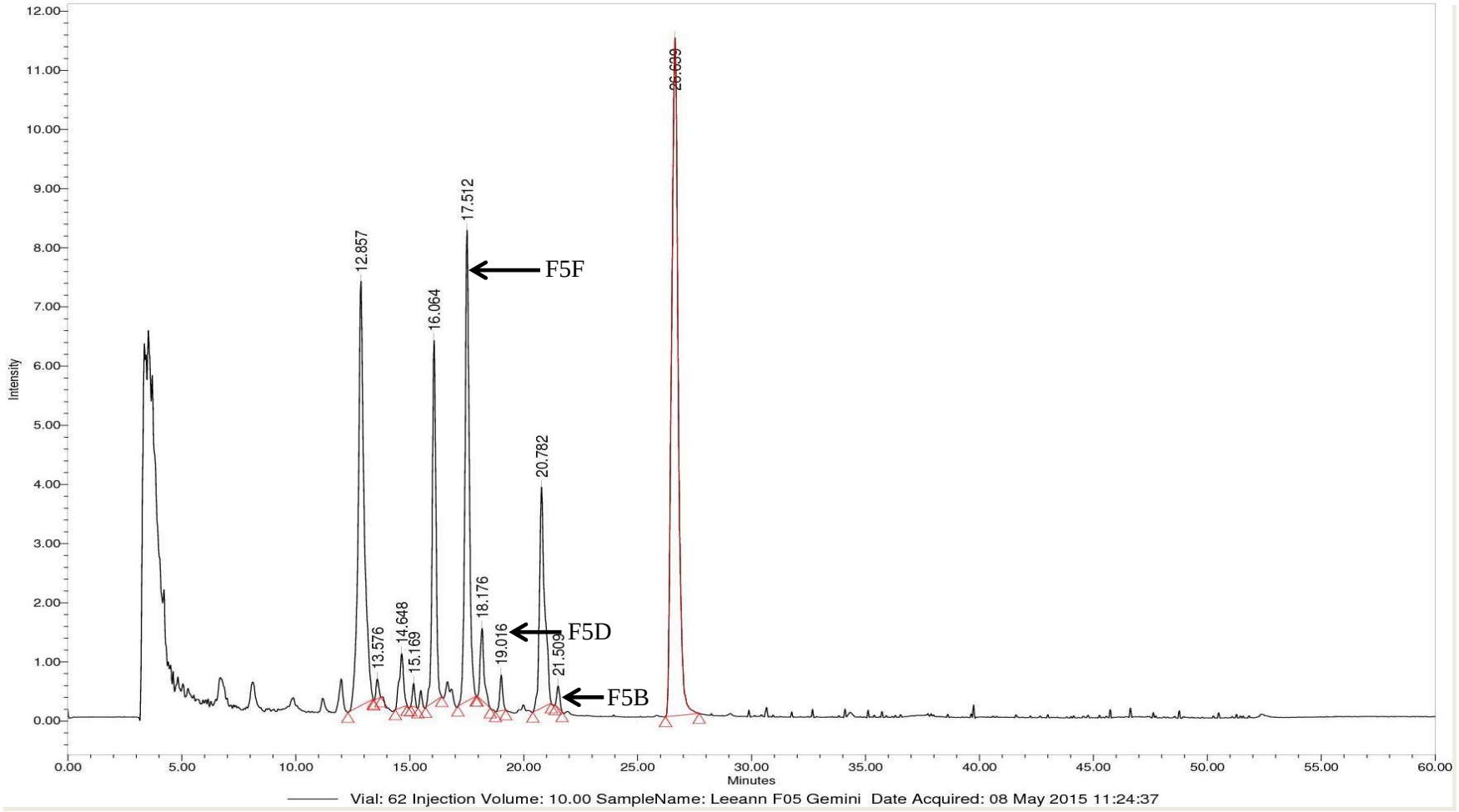

Figure 11: Chromatogram of fraction F5 showing the presence of seven distinct compounds of interest at varying retention times. F5B-Rt = 21.509, F5D-Rt = 19.016, F5F-Rt = 17.512.

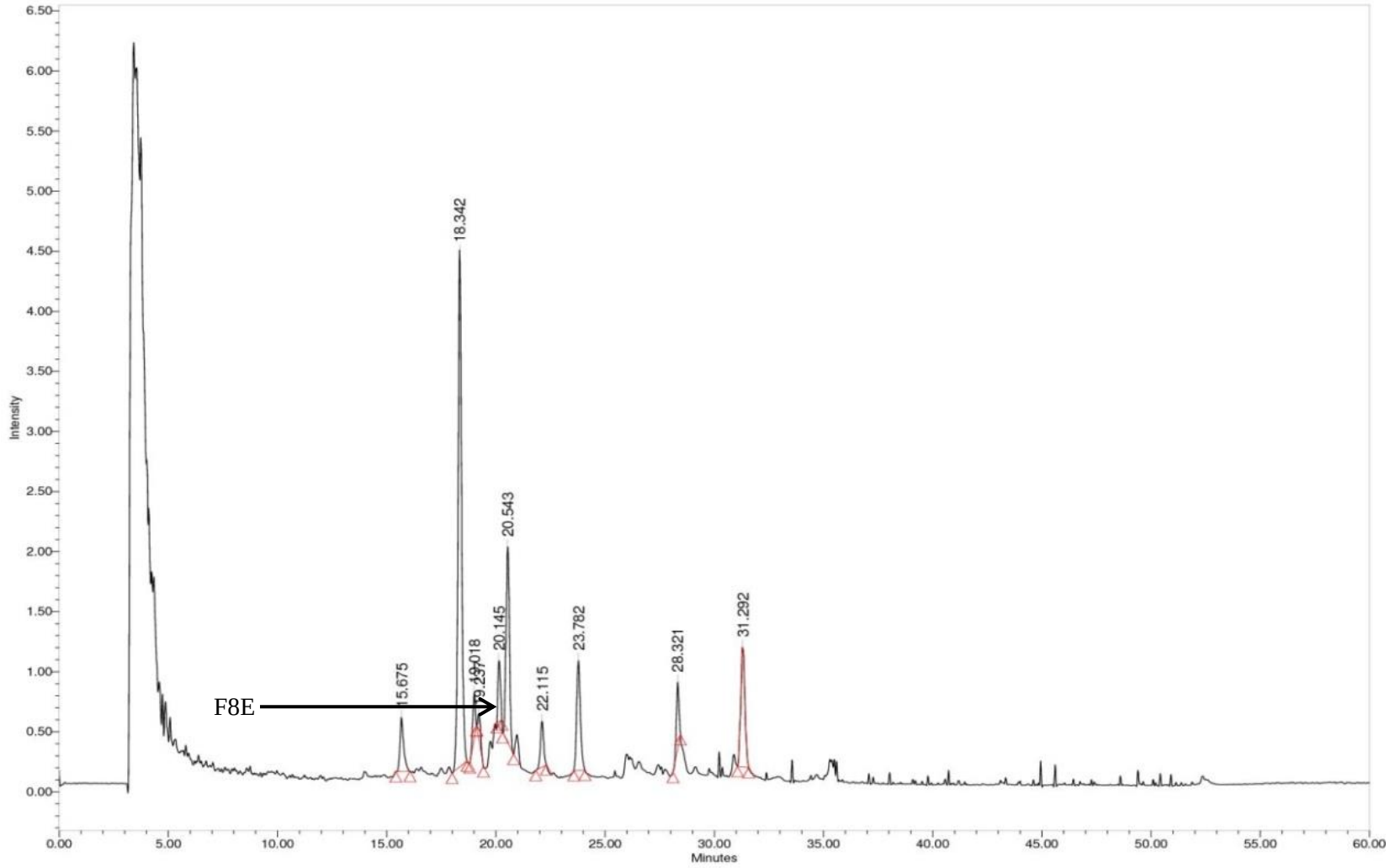

Figure 12: Chromatogram of fraction F8 showing the presence of six distinct compounds of interest at varying retention times. F8E-Rt = 20.145.

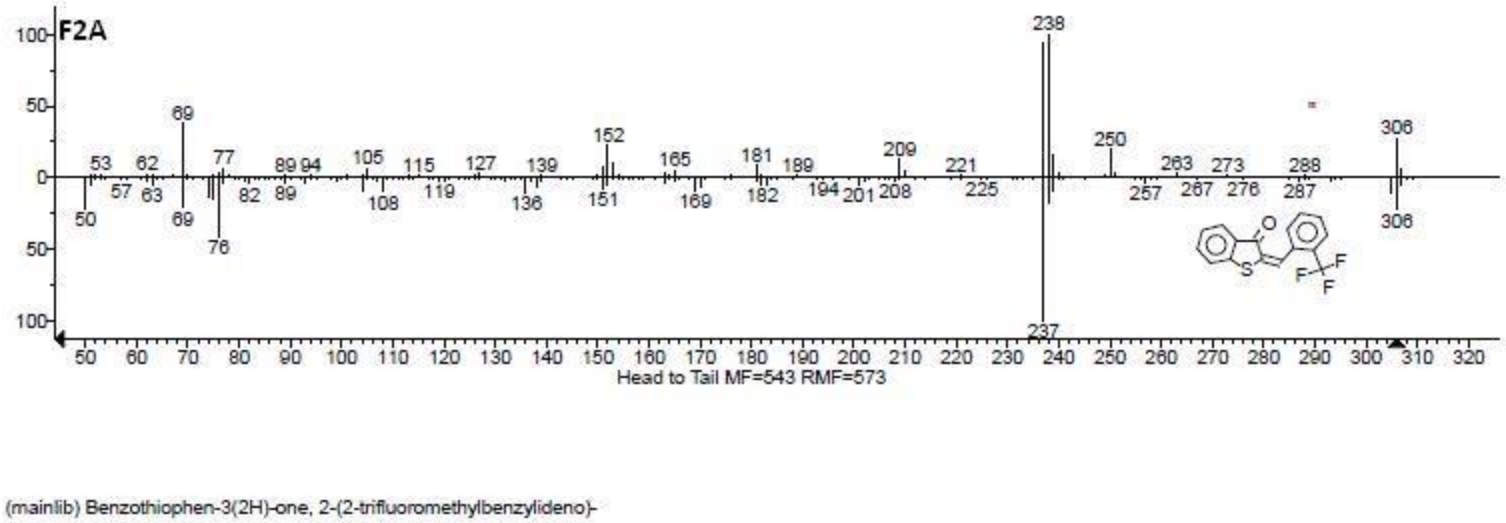

Figure 13: Mass spectra of compound F2A isolated from *C. triloba* root extract (top axis) matched the library template of benzothiophen-3(2H)-one, 2-(2-trifluoromethylbenzylideno)-(bottom axis).

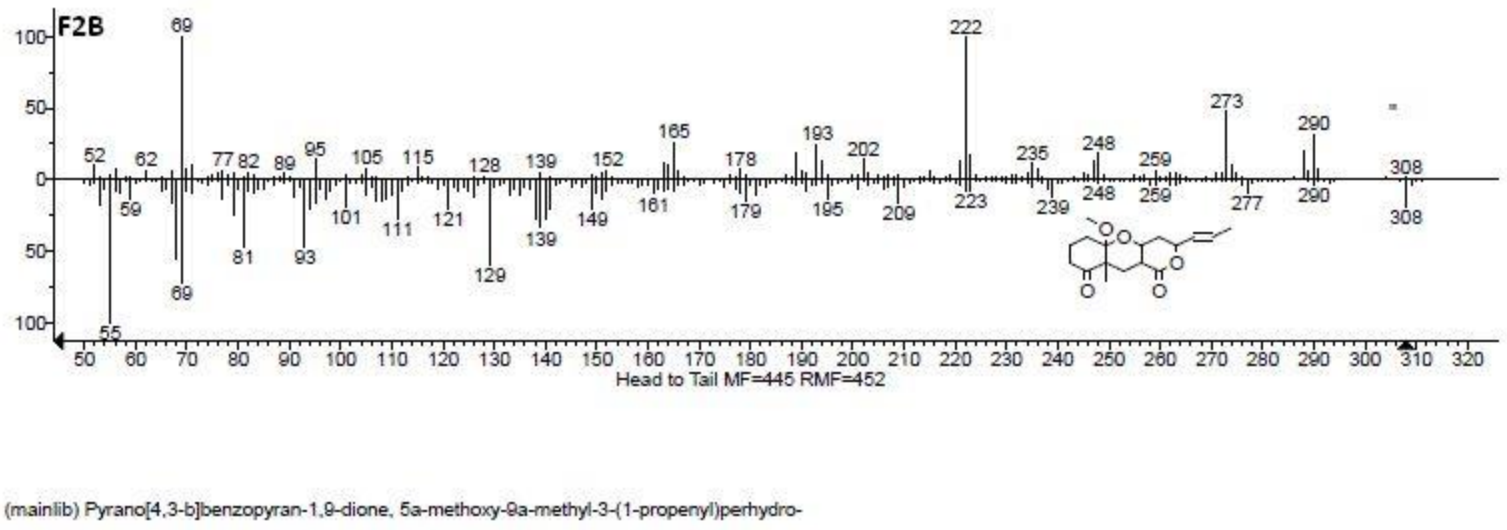

Figure 14: Mass spectrum of compound F2B isolated from *C. triloba* root extract (top axis) matched the library template of pyrano[4,3-b]benzopyran-1,9-dione, 5a-methoxy-9a-methyl-3-(1-propenyl)perhydro- (bottom axis).

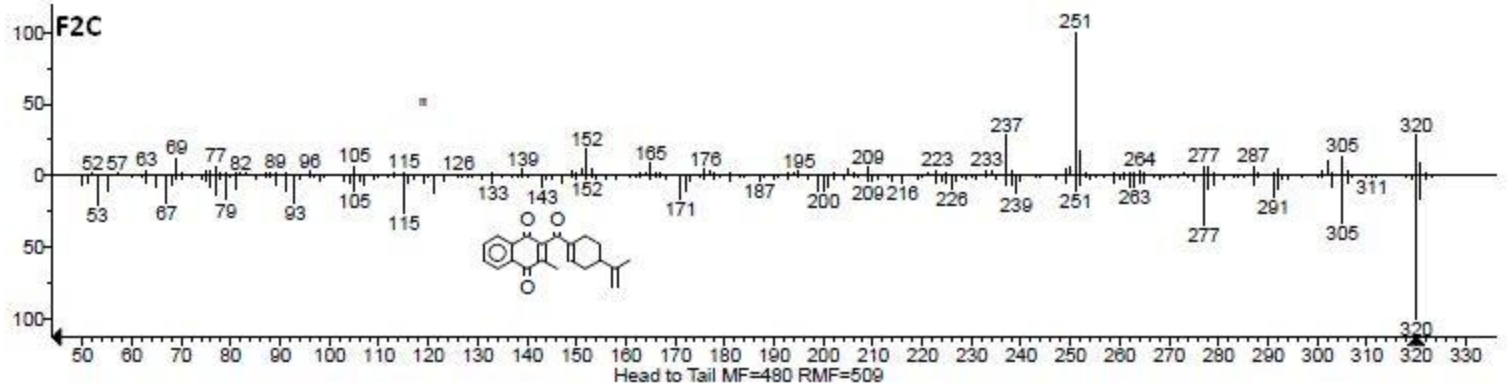

Figure 15: Mass spectrum of compound F2C isolated from *C. triloba* root extract (top axis) matched the library template of 1,4-naphthoquinone, 3-methyl-2-[(4-isopropenyl-1-cyclohexenyl)formyl]- (bottom axis).

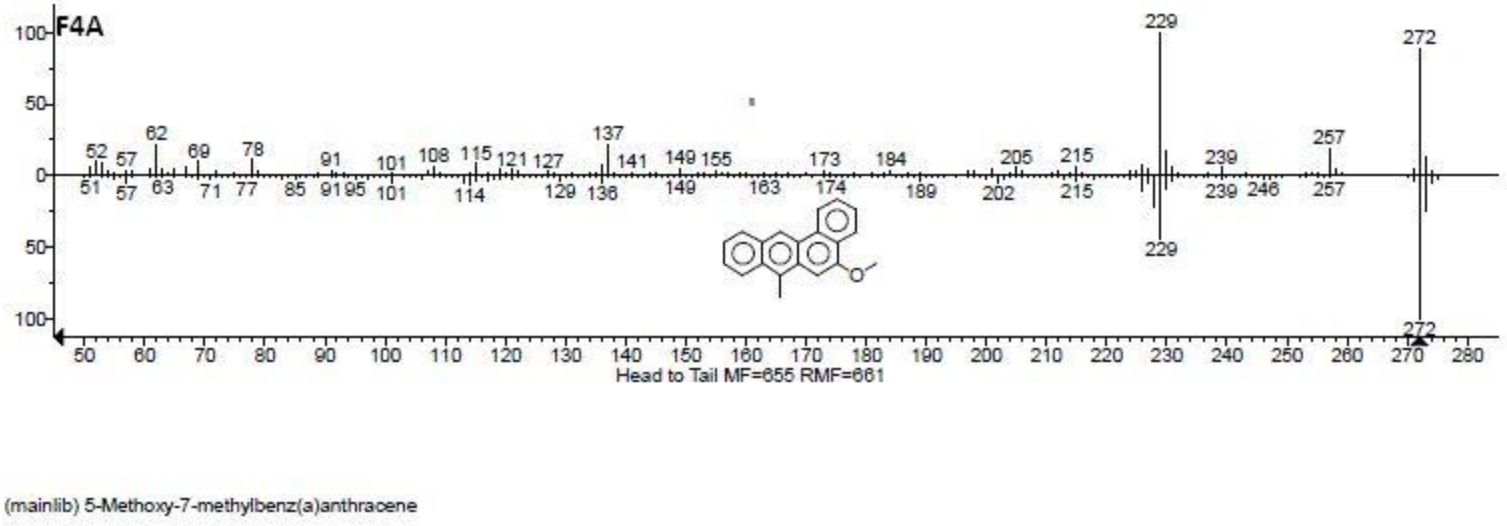

Figure 16: Mass spectrum of compound F4A isolated from *C. triloba* root extract (top axis) matched the library template of 5-methoxy-7-methylbenz(a)anthracene (bottom axis).

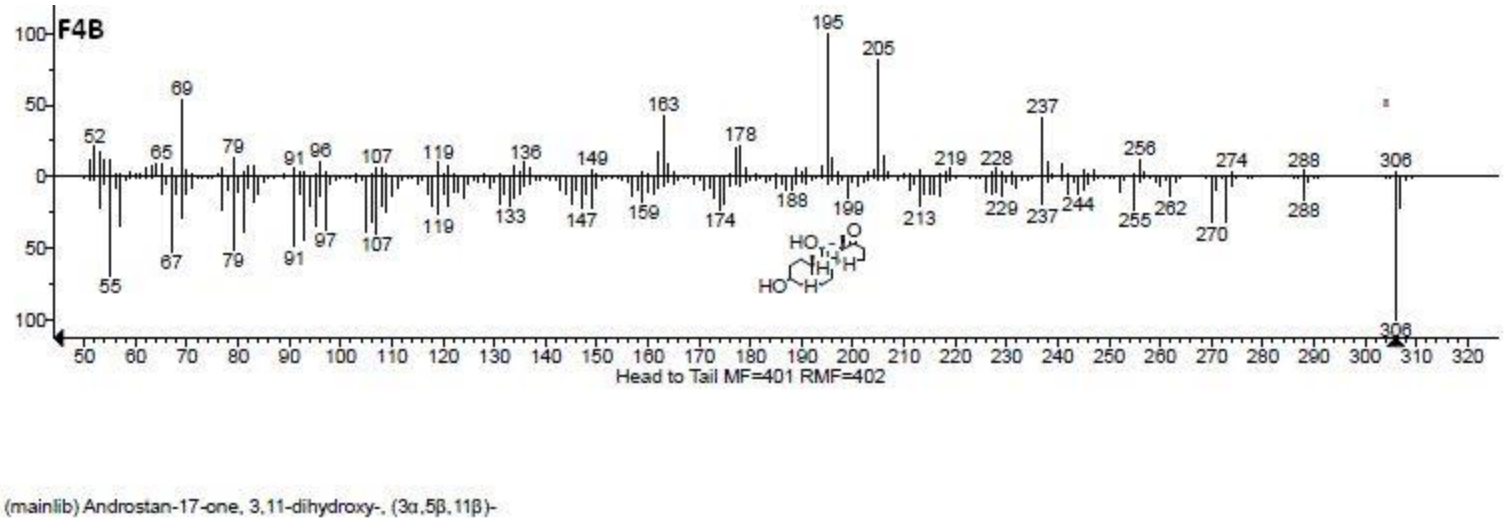

Figure 17: Mass spectrum of compound F4B isolated from *C. triloba* root extract (top axis) matched the library template of androstan-17-one, 3,11-dihydroxy-, (3α,5β,11β)- (bottom axis).

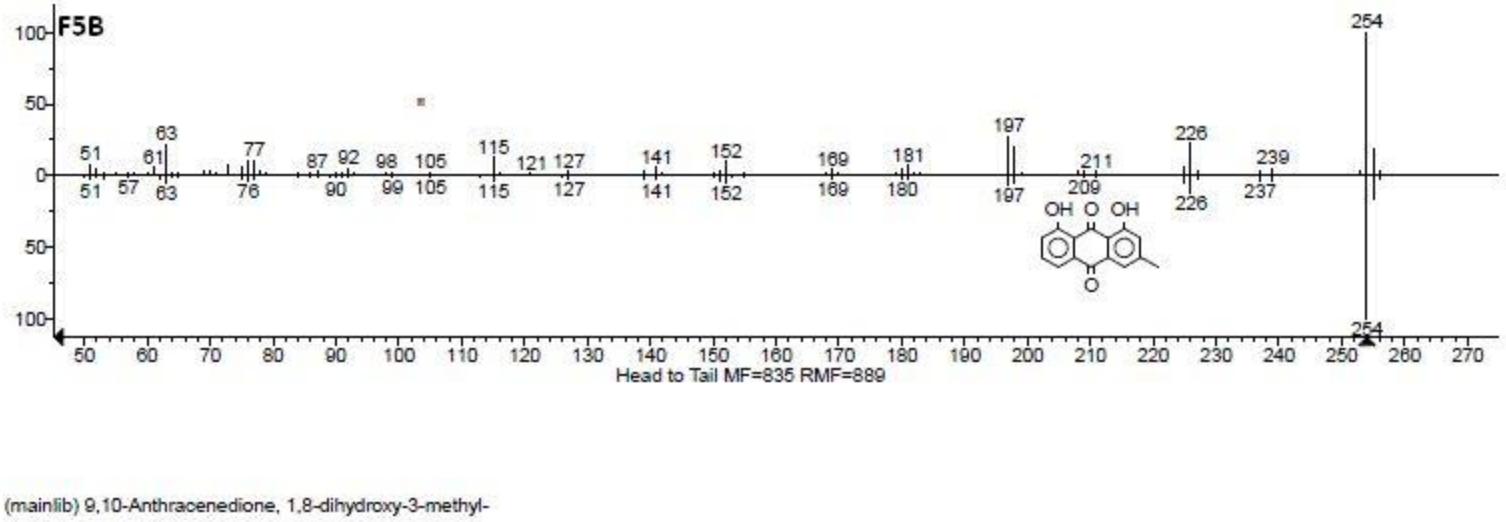

Figure 18: Mass spectrum of compound F5B isolated from *C. triloba* root extract (top axis) matched the library template of 9,10-anthracenedione, 1,8-dihydroxy-3-methyl (bottom axis).

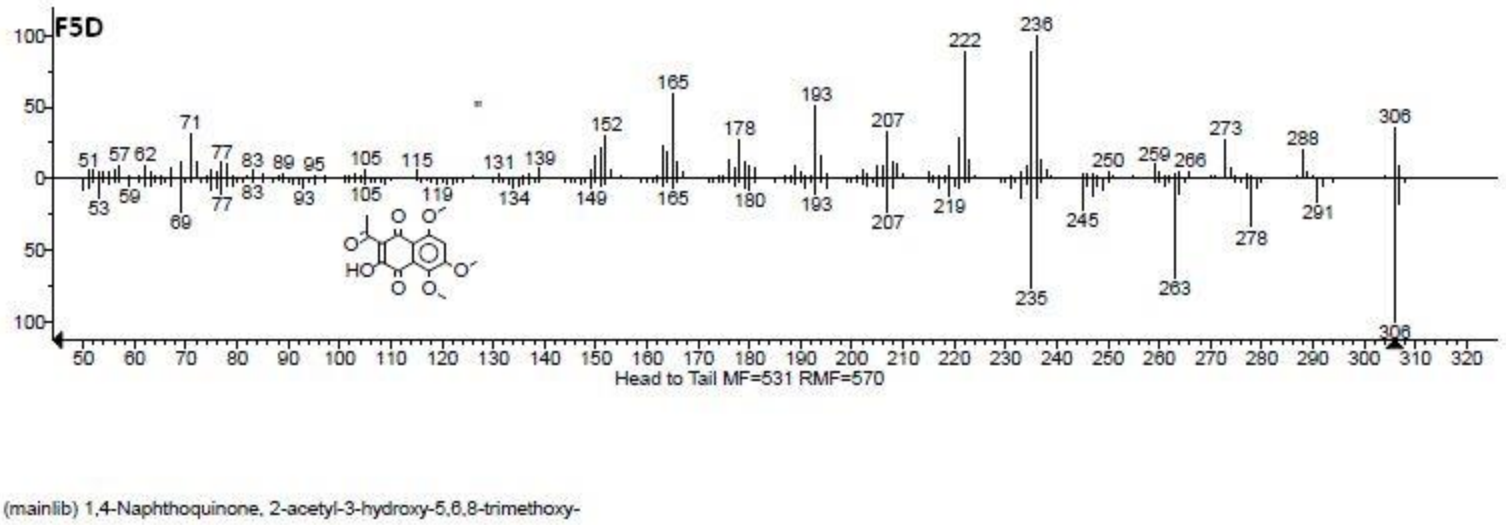

Figure 19: Mass spectrum of compound F5D isolated from *C. triloba* root extract (top axis) matched the library template of 1,4-naphthoquinone, 2-acetyl-3-hydroxy-5,6,8-trimethoxy- (bottom axis).

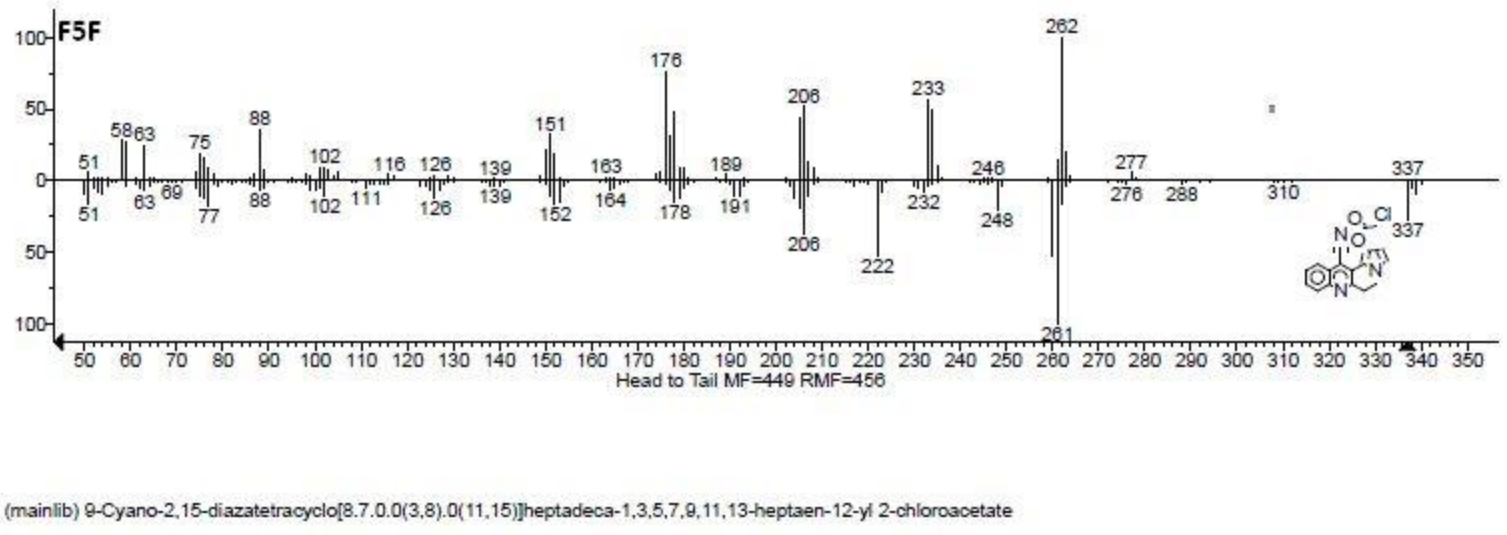

Figure 20: Mass spectrum of compound F5F isolated from *C. triloba* root extract (top axis) matched the library template of 9-cyano-2,15-diazatetracyclo[8.7.0.0(3,8).0(11,15)]heptadeca-1,3,5,7,9,11,13-heptaen-12-yl 2-chloroacetate (bottom axis).

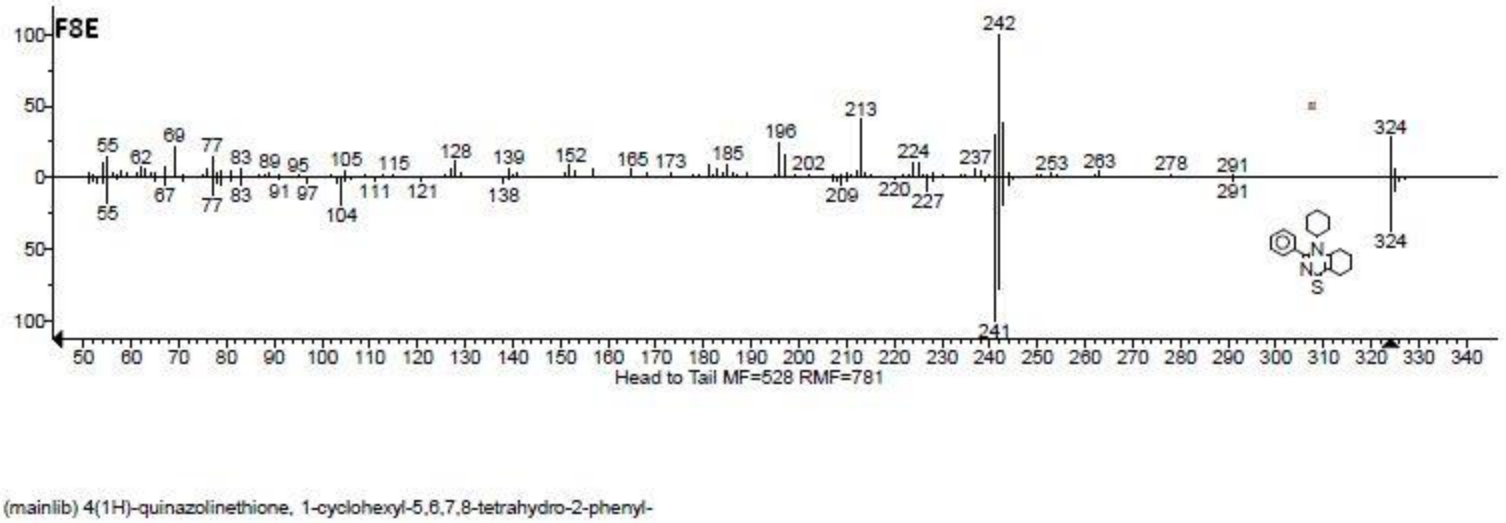

Figure 21: Mass spectrum of compound F8E isolated from *C. triloba* root extract (top axis) matched the library template of 4(1H)-quinazolinethione, 1-cyclohexyl-5,6,7,8-tetrahydro-2-phenyl (bottom axis).

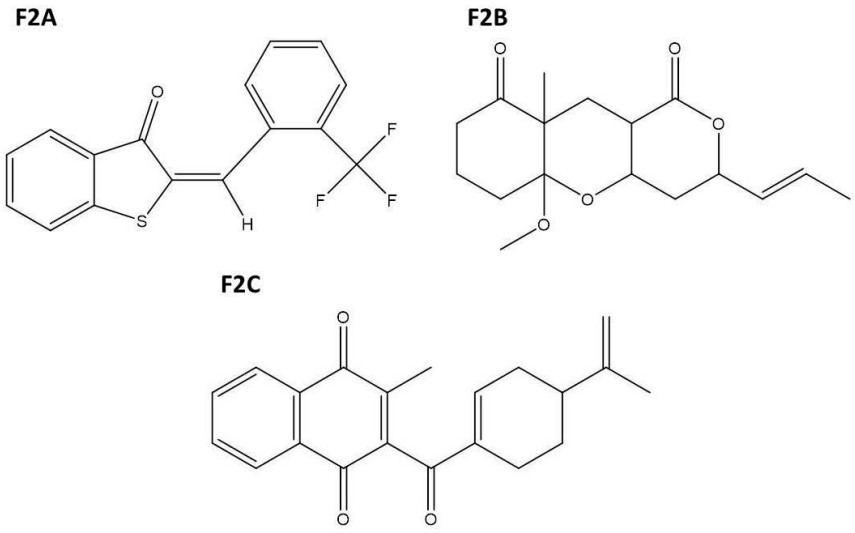

Figure 22: Compounds isolated from fraction F2. F2A-benzothiophen-3(2H)-one, 2-(2-trifluoromethylbenzylideno)-, F2B-pyrano[4,3-b]benzopyran-1,9-dione, 5a-methoxy-9a-methyl-3-(1-propenyl)perhydro, F2C-1,4-naphthoquinone, 3-methyl-2-[(4-isopropenyl-1-cyclohexenyl)formyl]-.

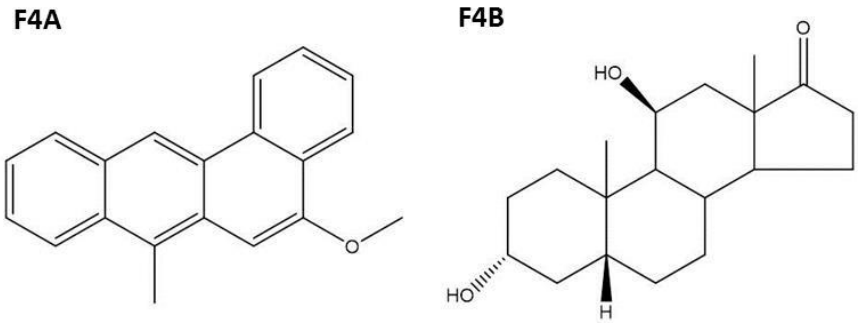

Figure 23: Compounds isolated from fraction F4. F4A-5-methoxy-7-methylbenz(a)anthracene and F4B-androstan-17-one, 3,11-dihydroxy-, (3α,5β,11β)-.

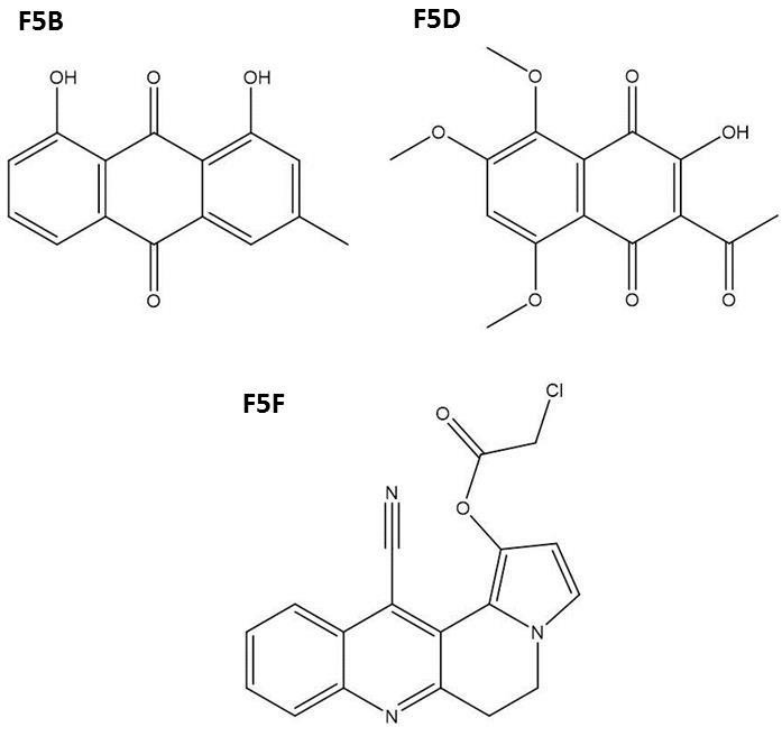

Figure 24: Compounds isolated from fraction F5. F5B-9,10-anthracenedione, 1,8-dihydroxy-3-methyl, F5D-1,4-naphthoquinone, 2-acetyl-3-hydroxy-5,6,8-trimethoxy and F5F-9-cyano-2,15-diazatetracyclo[8.7.0.0(3,8).0(11,15)]heptadeca-1,3,5,7,9,11,13-heptaen-12-yl 2-chloroacetate.

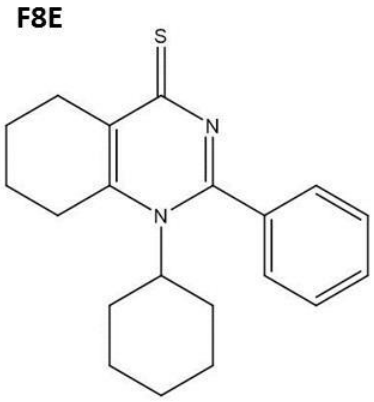

Figure 25: Compounds isolated from fraction F8. F8E-4(1H)-quinazolinethione, 1-cyclohexyl-5,6,7,8-tetrahydro-2-phenyl, F8F-2-methylenesuccinic acid, bis-(2-biphenyl-4-yl-2-oxoethyl ester).

4. Conclusions

Column chromatography allowed for separation of the hexane root extract into ten combined fractions. From the results obtained it was evident that the cytotoxic compounds were located in Fractions F2, F4, F5 and F8. Moreover according EI-LC-MS data, there were various classes of anticancer compounds (benzothiophenones, benzopyranones, naphthoquinones, anthraquinones, androstanes and quinazolines) present in these fractions. Mohanlall et al. (2011) previously found 9,10-anthracenedione; 1-hydroxy-4-methylanthraquinone; 5,8-dimethoxy-2,3,10,10a-tetrahydro-1H,4aH-phenanthrene-4,9-dione and androst-5-ene-3, 17, 19-triol. We were unable to find these compounds in the roots of *C. triloba* as derivatization (presence of similar structured compounds) made chromatographic analyse a challenge. Other techniques (such as mini-column chromatography, PTLC and PHPLC) would have to be employed to achieve maximum separation. Nevertheless, our study has revealed that the roots of *C. triloba* serve as a rich source of anticancer compounds. It was important to perform this study as Narang and Desai, (2009) reported that the "identification of cytotoxic compounds led to the development of anticancer therapeutics for several decades"[27]. Thus, the compounds characterized in this study could be used towards the development of new anticancer drugs.

Acknowlegements

This project was funded by National Research Foundation. We are thankful to Professor Himansu Baijnath (University of Kwa-Zulu Natal) for the collection of plant material. We are also grateful to Dr Catherine Kaschula (ICGEB, University of Cape Town) for the provision of cell lines.

References

1. Smithies, S. J. Pedaliaceae. 2000. In: Leistner OA. (ed.) Seed plants of Southern Africa: families and genera. Pretoria: National Botanical Institute.

2. Hutchings, A. (ed.) Zulu Medicinal Plants, an Inventory. University of Natal Press, Pietermaritzburg, 1996.

3. Wunderlin RP, Hansen BF. Atlas of Florida vascular plants [Online]. Tampa: University of South Florida, 2002, Available: http://www.plantatlas.usf.edu/. [Accessed: 23 July 2016]

4. Tredgold MH. (ed.) Food of plants of Zimbabwe. Gweru: Mambo Press, 1986.

5. Roberts M. Indigenous Healing Plants. Southern Book Publishers, South Africa, 1990.

6. Watt JM, Breyer-Brandwijk M.G. (eds.) The medicinal and poisonous plants of Southern and Eastern Africa. Livingstone, London, 1962.

7. Pooley E. (ed.) A field guide to wild flowers Kwazulu-Natal and the East Region. Natal Flora Publications Trust, South Africa, 1998.

8. Van Wyk BE, Gericke N. (eds.) People's plants. A guide to useful plants of Southern Africa. Briza Publications, South Africa, 2000.

9. Ramesar S, Baijnath H, Govender T, Mackraj I. Angiotensin I-Converting Enzyme Inhibitor Activity of Nutritive Plants in KwaZulu-Natal. Journal of Medicinal Food 2008; 11: 331-336.

10. Odhav B, Kandasamy T, Khumalo N, Baijnath H. Screening of African traditional vegetables for their alpha-amylase inhibitory effect. Journal of Medicinal Plants Research 2010; 4:1502-1507.

11. Mohanlall V, Odhav B. Antibacterial, anti-inflammatory and antioxidant activities of anthraquinones from *Ceratotheca triloba* (Bernh) Hook F. Journal of Medicinal Plant Research 2013; 7: 877-886.

12. Mohanlall V, Steenkamp PA, Odhav B. Isolation and characterization of anthraquinone derivatives from *Ceratotheca triloba* (Bernh.) Hook.f. Journal of Medicinal Plants Research 2011; 5: 3132-3141.

13. Balachandran C, Emi N, Arun Y, Yamamoto N, Duraipandiyan V, Inaguma Y, Okamoto A, Ignacimuthu S, Al-Dhabi NA, Perumal PT. In vitro antiproliferative activity of 2,3-dihydroxy-9,10-anthraquinone induced apoptosis against COLO320 cells through cytochrome c release caspase mediated pathway with PI3K/AKT and COX-2 inhibition. Chemico-Biological Interactions 2016; 5: 23-35.

14. García-Vilas JA, Quesada AR, Medina MA. Damnacanthal, a noni anthraquinone, inhibits c-Met and is a potent antitumor compound against Hep G2 human hepatocellular carcinoma cells. Scientific reports 2015; 5:1-9.

15. Preobrazhenskaya MN, Shchekotikhin AE, Shtil AA, Huang HS. Antitumor anthraquinone analogues for multidrug resistant tumor cells. Journal of Medical Sciences 2006; 26: 1-4.

16. Dhingra N, Bhardwaj TR, Mehta N, Mukhopadhyay T, Kumar A, Kumar M. Synthesis, antiproliferative activity, acute toxicity and assessment of the antiandrogenic activities of new androstane derivatives. Archives of Pharmacal Research 2011; 34: 1055-1063.

17. Hostettmann K. Strategy for the Biological and Chemical Evaluation of Plant Extracts. Invited lecture presented at the International Conference on Biodiversity and Bioresources: Conservation and Utilization. Phuket, Thailand: IUPAC. 1997.

18. Akhtar MS, Ali M, Mir SR, Singh O. New anthraquinones from Rubia cordifolia roots. Indian Journal of Chemistry 2006; 45B:1945-1950.

19. Kale A, Gaikwad S, Adsul V, Deshpande N, Salvekar J. Quantification of a phytotoxin from walnut species by HPTLC method. International Journal of Pharmacy and Pharmaceutical Sciences 2013; 5: 752-754.

20. Zhang Z, Daynard T, Kalmar G. Methods of using benzothiophenone derivatives to treat cancer or inflammation. 2006; United States patent application 60390589.

21. Chuang JY, Huang YF, Lu HF, Ho HC, Yang JS, Li TM, Chang NW, Chung JG. Coumarin induces cell cycle arrest and apoptosis in human cervical cancer HeLa cells through a mitochondria- and caspase-3 dependent mechanism and NF-kappaB down-regulation. In Vivo 2007; 21:1003-1009.

22. Xu TP, Shen H, Liu LX, Shu YQ. Plumbagin from Plumbago Zeylanica L induces apoptosis in human non-small cell lung cancer cell lines through NF- κB inactivation. Asian Pacific Journal of Cancer Prevention 2013; 14:2325-2331.

23. Hong JY, Chung HJ, Bae SY, Trung TN, Bae K, Lee SK. Induction of Cell Cycle Arrest and Apoptosis by Physcion, an Anthraquinone Isolated From Rhubarb (Rhizomes of Rheum tanguticum), in MDA-MB-231 Human Breast Cancer Cells. Journal of Cancer Prevention 2014; 19: 273-278.

24. Yeap S, Akhtar MN, Lim KL, Abu N, Ho WY, Zareen S, Roohani K, Ky H, Tan SW, Lajis N, Alitheen NB. Synthesis of an anthraquinone derivative (DHAQC) and its effect on induction of G2/M arrest and apoptosis in breast cancer MCF-7 cell line. Journal of Drug Design, Development and Therapy 2015; 9: 983-992.

25. Oklješa AM, Jovanović-Šanta SS, Klisurić OR, Sakaĉ MN, Djurendić EA, Jakimov DS, Aleksić LD, Penov Gaši, KM. Structural Analysis and Antitumor Activity of Androstane D-Seco-mesyloxy Derivatives. Journal of the Brazilian Chemical Society 2013; 24:1613-1622.

26. Wasfy AAF, Mohmed NA, Salman AA. Synthesis and anti-cancer properties of novel quinazoline derivatives. International Journal of Research in Pharmacy and Chemistry 2015; 5: 34-40.

27. Narang AS, Desai DS. Anticancer Drug Development. 2009. In: Lu Y, Mahato RI. (eds.) Pharmaceutical Perspectives of Cancer Therapeutics. Springer Science & Business Media, Heidelberg, London, New York.

Naicker et al., Afr J Tradit Complement Altern Med. (2016) 13(3):85-94
http://dx.doi.org/10.4314/ajtcam.v13i3.11

GENETIC TRANSFORMATION OF *CERATOTHECA TRILOBA* FOR THE PRODUCTION OF ANTHRAQUINONES FROM HAIRY ROOT CULTURES

Leeann Naicker, Viresh Mohanlall* and Bharti Odhav

Department of Biotechnology, Faculty of Applied Sciences, Durban University of Technology, P. O Box 1334, Durban 4001, South Africa

Corresponding Author: Dr V. Mohanlall, Telephone: +2731 327 5426; Fax: +2731 327 5351, E-mail: vireshm@dut.ac.za

Abstract

Background*: Ceratotheca triloba* was found to contain three anthraquinones (9, 10-anthracenedione, 1-hydroxy-4-methylanthraquinone and 5, 8-dimethoxy-2, 3, 10, 10a-tetrahydro-1H, 4aH-phenanthrene-4, 9-dione [DTP]) in its roots. Inhibition of the human topoisomerase II enzyme is the basis of some currently used cancer drugs such as doxorubicin which is shown to be cardio-toxic. For this reason we decided to investigate anthraquinones from *C. triloba* as a possible anticancer drug, however the main limitation was the large quantities of roots that are required to obtain a good yield of the active compound. Therefore the aim of this research was to obtain a higher yield of anthraquinones in hairy roots cultures than the parent plant as well as to compare yields of hairy root, cell suspension and shoot cultures.
Materials and Methods: Protocols for seed sterilization, seed germination, shoot cultivation, callus induction, *A. rhizogenes* mediated-transformation and hormone supplementations of hairy roots were developed.
Results*:*The results revealed that stem explants was susceptible to transformation by *Agrobacterium rhizogenes* at a low optical density of 0.2. Induced hairy roots were decontaminated by exposure to cefotaxime at 500mg.l^{-1} for five days and then 200mg.l^{-1} for eight days. Visualization of culture extract profiles by TLC revealed anthraquinones were present in all cultures. Analysis of the culture extracts by HPLC showed the highest yield of anthraquinones was produced in hairy root cultures supplemented with 1-Naphthaleneacetic acid [NAA] (8 mg). This was a 17 fold increase compared to field roots (0.47 mg).
Conclusion: Therefore *C. triloba* hairy root cultures are the preferable biological system for anthraquinones production over shoot (0.13 mg) and cell suspension cultures (0.70 mg).

Key words: anthraquinones, *Agrobacterium rhizogenes*, *Ceratotheca triloba*, topoisomerase II, hairy root cultures, hormone supplementations

Introduction

C. triloba is an annual plant that is found in the summer rainfall areas of South Africa. The root extract of the plant was found to contain three anthraquinones; 9, 10-anthracenedione, 1-hydroxy-4-methylanthraquinone and 5, 8-dimethoxy-2, 3, 10, 10a-tetrahydro-1H, 4aH-phenanthrene-4, 9-dione (DTP), and one steroid; androst-5-ene-3, 17, 19-triol (Mohanlall *et al*., 2011). Derivatives of the anthraquinones molecule have shown to exhibit various pharmacological and biological activities which include: anticancer, antibacterial, antitrypanosomal and antineoplastic activities (Baguley, 1991; Monneret, 2001; Dzierzbicka and Kolodziejczyk, 2005; Preobrazhenskaya *et al*., 2006). Experiments in our lab have revealed that DTP can inhibit the human topoisomerase II enzyme which transforms supercoiled DNA to linear DNA. This mechanism is the basis of some currently used cancer drugs. For example: doxorubicin is used to treat tumors of the mammary gland and gynaecological and haematological malignancies (Preobrazhenskaya *et al*., 2006). However the use of this compound can be life threatening due to its cardiotoxicity (Hsiao *et al*., 2008). Recent research has also shown that anthracenedione derivatives induce apoptosis in the human cervical cancer cell line, CaSki (Amin *et al*., 2009). Until now there has been no effective compound against this type of cancer.

Due to the applications of anthraquinones and the need for alternative anticancer molecules, we decided to conduct further research on the anthraquinones from *C. triloba*. There are certain limitations to extracting this anthraquinone from field grown plants. A large quantity of roots is required to obtain a reasonable yield of the active compound. The plant growth is negatively affected by cold winter conditions and is sensitive to pathogens and insects. Therefore we turned our attention to the *in vitro* production of anthraquinones. In a previous study, cell suspension cultures of *C. triloba* were cultured to elicit an overproduction of anthraquinones, but only 0.02µg.ml^{-1} and 0.75 µg.ml^{-1} were produced in the control and elicited cultures, respectively (Naicker, 2011). This was due to the undifferentiated state of the plant cells which synthesize low concentrations of secondary metabolites (Palazon *et al*., 2006). Hence in this study we cultured hairy root cultures. These are differentiated plant tissues which are cultured by infecting stem explants with the Gram negative bacterium, *Agrobacterium rhizogenes* which habours the Ri plasmid. The genes on this plasmid direct the transfer of tDNA into the plants genome. This DNA contains genes that are responsible for the hairy root phenotype and auxin and cytokine production that allow for growth without exogenous hormones. These cultures have been successfully employed towards producing important anticancer plant compounds (taxol, vinblastine and vincristine) due to several advantages (Rowinsky and Donehower, 1995; Kim *et al*., 2009; Ataei-Azimi *et al*., 2008; Schmelzer and Gurib-Fakim, 2008). Hairy root cultures can synthesize metabolites at a higher

level than the parent plant (Pietrosiuk *et al*., 2007). They can produce metabolites specific to the parent plant as well as novel metabolites that cannot be detected in the mother plant or other plant tissue cultures (Nader *et al*., 2006). When compared to other *in vitro* cultures they have a higher growth rate and secondary metabolite yield than untransformed cultures (Charlwood and Charlwood, 1991; Flores *et al*., 1999). Therefore aims of this research were to obtain a higher yield of anthraquinones in hairy roots cultures than the parent plant as well as to compare yields of hairy root, cell suspension and shoot cultures.

Materials and Methods

Plant Material

Seed pods and roots of *C. triloba* were collected from wild plants in Durban, Kwa-Zulu Natal, South Africa. The plant was identified by using taxonomic keys and a voucher specimen was deposited in the Ward Herbarium at the University of Kwa-Zulu Natal (Westville campus). The seed pods were broken to remove the seeds which were stored in a closed bottle at room temperature. The roots were dried in the laboratory at room temperature for 5-8 days or until they broke easily by hand. These were then ground to a fine powder using a Wareing blender and stored in a closed bottle at room temperature until required.

Seed Germination and Shoot Cultivation

In order to determine the optimum time for effective surface sterilization the seeds were exposed to 30% NaCIO for 0 (control), 5, 10, 15 and 20 minutes. The seeds were then washed with sterile distilled water and placed in a Petri dish containing solid MS medium (5 seeds per plate) (Murashige and Skoog, 1962). A replicate of 5 Petri dishes were prepared for each exposure time. The Petri dishes were incubated under visible light at room temperature. The seeds were examined for contamination after two weeks and the treatment regime that produced the highest percentage of sterile seeds was used for germination seeds to produce shoot cultures for the *in vitro* transformation experiment.
The germinated seedlings (3 weeks old) were cultivated into shoot cultures in 12 cm culture vessels containing MS medium which was supplemented with 1 $mg.l^{-1}$ of 6-Benzylaminopurine [6-BAP] (Sigma-Aldrich, Inc.) and 0.5 $mg.l^{-1}$ of Indole-3-acetic acid
[IAA] (Sigma-Aldrich, Inc.). The seedlings were incubated for 45 days in a growth chamber at 26˚C under standard cool white fluorescent light with a flux rate of 35 $\mu mols^{-1}m^{-2}$ and a 16 h photoperiod.

Callus Induction and Preparation of Cell Suspension Cultures

The leaves of *in vitro* shoot cultures were removed and cut into 1 cm square disks by using a scalpel. They (5 leaf disks per plate) were placed on MS medium supplemented with 1 $mg.l^{-1}$ of 2.4-D and 1 $mg.l^{-1}$ of 6-BAP (Sigma-Aldrich, Inc.). These plates were then placed in a cardboard box and incubated in the dark phase at 26˚C for 4 weeks. Induce calli were transferred onto fresh medium and maintained by sub-culturing at 3 week intervals.
Inoculum for the cell suspension cultures were initiated by transferring approximately 1 g of callus (three weeks old) from the second sub-culture into four 1000 ml Erlenmeyer flasks containing 50 ml of MS liquid medium which was supplemented with 1 $mg.l^{-1}$ of 2.4-D and 1 $mg.l^{-1}$ of 6-BAP. The flasks were agitated on a shaker (Infors Ecotron, Polychem supplies cc) at 100 rpm at 26˚C in the dark phase for one week. Thereafter, 150 ml of MS medium was added to the inocula and the flasks were incubated for a further 2 months. At the end of cultivation period the cell mass of suspension cultures was determined by centrifuging 50 ml volumes at 4000 rpm for 10 minutes at 20˚C. The total wet weight of the cell suspension cultures was determined by the following equation: (mass of beaker + cell mass) – (mass of beaker) = total wet weight of cell suspension cultures from four flasks.

Production of Hairy Root Cultures

Cultivation of *A. Rhizogenes*

A. Rhizogenes strain 15834 was provided on yeast extract peptone (YEP) agar plates by the Council of Scientific and Industrial Research (CSIR), South Africa. Plate cultures of *A. rhizogenes* were prepared by streaking the culture onto YEP agar (An *et al*., 1988). The strain was cultivated for 24 hours at 30°C. A loopful of this culture was used to inoculate a 250 ml Erlenmeyer flask containing 50 ml of YEP liquid medium. The flasks were placed on a shaker and incubated for 24 hours at 30˚C. The optical density (OD) of the culture was determined spectrophotometrically at 600 nm and the culture was diluted with YEP medium to an OD of 1, 0.5 and 0.2 for the transformation experiment.

Hairy Root Induction in *C. Triloba* Using *A. Rhizogenes*

Shoots of the *in vitro* grown plantlets were cut at the stems and the leaves and stems were used as explants. These were inoculated with a sterile scalpel dipped in three concentrations (OD of 1, 0.5 and 0.2) of the *A. rhizogenes* culture. Leaf explants were inoculated by pricking and stem explants were cut. Explants inoculated with a scalpel dipped in YEP medium served as the control. The infected and control explants were placed on MS medium (containing no hormones) and incubated for 3-4 weeks at 26˚C under standard cool white fluorescent light with a flux rate of 35 $\mu mols^{-1}m^{-2}$ and a 16 h photoperiod. The response of the explants to Agrobacterium in terms of hairy root emergence was measured by determining the transformation efficiency: (number of hairy roots/number of explants) X 100. Induced hairy roots were excised and then decontaminated by treating them with 500 $mg.l^{-1}$ of cefotaxime for five days, and thereafter with 200 $mg.l^{-1}$ of cefotaxime for eight days. The sterility of the hairy roots was confirmed by placing 1 cm of the root onto a
YEP plate which was incubated at 30˚C for three days. Once the roots were confirmed to be sterile the hairy root cultures were placed on

MS medium plates and maintained by sub-culturing onto fresh medium at three week intervals.

Effect of Auxins on Hairy Root Biomass Production

In order to improve the growth of hairy roots two auxins were used, NAA at 1 mg.l^{-1}and IAA at 1 mg.l^{-1}. Inoculum cultures were prepared by transferring approximately 200 mg hairy roots into 1 L flasks containing 30 ml of MS medium. Three flasks containing medium with no hormone served as the control cultures. All cultures were incubated at 26˚C in a shaker under standard cool white fluorescent light with a flux rate of 35 µmols^{-1}m^{-2} and a 16 h photoperiod. An aliquot of 70 ml of medium was added to the inoculum cultures after 3 weeks and a final volume of 100 ml of medium was added to the flasks after a further 3 weeks. Cultures were then incubated for 4 weeks. Thereafter the biomass was removed from the medium using a forceps and the increase in wet weight was determined by the following equation: (final wet weight – initial weight = increase in wet weight).

Examination of the Morphological Characteristics of Adventitious Roots and Hairy Roots

Shoot cultures were sub-cultured on Petri plates containing MS medium supplemented with 1 mg.l^{-1} of IBA to induce adventitious roots. Induced hairy roots were transferred onto plain MS medium and MS medium supplemented with 1 mg.l^{-1} of NAA.
The plates were incubated at 26˚C under standard cool white fluorescent light with a flux rate of 35 µmols^{-1}m^{-2} and a 16 h photoperiod. The morphology of adventitious roots and hairy roots were examined according to color and branching of the lateral roots.

Extraction and Analysis of Anthraquinones

The preparation of the field roots, shoot, cell suspension and hairy root cultures for extraction varied but the preparation of the different extracts was the same. This is outlined below:

Field roots: the ground material of the field roots was extracted with hexane by agitation on a shaker at 180 rpm for 24 hours at room temperature.

Shoot cultures*:* the shoot cultures were dried at 30˚C in an oven and crushed to a fine powder in a Waring blender. The powder was extracted in 100 ml of hexane at room temperature by agitation on a shaker at 180 rpm for 24 hours.

Cell suspension cultures*:* The cell mass was harvested by centrifuging 50 ml volumes of suspension culture at 4000 rpm for 10 minutes at 4˚C. The cell mass pellet was disrupted by sonication (Virsonic, Virtis) at 4 psi for 10 minutes. The cell mass (used to obtain the intra-cellular extract) and the supernatant (used to obtain the extra-cellular extract) were agitated in 100 ml of hexane in 1 L flasks on a shaker at 180 rpm for 24 hours at room temperature.

Hairy root cultures*:* The hairy root biomass was macerated using a scalpel. The macerated root mass (used to obtain the intra-cellular extract) and the supernatant (used to obtain the extra-cellular extract) were extracted in 200 ml of hexane on a shaker at 180 rpm for three days at room temperature.

Preparation of the intra-cellular extracts involved using the following protocol. Filtration was used to separate the powdered plant material, cells and macerated hairy roots from the hexane extract which was then concentrated by using a roto-evaporator (Heidolph Laborota 400 efficient) with the water bath set at a temperature of 50°C and the flask rotated at 60 rpm. The residue was dissolved in 10 ml of hexane and transferred to a glass bottle which was covered with foil to prevent light from degrading the compounds. The extract was dried under an air current for 3 days and used for chromatographic analyses. For the extra-cellular extract the hexane fraction was slowly poured out into a flask and concentrated as described above.

Profile of Compounds and Detection of Anthraquinones in the Field Root Extract and in Plant Cell and Tissue Culture Extracts by TLC

Thin layer chromatography (TLC) was performed to compare the compounds and detect anthraquinones in *C. triloba* field root extract and plant cell and tissue culture extracts by using commercial standards; 9,10-Anthracenedione and 1-Hydroxy-4-methylanthaquinone (Sigma-Aldrich, Inc) (1 mg.ml^{-1} dissolved ethyl acetate). Approximately 10 µl of each standard solution, 50 µl of the field root extract and plant cell and tissue culture extracts were applied to the TLC silica gel plate (Merck TLC F_{254}). Hexane: ethyl acetate (90:10) was used as the mobile phase. The developed TLC plate was visualized under ultraviolet light at 312 nm and 264 nm (Camag Universal UV lamp TL-600). The TLC plate was also sprayed with p-anisaldehyde solution (13.31 ml of anisaldehyde in 250 ml of ethanol and 2.5 ml of H_2SO_4) and heated at 120˚C in an oven for 15 minutes as described by Wagner *et al*. (1984)

Quantification of Anthraquinones by HPLC

HPLC analysis was carried out according to the method described by Fernand *et al*. (2008) using commercial standards. A standard curve was generated with 10, 20, 50, 5, and 2 µg.ml^{-1} of 9, 10- anthracenedione and 1-hydroxy-4-methylanthaquinone (Sigma-Aldrich, Inc.) which were dissolved in ethyl acetate. The field root extract, hairy root, shoot and cell suspension culture extracts were dissolved in ethyl acetate and filtered for HPLC analysis. Separation and quantitative analyses of anthraquinones were performed on a

Merck- Hitachi LaChrom system (Darmstadt, Germany) consisting of a D7000 system controller, four pumps (D7400), a Merck- Hitachi LaChrom (L-7200) auto injector and an Merck- Hitachi LaChrom (L-7200) UV-VIS detector (λ = 260 nm). Separation of the analytes was performed at 40 ˚C on a Licrospher C18 (2) column, 100 ˚A pore size, 5µm particle size, 250×4.6 mm i.d.column containing a guard column (Merck, Darmstadt, Germany). The analytes were eluted isocratically at a flow rate of 0.4 ml.min^{-1} using an acetonitrile/methanol/buffer (25:55:20, v/v). The buffer used as 10 mM ammonium acetate at pH 6.8. The injection volume was 10 µL.

Results and Discussion

Seed Germination and Shoot Culture

The optimum exposure time to NaClO for maximum seed germination and minimum contamination was determined by exposing the *C. triloba* seeds to 30% NaClO for 0, 5, 10, 15 and 20 minutes. It was found that the percentage of seed germination decreased as the exposure time of the seeds to NaClO increased (**Fig 1**). This could be due to damage of the seed by NaClO. The best exposure time for sterilization of *C. triloba* seeds with 30 % NaClO was 10 minutes as 26 % of seeds germinated and only 6 % was contaminated. The sterilized seeds germinated on MS medium within two to three weeks. The seedlings developed into shoots after 45 days.

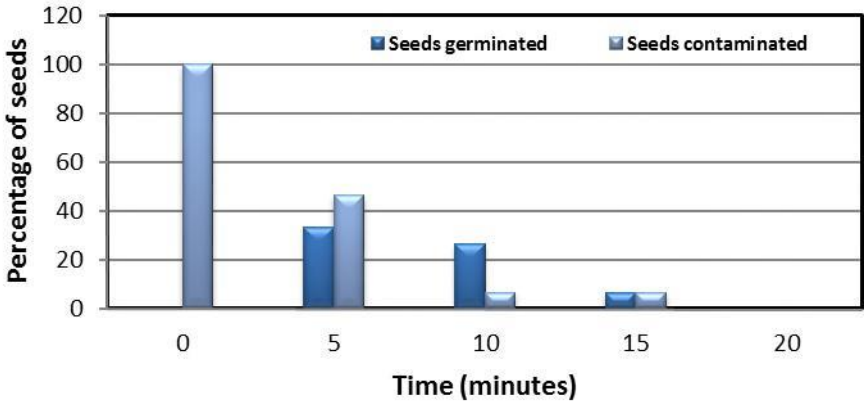

Figure 1: Percentage of seeds that germinated and the percentage of seeds that were contaminated after treatment with 30% NaClO at different time intervals.

Callus and Cell Suspension Cultures

Callus initiation was observed on the surface or cut ends of the leaf explants after 2-3 weeks of inoculation. Callus cultures induced from *C. triloba* leaf explants on MS medium were orange-yellow in color. When callus cultures were transferred into flasks containing MS liquid medium, the friable callus tissue dispersed into small aggregates after the flasks were agitated on the shaker. This allowed for semi-homogenous cell suspension cultures to form for scaling up to 200 ml. After two months of cultivation the cell suspension cultures turned from orange to brown in color. This phenomenon was observed in *Morinda elliptica* cells which turned brown when anthraquinones were produced (Abdullah *et al*., 1998). Thus the browning of these plant cell cultures can indicate the time to harvest the cells from suspension cultures for extraction of secondary metabolites.

Induction of Hairy Roots

The transformation of *C. triloba* to produce hairy roots was dependent on the type of explant used (young tissues of sterile plantlets, hypocotyl segments, cotyledons, petioles and young stems and leaves are normally used). In this study stem and leaf explants of shoot cultures were used and it was found that stem explants gave the highest transformation efficiency (73 %) while leaf explants were not responsive to transformation by *A. rhizogenes* (**Table 1, Fig 2A and 2B**). The concentration of *A. rhizogenes* used was also significant as it influenced the survival of the explants. A low concentration of *A. rhizogenes* (culture with an optical density of 0.2) transformed the stem explants whereas high concentrations (culture with an optical density of 0.5 or 1) killed the explants (**Table 1**). The concentration of cefotaxime used to decontaminate the induced hairy root cultures was also significant. Induced hairy roots were disinfected by transferring onto MS medium containing 500 mg.l^{-1} of cefotaxime. Hairy roots kept on this medium for more than five days resulted in browning and they stopped growing. Therefore, they were transferred onto MS medium containing a lower concentration of cefotaxime (200 mg.l^{-1}). After eight days on this medium, the sterility test showed that the hairy roots were sterile as no bacterial colonies grew on YEP solid medium.

Morphological Characteristics of Adventitious and Hairy Roots

Hairy roots cultured on MS medium containing no hormone were slow growing. Therefore, the morphology of adventitious roots (non-transformed roots) and hairy roots were examined to ensure that the hairy roots induced were as result of Agrobacterium transformation. Adventitious roots were induced in *C. triloba* shoot cultures using MS medium containing 1 $mg.l^{-1}$ of IBA Morphologically, these roots were highly branched and were white in colour. In contrast, the hairy roots cultured with no hormone or with NAA were less branched and turned brown as the biomass increased in the plate. Hence, based on the morphological features it can be assumed that in this study the induced hairy roots resulted from Agrobacterium transformation

Table 1: Concentration of *A. rhizogenes* used to transform *C. triloba* and the transformation efficiency of leaf and stem explants.

Explant	Concentration of bacteria (OD)	No. of explants transformed	Transformation efficiency (%)
Leaf	Control	None	0
	1	None	0
	0.5	None	0
	0.2	None	0
Stem	Control	None	0
	1	None	0
	0.5	None	0
	0.2	11	73.33

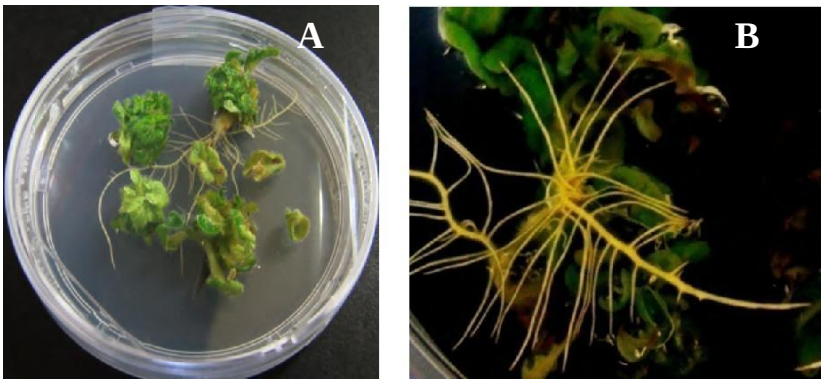

Figure 2:*C. triloba* hairy roots were induced on MS medium and became highly branched after 4 weeks (A). The hairy roots emerged from stem explants (B).

The Effect of Auxins Hairy Root Biomass

Hairy root cultures containing no hormone did not grow well as the entire hairy root biomass turned brown after four weeks. This result contradicted the findings of Estruch *et al*. (1991) who indicated that hairy roots can growth rapidly in hormone free medium. The mean doubling time of hairy roots after inoculation varies from 24 to 90 hours, but in some cultures this time is even longer, for example the doubling time of *Galphimia glauca* hairy roots was 6 days (Nader *et al*., 2006) and as long as 15 days has been reported for *Cinchona* hairy roots (Geerlings *et al*., 1999). Thus great variations exist from one species to another. It has been reported that the improvement of the culture medium can increase the growth rate of slow growing hairy roots as well as the yield of secondary metabolites. In our study we added auxins; IAA or NAA into the medium. Cultures containing either one of these hormones turned brown while their lateral roots were yellow in color and continued growing). Moreover the mean biomass of these cultures increased by 23.21 and 44.79 times, respectively in comparison to the control culture. Thus MS medium containing NAA produced the highest mean biomass (46.13 g) (**Fig 3**). A study by Balvanyos *et al*. (2001) also showed that the addition of NAA into the medium increased the biomass production of *Lobelia inflata* L. hairy root cultures.

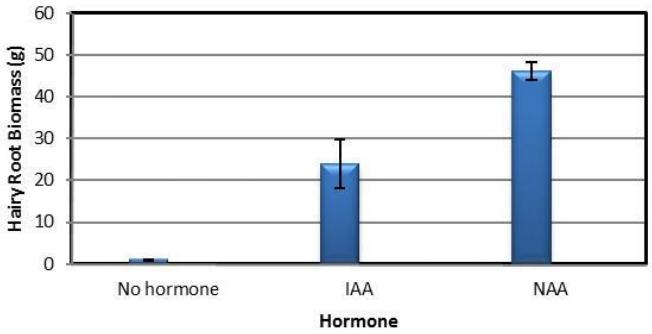

Figure 3: The biomass of hairy root cultures were cultivated in MS medium containing no hormone (control) and 1 mg.l^{-1} of IAA or 1 mg.l^{-1} of NAA

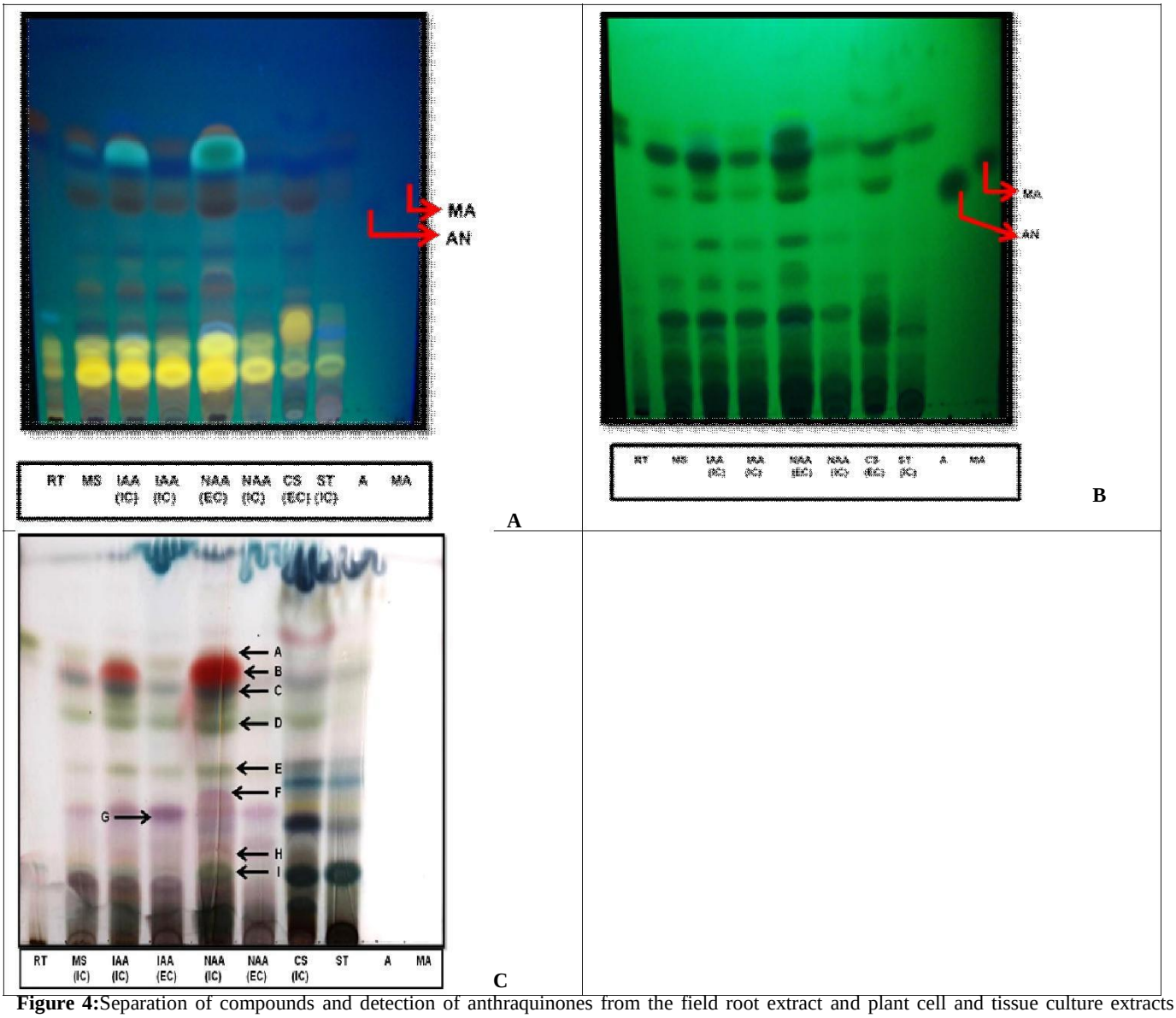

Figure 4: Separation of compounds and detection of anthraquinones from the field root extract and plant cell and tissue culture extracts of *C. triloba*. The TLC profiles of the field root extract and hairy root, shoot and cell suspension culture extracts of *C. triloba* were compared under UV light at 312 nm (A) and 264 nm (B) and by using p-anisaldehyde spray reagent (C). Field root extract (RT) (lane 1). Hairy root extract from the cultures cultivated with no hormone (lane 2), hairy root extracts from the cultures supplemented with IAA or NAA (lane 3-6). Cell suspension culture extract (CS) (lane 7). Shoot culture extract (ST) (lane 8). 9, 10-Anthracenedione (AN) (lane 9), 1-Hydroxy-4-methylanthaquinone (MA) (lane 10). Intra-cellular extract (IC), Extra-cellular extract (EC).

Profile of Compounds and Detection Of Anthraquinones in the Field Root Extract and Plant Cell and Tissue Culture Extracts by TLC

The TLC and R*f* value profiles of the field roots and hairy root, shoot and cell suspension cultures are shown in **Fig 4**. Different visualization methods were used as not all bands were visible when only one method was used. For instance band A was only shown clearing on the TLC viewed under UV light at 312 nm. The TLC viewed at 264 nm showed the standards clearly. This allowed for the Rf values of 9, 10-Anthracenedione (0.55) and 1-hydroxy-4-methylanthaquinone (0.60) to be compared to the R*f* values of the bands in the extracts. The R*f* value of band D (0.55) in the hairy root and cell suspension culture extracts correlated to R*f* value of 9,10-Anthracenedione. There were three other bands that had a R*f* value similar to1-hydroxy-4-methylanthaquinone. These were: band A (0.71) (**Fig 4A**) which was present in field root and hairy root extracts, band B (0.70) (**Fig 4B**) which was present only in hairy root culture extracts and band C (0.64) (**Fig 4B**) which was present in the field root and hairy root, shoot and cell suspension culture extracts. The TLC sprayed with p-anisaldehyde showed most of the bands present the extracts, however the standards were not visible (**Fig 4C**). Thus the TLC results gave indication that anthraquinones were present in the extracts.

Quantification of Anthraquinones by HPLC

HPLC analysis showed that the 9, 10-Anthracenedione and 1-Hydroxy-4-methylanthaquinone standards eluted at retention times (R_t) of 3.72-3.75 minutes and 4.07-4.12 minutes, respectively (**Table 2**). The field root extract showed peak at 3.57 minutes. The hairy root culture extracts showed a peak between 3.60-3.70 minutes. The shoot and cell suspension cultures extracts showed a peak at 3.55 and 3.68 minutes, respectively. Thus anthraquinones were present in the plant cell and tissue culture extracts. However, individual anthraquinones were not identified due to co-elution and therefore, the total amount of anthraquinones was calculated.

Table 3: Retention times of anthraquinones from *C. triloba* field root, plant cell and tissue culture extracts

Sample/Standard	9.10-Anthracenedione Retention Time (R_t) - minutes	1-Hydroxy-4-methylanthaquinone Retention Time (R_t) - minutes
Standard 9.10-Anthracenedione	3.72	
Standard 1-Hydroxy-4-methylanthaquinone		4.07
C. triloba field root extract	3.57	-
Hairy root (cultivated in MS medium without hormone) intra-cellular extract	3.60	-
Hairy root (cultivated in MS medium supplemented with IAA) intra-cellular extract	3.62	-
Hairy root (cultivated in MS medium supplemented with NAA) intra-cellular extract	3.70	-
Shoot culture extract	3.55	-
Cell suspension culture intra-cellular extract	3.68	-

The concentration of anthraquinones in *C. triloba* field root extract and plant cell and tissue culture extracts were calculated by using the standard curve of 9,10-Anthracenedione (Table 3). Hairy root cultures supplemented with IAA (125.03 µg.mg^{-1} [intra-cellular extract]) or NAA (98.25 µg. mg^{-1} [intra-cellular extract]) produced a higher concentration of anthraquinones compared to the control culture (13.33 µg.mg^{-1} [intra-cellular extract]). This was a 9.38 and a 7.37 fold increase, respectively. Also hairy root cultures supplemented with IAA or NAA produced a higher concentration of anthraquinones compared to the field roots of *C. triloba* (33.51 µg. mg^{-1}). This was a 3.73 and a 2.93 fold increase, respectively. This is possible as there is evidence that the secondary metabolites produced by hairy roots in culture are same as those usually synthesized in the intact parent roots and have similar or higher yields. For instance similar results were obtained in *C. roseus* hairy root cultures (Pietrosiuk *et al*., 2007). Studies show that the biosynthesis of secondary metabolites in hairy root cultures is directed by the effect of the oncogenes (the four *rol* genes A, B, C and D) (Schmülling *et al*., 1988; Petersen *et al*., 1989; Estruch *et al*., 1991). For example, it has been reported that a correlation exists between the expression of the *rol*C gene and the production of *C. roseus* alkaloids (Palazon *et al*., 1998). Furthermore a study reported by Bulgakov *et al*. (2002) showed that an association exists between the *rol* genes and anthraquinone production. In this study callus cultures of *Rubia cordifolia* were transformed with *rol* genes and the level of anthraquinones (purpurin and munjistin) was as high as 4.8% of the dry weight extract. This was much higher than the yields reported by Mischenko *et al*. (1999) for *R. cordifolia* field roots (0.2% of the dry weight extract) and non-transformed callus cultures (0.62-1.22% of the dry weight extract). The *rol* genes have also been considered to be potential activators of secondary metabolism in transformed plants as shown in Solanaceae, Araliaceae, Rubiaceae, Vitaceae and Rosaceae families (Bulgakov, 2008). Thus, the effect of the *rol* genes on secondary metabolism may probably be the reason for the higher anthraquinone yields in hairy root cultures of *C. triloba*. Shoot (3.23 µg.mg^{-1}) produced a lower concentration of the anthraquinones in comparison to the field roots and hairy roots (supplemented with hormones). According to literature shoot cultures can produce high yields of secondary metabolites for example; *Frangula alnus* and *Frangula rupestris* shoot cultures (Kovačević and Grubišić, 2005). However, some shoot cultures produce lower quantities of secondary metabolites than the parent plant for example; *Gentianella austriaca* shoot culture (Vinterhalter *et al*., 2008).

Cell suspension cultures (13.17 µg.mg^{-1}) also produced a lower concentration of the anthraquinones in comparison to the field roots and hairy roots (supplemented with hormones). A major limitation of cell suspension cultures is their lack of ability to synthesize secondary metabolites at the same level as the intact parent plant. This could be due to the lower degree of differentiation and organization of cell suspension cultures compared to organ cultures, and the location of key enzymes involved in the biosynthetic pathways (Palazon *et al*., 2006). There are certain genes and proteins that are required to produce the secondary metabolites of interest. For example, the expression *pmt* gene is essential for the synthesis of

scopolamine and the expression of this gene is specific to the pericycle of the roots (Suzuki *et al*., 1999). In the case of *C. triloba* the anthraquinones of interest are predominantly synthesized in the roots and thus root differentiation of the plant tissue is required to express certain genes in order for high yields of anthraquinones to be synthesized.

Table 3: Concentration and yield of anthraquinones from *C. triloba* field root and plant cell and tissue culture extracts

Plant material	Hormones	Extract (mg)	Anthraquinones ($\mu g.mg^{-1}$)	Yield of anthraquinones in the extract (mg)	Fold increase (comparison to field roots)
Natural roots		14	33.51	0.47 ± 0.11*	-
Hairy roots	No hormones (control) (IC)	37.7	13.33	0.50 ± 0.09	-
	IAA (IC)	38.8	125.03	4.85 ± 0.17	3.73
	IAA (EC)	13.3	0.0037	0.00005 ± 0.05	-
	NAA (IC)	81.4	98.25	8.00 ± 0.25	2.93
	NAA (C)	5.3	117.23	0.62 ± 0.13	3.50
Cell suspension	2,4-D and 6-BAP (IC)	53.1	13.17	0.70 ± 0.14	-
Shoot culture	6-BAP and IAA	39.6	3.23	0.13 ± 0.09	-

IC (Intra-cellular extract), EC (Extra-cellular extract). Fold increase is representative of the increase in the concentration of anthraquinones found in hairy roots cultures compared to *C. triloba* field roots. * n=3

In this study, we established the *C. triloba* hairy root system that exhibits the biosynthetic capacity for anthraquinones production. This was achieved by obtaining the following objectives. Protocols have been developed for the surface sterilization and germination of *C. triloba* seeds for the cultivation shoot cultures to serve as a source of explants for transformation. Hairy root cultures were induced by employing a low cell density inoculum of *A. rhizogenes* and antibiotic decontamination to induced cultures. Improvement of the biomass yield of the hairy root cultures by hormone supplementation; allowed for the comparison of the TLC profiles of the hairy root culture extracts to the field roots, shoot and cell suspension culture extract profiles. Also the highest yield of anthraquinones was produced in hairy root cultures supplemented with NAA (8 ± 0.25 mg). This was a 17 fold increase compared to field roots (0.47 ± 0.11 mg). Therefore *C. triloba* hairy root cultures are the preferable mode of anthraquinones production over shoot and cell suspension cultures.

Conclusion

This is the first study that shows the induction of *C. triloba* hairy root cultures and compares concentration of anthraquinones from *C. triloba* hairy root extracts to the field root, shoot and cell suspension culture extracts. The levels of anthraquinones produced by hairy root cultures showed a 17 fold increase as compared to the filed roots. Further optimization of culture parameters (the selection of

A. rhizogenes strain, medium composition, influence of pH and temperature and the effect of elicitors) can allow for the scale-up of the cultivation of *C. triloba* hairy roots for the mass production of anthraquinones in bioreactors. For example, *Catharanthus trichophylleus* hairy roots were cultivated at a 20 L scale and 17 monomeric indole alkaloids were isolated including vindoline, ajmalicine, lochnericine and tabersonine (Pietrosiuk *et al*., 2007). Advances in bio-techniques and plant tissue culture technology have provided new means for commercial processing of medicinal plants and their valuable phytochemicals. For example, the German company ROOTec has specialized in the large-scale cultivation of hairy root cultures for the production of valuable secondary metabolites such as camptothecin and podophyllotoxin (anticancer drugs) (Shuler and Kargi, 1992).

Acknowledgements

The National Research Foundation and the Durban University of Technology are acknowledged for support.

References

1. Abdullah, M. A., Ali, A. M., Marziah, M., Lajis, N. H and Ariff, A. B. (1998). Establishment of cell suspension cultures of *Morinda elliptica* for the production of anthraquinones. Plant Cell, Tissue and Organ Culture. 54: 173-182.
2. Amin, A., Gali-Muhtasib, H., Ocker, M and Schneider-Stock, R. (2009). Overview of Major Classes of Plant-Derived Anticancer Drugs. International Journal of Biomedical science. 5: 1-11.
3. Ataei-Azimi, A., Hashemloian, B. D., Ebrahimzadeh, H and Majd, A. (2008). High *in vitro* production of ant-canceric indole alkaloids from periwinkle (*Catharanthus roseus)* tissue culture. African Journal of Biotechnology. 7: 2834-2839.
4. Baguley, B. C. (1991). DNA intercalating anti-tumour agents. Anticancer Drug Des. 6: 1-35.
5. Bulgakov, V. P., Tchernoded, G. K., Mischenko, N. P., Khodakovskaya, M. V., Glazunov, V. P., Radchenko, S. V., Zvereva, E. V., Fedoreyev, S. A. and Zhuravlev, Y. N. (2002). Effect of salicylic acid, methyl jasmonate, ethephon and cantharidin on anthraquinone production by *Rubia cordifolia* callus cultures transformed with the *rolB* and *rolC* genes. Journal of Biotechnology. 97: 213-221.
6. Charlwood, B. V and Charlwood, K. A. (1991). Terpenoid production in plant cell culture. In: Harborne, J.B. and Tomas-Barberan, F. (Eds*.) Ecological Chemistry and Biochemistry of Plant Terpenoids.* Oxford: Clarendon Press, 95-132.
7. Dzierzbicka, K and Kolodziejczyk A. M. (2005) Anthracenedione analogues – synthesis and biological activity. Pol. J. Chem. 79: 1-29.
8. Estruch, J. J., Chriqui, D., Grossmann, K., Schell, J and Spena, A. (1991). The plant oncogene rolC is responsible for the release of cytokinins from glucoside conjugates. EMBO J. 10: 2889-2895.
9. Fernand, V. E., Dinh, D. T., Washington, S. J., Fakayode, S. O., Losso, J. N., Ravenswaay, R. O. V and Warner, I. M. (2008). Determination of pharmacological active compounds in root extracts of *Cassia alata* L. by use of high performance liquid chromatography. Talanta. 74: 896.
10. Flores, H. E., Vivanco, J. M and Loyola-Vargas, V. M. (1999). Radicle bio-chemistry: the biology of root-specific metabolism. Trends Plant Sci. 4: 220-226.
11. Geerlings, A., Hallard, D., Martinez, C. A., Lopes, C. I., van der Heijden, R and Verpoorte, R. (1999). Alkaloid production by a *Cinchona officinalis* 'ledgeriana' hairy root culture containing constitutive expression constructs of tryptophan decarboxylase and strictosidine synthase cDNA from *Catharanthus roseus*. Plant Cell Rep. 19: 191-196.
12. Hsiao, C. J., Li, T. K., Chan, Y. L., Hsin, L. W., Liao, C. H., Lee, C. H., Lyu, P. C and Guh J. H. (2008).WRC-213, an L-methionine-conjugated mitoxantrone derivative, displays anticancer activity with reduced cardiotoxicity and drug resistance: Identification of topoisomerase II inhibition and apoptotic machinery in prostate cancers. Biochem Pharm. 75: 847-856.
13. Kim, J. A., Baek, K. H., Son, Y. M., Son, S. H and Shin, H. (2009). Hairy root cultures of *Taxus cuspidata* for enhanced production of paclitaxel. J. Korean Soc. Appl. Biol. Chem. 52: 144-150
14. Kovačević, N. and Grubišić, D. (2005). *In vitro* cultures of plants from the rhamnaceae: shoot propagation and anthraquinones production. Pharm Biol. 43: 420- 424.
15. Mischenko, N. P., Fedoreyev, S. A., Glazunov, V. P., Chernoded, G. K., Bulgakov, V. P and Zhuravlev, Y. N. (1999) Anthraquinone production by callus cultures of *Rubia cordifolia*. Fitoterapia. 70: 552-557.
16. Mohanlall, V., Steenkamp, P. A and Odhav, B. (2011). Isolation and characterization of anthraquinone derivatives from *Ceratotheca triloba* (Bernh.) Hook. F. J. of Med. Plants Res. 5: 3132-3141
17. Monneret, C. (2001). Recent developments in the field of antitumour anthracyclines. Eur J Med Chem. 36: 483-493.
18. Nader, B. L., Taketa, A. T., Pereda-Miranda, R and Villarreal, M. L. (2006) Production of triterpenoids in liquid-cultivated hairy roots of *Galphimia glauca*. Planta Med. 72: 842-844.
19. Naicker, L., Mohanlall, V and Odhav, B. (2010). Methyl jasmonate induced over-production of anthraquinones from cell suspension cultures of *Ceratotheca triloba* (Bernh.) Hook. F. Int. J of Biotech and Biochem. 7: 529-541.
20. Palazon, J., Moyano, E., Bonfill, M., Cusido, RM and Pinol, MT. (2006). In: Teixeira da Silva, J. A. (Ed.) *Floriculture, Ornamental and Plant Biotechnology: Advances and Topical Issues*. London, United Kingdom: Global Science Books, 209-221.
21. Petersen, S. G., Stummann, B. M., Olesen, P and Henningsen, K. W. (1989). Structure and function of root-inducing (Ri) plasmids and their relation to tumor-inducing (Ti) plasmids. Physiol Plantarum. 77: 427-435.
22. Preobrazhenskaya, M. N., Shchekotikhin, AE., Shtil, AA and Huang, HS. (2006). Antitumor anthraquinone analogues for

multidrug resistant tumor cells. J Med Sci. 26: 1-4.
23. Pietrosiuk, A., Furmanowa, M and Lata, B. (2007) *Catharanthus roseus*: micropropagation and *in vitro* techniques. Phytochem Rev. 6: 459-473.
24. Rowinsky, E. K and Donehower, R. C. (1995). Paclitaxel (taxol). N Engl J Med. 332: 1004- 1014.
25. Schmelzer, G. H and Gurib-Fakim, A. (2008). Plant resources of tropical Africa II, Medicinal plants I. Wageningen, Netherlands: Backhuys Publishers, 155.
26. Schmülling, T., Schell, J. and Spena, A. (1988). Single genes from *Agrobacterium rhizogenes* influence plant development. EMBO J. 7: 2621-2629.
27. Shuler, M. L. and Kargi, F. eds., (1992). Bioprocess engineering: basic concepts. Prentice Hall, Upper Saddle River.
28. Suzuki, K., Yamada, Y. and Hashimoto, T. (1999). Expression of *Atropa belladonna* putrescine *N*-methyltransferase gene in root pericycle. Plant Cell Physiol. 40: 289-297.
29. Vinterhalter, B., Jankovic, T., Sovikin, L., Nikolic, R. and Vinterhalter, D. (2008). Propagation and xanthone content of *Gentianella austiaca* shoot cultures. Plant Cell Tiss. Org. Cult. 94: 329-335.
30. Wagner, H., Bladt, S and Zgainski, E. M. (1984). Plant Drug Analysis, Springer-Verlag, Berlin. ISBN 0-387-13195-7.